UNIVERSITÉ DE MONTRÉAL

DECARBONIZATION OF RESIN-BONDED MAGNESIA-GRAPHITE COMPOSITE REFRACTORIES

par

Xiangmin LI

DÉPARTEMENT DE MÉTALLURGIE ET DE GÉNIE DES MATÉRIAUX

ÉCOLE POLYTECHNIQUE

THÈSE PRÉSENTÉE EN VUE DE L'OBTENTION

DU GRADE DE PHILOSOPHIAE DOCTOR (Ph.D.)

(GÉNIE MÉTALLURGIQUE)

Juillet 1993

© droits réservés de Xiangmin LI 1993.

National Library of Canada
Bibliothèque nationale du Canada

Acquisitions and Bibliographic Services Branch
Direction des acquisitions et des services bibliographiques

395 Wellington Street
Ottawa, Ontario
K1A 0N4

395, rue Wellington
Ottawa (Ontario)
K1A 0N4

Your file *Votre référence*

Our file *Notre référence*

The author has granted an irrevocable non-exclusive licence allowing the National Library of Canada to reproduce, loan, distribute or sell copies of his/her thesis by any means and in any form or format, making this thesis available to interested persons.

L'auteur a accordé une licence irrévocable et non exclusive permettant à la Bibliothèque nationale du Canada de reproduire, prêter, distribuer ou vendre des copies de sa thèse de quelque manière et sous quelque forme que ce soit pour mettre des exemplaires de cette thèse à la disposition des personnes intéressées.

The author retains ownership of the copyright in his/her thesis. Neither the thesis nor substantial extracts from it may be printed or otherwise reproduced without his/her permission.

L'auteur conserve la propriété du droit d'auteur qui protège sa thèse. Ni la thèse ni des extraits substantiels de celle-ci ne doivent être imprimés ou autrement reproduits sans son autorisation.

ISBN 0-315-90021-0

Canada

UNIVERSITÉ DE MONTRÉAL

ÉCOLE POLYTECHNIQUE

Cette thèse intitulée:

DECARBONIZATION OF RESIN-BONDED

MAGNESIA-GRAPHITE COMPOSITE REFRACTORIES

présentée par: Xiangmin LI

en vue de l'obtention du grade de: Philosophiae Doctor (Ph.D.)

a été dûment acceptée par le jury d'examen constitué de:

M. AJERSCH Frank, Ph.D., président

M. RIGAUD Michel, D.Sc.A., directeur de recherche

M. LANDY Richard, Ph.D., examinateur externe

M. ALLAIRE Claude, Ph.D., membre

Sommaire

Le sujet de ce thèse porte sur la décarburation des réfractaires de magnésie-graphite à liaison résine, en fonction de la quantité de graphite (de 5 à 20% en poids), de la distribution granulométrique des agrégats de magnésie, de la quantité de résine (2.5 ou 3.5% en poids) et de la nature des anti-oxydants (Al, Si et SiC), de la température (entre 1000 et 1600°C) essentiellement dans l'air et accessoirement dans divers atmosphères.

Pour évaluer le comportement de ces matériaux, un protocole et des montages expérimentaux appropriés ont dus être mis au point. En effet, pour des briques de MgO-C contenant des anti-oxydants, l'évaluation de la résistance à l'oxydation à partir de mesures de changement de poids n'est pas significative, car l'oxydation des anti-oxydants correspond à un gain et non à une perte de poids et rend très difficile l'évaluation de la perte de poids en carbone. Dès lors l'évaluation doit être basée sur la mesure de l'épaisseur (ou de l'aire) décarburée et de la perte relative de résistance mécanique, ainsi que sur les changements de composition, de microstructure et de propriétés physiques (dimensions, densité, porosité) des matériaux. Dans ce contexte, la mesure de la variation en CO_2, des gaz éluants après décarburation, qui a été mise au point, s'avérera très utile. La plupart des échantillons qui ont été oxydés au cours de l'étude, ont été au préalable pyrolysés sous atmosphère réductrice. Les propriétés des matériaux graphités évoluent

considérablement durant cette réaction dite de carbonisation et cette évolution a été bien documentée. Compte tenu du protocole développé l'oxydation des échantillons ne peut être qu'unidirectionnel, ce qui élimine l'effet de la géométrie de l'échantillon sur la perte de poids par unité de surface et fait que les résultats représentent mieux l'effet du débit de la circulation et de la pression partielle d'oxygène dans le gaz, qui sont autant de paramètres importants, jouant sur les taux d'oxydation.

Les résultats obtenus confirment que la décarburation, en fonction de la température et de la nature des gaz, se déroule soit par oxydation directe du carbone par l'oxygène gazeux soit par oxydation indirecte, résultant de l'interaction MgO-C. L'oxydation directe correspond à la réaction solide-gaz C-O_2 alors que l'interaction MgO-C correspond à la réaction de la magnésie, initialement une réaction de type solide-solide. Aux températures inférieures à 1400°C c'est l'oxydation directe qui est la réaction prédominante et le taux de décarburation est en grands partie contrôlé par la diffusion de l'oxygène à l'intérieur de l'échantillon. Aux températures supérieures à 1400°C, la réduction de la magnésie devient inévitable et la décarburation est alors contrôlée par l'apport d'oxygène provenant de la magnésie. La diffusion vers l'extérieur de l'échantillon du magnésium gazeux et du CO, résultant de la réduction de la magnésie, devient le facteur dominant le taux de décarburation. En diffusant hors de l'échantillon le magnésium gazeux en contact avec un gaz s'enrichissant en oxygène, se déposera sous forme de magnésie secondaire. Ce dépôt ne peut pas se faire en présence de carbone,

mais dans la zone décarburée. L'endroit où cette déposition va s'effectuer est critique; cet endroit dépend du gradient de pression partielle de l'oxygène dans la zone décarburée; selon la valeur de ce gradient le dépôt pourra ou non conduire à la formation d'un dépôt dense. Ce dépôt dense pourra ou non constituer une barrière infranchissable et prévenir la diffusion vers l'extérieur de Mg(g) et de CO(g), limitant ainsi l'interaction MgO-C. Dès lors la porosité du matériau est importante. En ajustant la pression partielle d'oxygène il a été démontré que, de fait, il était possible de contrôler la réduction de la magnésie et la formation du dépôt dense de magnésie à l'endroit désirable pour ralentir la décarburation du matériau.

Les résultats obtenus démontrent aussi clairement que les teneurs en graphite, la distribution granulométrique des agrégats de magnésie et la quantité de résine utilisée dans les échantillons influencent l'oxydation directe et indirecte du carbone, essentiellement en jouant sur la porosité des matériaux, durant la décarburation.

Un modèle cinétique, basé sur l'interdiffusion des espèces gazeuses dans le matériau, valide jusqu'à 1400°C, a été développé, mettant en lumière le rôle prépondérant de la diffusion de l'oxygène de l'extérieur vers l'intérieur de l'échantillon. Ce modèle cinétique tient compte de la diffusion externe, de la diffusion dans un milieu poreux et de la réaction chimique C-O_2.

Les différents rôles des anti-oxydants sur la protection du carbone, compte tenu des aspects physiques et chimiques, ont été clarifiés, selon le régimes de décarburation aux températures inférieures et supérieures à 1400°C. Les différences d'oxydation de ces additifs sous CO et sous oxygène, et les conséquences sur la protection du carbone, ont été mises à jour. Le point le plus important concernant le rôle des anti-oxydants, à savoir le renforcement de la résistance mécanique, a été bien documenté.

Abstract

Decarbonizing behaviour of resin-bonded MgO-graphite refractories has been intensively studied, by varying graphite content (from 5 to 20 wt%), MgO grain-size distribution (either regular or small size distribution), the amount of resin binder (either 2.5 or 3.5 wt%), and the types of antioxidants (Al, Si, and SiC) between 1000 and 1600°C in air and other atmospheres.

In order to evaluate the decarbonizing behaviour, special efforts have been made to select and develop appropriate experimental methods and setups. For the bricks containing antioxidants, the evaluation of oxidation resistance based only on the measurement of weight changes is not meaningful because the oxidation of antioxidants contributes a weight gain to the overall weight change and creates difficulties in assessing the amount of lost carbon in the materials. Thus, the overall brick evaluation needs to be based on the measurements of the depth or area of decarbonized zone and the extent of strength loss, as well as the changes in phase composition, microstructure, and physical properties (e.g. dimension, bulk density, and porosity). The measurement of CO_2 concentration in the exhaust gas was also used successfully to estimate the rate of carbon burnout. In this study, most of the samples have been previously carbonized before oxidation tests. The properties of MgO-C bricks change considerably during the process of carbonization. Thus, to assess how this process changes the brick properties

is essential for the prediction of brick performance in the later stage. Under the unidirectional conditions of oxidation, the sample geometry does not affect the value of weight change per surface area. The results under such conditions better represent the effect of gas flow rate, flow direction, and the Po_2 in the flow, which are very important to the evaluation of oxidation rate.

It has been confirmed that decarbonization, as a function of both temperature and atmosphere, takes place either through carbon burnout by gaseous oxygen or/and MgO-C interaction. Carbon burnout corresponds to the solid-gas reaction between C and O_2, while MgO-C interaction corresponds to the reduction of magnesia, initially as a solid-solid reaction. At temperatures lower than 1400°C, carbon burnout is the dominant decarbonizing reaction, and the overall rate of decarbonization is largely determined by inward diffusion of oxygen. At higher temperatures (>1400°C), MgO decomposition becomes inevitable, and decarbonization takes place by the oxygen released from MgO. Outward diffusion of gaseous products Mg and CO generated by the MgO-C interaction becomes very important to the overall rate of decarbonizing process. As Mg vapour diffuses outwards, this vapour will deposit and form a so-called "secondary MgO" when it encounters a higher Po_2. The deposition of Mg vapour can not occur if carbon materials are present. However, the presence of a decarbonized layer does not necessarily make a MgO dense zone form unless a proper gradient of Po_2 is established. Preventing outward diffusion of Mg(g) and CO(g) can effectively inhibit MgO-C interaction; thus,

reduction of material porosity is important. Adjustment of Po_2 in the reaction system can not only control MgO decomposition, but also enhance MgO dense zone formation to hinder further decarbonization.

Variations of graphite content, MgO grain-size distribution, and the amount of resin binder in the bricks can affect greatly their resistance to direct oxidation of carbon, mainly due to the changes in material porosity.

A diffusion-limited model valid up to 1400°C for the direct oxidation of carbon has been developed, wherein the inward diffusion of oxygen from the exterior is rate-controlling. This kinetic model has combined the effects of gaseous mass transfer, gaseous diffusion in porous media, and chemical reaction between C and O_2.

The roles of antioxidants on carbon protection have been clarified based on their physical and chemical aspects in the two different decarbonizing regimes corresponding to the two different temperature ranges ($T \leq 1400°C$ and $T > 1400°C$). The difference in oxidation of antioxidants by CO and O_2 and its impact on the roles of antioxidants on carbon protection has been pointed out. Another important feature of antioxidants, i.e. their effects on strength improvement have also been discussed.

Résumé

Cette thèse porte sur la décarburation des réfractaires de magnésie-graphite à liaison résine. Ce phénomène de décarburation demeure l'élément le plus controversé qui conditionne les performances de ces matériaux composites dans l'industrie sidérurgique.

Les réfractaires graphités à liaison carbone constituent une classe de matériaux réfractaires dont l'importance est devenue manifeste au cours de la dernière décennie, et qui ne cesse de croître dans les années 1990. Ces matériaux sont utilisés dorénavant dans les convertisseurs à oxygène, les fours à arcs électrique, les poches de coulée de transfert et les fours-poches, dans la majorité des aciéries, à l'échelle mondiale. Grâce à ces matériaux, la consommation spécifique de réfractaires dans ces unités de production a chuté de façon très spectaculaire, de 6 à 8 kg par tonne d'acier à 2.0 kg par tonne d'acier dans les convertisseurs à oxygène par exemple, ce qui se traduit par des durées de vie, dans certains convertisseurs, de 800 coulées avec des briques cuites à 8000 coulées avec des briques à liaison résine. Ces quelques chiffres sont présentés à titre indicatif, pour souligner que ces matériaux composites façonnés mais non cuits, sont réellement très utiles. De nombreux efforts sont encore déployés pour atteindre des consommations spécifiques de l'ordre de 1.5 kg de réfractaires par tonne d'acier, et tous ces efforts sont centrés sur l'amélioration de la résistance à l'oxydation. En effet, irrémédiablement, ces produits pouvant contenir de 5 à 30% en poids de graphite et de 2.5 à 3.5% de résine

phénolique (Resol ou Novalak) sont très susceptibles aux réactions d'oxydoréduction, d'autant plus que leurs températures d'utilisation se situent autour de 1600°C et qu'à cette température, la réactivité du carbone est très grande. Toute trace d'oxygène gazeux se traduit par une oxydation rapide de toute matière carbonée présent; la plupart des oxydes (solides ou liquides) sont aussi réductibles par le carbone à ces températures et servent de source d'oxygène.

La présente thèse a donc été entreprise en vue de contribuer à la compréhension intime des réactions qui se déroulent dans les matériaux industriels à base d'agrégats de magnésie d'eau de mer et de paillettes de graphite naturel, liés avec un minimum de résine phénolique et de mieux saisir le rôle des anti-oxydants, des additifs maintenant usuels, comme des poudres fines d'aluminium, de silicium ou de carbure de silicium.

Le protocole expérimental qui a été développé est centré sur l'obtention de conditions expérimentales reproductibles, faisant intervenir une oxydation unidirectionnelle d'échantillons cylindriques, de 44 mm de diamètre et d'environ 40 mm de hauteur. Ces échantillons ont été découpés dans des briques expérimentales obtenues à partir de mélanges totalisant 100 kg, pour chaque composition. Un total de 9 compositions ou lots distincts ont été élaborés, en faisant varier la teneur en graphite pour une distribution granulométrique des agrégats (D1) et un pourcentage (2.5%) de résine donnés (4 lots à 5, 10, 15 et 20% en poids de graphite), en faisant varier la

distribution granulométrique à un pourcentage de graphite donné (15%), en faisant varier la teneur en résine de 2.5 à 3.5% en poids, au même pourcentage de graphite (15%), et finalement en ajoutant 3% d'anti-oxydants (3 lots avec 3% Al, 3% Si, 3% SiC).

Après mélange et mise en forme, toutes les briques ont subi un premier tempérage à 150°C pour volatiliser une partie des activateurs de prise de la résine (0.1 d'hexamine). La densité en vrac des briques produites était fonction de leur composition; dans un même lot, la densité des briques étant reproductible à 0.01 g/cm^3 près; la densité de celles-ci variant d'un lot à l'autre, de 2.94 à 3.01 g/cm^3. Par la suite la plupart des échantillons, avant oxydation, ont été pyrolisés sous atmosphère réductrice, 5 heures à 1000°C, selon la norme ASTM C607-88. Un certain nombre d'échantillons ont été oxydés sans carbonisation préalable.

La plupart des échantillons ont été oxydés, dans une enceinte, avec un débit d'air imposé de 500 ml/min, à 4 différentes températures, 1000, 1200, 1400 et 1600°C. Dans un nombre restreint de cas, des essais ont été effectués soit sous CO pur, soit sous oxygène pur et enfin sous un mélange de 90% N_2 et 10% O_2.

Au total, un ensemble de près de 200 échantillons ont été testés. Pour la très grande majorité des tests, des mesures de poids sur chaque échantillon ont été effectués après tempérage, après carbonisation et après oxydation. Des mesures de densité et de

porosité, à partir d'une méthode pycnométrique faisant intervenir un pycnomètre à hélium; des mesures de changements dimensionnels, et ce à chaque étape: tempérage, carbonisation, oxydation, doublées dans plusieurs cas d'étude dilatométrique (dilatomètre vertical avec contrôle de l'atmosphère); des mesures de résistance mécanique à l'écrasement et des mesures d'épaisseur de couche décarburée (essais destructifs après oxydation) ainsi que des analyses de diffraction X et des observations au microscope optique. Pour la plupart des essais, les tests d'oxydation se sont déroulés sur 5 heures, nécessitant au total 12 heures par essai en incluant les périodes de montée en température et de refroidissement.

Tous ces essais ainsi que les méthodes expérimentales mises en œuvre sont décrits dans la thèse. Celle-ci a été divisée en sept chapitres distincts. Le premier chapitre est un chapitre d'introduction générale où sont précisés les objectifs de départ et les questions qui sont demeurées en suspens après la recherche bibliographique portant sur une centaine de documents disponibles. Un sommaire de cette recherche est présenté dans ce chapitre ainsi que la discussion relative aux questions suivantes: quel est le contenu optimal en graphite? quels sont les mécanismes prépondérants lors de la décarburation? quelles sont les conditions favorables à la formation d'une couche dense de magnésie? quelle est la méthode la plus appropriée pour mesurer la décarburation? les anti-oxydants: protègent-ils vraiment le carbone? jouent-ils que des rôles bénéfiques? Dans le deuxième chapitre, l'envergure de la thèse est détaillé sur le plan expérimental, le protocole et les

méthodes de mesures y sont alors décrites en détails. Les résultats sont par la suite décrits dans les chapitres III à VI; ceux se rapportant à la composition dite de référence, 15% de graphite avec la distribution granulométrique optimale (D1) et la quantité de résine minimale (B1), sans anti-oxydant, en fonction de la température et de la pression partielle de l'oxygène (Chapitre III); ceux se rapportant aux changements structuraux, avec différents contenus en graphite (5, 10, 15 et 20%) ou avec une distribution granulométrique D2 correspondant à une porosité initiale accrue (D2-B1) et avec une teneur en résine accrue, correspondant à une porosité après carbonisation accrue (D1-B2) (Chapitre IV); enfin ceux se rapportant aux essais, dits de cinétique, où la teneur en CO_2 des gaz de sortie a été mesurée en continue, ce qui a permis d'établir les courbes de décarburation des échantillons dits de référence en continu (Chapitre V), et ceux se rapportant aux échantillons avec anti-oxydants (Chapitre VI). Dans le dernière chapitre, VII, les conclusions de l'étude sont présentées, après une discussion en vue de fournir des réponses aux questions posées dans l'introduction, et suivies de recommandations pour la poursuite de travaux ultérieurs, car toutes les réponses ne sont pas encore assurées.

Ce qui est à retenir c'est que définitivement il faut distinguer deux types d'oxydation du carbone, l'oxydation directe par l'oxygène gazeux, prédominante jusqu'à 1400°C et l'oxydation indirecte provenant de la réduction de la magnésie et de tous les oxydes plus facilement réductibles que la magnésie à partir de 1400°C. Le passage d'un

régime à l'autre se fait graduellement. À 1600°C le régime deux est le plus dominant, après seulement une heure d'oxydation environ, lorsque l'oxydation se fait dans l'air, en convection forcée. La valeur de la pression partielle d'oxygène dans l'atmosphère environnant joue un rôle prépondérant, mais plus important encore est le gradient de pression partielle à l'intérieur de la couche décarburée.

L'oxydation directe correspond à la réaction solide-gaz C-O_2 alors que l'interaction MgO-C correspond à la réaction de la magnésie, initialement une réaction de type solide-solide. Aux températures inférieures à 1400°C c'est l'oxydation directe qui est la réaction prédominante et le taux de décarburation est en grands partie contrôlé par la diffusion de l'oxygène à l'intérieur de l'échantillon. Aux températures supérieures à 1400°C, la réduction de la magnésie devient inévitable et la décarburation est alors contrôlée par l'apport d'oxygène provenant de la magnésie. La diffusion vers l'extérieur de l'échantillon du magnésium gazeux et du CO, résultant de la réduction de la magnésie, devient le facteur dominant le taux de décarburation. En diffusant hors de l'échantillon le magnésium gazeux en contact avec un gaz s'enrichissant en oxygène, se déposera sous forme de magnésie secondaire. Ce dépôt ne peut pas se faire en présence de carbone, mais dans la zone décarburée. L'endroit où cette déposition va s'effectuer est critique; cet endroit dépend du gradient de pression partielle de l'oxygène dans la zone décarburée; selon la valeur de ce gradient le dépôt pourra ou non conduire à la formation d'un dépôt dense. Ce dépôt dense pourra ou non constituer une barrière infranchissable

et prévenir la diffusion vers l'extérieur de Mg(g) et de CO(g), limitant ainsi l'interaction MgO-C. Dès lors la porosité du matériau est importante. En ajustant la pression partielle d'oxygène il a été démontré que, de fait, il était possible de contrôler la réduction de la magnésie et la formation du dépôt dense de magnésie à l'endroit désirable pour ralentir la décarburation du matériau.

Les résultats obtenus démontrent aussi clairement que les teneurs en graphite, la distribution granulométrique des agrégats de magnésie et la quantité de résine utilisée dans les échantillons influencent l'oxydation directe et indirecte du carbone, essentiellement en jouant sur la porosité des matériaux, durant la décarburation. Pour l'oxydation directe une teneur accrue en graphite se manifeste par une épaisseur de couche décarburée moindre, mais une plus grande porosité dans cette couche. Cette porosité accrue s'explique par la plus grande quantité de graphite consumée et par l'expansion irréversible plus sensible des paillettes avant oxydation. Dès lors il apparaît que la teneur optimale en graphite soit de 15% en poids et qu'au delà de la résistance à l'oxydation, mesurée par l'inverse de l'épaisseur de la couche décarburée, décroît. La distribution granulométrique des agrégats de magnésie, de même que la quantité de résine utilisée jouent aussi un rôle déterminant sur la porosité, pas seulement dans la zone décarburée comme précédemment, mais de façon plus critique dans la zone non-encore décarburée. Nos résultats ont permis de mettre en relief ces deux porosités, l'une dans la couche décarburée qui influencera surtout le lieu de déposition de la couche dense,

l'autre dans la couche non décarburée qui affectera le régime d'oxydation directe du carbone. Nos résultats indiquent aussi clairement qu'il y a tout avantage à utiliser la quantité minimale de résine même si une quantité plus importante (3.5% par rapport à 2.5%) se traduit par une résistance mécanique après tempérage plus élevée. Encore là, il faudra chercher en pratique le bon compromis; pour la résistance à l'oxydation la meilleure, le minimum de résine s'impose. Bien sûr, il ne faudra pas minimiser le rôle des impuretés du graphite, le recouvrement en carbone de la résine après pyrolise, et le rôle des impuretés des agrégats et autres additifs, pour bien contrôler la résistance à l'oxydation des magnésies-graphitées.

Le modélé cinétique qui a été développé, a permis de rationaliser par une équation mathématique nos résultats expérimentaux jusqu'à 1400°C, de façon satisfaisante. Cette expression

$$\frac{\rho_m}{4D_{eff}\,C_{O_2,s}}L_t^2 + \frac{\rho_m}{2k_c\,C_{O_2,s}}L_t = t$$

fait intervenir le coefficient de diffusion effectif de l'oxygène D_{eff} dans la couche décarburée d'épaisseur L_t, la concentration en oxygène à l'interface échantillon - atmosphère, $C_{O2,s}$ et la constante cinétique k_c de la réaction chimique $C(s) + 1/2\ O_2(g) = CO(g)$, qui se déroule à l'interface graphite - zone décarburée. Cette équation met en lumière le rôle prépondérant de la diffusion de l'oxygène de l'extérieur vers l'intérieur

de l'échantillon. Ceci n'est toutefois qu'une première approximation qui ne tient pas compte de la différence de réactivité du carbone secondaire initialement présent et de son taux de disparition plus rapide que celui du graphite. Bien sûr l'importance relative du carbone secondaire décroît lorsque le pourcentage de graphite augmente. Cette équation doit donc être utilisée avec prudence, car elle ne représente pas tous les phénomènes observés, notamment l'importance croissante de la réduction de la magnésie en fonction de la température.

Les différents rôles des anti-oxydants sur la protection du carbone, compte tenu des aspects physiques et chimiques, ont été clarifiés, selon les régimes de décarburation aux températures inférieures et supérieures à 1400°C. Les différences d'oxydation de ces additifs sous CO et sous oxygène, et les conséquences sur la protection du carbone, ont été mises à jour. Le point le plus important concernant le rôle des anti-oxydants, à savoir le renforcement de la résistance mécanique, a été bien documenté. Ce qui importe de retenir c'est que les anti-oxydants réagissent rapidement avec les constituants des briques et ont tendance à former rapidement des composés intermédiaires, carbures, oxynitrures, nitrures et oxydes mixtes, bien avant 1600°C. Dès lors la granulométrie des anti-oxydants est vitale. Les actions locale et globale des anti-oxydants sont deux modes à clarifier par des travaux ultérieurs. C'est sur cette dernière considération qu'a été conclue cette thèse.

Au total nous avons fourni des éclaircissements nouveaux au phénomène de décarburation des réfractaires de magnésie graphités, à liaison résine, qui conduisent à distinguer deux régimes cinétiques distincts et qui conduiront dans les travaux ultérieurs à considérer deux stratégies distinctes pour lutter contre l'oxydation des matériaux carbonés, dans ces composites industriels de haute technicité.

Acknowledgements

First of all, I would like to express my sincere gratitude and respect to my supervisor, Professor Michel Rigaud for his valuable guidance and constructive criticism throughout this work. I am very much appreciative of his continuing support and encouragement during my Ph.D. study program at École Polytechnique.

I wish to thank the industrial partners of the NSERC Chair on Refractory Materials for their active interest in this work. My special thanks go to Drs. C. F. Cooper, R. A. Landy, B. Brezny, R. E. Farris, and I. Peretz for their helpful suggestions and enlightening discussion during the course of my research work.

I am very much thankful to my colleagues for their valuable discussion and assistance, including B. Guéroult, S. Palco, S. Panigrahy, K. Adams, P. Bombard, C. Zhou, J. Xia, K. Chérif, B. Robert, F. Bossler, P. Hovington, M. Lagacé, N. Wang, and others. I also greatly appreciate the help of technicians and secretaries, especially from Messrs. J. Desrochers, A. Desilets, J-P. Bouchard, and Miss J. Chamberlain.

Lastly, I wish to express my sincere gratitude to my parents for their support and encouragement, and also acknowledge a great debt that I owe to my wife and daughter for my giving-up of many holidays and weekends to complete my study program.

Table of Contents

SOMMAIRE iv

ABSTRACT viii

RÉSUMÉ xi

ACKNOWLEDGEMENTS xxi

TABLE OF CONTENTS xxii

LIST OF FIGURES xxvii

LIST OF TABLES xxxvi

LIST OF APPENDICES xli

NOTATION xlii

CHAPTER I Introduction 1

1.1 Literature Review 4

1.1.1 Selection of brick compositions 4

1.1.2 Evaluation of carbon oxidation resistance 11

1.1.3 Kinetic approaches to MgO-C interaction 16

1.2 Questions Yet to Be Answered 18

1.3 Objectives and Significance of Present Study 24

1.4 Experimental Scheme 25

1.5 Plan of the Manuscript 26

CHAPTER II Experimental Design and Procedure 29

2.1 Design and Preparation of Experimental Bricks 29

2.2 Preparation of Samples for Testing 33

2.3 Selection of Protective Gases for Carbon Materials 34

2.4 Carbonization 35

2.5 Pre-oxidation and Oxidation Firing 36

2.6 Measurement of CO and CO_2 Concentrations 38

2.7 Characterization of Physical Properties 39

2.7.1 Weight, pycnometric volume, and dimension 39

2.7.2 Bulk density and open porosity 40

2.7.3 Relative cold crushing strength 41

2.8 Microstructural Examination 43

2.9 Analysis of X-Ray Diffraction 43

2.10 Evaluation of Experimental Measurements and Their Precision 44

CHAPTER III Decarbonization as a Function of Temperature and Atmosphere . . 46

3.1 Thermochemical Considerations of Decarbonizing Process 46

3.2 Decarbonization at Temperatures up to 1400°C 53

3.2.1 Experimental results 53

3.2.2 Discussion of the results and comparison with others 55

3.3 Decarbonization at Temperatures above 1400°C 59

3.3.1 Experimental results 59

3.3.2 Discussion of the results and comparison with others 66

3.4 Importance of Material Reactivity during Decarbonization 76

3.5 Chapter Summary 80

CHAPTER IV Direct Carbon Oxidation as a Function of Brick Composition . . . 84

4.1 Comparison of Properties before and after Carbonization 84

4.1.1 Effect of graphite content 85

4.1.2 Effect of MgO grain size distribution 92

4.1.3 Effect of carbon binder content 96

4.2 Resistance to Direct Carbon Oxidation 100

4.2.1 Effect of graphite content 101

4.2.2 Effect of MgO grain size distribution 109

4.2.3 Effect of carbon binder content 114

4.3 Chapter Summary 118

CHAPTER V Decarbonizing Kinetics in Direct Carbon Oxidation 124

5.1 Kinetic Considerations of Decarbonizing Process 125

5.2 Important Parameters Affecting Kinetics of Direct Oxidation 128

5.3 Derivation of Mathematical Equations for Kinetics 130

5.3.1 Mass transfer of oxygen through gas flow 131

5.3.2 Diffusion of oxygen through the decarbonized layer 134

5.3.3 Chemical reaction rate 135

5.3.4 Controlling step of the overall process 136

5.4 Experimental Results and Their Fit with Kinetic Modelling 138

5.4.1 Relations of thickness of decarbonized layer with reaction time 139

5.4.2 Evaluation of D_{eff} and k_c 143

5.4.3 Temperature dependence of the oxidation process 149

5.5 Chapter Summary 151

CHAPTER VI Roles of Antioxidants (Al, Si, and SiC) on Carbon Protection . . 156

6.1 Changes of Properties due to Reactions during Carbonization 156

6.2 Effect of Antioxidants on Direct Carbon Oxidation 165

6.2.1 Changes of properties during oxidation 167

6.2.2 Chemical roles of antioxidants 172

6.2.3 Physical roles of antioxidants 185

6.2.4 Stability and roles of nitrides 189

6.3 Effect of Antioxidants on Indirect Carbon Oxidation 198

6.4 Effect of Antioxidants on Mechanical Strength 204

6.4.1 Comparison of strength before and after carbonization 204

6.4.2 Comparison of strength after firing in CO at 1200°C 205

6.4.3 Comparison of strength before and after oxidation 208

6.4.4 Negative roles of antioxidants on strength 209

6.5 Further Discussion on Antioxidants 212

6.5.1 Confusions in oxidation resistance evaluation 212

6.5.2 Hydration of Al_4C_3 213

6.6 Chapter Summary 215

CHAPTER VII Summary and Conclusions 220

7.1 The Process of Decarbonization 220

7.2 Control of Decarbonization 221

7.3 Effect of Brick Compositions on Oxidation Resistance 222

7.4 Roles of Antioxidants on Carbon Protection 223

7.5 Changes of Brick Mechanical Strength 225

7.6 Characterization of Brick Properties 225

7.7 Conclusions from Present Research Work 227

7.8 Recommendations on Further Research Work 228

References 230

APPENDICES 241

List of Figures

Figure 1.1 Thirty years of continued progress in the production of carbon-containing magnesia refractories 3

Figure 1.2 Flow chart of the experimental scheme of this study 26

Figure 2.1 Two different grain size distributions of MgO grains 31

Figure 2.2 Oxidation of graphite flakes by thermogravimetric analysis 31

Figure 2.3 Preparation of samples for testing 33

Figure 2.4 Carbonization of samples for testing 36

Figure 2.5 Experimental set-up to achieve unidirectional oxidation 37

Figure 2.6 Experimental configuration for oxidation tests 38

Figure 2.7 Measurement of relative cold crushing strength 42

Figure 2.8 A view of both oxidized and unoxidized samples after crushing tests . 42

Figure 3.1 Equilibrium partial pressures of gaseous species in the C-O_2-CO-CO_2 system 49

Figure 3.2 Changes of Pco_2/Pco ratio (in logarithm) as a function of both temperature and Po_2 50

Figure 3.3 Reaction free energy of MgO-C interaction with changes of temperature and atmosphere 51

Figure 3.4 Partial pressures of gaseous species for MgO decomposition in the presence of carbon 51

Figure 3.5 Loss of weight or pycnometric volume after (unidirectional) oxidation in air at different temperatures 54

Figure 3.6 Weight loss as a function of temperature for two types of carbonized (1000°C for 1 h) brick samples after firing in vacuum for 60 min (from Tabata et al.) 58

Figure 3.7 Weight loss as a function of temperature for carbonized (at 1000°C) samples after firing in an oxidizing atmosphere with 14% O_2 (from Zoglmeyr) 58

Figure 3.8 Comparison of physical appearances (sectioned surface) of oxidized samples (with 15 wt% graphite) at three different temperatures, showing the difference in the depth of decarbonized layer 60

Figure 3.9 Micrograph of oxidized sample with 15 wt% graphite after oxidation for 5 h, showing neither graphite phase nor MgO dense zone in the decarbonized layer 61

Figure 3.10 Micrograph of oxidized sample with 15 wt% graphite after oxidation for 5 h, showing a dense MgO zone and, under this zone the graphite phase is protected from oxidation 61

Figure 3.11 Observation of MgO whiskers formed on the thermocouple tube after firing MgO-C brick sample with 15 wt% graphite in CO at 1600°C for 5 h as a result of Mg vapour deposition 63

Figure 3.12 Micrograph of brick sample with 15 wt% graphite after firing in CO for 5 h, showing the gaps between MgO grains and graphite flakes at hot face . . 64

Figure 3.13 Micrograph of brick sample with 15 wt% graphite after firing in CO at 1600°C for 5 h, showing the difference in microstructure in the interior of the sample compared to that at hot face 64

Figure 3.14 Micrograph of brick sample with 15 wt% graphite after oxidation in air for 5 h and then firing in CO for 5 h, showing the microstructure of decarbonized layer 65

Figure 3.15 Observation of MgO whiskers formed on the hot face of brick sample with 15 wt% graphite (pre-oxidized in air at 1000°C for 5 h) after firing in CO at 1600°C for 5 h as a result of Mg vapour deposition 65

Figure 3.16 Gap distance between MgO grains and carbon phase as a function of holding time at 1600°C in vacuum (from Tabata et al.) 68

Figure 3.17 Reaction free energies for carbon oxidation and Mg vapour deposition as a function of Po_2 in the reaction system 68

Figure 3.18 Weight loss of MgO-C brick samples (carbonized at 1200°C for 5 h) as a function of temperature in two different firing atmospheres (from Ishibashi et al.) 71

Figure 3.19 Schematic illustration of the relation between the Po_2 gradient and the position of Mg vapour deposition 74

Figure 3.20 Micrograph of MgO dense zone in the brick sample with 15 wt% graphite

after oxidation in air at 1600°C for 5 h 75

Figure 3.21 Thermogravimetric curves for MgO-C brick samples with 20 wt% graphite (from Wolfert et al.) 78

Figure 3.22 Relation between weight loss (in TGA) during firing in CO atmosphere and (SiO_2 + Fe_2O_3) content in MgO grain (from Uchimura et al.) 78

Figure 4.1 Changes of properties for brick samples (Gx-D1-B1) during carbonization (1000°C - 10 h) 86

Figure 4.2 Changes in cold crushing strength before and after carbonization (1000°C - 10 h) 86

Figure 4.3 Variation of porosity with graphite content for MgO compacts before and after firing in a reducing atmosphere (from Lubaba et al.) 89

Figure 4.4 View of cracked surfaces of brick samples as-received with 5 wt% graphite after crushing test, showing crack propagation through large MgO grains . . 91

Figure 4.5 View of cracked surfaces of brick samples as-received with 20 wt% graphite after crushing test, showing crack propagation through large MgO grains . . 91

Figure 4.6 Variation of strength of MgO-graphite composites with carbon content after carbonization in a reducing atmosphere (from Lubaba et al.) 93

Figure 4.7 Weight loss (unidirectional oxidation) as a function of graphite content at different oxidation temperatures 101

Figure 4.8 Weight loss (unidirectional oxidation) as a function of reciprocal temperature

for different levels of graphite content 105

Figure 4.9 Change of porosity (unidirectional oxidation) as a function of graphite content at different oxidation temperatures 105

Figure 4.10 Depth of decarbonized layer (unidirectional oxidation) as a function of graphite content at different oxidation temperatures 107

Figure 4.11 Loss of crushing strength as a function of graphite content after oxidation at different temperatures 107

Figure 4.12 Weight loss (unidirectional oxidation) as a function of oxidation temperature for both the regular MgO grain-size distribution, D1, and the small MgO grain-size distribution, D2 110

Figure 4.13 Weight loss (unidirectional oxidation) as a function of reciprocal temperature for the samples (15 wt% graphite) with either the regular MgO grain-size distribution D1 or small MgO grain-size distribution D2 111

Figure 4.14 Depth of decarbonized layer as a function of oxidation temperature for the samples (15 wt% graphite) with either the regular MgO grain-size distribution, D1, or the small MgO grain-size distribution, D2 111

Figure 4.15 Change of porosity as a function of oxidation temperature for the samples (15 wt% graphite) with either the regular MgO grain-size distribution, D1, or the small MgO grain-size distribution, D2 113

Figure 4.16 Loss of crushing strength as a function of oxidation temperature for the samples (15 wt% graphite) with either the regular MgO grain-size distribution, D1,

or the small MgO grain-size distribution, D2 113

Figure 4.17 Weight loss (unidirectional oxidation) as a function of oxidation temperature for brick samples (15 wt% graphite) with carbon binder either B1 (2.5 wt%) or B2 (3.5 wt%) 115

Figure 4.18 Depth of decarbonized layer as a function of oxidation temperature for the brick samples (15 wt% graphite) with carbon binder either B1 (2.5 wt%) or B2 (3.5 wt%) 115

Figure 4.19 Change of porosity as a function of oxidation temperature for the brick samples (15 wt% graphite) with carbon binder either B1 (2.5 wt%) or B2 (3.5 wt%) 117

Figure 4.20 Loss of crushing strength as a function of oxidation temperature for the brick samples (15 wt% graphite) with carbon binder either B1 (2.5 wt%) or B2 (3.5 wt%) 117

Figure 4.21 Comparison of the effect of changing either MgO grain size distribution (from D1 to D2) or amount of carbon binder (from B1 to B2) on the resistance of carbon oxidation 120

Figure 5.1 Schematic of the diffusion-controlled kinetic model for graphite oxidation in MgO-C refractories 132

Figure 5.2 CO and O_2 concentrations in the exhausting gas flow during oxidation as a function of oxidation temperature 140

Figure 5.3 Variation of CO_2 concentration with reaction time as a function of oxidation temperatures 142

Figure 5.4 Variation of depth of decarbonized layer with reaction time as a function of oxidation temperatures 142

Figure 5.5 Comparison of effective diffusion coefficients obtained from either experimental measurement or theoretical estimation 148

Figure 5.6 Arrhenius plots for the effective diffusion coefficients, D_{eff}, and chemical reaction rate constants, k_c 150

Figure 5.7 Values of depth of the decarbonized layer obtained from the measurement of either CO_2 concentration or total weight loss 154

Figure 6.1 Equilibrium partial pressures of CO for the reactions forming spinel, $MgO \cdot Al_2O_3$ (MA), or for carbon oxidation at different temperatures 159

Figure 6.2 Equilibrium partial pressures of CO for the reactions forming forsterite, $2MgO \cdot SiO_2$ (M_2S), or for carbon oxidation at different temperatures 159

Figure 6.3 Comparison of results of XRD analysis (relative intensities of peaks) for the carbonized (at 1000°C for 10 h) samples with Si addition before and after firing in CO atmosphere 166

Figure 6.4 Micrograph of as-received brick sample (15 wt% graphite) after direct oxidation in air at 1200°C for 10 h, showing partially oxidized Al particles left in the decarbonized layer 174

Figure 6.5 Micrograph of as-received brick sample (15 wt% graphite) after direct oxidation in air at 1200°C for 10 h, showing partially oxidized SiC particles left in the decarbonized layer 174

Figure 6.6 (a) Volatility diagram of the system Al-C-O at 1000°C 179

Figure 6.6 (b) Volatility diagram of the system Al-C-O at 1200°C 179

Figure 6.6 (c) Volatility diagram of the system Al-C-O at 1400°C 180

Figure 6.7 (a) Volatility diagram of the system Si-C-O at 1000°C 180

Figure 6.7 (b) Volatility diagram of the system Si-C-O at 1200°C 181

Figure 6.7 (c) Volatility diagram of the system Sil-C-O at 1400°C 181

Figure 6.8 Micrograph of carbonized brick sample (15 wt% graphite) after oxidation in air at 1400°C for 5 h, showing the newly formed glassy phase between MgO grains in the decarbonized layer (with Si addition) 184

Figure 6.9 Micrograph of carbonized brick sample (15 wt% graphite) after oxidation in air at 1400°C for 5 h, showing the newly formed glassy phase between MgO grains in the decarbonized layer (with SiC addition) 184

Figure 6.10 Reaction free energy for the formation of nitrides (AlN or Si_3N_4) and oxides (MA or M_2S) from Al or Si in air as a function of temperature 190

Figure 6.11 Reaction free energy for the formation of nitrides (AlN or Si_3N_4) and oxides (MA or M_2S) from Al_4C_3 or SiC in air as a function of temperature 190

Figure 6.12 (a) Predominance diagram of Al-C-O-N system at 1000°C 192

Figure 6.12 (b) Predominance diagram of Al-C-O-N system at 1200°C 192

Figure 6.12 (c) Predominance diagram of Al-C-O-N system at 1400°C 193

Figure 6.12 (d) Predominance diagram of Al-C-O-N system at 1600°C 193

Figure 6.13 (a) Predominance diagram of Si-C-O-N system at 1000°C 195

Figure 6.13 (b) Predominance diagram of Si-C-O-N system at 1200°C 195

Figure 6.13 (c) Predominance diagram of Si-C-O-N system at 1400°C 196

Figure 6.13 (d) Predominance diagram of Si-C-O-N system at 1600°C 196

Figure 6.14 Reaction free energy for the oxidation of nitrides (AlN or Si_3N_4) or carbon as a function of temperature 197

Figure 6.15 Equilibrium Mg partial pressures in the MgO-C systems in or not in the presence of Al compound as a function of temperature 200

Figure 6.16 Equilibrium Mg partial pressures in the MgO-C systems in or not in the presence of Si compound as a function of temperature 200

Figure 6.17 Comparison of crushing strength before and after carbonization for the as-received brick samples (15 wt% graphite) with or without antioxidant . . . 206

Figure 6.18 Comparison of crushing strength before and after firing in CO for the carbonized (at 1000°C for 10 h) samples with or without antioxidant . . . 206

Figure 6.19 Changes of crushing strength before and after oxidation as a function of oxidation temperature for carbonized (at 1000°C for 10 h) samples with or without antioxidant 209

Figure 6.20 Physical appearances of oxidized samples (fired at three temperatures) with Al addition after exposure to ambient moist atmosphere 216

List of Tables

Table 1.1 Evaluation of typical properties for carbon-containing refractories 3

Table 2.1 Designation of experimental bricks 30

Table 2.2 Chemical composition of sea-water sintered magnesia (wt%) 30

Table 2.3 Bulk densities of the experimental bricks as received (g/cm^3) 33

Table 3.1 Thermochemical data of redox reactions in the system of MgO-C-O_2-CO-CO_2 48

Table 3.2 Effect of oxygen concentration on carbon burnout (the brick samples G3-D1-B1 with 15 wt% graphite fired at 1200°C for 10 h) 54

Table 3.3 Property changes of the brick samples (15 wt% graphite, D1, and B1) after firing in air or CO at 1200°C for 5 h 55

Table 3.4 Properties of brick specimens A and B (from Tabata et al.) 57

Table 3.5 Effect of temperature on decarbonization (the samples with 15 wt% graphite fired in air at given temperatures for 5 hours) 60

Table 3.6 Effect of atmosphere on decarbonization (the brick samples D1-B1 with 15 wt% graphite fired at given temperatures for 5 h) 63

Table 3.7 Characteristics of MgO grains used in MgO-C bricks with 20 wt% graphite (from Wolfert et al.) 79

Table 3.8 Decarbonization of MgO-C refractories with 15 wt% graphite after carbonization at 1200°C (from Baker et al.) 81

Table 3.9 Decarbonization of MgO-C samples with 10 wt% graphite after firing in air at 1600°C (from Lin et al.) 81

Table 4.1 Comparison of properties for the brick samples (15 wt% graphite) with either the regular (D1) or small (D2) MgO grain size distribution before and after carbonization 93

Table 4.2 Changes of properties for brick samples (15 wt% graphite) with either the regular (D1) or small (D2) MgO grain size distribution due to carbonization process 93

Table 4.3 Comparison of properties for brick samples (15 wt% graphite) with either 2.5 wt% (B1) or 3.5 wt% (B2) resin binder before and after carbonization . . . 97

Table 4.4 Changes of properties for brick samples (15 wt% graphite) with either 2.5 wt% (B1) or 3.5 wt% (B2) resin binder before and after carbonization . . . 97

Table 4.5 Properties of MgO-graphite (80:20 in weight) compacts as a function of resin binder content before and after firing at 1500°C for 3 h in a reducing atmosphere (from Lubaba et al.) 100

Table 4.6 Oxidation behaviour of MgO-Carbon bricks in air at 1400°C (from Brant et al.) 122

Table 5.1 Effect of air flow rate on carbon burnout 130

Table 5.2 Effect of air flow direction (at a same flow rate) on carbon burnout . 130

Table 5.3 Oxygen concentrations at the hot surface of oxidizing sample at different temperatures of oxidation through gaseous mass transfer of air flow 134

Table 5.4 Values of coefficients A and B in Equation 5.28 and their coefficients of variation, CV%, at different temperatures 143

Table 5.5 Values of effective diffusion coefficients, D_{eff}, and rate constants of chemical reaction, k_c, at different temperatures (from experimental data) 144

Table 5.6 Theoretical prediction of diffusivity for oxygen in CO and in the porous decarbonized layer of brick samples with 15 wt% graphite at different temperatures 145

Table 6.1 Comparison of the changes in the weight and volume of samples due to the process of carbonization at 1000°C for 10 h with or without antioxidant . 157

Table 6.2 Results of XRD analysis on antioxidant-containing samples after carbonization at 1000°C for 10 h 158

Table 6.3 Change of Al vapour pressure as a function of temperature 162

Table 6.4 Comparison of the changes in weight and volume of carbonized (at 1000°C for 10 h) samples after firing in CO at 1200°C for 5 h 166

Table 6.5 Comparison of decarbonized layer depths (mm) of carbonized samples after oxidation in air at given temperatures for 5 h 168

Table 6.6 Comparison of weight changes ($\Delta W/W_0$ %) of carbonized samples after oxidation in air at given temperatures for 5 h 168

Table 6.7 Comparison of pycnometric volume changes ($\Delta V/V_0$ %) of carbonized samples after oxidation in air at given temperatures for 5 h 168

Table 6.8 Results of XRD analysis on oxidized samples with Al addition in the regions of both decarbonized layer (D.L.) and undecarbonized layer (U.L.) 170

Table 6.9 Results of XRD analysis on oxidized samples with Si addition in the regions of both decarbonized layer (D.L.) and undecarbonized layer (U.L.) 170

Table 6.10 Results of XRD analysis on the oxidized samples with SiC addition in the regions of both decarbonized layer (D.L.) and undecarbonized layer (U.L.) 171

Table 6.11 Effects of antioxidants on direct oxidation of uncarbonized brick samples (as-received) with 15 wt% graphite in air at 1200°C for 10 h 171

Table 6.12 Effects of metal additions on the MgO dense zone formation and carbon protection in MgO-C bricks with 96 wt% MgO quality grain and 15 wt% graphite (from Baker et al.) 203

Table 6.13 Hot modulus of rupture measured in argon atmosphere for MgO-C bricks with or without Al metal addition (from Tammermann et al.) 207

Table 6.14 Effect of Al metal addition on hot crushing strength in a reducing atmosphere for MgO-C bricks with 20 wt% carbon (from Troell et al.) . . 210

Table 6.15 Effect of Si metal additions on hot crushing strength in a reducing atmosphere for MgO-C bricks with 20 wt% carbon (from Troell et al.) . . 210

Table 6.16 Comparison of the results of XRD analysis on carbonized samples with Al addition before and after hydration (exposed to ambient moist air) 216

List of Appendices

APPENDIX I Thermochemical Diagrams 241

I.1 Predominance Diagrams 241

I.2 Volatility Diagrams 243

APPENDIX II Oxidation Kinetics 244

II.1 Oxygen Concentration in Air Flow at Given Temperatures 244

II.2 Rate of First-Order Chemical Reaction 246

II.3 Gas Phase Diffusivities 247

APPENDIX III Lists of Experimental Data and Their Statistical Analyses 249

Notation

C	molar concentration of gas, mole/m^3
C_s, C_i	molar concentration of gas at surface or interface, mole/m^3
D	coefficient of molecular diffusion, cm^2/min
D_{eff}	effective diffusion coefficient of oxygen through a porous solid under conditions of molecular diffusion, cm^2/min
E	activation energy, KJ/°K·mole
K_E	equilibrium constant for chemical reaction
k	Boltzmann constant
k_c	chemical reaction-rate constant for surface reaction, cm/min
L	depth of decarbonized layer, cm
M	March number, the ratio between flow velocity and sonic velocity
M_C	molecular weight of carbon, 12.01 g/mole
P	absolute total pressure, atm
p	partial pressure, atm
Q	volumetric flow rate of air, l/min
$\mathbf{R}$	reaction rate, mole/cm^2·min
R	gas constant, 8.314 J/°K·mole or 1.987 Cal/°K·mole
S	surface area of reaction during unidirectional oxidation, cm^2
T	absolute temperature, °K

t	reaction time, min
u	flow velocity, m/s
V_M	molar volume of ideal gases, 22.4140 L/mole at 0°C (273.15°K) and 24.4654 L/mole at 25°C (298.15°K)
γ	adiabatic exponent (C_P/C_V), 1.4 for air
ΔW	total weight loss of sample after oxidation, g
ε	material porosity, vol%
ρ_m	molar density of carbon in MgO-C samples, mole-(C)/cm^3-(MgO-C)
Φ	mass flux density of gas, mole/cm$^2 \cdot$ min

CHAPTER I

Introduction

In recent years, developments in the steelmaking industry have exposed refractory materials to more and more severe service conditions, which have paved the way to a considerable increase in the use of carbon-containing refractories. Within the last decennial, the resin-bonded, magnesia-graphite refractories have found widespread applications in the linings of electric arc furnaces, basic oxygen-blown converters, and various ladles for secondary-steelmaking processes. These refractories are mostly installed in the areas of intense slag wearing, such as the trunnion, slag line, tap hole, the tuyere, etc.[1]

The development of carbon-containing refractories started with pitch impregnation of dolomite bricks, which protected them from hydration. Later, the presence of carbon in these refractories was also found to contribute to the improvement of brick performance in service. Carbon materials have some important characteristics, i.e. high thermal conductivity and nonwettability in molten slag, both of which enhance the performance of the bricks used at high temperatures. Thus, carbon materials, as a constituent, have been intentionally introduced into the magnesia, alumina, and dolomite refractories.

According to Buchebner,[2] the development of magnesia-carbon bricks has taken five major steps since its beginning. Initially starting with the pitch-impregnated, burned magnesia bricks, people found later that the pitch-bonded magnesia bricks were both economically and technically better than the former. Because of the usage of coal-tar pitch as the bonding agent, especially when used together with dehydration agents, and then by means of purposeful addition of carbon black, important progress was made. A further step in the development of the magnesia-carbon bricks was the pitch post-impregnation. Since the residual carbon content was increased, an improvement in performance had been achieved. For the purpose of further increasing carbon content, introduction of graphite was made, and it had been proven to be very successful in practice. Important advances were then encountered in the development of magnesia-graphite bricks with the addition of antioxidants. Initially, the antioxidants consisted of mainly metals with a high affinity for oxygen, i.e. magnesium, aluminum, silicon, or their alloys. They were used, during operation, to influence through complex reactions the brick microstructure and properties in various ways. The flow chart shown in *Figure 1.1* summarizes the above development steps in the production of carbon-containing magnesia refractories.[2] In order to achieve better performance, carbon content has been increased from about 2 wt% in pitch-impregnated magnesia bricks to almost up to 30 wt% in magnesia-graphite bricks. However, with the increase of carbon content, the problems caused by carbon oxidation have become more apparent. *Table 1.1* gives a general evaluation of the main characteristics for these products.[2]

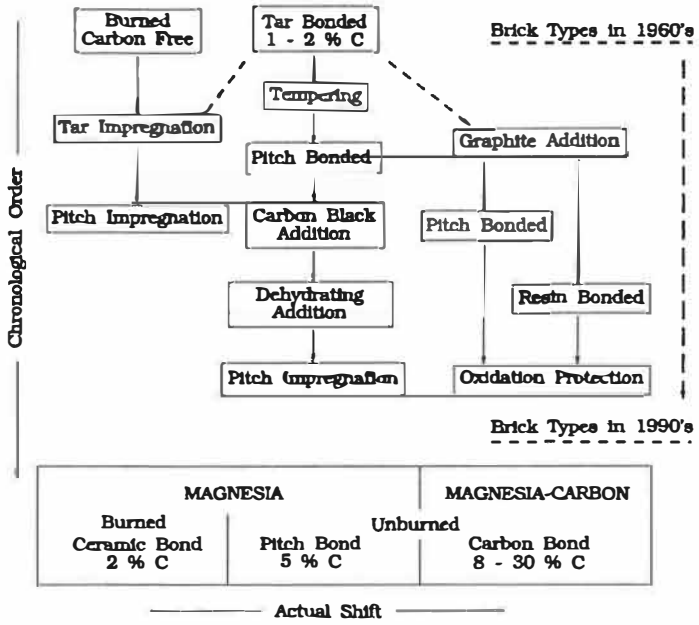

Figure 1.1 Thirty years of continued progress in the production of carbon-containing magnesia refractories.[2]

Table 1.1 Evaluation of typical properties for carbon-containing magnesia refractories[2]

Type of bricks	Magnesia		Magnesia - Carbon	
	Pitch-impregnated burned	Pitch bonded	Conventional type	With high oxidation resistance
Residual carbon	2%	5%	14%	14%
Thermal conductivity	Medium	Medium	High	High
Brick flexibility	Very low	Medium	Very high	High
Hot erosion strength	High	Medium	Medium	High
Oxidation resistance	Very high	Medium	Low	Medium~high
Corrosion resistance	Medium	High	Very high	Medium~very high
Redox stability	Very high	High	Medium	Low~high

The improved performance of magnesia-graphite refractories in practice is characterized by their high refractoriness, excellent thermal shock resistance, and very good slag penetration and corrosion resistance. However, the potential weakness of magnesia-graphite refractories is the easy decarbonization of carbon materials in service, which can result in progressive carbon loss and thus, degrade brick properties and shorten service lifetime of the linings. In addition, the strength of magnesia-graphite bricks is expected to decrease when the carbon binder is oxidized. Since decarbonization of carbon materials in service leads to significant degradation of brick properties, continuing efforts to better understand and further improve the decarbonizing resistance and performance of magnesia-graphite refractories are still being pursued.[3]

1.1 Literature Review

In this section, a brief literature review related to the decarbonization of MgO-C refractories will be given in order to provide a background on the issues on which the present study will focus.

1.1.1 Selection of brick compositions

The MgO-C refractories which are currently used in steelmaking generally have 4 major constituents, including MgO grains, graphite, carbon binder, and antioxidants. Selection of the proper raw materials and proper portion of each constituent is a very important step to produce high-quality bricks. Two recently published papers by Peretz

et al.[4] and Moore et al.,[5] respectively, have provided general reviews on this subject, but their emphases have been put on the wear resistance of the bricks.

(1) Magnesia grains

There are mainly 3 types of MgO grains used in MgO-C refractories, including sintered MgO from natural magnesite, synthetic MgO by extraction from sea water or brines, and electrically fused MgO. The chemical compositions and crystal sizes of sintered magnesite depend on the different sources. The processes of beneficiation and calcination can also have an important effect on these physical and chemical properties of MgO grains. Sea water-derived MgO can be more easily produced to higher grades. The common impurity in sea-water MgO is the boric oxide which can act as a powerful fluxing agent and has a great influence on the properties of MgO grains.[6] Electrofused MgO is available in high purity and big crystals. The fused MgO grains are less porous, but more costly. Since MgO grains are the largest portion of the MgO-C refractories, the nature of MgO grains, including the purity, density, and crystal size, is one of the most important properties affecting the overall performance of the products.

Ishibashi et al.[7] have found that with a lower CaO/SiO_2 ratio, SiO_2 and B_2O_3 in MgO grains are more likely to migrate to grain surface and then to be reduced by carbon. Also, the volatilization of SiO_2 and B_2O_3 can cause periclase surfaces to be activated, which promotes MgO-C interaction. On the other hand, the results of Baker

et al.[8] have indicated that the MgO-C bricks with standard purity grain have a smaller decarbonized area compared to those bricks with high purity grain, after oxidation in air at 1650°C.

Several studies[7,9,10] have demonstrated that the use of MgO grains with large periclase crystals, mainly available from the fused grains, can decrease the extent of MgO-C interaction, as well as the wear rate of the bricks. The size of MgO grains has been shown to be another important feature which affects the properties of MgO-C bricks. Lin et al.[3] have found that when being heated in air, the samples with finer grains have a higher effective diffusion coefficient of Mg vapour and show a lower weight loss than the coarser-grained samples. Their results indicate that the smaller grain sizing of MgO enhances the formation of a protective MgO dense layer near the outer face and limits the graphite oxidation. On the other hand, if heated in a reducing atmosphere, the volatilization of MgO with fine grains is enormous due to the large surface area, and thus a higher weight loss has been recorded.[9]

(2) Graphites

The graphites used in MgO-C bricks are mostly the natural flakes which are described loosely as coarse flake (-20 to +60 mesh), medium flake (-60 to +200 mesh), and fine flake (-200 mesh and down).[11] The main differences are the flake size and the impurity level. The carbon levels can vary from 80 to 99 wt%, and the major

components in ash are quartz and other silicates, in which SiO_2 can run over 50 wt%. Sakaguchi et al.[12] have reported that the MgO-C bricks with large-size graphite flakes have better mechanical strength and spalling resistance; but the use of small-size flakes can result in a dense brick texture which retards chemical reactions and improves oxidation and wear resistance. The results of Ishibashi et al.[7] have indicated that the SiO_2 from graphite ash can not only react directly with carbon to form the gaseous species SiO and CO, but activate the surfaces of MgO grains and promote the MgO-C interaction. Both Horio et al.[13] and Naruse et al.[10] have also shown that with the increase of impurity level in graphite, the wear rate of MgO-C bricks becomes greater. On the other hand, the results of Brant et al.[14] have demonstrated that the MgO-C bricks containing regular grade graphite have a smaller oxidized area compared to those bricks containing high purity graphite, after oxidation in air at 1400°C.

The graphite content in MgO-C bricks may range from 5 to 30 wt%. A 20 wt% of graphite in a MgO-C brick is equivalent to nearly 30% by volume. With graphite levels greater than about 10 wt%, the graphite phase can form a continuous matrix, resulting in a significant change in properties compared with traditional burned MgO bricks.[15] As reported by Kyoden et al.,[16] the spalling resistance of MgO-C bricks is improved as the graphite content increases, and the bricks with a graphite content over 15 wt% are unaffected by spalling. Yoshino et al.[17] have also shown that corrosion resistance increases with increasing graphite content up to 35 wt%, beyond that the

resistance tends to reduce because of the decrease in abrasion resistance. In addition, the results of Lubaba et al.[18] have indicated that increasing graphite content can significantly reduce the porosity of the "as-pressed" MgO-C compacts, but after carbonization this trend changes and the minimum porosity is achieved at the graphite level of ~25 wt%.

(3) Carbon binders

Resins and pitches are the two mostly used carbon binders for MgO-C refractories. The introduction of pitch as a carbon component into MgO bricks for basic oxygen furnace (BOF) applications was initially made by impregnating the pitch into the burned bricks. A more current process is to use a pitch or pitch/carbon mixture to actually bond the refractory particles. MgO grains and graphite flakes are mixed in sequence with pitch and pressed into refractory shapes. Like pitches, resin binders are also mixed with MgO grains and graphite flakes, in either powder or liquid form. The bricks after compaction normally need to be cured, resulting in improved mechanical properties of the green refractory products.

A comparative summary of the properties of resin- and pitch-carbons has been given by Rand and McEnaney.[19,20] They have reported that the oxidation resistance of pitch carbons is higher than resin carbons, but the strength and elastic modulus of pitch carbons is likely to be lower than resin carbons. Lubaba et al.[21] have made a thermogravimetric analysis in an atmosphere of continuous flowing nitrogen for both the

resin polyethylene and finely-ground pitch. Their results have indicated that resin carbon not only has a higher pyrolysing temperature (540°C), but also a higher carbon yield (58%) compared to those (450°C and 50%) of pitch carbon.

The carbon binders can determine many of the brick properties critical to the successful applications of the MgO-C refractories. The influence of the binder is related to its volume fraction and distribution (as determined by the manufacturing process) as well as to its inherent physical and chemical characteristics. Fitchett et al.[22,23,24] have systematically investigated the mechanical properties of pitch- and resin-bonded MgO or MgO-graphite materials. Their results have shown that the strength of the bonded materials changes considerably with the temperature, and the process of tempering for pitch binder or curing for resin binder has a great influence on this change in strength. The effect of carbon binders on the development of porosity in MgO-graphite refractories has also been studied by Lubaba et al.[21] They have reported that the relative contributions to porosity in the carbonized samples from binder carbonization, bulk volume expansion, and green porosity are comparable in the range up to about 6 wt% binder. As reported recently by Zoglmeyr,[25] the pitch binder has been gradually replaced by the resin binder in modern-day refractories to satisfy the environmental and safety regulations.

(4) Antioxidants

The antioxidants included in MgO-C refractories are mainly to improve the high

temperature strength and oxidation resistance. Both metallic and nonmetallic additions have been adopted so far, including Mg, Al, Si, and their alloys (metallic); SiC, ZrB_2, and B_4C (nonmetallic).

Various kinds of mechanisms have been proposed to explain the roles of antioxidants, and they are summarized as follows:

1) because of oxygen affinity, antioxidants can preferentially react with oxidizing agents so as to retard carbon oxidation;[10,26]

2) the presence of antioxidants can increase Mg vapour pressure or the rate of Mg vapour formation and enhance the formation of protective MgO dense zone, so as to restrict further decarbonization;[8,27]

3) antioxidants can produce vapour species during the process of reaction, which migrate to hot surface and react with oxidizing agents, inhibiting further oxidation of carbon;[28,29]

4) the formation of metastable carbides and stable mixed-oxides can increase the hot strength significantly;[30,31]

5) the induced volume expansion during phase transformation can contribute to the reduction of porosity for gas diffusion;[31,32]

6) and finally, the liquid phase, if any may form, accelerates densification and blocks the pores for gas diffusion.[33,34]

Although the additions can function as a strength improver and antioxidant, they

will eventually transform into the "impurities" which may then deteriorate other brick properties, such as spalling and corrosion resistance, and the strength at high temperatures as well. Kiryu et al.[35] have shown a relation between the improvement of oxidation resistance and the deterioration of spalling resistance with the increase in the amount of metal added. Toritani et al.[36] have also reported that the bricks with the addition of Al or Si have a higher corrosion rate after slag tests at 1750°C for 1 h. Recently, Troell et al.[37] have found that the presence of Si metal addition can deteriorate the hot strength of MgO-C bricks, and the values of crushing strength at 1540°C decrease with the amount of silicon added. Thus, in consideration of the overall performance, the amount of antioxidants added has to be controlled carefully.

1.1.2 Evaluation of carbon oxidation resistance

Many studies[3,10,14] have reported that the wear rate of MgO-C bricks has a strong dependence on the rate of formation of a decarbonized zone. As decarbonization proceeds, MgO-C bricks will lose their integrity and mechanical strength. Eventually, the bricks can become a loose pile of MgO grains without cohesiveness. Thus, it is of great importance to characterize and evaluate the resistance of MgO-C bricks to carbon oxidation.

(1) Weight changes

When MgO-C bricks are heated to high temperatures, carbon will first react with

oxygen from an oxidizing atmosphere, producing CO and/or CO_2:

$$2\ C(s) + O_2(g) = 2\ CO(g)$$

$$C(s) + O_2(g) = CO_2(g)$$

The interaction between MgO and C can also generate the gaseous species Mg and CO:

$$MgO(s) + C(s) = Mg(g) + CO(g)$$

All these reactions lead to a release of gaseous products with a net weight loss. However, if the Mg vapour generated through MgO-C interaction absorbs the oxygen from the atmosphere and forms a condensed MgO solid within the materials, i.e.

$$2\ Mg(g) + O_2(g) = 2\ MgO(s)$$

a weight gain is consequential, which may or may not balance the initial weight loss. Thus, the weight change of MgO-C bricks during the process of decarbonization is a reflection of the extent of several reactions occurring in the system.

The results of Zoglmeyr[38] have indicated that the rate of weight loss at 1350°C increases proportionally with the residual carbon content in the bricks. This means that there is an expected trend for higher carbon containing materials to show higher weight losses for a given reaction time. The higher surface area of carbon materials due to high carbon content is obviously a major cause for such a higher oxidation rate. For a given carbon content, the rate of weight loss is also dependent on the oxidizing temperature and time. Zoglmeyr[38] has found that there is a drop in the rate of weight loss when the oxidizing temperature is over 1400°C. He considered that this drop resulted from the

sintering effect at the surface of the oxidizing samples, making the surface increasingly impervious for the oxygen and thus retarding the oxidation of carbon materials.

Several studies[39,40] have also confirmed that the atmosphere is another important factor controlling the decarbonization in MgO-C bricks. Through the thermogravimetric analysis, Darroudi et al.[39] have found that an interaction exists between oxidation rate and atmosphere; at low and moderate temperatures air is more destructive than CO_2 for the MgO-C bricks, while at high temperatures CO_2 becomes more corrosive (a higher weight loss was recorded). Leonard et al.[40] have also observed that when the temperature reaches above 1500°C, the highest weight loss occurs in the neutral atmosphere rather than in air or CO.

On the other hand, if the bricks contain any oxidizable elements, such as the antioxidants or volatile species, besides carbon materials, the extent of weight loss does not necessarily correspond to the amount of lost carbon. Thus, from the data of weight loss, it is sometimes confusing in judgment on the resistance of the bricks to carbon oxidation. However, in the literature, there is no lack of reports[36,41] in which the weight loss is still used as an indicator of the extent of carbon loss in the cases of additions.

(2) Microstructural changes

The redox reactions occurring in the MgO-C bricks can not only cause a weight

change, but also significant microstructural changes. When MgO-C bricks are exposed to an oxidizing atmosphere at high temperatures, one typical structural change is the formation of a decarbonized layer. Thus, the measurement of the depth or area of decarbonized layer has also been used to evaluate the oxidation resistance of the bricks.

Brant et al.[42] have found that the oxidized area decreases with the carbon content, although the weight loss increases in the same direction. The results of both Leveque et al.[30] and Naruse et al.[10] have also shown that the metallic additions can significantly reduce the depth of decarbonized layer during oxidation tests, and this effect becomes more evident as the increase of metal content. However, Guenard et al.[43] have claimed that the values of the depth of decarbonized layer are less sensitive to the different types of bricks than the measurements of weight change.

When the oxidizing temperature is around 1600°C, a dense MgO zone has been frequently observed[3,8] to form somewhere in the decarbonized layer between the outer face and the reaction interface of the bricks. According to Baker et al.,[44] this dense zone is characterized by three prominent microscopic features: 1) periclase enlargement; 2) a bridging effect between coarse grains in the matrix; and 3) perimeter densification of periclase crystals.

The formation of the dense MgO zone via a vapour phase transport mechanism

has been studied extensively by many researchers.[45,46,47] Watanabe et al.[47] have found by the scanning electron microscopy examination that the needlelike MgO crystals (whiskers) exist at the interface between the dense layer and the original layer. A preferred orientation of the MgO crystals in this dense layer has also been confirmed by Leonard et al.[40] through x-ray diffraction. In addition, both Brezny et al.[27] and Baker et al.[8] have reported that the presence of antioxidants can significantly influence the thickness, quality, and temperature of formation of this dense zone, and the addition of Mg metal can not only increase its thickness but also reduce its forming temperature. Furthermore, Baker et al.[44] and Kim et al.[46] have noticed that the slag composition has an important effect on the formation and destruction of the dense MgO zone due to the very different oxygen partial pressures in the systems, and iron oxide must be present in the slag to establish a Po_2 high enough to allow the dense zone to form.

Because of the impervious nature of the dense MgO layer, the inward diffusion of oxygen to the materials and the escape of gaseous products Mg and CO from the interior of the materials are repressed so that carbon is inhibited from further oxidation by either oxygen or MgO. There are also many reports[8,44,46] indicating that the slag wear resistance of the bricks is improved due to the formation of this dense zone. However, Lin et al.[3] have found that the progressive build-up of internal pressure of gaseous species Mg and CO may cause the structure to crack, bloat or spall to relieve this pressure.

1.1.3 Kinetic approaches to MgO-C interaction

The interaction between MgO and C is an important reaction during the decarbonizing process of MgO-C refractories. Carniglia[48] was the first to make an effort to establish a diffusion-limited model for the kinetics of MgO-C interaction process in which the rate of escape of CO and Mg vapour species from the interior is controlling. His kinetic modelling was based on the one-dimensional, steady-state diffusion case with either uniform temperature distribution or a temperature gradient along the diffusion direction. In the case with uniform temperature distribution, the kinetic equation was given as

$$\Phi_s \cong \frac{\Pi}{\frac{1}{\Phi_a} + \frac{(x_s - x_c)}{D_s}} \qquad (1.1)$$

where Φ_s is the product gas flux at the exposed surface; Π, the equilibrium value of the product gas pressure at temperature T; Φ_a, the sweep rate of the external atmosphere; x_s-x_c, the thickness of decarbonized layer; and D_s, the effective diffusion coefficient. Although Carniglia's model was developed nearly 20 years ago, the model has not been satisfactorily justified since then. The main reason is that through the conventional method of thermogravimetric analysis unidirectional gas diffusion can hardly be achieved.

Tabata et al.[49] have also proposed another kinetic model for MgO-C interaction based on the growth rates of gaps between MgO and C and the reaction (gap forming)

layer. Depending on the rate-determining step for the chemical reaction at the MgO-C interface or the outward diffusion of Mg and CO gaseous products, different rate equations were derived. If the diffusion of product gases is the rate-controlling step, the total weight loss can be given as

$$(\Delta W)^2 = 2\ K_d\ t \qquad (2.2)$$

where t is the reaction time, and K_d is the reaction rate constant which is a function of the concentrations of Mg(g) and CO(g) at reaction interface, the diffusion coefficients of Mg(g) and CO(g), and the cross-sectional area of diffusion path (as expressed in a complicated formula). The value of ΔW is calculated based on the measurements of gap distance between MgO and C and the length of reaction layer at a given time t, and also some other material parameters. Unfortunately, from these results, the predicted values do not have a fair agreement with the measured values due to the difficulty in precise evaluation of gap distance between the MgO and C phases.

Besides kinetic modelling, Komarek et al.,[50] Leonard et al.,[40] Carniglia,[48] and Tabata et al.[49] have also evaluated the overall rate of reaction process by measurements of thermogravimetric analysis (continuous recording) or weight loss (discontinuous recording) in the reaction systems with low Po_2. The activation energy values obtained fall in the range of 35 ~ 150 kcal/mole (in the temperature range 1300 ~ 1600°C), depending mainly on the reaction systems. In addition, both Brezny et al.[27] and Lin et al.[3] have made quantitative evaluations of the effective diffusion coefficient of Mg vapour through

the measurement of the rate of MgO dense zone growth in an oxidizing atmosphere at temperatures ~ 1600°C. However, this method is tedious, and can only be carried out on a discontinuous basis. Moreover, the larger variation in the dense-zone thickness could make the measured values less precise.

1.2 Questions Yet to Be Answered

The research work on the decarbonization of MgO-C refractories has been conducted frequently during the last decade due to its importance. However, there are still many questions which need to be answered after having reviewed extensively the literature available (more than 100 papers/publications since 1970),[51] and the following questions have been raised in order to understand the nature of the problems.

QUESTION 1.

What optimum mixture of carbon materials should be used?

Among the carbonaceous materials normally used to produce MgO-C bricks are the resins, pitches, carbon blacks, synthetic and natural graphites. Their physical and chemical properties are totally different from one to another.[52,53,54] But what proportion of each type should be adopted for the brick composition? Also, the available literature does not help to clarify the issues related to the selection of carbon materials, including the purity, size, and mixing procedure.

QUESTION 2.

What are the mechanisms of decarbonization?

Graphite can be very stable in a reducing atmosphere at temperatures up to 3000°C. However, in an oxidizing atmosphere, the situation is completely different, and graphite will begin to oxidize at a significant rate if the temperature is over about 600~700°C.[11] The oxidizing temperature of carbon binders is even lower.[55] At high temperatures (T >1400°C), the chemical incompatibility of magnesia and carbon can inevitably induce the MgO-C interaction, even in an inert or reducing atmosphere. Thus, decarbonization through a series of redox reactions can occur in MgO-C bricks when they are heated up from ambient temperature to service temperature, i.e. ≥1600°C. With the changes of both temperature and atmosphere in the reaction system, which decarbonizing mechanism is dominant and how to control the reaction rate are still two questions which have not been clearly answered in the literature.

QUESTION 3.

Is atmospheric oxidation important?

Because of the use of MgO-C bricks for steelmaking at high temperatures above 1600°C, previous research work was primarily limited to the study of corrosion resistance to molten slags and steels.[9,15,56] Carbon oxidation in air on a bare working face at low temperatures has received much less attention. In fact, decarbonization at low temperatures always preconditions the reactions occurring at high temperatures, and

affects the performance of the brick linings in the later stage. As importantly, there have been reports[38,57] that at cold face of furnace linings where temperature may reach 900°C or so, the burnout of carbon materials in air may, under practical service conditions, become significant. Unlike what happens at the hot face, no protection from a slag layer or/and dense MgO layer can occur at the cold face. Therefore, decarbonization at the cold face can also become a serious problem, and an investigation on this subject is meaningful and necessary.

QUESTION 4.

What are the prevailing conditions to form a dense MgO zone?

Although it has been very well documented[46,47,58] that a dense MgO zone can be formed in the interior of brick body as a result of MgO-C interaction, the conditions for the formation of dense MgO zone have not been well delineated yet. In fact, the dense zone formation is frequently observed in laboratory tests, but is randomly reported on the bricks after in-plant service. Since the formation of Mg vapour is inevitable because of the chemical incompatibility between MgO and carbon, it is more beneficial that the Mg vapour deposit in the interior of bricks or at the brick surface rather than escape to the exterior. Thus, further study is needed in order to improve the understanding of the criteria that control the presence or absence of a dense zone in the bricks used in steelmaking furnaces.

QUESTION 5.

What are the optimum microstructure, compaction, and grain-size distribution?

Although the addition of carbon materials to magnesia refractories is very helpful for the improvement of performance, in terms of carbon oxidation, the increase of graphite content will result in losing more carbon, which can, in turn, cause more significant brick structure damage. But then, what is the optimum graphite content? The increase of carbon binder content can increase the amount of carbon in the bricks and also improve their strength, but is a high carbon binder content in MgO-C refractories worthwhile? When MgO grains mix with graphite, their size distribution has to be modified in order to produce the bricks of high quality. However, does the MgO grain-size distribution have a significant effect on the decarbonizing resistance of the bricks?

In fact, with the changes of graphite content, carbon binder content, and MgO grain-size distribution, the only systematic study on the compaction behaviour of MgO-graphite composites has been published by Lubaba et al.,[18,21] in which porosity changes before and after carbonization were stressed. These porosity changes are expected to have an influence on oxidation resistance of MgO-graphite bricks at high temperatures. Unfortunately, this part was missing in their study, and hence the relationship between microstructural features and carbon oxidation has yet to be established.

QUESTION 6.

What are the effective methods to characterize decarbonization?

Currently, no accepted standard test method to evaluate decarbonizing behaviour of MgO-C refractories is available from either ASTM (American Society for Testing and Materials) or ISO (International Organization for Standardization). The European Association of Refractory Producers is still working on an ISO standard.[59]

In the literature, many different procedures are being followed, but they include at the end the measurements of weight loss and/or depth of decarbonized layer, even if there is no report so far concerning the concordance of these two measures.

QUESTION 7.

Is the binder pyrolysis or carbonization process significant?

In commercially available MgO-C bricks, the binder phase is cured, but not pyrolysed. However, the bricks in a furnace lining will inevitably undergo the process of carbonization as they perform their functions in service. During this process, the brick properties can change considerably. However, in most published work on oxidation tests,[38,60,61] the competition between carbonization and decarbonization is not especially considered. Even though the carbonization method for MgO-C refractories is duly standardized for both ASTM (C607-88) and ISO/DIS (10060-1), how important to pre-carbonize the bricks in order to develop a standard oxidation test procedure is still an unanswered question.

QUESTION 8.

What are the dominant roles of antioxidants?

So far, a variety of antioxidants have been selected to add to MgO-C bricks for the purpose of protecting carbon materials. In terms of anti-oxidation and strength improvement, various kinds of mechanisms have been proposed. Although all these mechanisms are possible in practice, it is still not clear which mechanism will play the dominant role on hindering decarbonization under service conditions. Will the effectiveness of antioxidants vary with the types of raw materials in the bricks and/or the service conditions in terms of the changes in temperature and atmosphere? And what type of antioxidants is most effective? So far, these questions have not been well answered. Thus, a better understanding of the on-going mechanisms is still essential to the selection of new and better antioxidants.

Although many researchers have reported[10,62] that the addition of antioxidants is beneficial to the protection of carbon materials, other studies[36,63] have claimed that the superior slag resistance of the bricks can deteriorate when the additives transfer to impurity oxides. Results on slag-wear resistance are indeed controversial; "improved", "not-improved", and even "worse" corrosion resistances have all been reported in the literature.[10,13,36] A contradiction appears to exist; on the one hand, very high prices are paid for very pure raw materials, but, on the other hand, certain impurities are added on purpose as antioxidants. Therefore, in terms of the overall performance in practice, is

adding antioxidants worthwhile? Under what conditions do advantages outweigh disadvantages?

In summary of all questions brought up, the decarbonization of MgO-C refractories is an important characteristic to assess, but, many questions are still unanswered regarding this behaviour. No standardization for characterization of decarbonizing behaviour exists. Many parameters are known to influence this behaviour, and therefore, comparison of experimental results between different authors is very difficult. Contradictions among results in the previous work are often found because not all parameters are carefully defined.

1.3 Objectives and Significance of Present Study

The aims of the present research work were defined in order to be able to answer most of the questions formulated previously. They include:

1) the definition of an acceptable standard test method to evaluate the properties of resin bonded, MgO-graphite refractories, which could be easily standardized;
2) the investigation of decarbonizing behaviour and mechanisms in a wide range of temperature and atmosphere;
3) the evaluation of the roles of single antioxidants (Al, Si, and SiC) on the improvement of oxidation resistance.

The emphasis of this study focuses on the mechanisms of the redox reactions occurring in MgO-C materials as a function of both temperature and atmosphere. Both thermochemical and kinetic analyses of decarbonization (mainly in air) will be made. Brick-slag interaction is not part of this study.

This research work is intended to lead to a better understanding of decarbonizing behaviour of MgO-C refractories, i.e. the reactions of carbon materials with "free" and "bound" oxygen, on both practical and theoretical bases, and to provide possible directions for further improvement of performance, in terms of both brick properties and control of environmental conditions (temperature and atmosphere).

1.4 Experimental Scheme

The experimental scheme of this work is shown in *Figure 1.2*. The experimental bricks will be prepared with different graphite content, carbon binder content, size distribution of MgO grains, and type of antioxidants. Most experiments will be carried out isothermally in the temperature range of 1000 to 1600°C. The effects of atmosphere and convection in the furnace will be considered. Attempts will be made to control carbon oxidation of MgO-graphite bricks in air by unidirectional counter-diffusion, to simulate the operating conditions in practice. The characterization of the resistance to decarbonization will be attempted through the measurements of total weight loss, depth of decarbonized layer, change of open porosity, loss of mechanical strength, and changes

in microstructure.

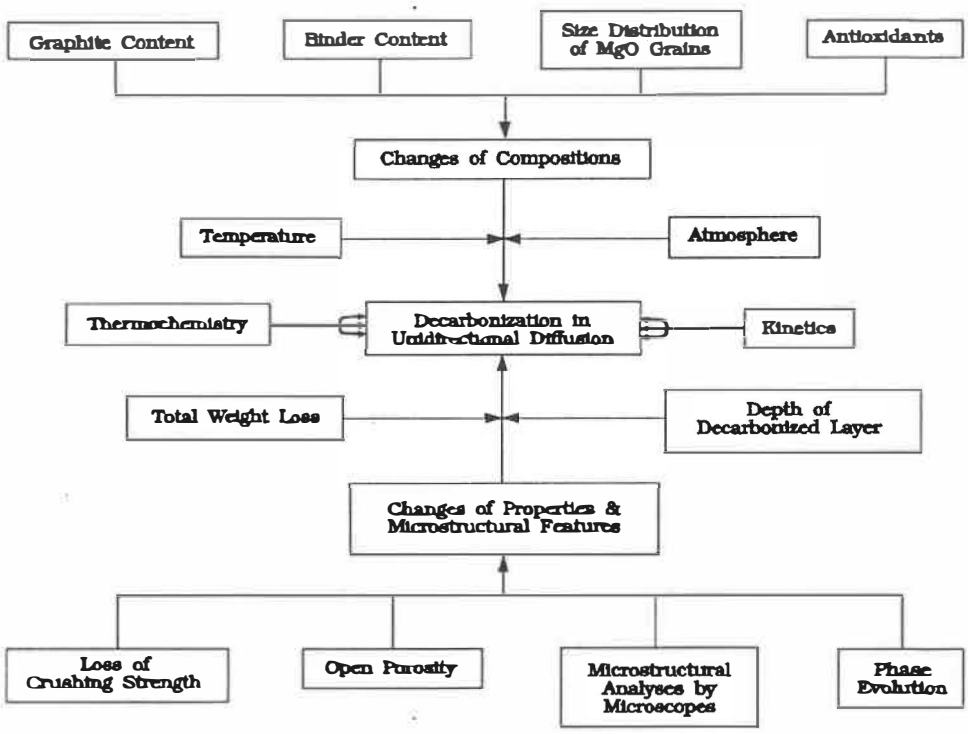

Figure 1.2 Flow chart of the experimental scheme of this study.

1.5 Plan of the Manuscript

The formulation and preparation of experimental bricks are described in Chapter II, where the experimental design and procedure are also presented. Emphasis is put on the discussion of selection and design of appropriate experimental methods and set-ups to better characterize the decarbonizing behaviour of MgO-C refractories.

Experimental results and discussion are presented in Chapter III through Chapter VI, which are the major part of this thesis.

According to the results of oxidation tests, the decarbonizing behaviour with the changes of both temperature and atmosphere in the reaction system is reviewed in Chapter III. The possible decarbonizing mechanisms are discussed, and the explanations of the results from this work and the contradictions of previous research work are made.

In Chapter IV, the changes of brick properties during the process of carbonization with variations of brick compositions and the effect of these changes on carbon oxidation resistance are discussed.

In Chapter V, a kinetic model for graphite oxidation in MgO-C bricks in the temperature range from 1000 to 1400°C is presented, and then comparison with experimental results from continuous measurement of CO_2 concentration during the process of oxidation is made.

Both the positive and negative roles of antioxidants (Al, Si, and SiC) on carbon protection and strength improvement are discussed in Chapter VI along with the results of x-ray diffraction analysis, oxidation tests, and crushing strength measurements. The emphasis is put on the discussion of phase evolution with the changes of both temperature

and atmosphere in the reaction system by means of thermochemical analyses, e.g. predominance diagrams and volatility diagrams.

Chapter VII summarizes the discussions of the experimental results presented in Chapter III through Chapter VI, and then the conclusions are drawn. Suggestions on further research work are also made.

In Appendix I, the principles of predominance diagrams and volatility diagrams, and the methods of diagram construction are presented. Appendix II supplements the derivation of the kinetic model for graphite oxidation with the development of certain mathematical equations. Part of the experimental raw data and their statistical analyses are listed in Appendix III to show the range of data variations and the data treatments.

CHAPTER II

Experimental Design and Procedure

In order to better evaluate and characterize the decarbonizing behaviour of resin-bonded, MgO-graphite bricks, efforts have been made to select the most important parameters and to investigate the effects of these parameters on decarbonization by adopting an appropriate experimental design and procedure.

2.1 Design and Preparation of Experimental Bricks

The designation of experimental bricks was based on the following five major parameters:

1) MgO grain-size distribution (D)
2) the content of graphite (G)
3) the amount of carbon binder (B)
4) the type of antioxidants (A)

The formulations which combine all above parameters are shown in *Table 2.1*.

The same sea-water sintered magnesia with average crystallite size 40 ~ 60 μm was used throughout this study, and its chemical composition is listed in *Table 2.2*. Two different grain-size distributions, as shown in the histogram of *Figure 2.1*, were selected.

The selection of regular grain-size distribution, D1, was based on the optimum packing density of MgO-graphite compacts. For the second grain-size distribution, a higher percentage of finer grains was intentionally adopted to reduce the portion of larger grains, and the mix of the grains was referred to as the small grain-size distribution, D2.

Table 2.1 Designation of experimental bricks

Mix No.	MgO grain-size	Graphite content	Binder level	Antioxidant
1	D1-regular	G1-5	B1-2.5	-
2	D1-regular	G2-10	B1-2.5	-
3	D1-regular	G3-15	B1-2.5	-
4	D1-regular	G4-20	B1-2.5	-
5	D2-small	G3-15	B1-2.5	-
6	D1-regular	G3-15	B2-3.5	-
7	D1-regular	G3-15	B1-2.5	A1-Al
8	D1-regular	G3-15	B1-2.5	A2-Si
9	D1-regular	G3-15	B1-2.5	A3-SiC

Table 2.2 Chemical composition of sea-water sintered magnesia (wt%)

MgO	CaO	SiO_2	Al_2O_3	Fe_2O_3	B_2O_3
98.1	0.8	0.6	0.2	0.2	0.1

For the graphite, natural flake with ash content of 8.0 wt% and flake size 80% +80 mesh was utilized. SiO_2, Al_2O_3, and Fe_2O_3 are the majors in the composition of ash. *Figure 2.2* shows the result of thermogravimetric analysis of the graphite flakes that we

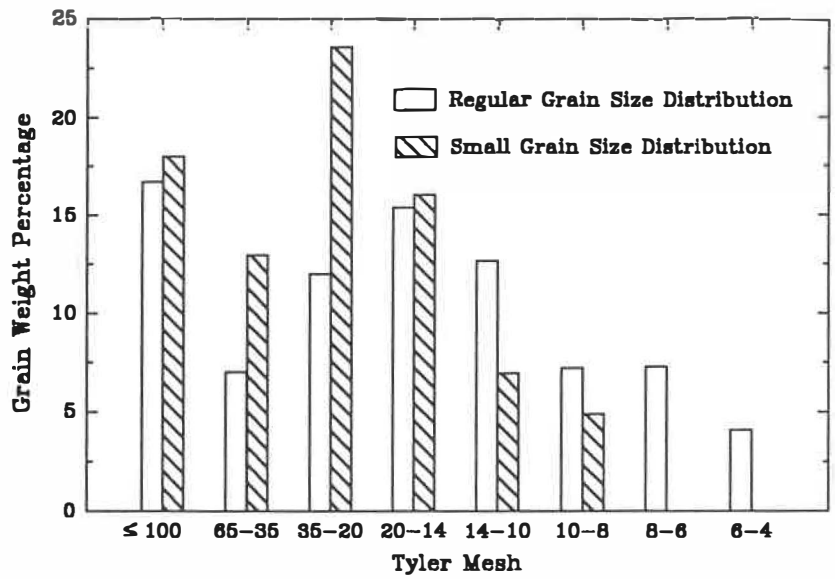

Figure 2.1 Two different grain size distributions of MgO grains.

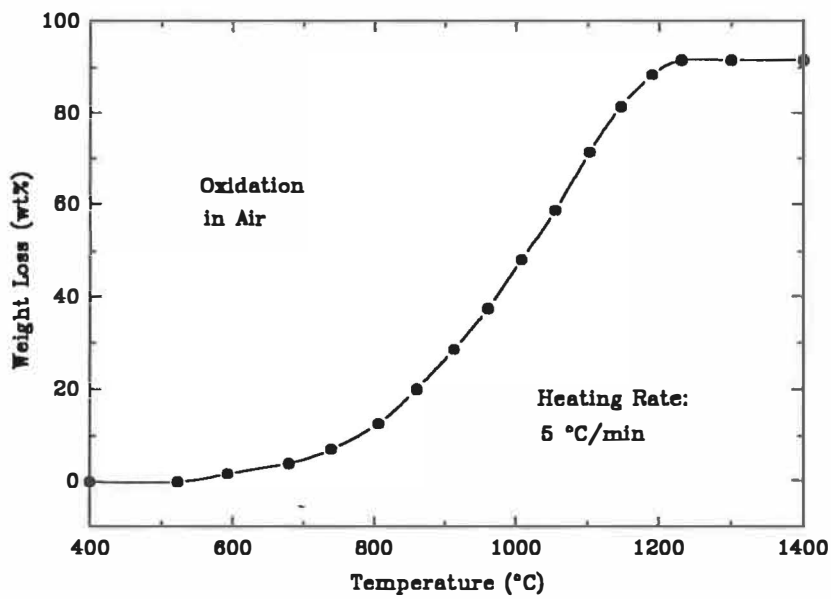

Figure 2.2 Oxidation of graphite flakes by thermogravimetric analysis.

used. The graphite content in the experimental bricks was set at 5 (G1), 10 (G2), 15 (G3), and 20 (G4) wt%.

Liquid phenolic resin with specific gravity 1.18 ~ 1.20 was adopted as carbon binder and its level was set at 2.5 wt%, B1 (a novolac 2.5% with hexamine 0.1%). The purpose of adding 0.1 wt% hexamine was to cure the resin properly. For the second binder amount, B2, an additional 1 wt% resin was added to B1, i.e. 3.5 wt% in total.

The antioxidants - aluminium (Al), A1; silicon (Si), A2; or silicon carbide (SiC), A3 - were included separately, all at the level of 4 wt%. They were added in the form of fine powders, i.e. 100 ~ 325 mesh Alcoa uncoated aluminum, -200 mesh silicon, or -200 mesh silicon carbide.

The experimental bricks were prepared by a refractory manufacturer in the same way as commercial ones. An intensive-type mixer with a standard mixing procedure and sequence of additions was used to mix each of the components together. The bricks, in the size of 76 mm (thickness) x 114 mm (width) x 229 mm (length), were pressed using multiple impacts to deair and densify the material properly. Eight bricks were prepared for each batch of the 9 mixes, and thus, the total number of the bricks with different compositions was 72. After pressing, the bricks were cured using a programmed heat-up schedule with a final hold of 6 h at a minimum temperature of 175°C. The average bulk

densities of these brick batches after curing are listed in *Table 2.3*.

Table 2.3 Average bulk densities of the cured experimental bricks as received (g/cm^3)

No.1 (G1)	No.2 (G2)	No.3 (G3)	No.4 (G4)	No.5 (D2)	No.6 (B2)	No.7 (A1)	No.8 (A2)	No.9 (A3)
3.01	3.00	2.98	2.95	2.94	2.95	2.95	2.95	2.90

2.2 Preparation of Samples for Testing

The samples for testing were prepared in cylindrical shape (ϕ44x40 mm) by drilling into the experimental brick with a core drill in the direction perpendicular to the pressing axis of the brick during manufacture and parallel to the longest brick direction (see *Figure 2.3*). The purpose was to evaluate the brick performance by simulating the service condition in consideration of the dominant graphite orientation.[64] The measurement of oxidation resistance in this direction is believed to represent better the practical situation. Eight samples in total were prepared from one brick.

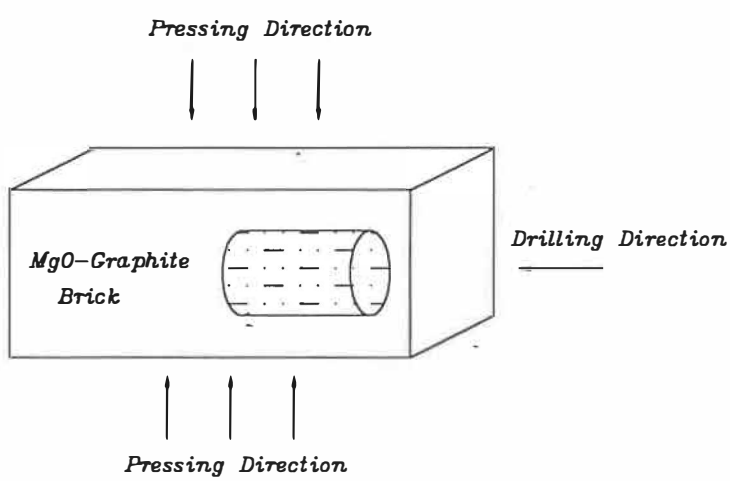

Figure 2.3 Preparation of samples for testing.

2.3 Selection of Protective Gases for Carbon Materials

Several gases are available to be used for preventing carbon from burning out by oxygen during heat treatments, but the selection of proper protective gases should be based on suppressing the dominant reaction of carbon oxidation:

$$2\ C(s) + O_2(g) = 2\ CO(g)$$

or in other words, any gas which does not react with the components of MgO-graphite bricks, and, at the same time, has a low level of oxygen concentration or/and a high level of CO concentration can be used as the protective gas for carbon materials.

Commercially available inert gases, such as Ar or He, can be used as the protective gases, but they are not very effective, especially when the temperature is rather high, because of their oxygen concentration. Oxygen as an impurity, at a level of 1 to 10 ppm (partial pressure of 10^{-5} atm), will cause a certain carbon loss, particularly at high temperatures where carbon oxidation can take place very quickly, even at such a low level of oxygen. N_2 is not considered to be a good protective gas either because it not only contains oxygen impurity, but also can react with the antioxidants in the bricks. Pure CO gas is quite effective for carbon protection, even though interactions between CO and antioxidants may occur. However, considering that the MgO-C material generates CO itself as the temperature rises, the use of CO gas may not have the

possibility of artificially imposed property changes.

2.4 Carbonization

As already mentioned in *Section 2.1*, the experimental bricks received were cured by the manufacturer. Most of the samples for testing were carbonized at 1000°C for 10 hours to remove the volatiles, especially from the resin binder. The procedure of carbonization mainly followed ASTM C607-88.

A Lindberg® metallic retort, as shown in *Figure 2.4*, was used for the atmosphere-controlled carbonization process. Within the retort, eight cylindrical samples were embedded in coke powder for each batch of the carbonizing treatment. After having loaded the samples and packed them in coke powder, the air remaining in the retort was evacuated by a vacuum pump, and then argon gas was introduced. Subsequently, a positive pressure within the retort was retained with a sufficient flow of argon throughout the entire period of carbonization process so that the air from the exterior was kept away. The retort loaded with samples was heated in an electric furnace to the carbonizing temperature 1000°C, at which the furnace was maintained for 10 h, and then cooled down naturally. Re-heating the carbonized samples in the same procedure as described above, or doubling the holding temperature at 1000°C, i.e. 20 h, only resulted in a negligible change in both weight loss and pycnometric volume (less than 0.03%).

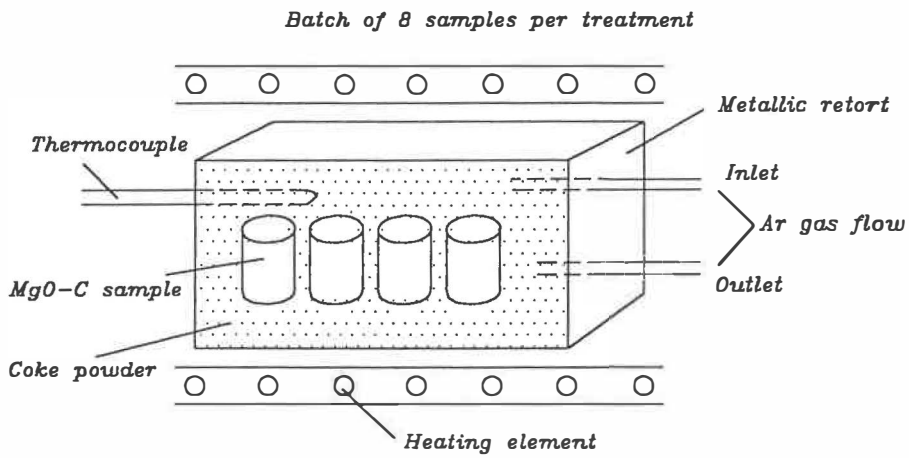

Figure 2.4 Carbonization of samples for testing.

2.5 Pre-oxidation and Oxidation Firing

A limited number of carbonized samples were pre-oxidized at 400°C for 50 h in air to remove secondary carbon pyrolysed from the resin binder during carbonization. This procedure was adopted for the purpose of minimizing the influence of carbon from the binder. According to the calculation from the measurement of weight loss during pre-oxidation, about 60 to 70 wt% of secondary carbon was burnt out. The preliminary tests showed no evidence of graphite oxidation under such a condition of pre-oxidation.

For oxidation firing, the carbonized or pre-oxidized (in some cases) samples were loaded in a specially designed experimental holder (see *Figure 2.5*). All surfaces of the sample except the top were protected by an alumina tube in order to control unidirectional oxidation at only one surface. The purpose of this orientation is to simulate

the situation under service conditions, and also to simplify the possible relation between weight loss and depth of decarbonized layer.

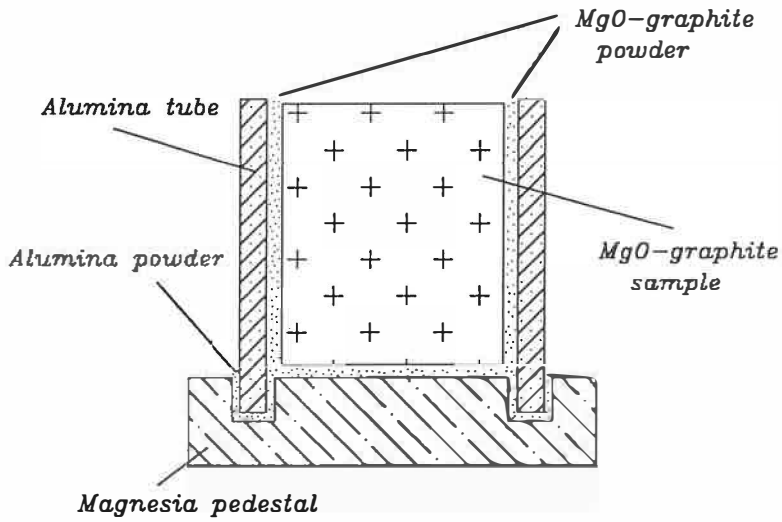

Figure 2.5 Experimental set-up to achieve unidirectional oxidation.

An electric furnace, heating an alumina tube with gas inlet and outlet at each end (see *Figure 2.6*), was used for the oxidation tests. The sample with the holder was placed in the centre of the heated alumina tube of the furnace, with the exposed sample surface facing the gas flow. Before heating, the furnace tube was flushed with pure CO gas for 10 min to minimize the influence of the remaining air in the tube. Isothermal firings at 1000, 1200, 1400, and 1600°C, respectively, for 5 h (or longer) were then conducted at a constant flow rate of dry air (500 ml/min). During the period of either heating-up or cooling-down, pure CO gas was circulated to prevent possible carbon oxidation. For CO atmosphere firing, pure CO gas rather than air flowed around the sample during the

time period of isothermal holding. Besides, pure oxygen and a gas mixture of oxygen and nitrogen were also selected as the oxidizing gases.

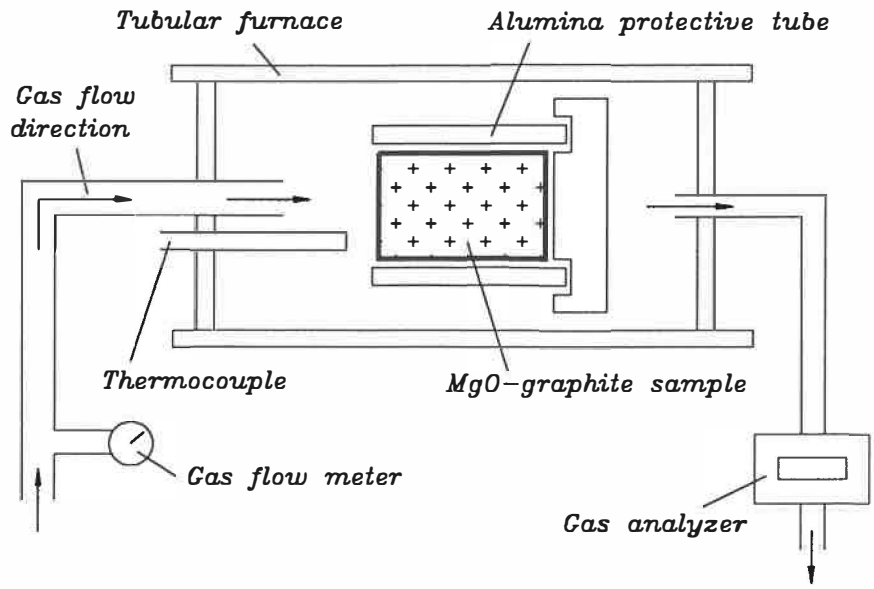

Figure 2.6 Experimental configuration for oxidation tests.

2.6 Measurement of CO and CO_2 Concentrations

In order to investigate oxidation kinetics of the graphite phase, the amounts of CO and CO_2 released during oxidation in a given time period were also chosen as an indication of the rate of carbon burnout. An ENERAC™ 2000 gas analyzer with electrochemical sensor was utilized to determine CO volumetric concentration in the composition of the exhaust gas after oxidation (also see *Figure 2.6*). The measurement of CO_2 concentration was made with a non-dispersive infrared analyzer from Rosemount Analytical Inc. (Model 880). The measurements from the gas analyzers were recorded

continuously through a chart recorder. Before each oxidation test, the analyzers were calibrated with both zero gas and span gas. In this work, the portions of CO and CO_2 in the exhaust gas were found to change with temperature, which will be discussed in detail in Chapter V.

2.7 Characterization of Physical Properties

The weight, pycnometric volume, dimensions, bulk density, open porosity, and cold crushing strength were recorded before and after each heat treatment, including carbonization, pre-oxidation, and oxidation.

2.7.1 Weight, pycnometric volume, and dimension

The weight-loss of each sample was measured on an electronic balance, the change in pycnometric volume was determined using a PMI gas (He) pycnometer, and the measurement of dimensional change was made with a vernier caliper (micrometer).

The pycnometric volume obtained from a gas pycnometer is actually a measurement of solid volume plus the closed pore volume of a sample. If the solid volume is unchanged after heat treatment (either carbonization or oxidation), i.e. no loss of material, opening-up of closed porosity in the sample can lead to a decrease in the value of pycnometric volume, and vice versa, the increase of closed porosity increases its value. If a loss of solid material occurs, open porosity of the sample increases and as

a result, the value of pycnometric volume decreases. Therefore, the change in pycnometric volume value for a sample after a heat treatment is relevant to the change of its porosity.

2.7.2 Bulk density and open porosity

The wax-impregnation method was used to measure bulk density and open porosity to minimize the hydration of MgO-C samples, especially after carbonization. A wax container was electrically heated and temperature-controlled at about 80°C to avoid overheating. The wax was heated only slightly above its melting point not only to permit easy impregnation of wax into the pores of the sample, but to avoid flashing of the wax vapour. Once the wax was completely melted, the sample was entirely immersed in the wax until no visible air bubbles were detected. After saturation, the sample was taken from the container. A blotting operation was performed as quickly as possible in order to remove the superfluous wax coating before it became hard. Each surface of the saturated sample was blotted with absorbent paper by rolling the sample lightly on the paper. Precaution was taken to avoid excessive blotting caused by withdrawing the wax from the pores of the sample.

The sample volumes before and after wax-impregnation were measured using the gas pycnometer. Supposing that the wax impregnates and seals all open pores and the volume of wax directly coated on the sample surface is negligibly small, the difference

between the volume of the wax-impregnated sample and that before wax-impregnation is equivalent to the total volume of open pores of the sample, and, in this way, both open porosity and bulk density of the sample can be measured. Although this method is not totally accurate, it was the solution adopted for the present work.

2.7.3 Relative cold crushing strength

As we know, one of the consequences of carbon oxidation is the loss of strength. The sample after oxidation contains both the decarbonized and undecarbonized zones whose mechanical properties are quite different. Such a nonuniform structure makes the conventional methods unapplicable for strength evaluation. In order to assess the strength change in such a situation, the oxidized samples were crushed in the way as illustrated in *Figure 2.7*. As we can see from *Figure 2.8*, under such a compressive loading, the samples (either before or after oxidation) cracked in the same manner along the longitudinal direction of the cylinders, that made it possible to evaluate the contribution of decarbonization to the loss in strength for the oxidized samples. However, it should be noted that the crushing strength value from this measurement is related to the thickness of the decarbonized layer (representing the extent of oxidation) as well as the sample geometry, so that this measurement can only be used for comparative purposes.

An INSTRON mechanical testing instrument (Model 1125) was used to carry out the crushing strength measurement at room temperature. A slow constant crosshead speed

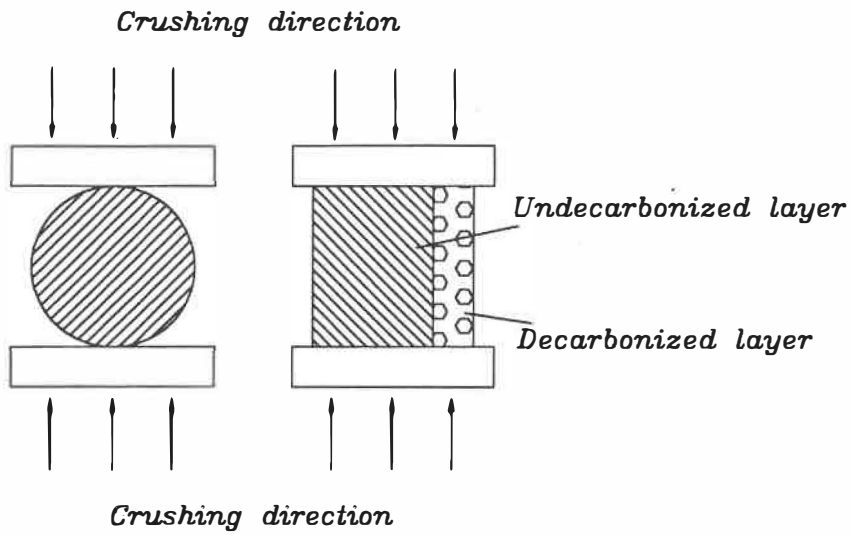

Figure 2.7 Measurement of relative cold crushing strength.

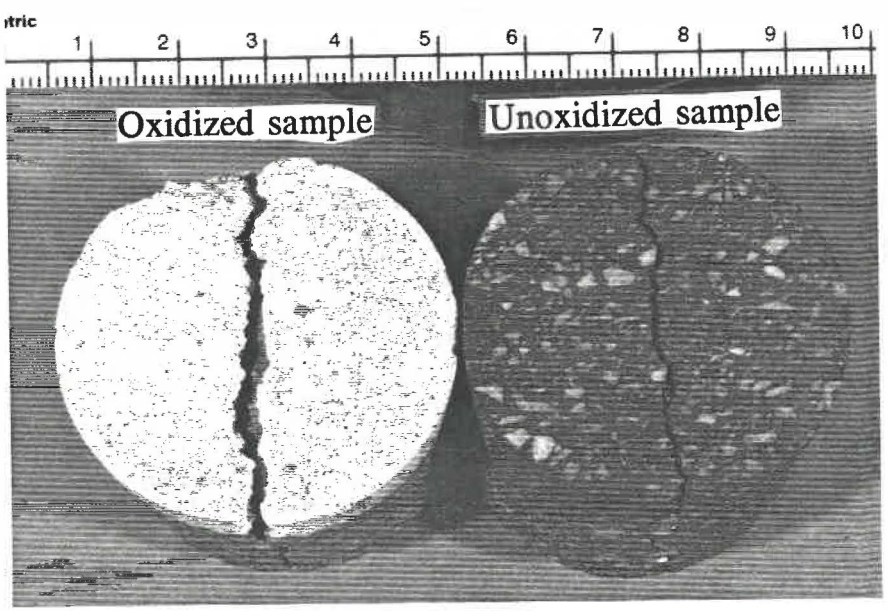

Figure 2.8 A view of both oxidized and unoxidized samples after crushing tests.

of 0.2 mm/min was selected to avoid possible overloading which would cause inaccurately higher values of crushing strength. The maximum load (pressure) before cracking divided by the sectioned area of the sample along the cylinder axis was adopted as the relative cold crushing strength of the sample.

2.8 Microstructural Examination

In order to prepare samples for microstructural examination, the following procedures were adopted to avoid the disintegration of the loose parts of the oxidized sample and to eliminate the risk of removal of fine particles from the polished section. Initially, the entire cylindrical sample was vacuum-impregnated with a special epoxy-resin from Epofix (low viscosity before curing, and low shrinkage and good mechanical properties after curing) before sectioning in half along the cylinder axis, and then re-impregnation of the cut-face was made also under vacuum. After that, the sectioned surface was ground flat and polished.

The measurement of the depth of decarbonized layer in an oxidized sample was carried under a light microscope with a vernier-scaled stage. The depth value for each sample is the average of about 30 measurements. All the micrographs of specific regions of the samples were taken using a LEITZ reflecting light microscope.

2.9 X-Ray Diffraction Analysis

X-ray diffraction analyses, mainly on the samples with antioxidants (in the form of ground powder), were performed using a Philips PW1130 (Cu Kα radiation, Ni filter) x-ray diffractometer. The phase compositions of the samples after each heat treatment, including both carbonization and oxidation, were identified. For the samples after oxidation, the decarbonized and undecarbonized parts of the sample were separated and then ground individually to fine powders in order to analyze the difference in phase composition between these two parts.

2.10 Evaluation of Experimental Measurements and Their Precision

Because of the time limit for the study program, in most of the measurements, only three parallel tests were carried out on three individual samples from different bricks from each batch of the 9 mixes under the same conditions. The values of the measurements were then averaged. From a statistical point of view, such a size of sampling may not be large enough to obtain a stable estimate of the true value. However, the average of the measurements is believed significant enough to follow the trend of change as a function of test conditions, e.g. oxidation temperature or time, and material parameters, e.g. graphite or binder content. The value of measurement itself may not be very meaningful if we just look at the number individually.

Experimental errors can come from several sources, including human operations, materials for testing, and instruments. The dispersion of values from experimental

measurements actually estimates the extent of these errors. The higher the repeatability of the values (as definded in Appendix III), the more precise the experimental measurements. The oxidation tests of this work were carried out on one sample for each firing. As a typical example for the samples with 15 wt% graphite, the experimental results have shown that, in terms of the weight-loss measurement, the repeatability of three parallel tests is 96% at 1000°C, 95% at 1200°C, and 94% at 1400°C.

CHAPTER III

Decarbonization as a Function of Temperature and Atmosphere

In order to find effective ways to prevent decarbonization, it is necessary to understand how decarbonization takes place in the refractories and what are the major factors controlling the overall process. In this chapter, we are going to discuss, based on the experimental results of this work (only limited to the brick samples with 15 wt% graphite, G3; regular MgO grain-size distribution, D1; and 2.5 wt% resin binder, B1) and those from previous studies, the process of decarbonization as a function of both temperature and atmosphere, emphasising the importance of the decarbonizing mechanisms. The main point to be made is to distinguish two different regimes in the decarbonizing process of MgO-C materials: i) the direct oxidation of carbon by gaseous oxygen and ii) the oxidation of carbon by oxides, or the so-called indirect oxidation.

3.1 Thermochemical Considerations of Decarbonizing Process

The major redox reactions taking place in MgO-C materials include carbon burnout by oxygen, MgO decomposition and vaporization, MgO-C interaction, and deposition of Mg vapour, i.e.:

$$2\ C(s) + O_2(g) = 2\ CO(g) \qquad (3.1)$$

$$K_{p1} = P_{CO}^2 / P_{O2}$$

$$C(s) + O_2(g) = CO_2(g) \quad (3.2)$$

$$K_{p2} = P_{CO2} / P_{O2}$$

$$2\ CO(g) + O_2(g) = 2\ CO_2(g) \quad (3.3)$$

$$K_{p3} = P_{CO2}^2 / P_{CO}^2 \cdot P_{O2}$$

$$C(s) + CO_2(g) = 2\ CO(g) \quad (3.4)$$

$$K_{p4} = P_{CO}^2 / P_{CO2}$$

$$MgO(s) + C(s) = Mg(g) + CO(g) \quad (3.5)$$

$$K_{p5} = P_{Mg} \cdot P_{CO}$$

$$2\ Mg(g) + O_2(g) = 2\ MgO(s) \quad (3.6)$$

$$K_{p6} = 1 / P_{Mg}^2 \cdot P_{O2}$$

As can be seen, not only solid-solid, but solid-gas or even gas-gas reactions can all take place during the process of decarbonization. The log K_p values listed in *Table 3.1* for the above reactions are calculated from the thermodynamic database, FACT, with the activities of MgO and C as condensed phases taken as unity in the temperature range 1000-1800°C. The following thermochemical calculations and considerations are based on these values.

Obviously, to be inclusive, one would also have to consider the redox reactions involving the silicates and other oxides that are always present as the material impurities, and nitrogen and other gaseous species from the actual industrial atmosphere. However,

we only focus ourselves on those most important reactions at this point, deliberately not embarking on the others in the way of microstructural characterization at a micron level. In Chapter VI, we then make an effort to explore these redox reactions more inclusively, including the role of nitrogen.

Table 3.1 Thermochemical data of redox reactions in the system MgO-C-O_2-CO-CO_2

Equilibrium constants	1000°C	1100°C	1200°C	1300°C	1400°C	1500°C	1600°C	1700°C	1800°C
log K_{p1}	18.4004	17.7186	17.1256	16.6046	16.1432	15.7312	15.3610	15.0264	14.7220
log K_{p2}	16.2554	15.0725	14.0495	13.1559	12.3688	11.6700	11.0457	10.4844	9.9772
log K_{p3}	14.1104	12.4264	10.9734	9.7072	8.5944	7.6088	6.7304	5.9426	5.2322
log K_{p4}	2.1450	2.6460	3.0761	3.4487	3.7744	4.0612	4.3154	4.5419	4.7449
log K_{p5}	-10.0855	-8.2268	-6.6259	-5.2334	-4.0116	-2.9315	-1.9702	-1.1095	-0.3346
log K_{p6}	38.5714	34.1720	30.3772	27.0714	24.1664	21.5942	19.3014	17.2452	15.3912

The reactions between carbon and oxygen are considered here first. At the beginning, as the temperature increases, the carbon materials in contact directly with the atmosphere will be oxidized first and *Reactions 3.1* to *3.4* can be involved concurrently. On the condition of $P_{CO} + P_{CO_2} + P_{O_2} = 1$ atm, the change of equilibrium partial pressures for these gaseous species with temperature can be calculated thermochemically. The results of the calculation, as shown in *Figure 3.1*, indicate that the CO gas becomes the major gas phase at temperatures above ~700°C, and both CO_2 and O_2 are suppressed to very low levels when the temperature exceeds 1000°C. Therefore, *Reaction 3.1*, i.e. carbon burnout by oxygen, should be the dominant above 1000°C, as long as carbon is

present.

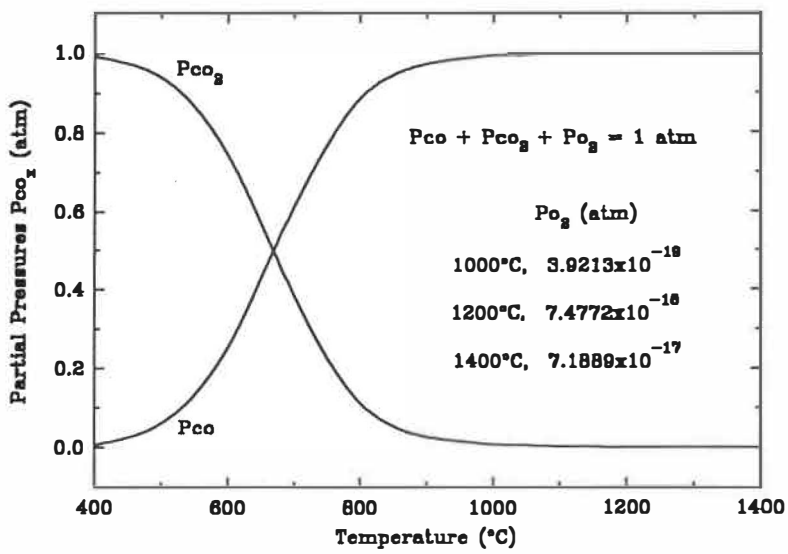

Figure 3.1 Equilibrium partial pressures of gaseous species in the C-O_2-CO-CO_2 system.

As carbon oxidation proceeds, the C(s)-O_2(g) reaction interface will move inwards, which results in the formation of a decarbonized layer at the outer face of the MgO-C brick. Microstructurally, this layer is a carbon-free porous layer of MgO grains since the carbon materials have burnt out and the voids are left at their positions. Because carbon is not present, only *Reaction 3.3* can possibly occur in this layer as long as oxygen is available, leading to a rise of Pco_2 in this region. *Figure 3.2* provides the ratio of Pco_2/Pco as a function of temperature; note that this ratio increases with the rise of Po_2 from 10^{-15} atm to 0.21 atm which represents the Po_2 gradient from the C-O_2 reaction interface to the hot face.

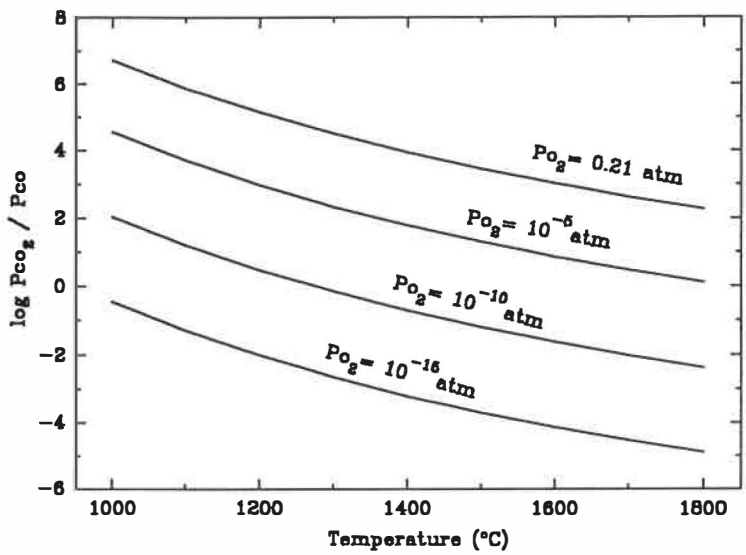

Figure 3.2 Changes of Pco_2/Pco ratio (in logarithm) as a function of both temperature and Po_2.

Besides the reactions between carbon and oxygen, the MgO-C interaction, i.e. *Reaction 3.5*, can also cause a loss of carbon materials. If only *Reaction 3.5* is considered, i.e. $P_{Mg} = P_{CO}$ in the reaction system, the starting temperature of this reaction is in the range of 1400 to 1800°C with the changes of P_{Mg} and P_{CO} from 0.01 atm to 1 atm (see *Figure 3.3*). Accordingly, if the Pco is close to the atmospheric pressure (see *Figure 3.1*), this reaction will become possible only at a relatively high temperature. However, because of both the high Pco and low Po_2 in the reaction system as a result of the reactions between carbon and oxygen, the P_{Mg} due to the MgO-C interaction can still reach as high as almost 1 atm when the temperature rises to about 1800°C, as can be seen in *Figure 3.4*. The calculation is based on the assumption that

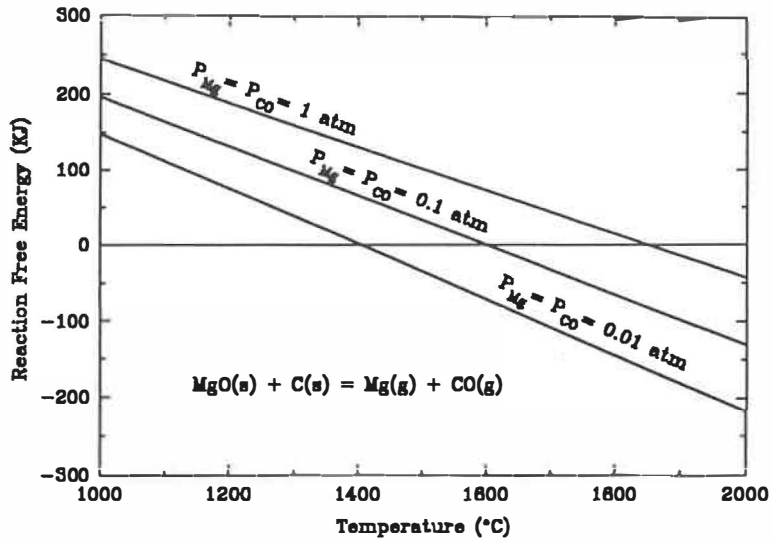

Figure 3.3 Reaction free energy of MgO-C interaction with changes of temperature and atmosphere.

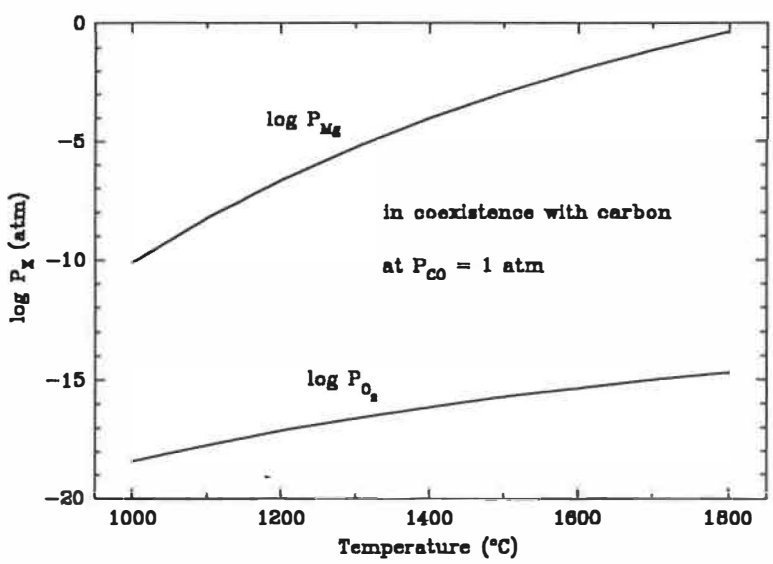

Figure 3.4 Partial pressures of gaseous species for MgO decomposition in the presence of carbon.

both Pco and Po_2 in the reaction system is controlled by the C-O_2 reactions. The results indicate that the MgO-C interaction should not be neglected, especially when the temperature is quite high.

The MgO-C interaction only occurs behind the decarbonized layer, where carbon is still available. The CO and Mg vapours generated at the reaction interface will diffuse outwards as the internal pressure increases, and then encounter the oxygen from the atmosphere, where *Reactions 3.3* and *3.6* can take place concurrently. The deposition of Mg(g) by *Reaction 3.6* may form an impervious MgO dense zone in the decarbonized layer if the Po_2 in the atmosphere is high enough. The minimum Po_2 needed to allow Mg vapour to condense can be read from *Figure 3.4* and is also a function of temperature.

Therefore, the decarbonization of MgO-C materials can result mainly from carbon burnout by oxygen (*Reaction 3.1*) or/and the MgO-C interaction (*Reaction 3.5*). Both reactions are strongly dependent on both temperature and atmosphere in the reaction system. However, not many people have realized the importance of the interrelation between temperature and atmosphere during the process of decarbonization. In most cases, only one of the two aspects was stressed and the other was neglected. As a matter of fact, many reported results, e.g. those from Wolfert et al.[65] and Baker et al.,[8] and from Uchimura et al.[9] and Lin et al.,[3] which seem contradictory, are actually consistent if the effects of both temperature and atmosphere on the decarbonizing mechanisms are

considered at the same time. In the following sections, we are going to compare the results of previous studies with the data from this work and rationalize them based on the understanding of the process of decarbonization.

3.2 Decarbonization at Temperatures up to 1400°C

3.2.1 Experimental results

Figure 3.5 shows the experimental results on carbon oxidation in the temperature range from 1000 to 1400°C, for the carbonized brick samples with 15 wt% graphite (D1-B1). The oxidation conditions have already been described in Chapter II. After the samples were fired in air at a fixed flow rate of 500 ml/min for 5 h, considerable loss in both weight and volume due to carbon burnout was recorded; and the amount of weight or volume loss increased with the temperature. As can be seen from *Figure 3.5*, the incurred weight loss increases from 0.24 g/cm^2 at 1000°C to 0.35 g/cm^2 at 1400°C. Since the amount of oxygen available at the outer face of the sample is kept constant, the difference in oxidation rates of the samples is due to the effect of temperature.

If we keep the flow rate of the reacting gas constant, but change its oxygen concentration, or say, the Po_2 in the atmosphere of the reaction system, we can see, from the results in *Table 3.2*, that considerable change in the rate of carbon oxidation takes place. As the Po_2 in the atmosphere changes from 0.1 atm (considering the total pressure 1 atm) to 1 atm, the extent of carbon burnout can reach about six times higher, which

indicates the very important role of Po_2 on the rate of decarbonization.

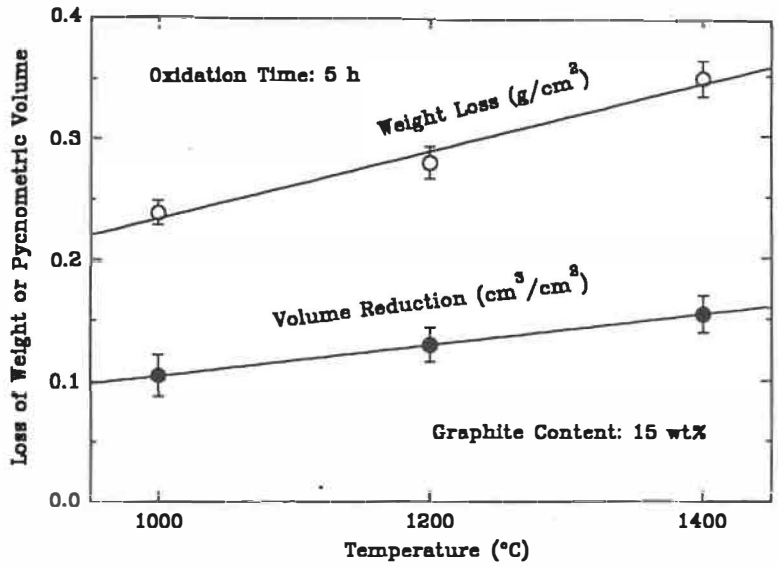

Figure 3.5 Loss of weight or pycnometric volume after (unidirectional) oxidation in air at different temperatures.

Table 3.2 Effect of oxygen concentration on carbon burnout (the brick samples G3-D1-B1 with 15 wt% graphite fired at 1200°C for 10 h)

Gas composition (vol%)	Gas mixture 10% O_2, 90% N_2	Air 21% O_2, 78% N_2	Pure oxygen 100% O_2
Weight loss (g/cm²)	0.22	0.52	1.25
Depth of decarbonized layer (mm)	3.56	8.80	21.28

The comparison of the effect of air and CO on carbon oxidation is shown in *Table 3.3*. Both tests were carried out on carbonized samples with 15 wt% graphite. The results indicate that carbon oxidation in CO at 1200°C is almost trivial, compared to that in air,

and, in terms of weight loss, the former has only less than 2% of the latter. The change in pycnometric volume can also be considered as an indication of the extent of carbon loss if the change in closed porosity is negligible, as we have mentioned in *Section 2.7.1*.

Table 3.3 Property changes of the brick samples (15 wt% graphite, D1, and B1) after firing in air or CO at 1200°C for 5 h.

Firing atmosphere	Weight change ($\Delta W/W_0$ %)	Pycnometric volume change ($\Delta V/V_0$ %)	Crushing strength loss ($\Delta\sigma/\sigma_0$ %)
Air	-2.54	-3.21	-37.89
CO	-0.05	+0.05	-5.11

3.2.2 Discussion of the results and comparison with others

Based on the results of previous studies,[49,66,67] we consider that the overall reaction process of decarbonization (including both carbon burnout by oxygen and MgO-C interaction) is controlled by the chemical reaction rate at lower temperatures or in the initial stage of the process. At higher temperatures or in the later stage, the reaction process is then determined by the diffusion rate of oxygen and gaseous products. In the temperature range $\leq 1400°C$, although we could not say that the MgO-C interaction does not occur, we do believe that, based on above thermochemical considerations in *Section 3.1*, its reaction rate is rather low and its effect on the overall process of decarbonization is relatively trivial so that the mechanism of carbon burnout by oxygen is considered dominant.

Once the decarbonizing process becomes diffusion-controlled, the increase in both diffusivity of gas species and reactivity of materials, as temperature increases, can greatly accelerate the carbon oxidation process. This condition is actually what happened in our case (see *Figure 3.5*). In addition, since Po_2 at the outer face determines the driving force for oxygen diffusion through the decarbonized layer, the increase of Po_2 in the atmosphere can also speed up decarbonization greatly if the process is in the diffusion-controlling step. The results in *Table 3.2* have confirmed the above interpretation.

As can be expected from *Reaction 3.1*, the high Po_2 in air (0.21 atm) leads to a significant carbon loss in the samples, which has resulted in large changes in weight, volume, and strength (see *Table 3.3*). The small amounts of weight and strength losses during CO atmosphere firing are believed due mainly to the further pyrolysis of resin binder at a higher temperature (200°C higher than the temperature of carbonization, 1000°C). As a result, the volume change of the samples is very small, and its positive value may be caused by the irreversible expansion (i.e. an increase in closed porosity) which will be discussed in more detail in the next chapter. CO gas has two effects on suppressing carbon oxidation; i.e. i) forcing *Reaction 3.1* leftwards and reducing the loss of carbon; ii) decreasing the Po_2 in the reaction system through *Reaction 3.3* and reducing the chance of carbon oxidation. In fact, our results further confirm that carbon burnout proceeds mainly through *Reaction 3.1* because an increase in Pco can greatly reduce the extent of carbon burnout.

In fact, the results of Tabata et al.[49] (see *Figure 3.6* and *Table 3.4*) have shown that in an atmosphere with low Po_2 (vacuum at P_{total} = 0.001 atm) MgO-C brick samples did not have a significant weight loss until the temperature reached 1400°C, and the change in material composition and MgO grain size distribution between Specimens A and B did not make a big difference in weight loss up to 1400°C. In these two types of brick samples, the same fused magnesia grains (99.5% MgO) and graphite flakes (99% C) were used. The results tell us two things: i) carbon burnout is negligible at a low Po_2; ii) MgO-C interaction is insignificant at temperatures up to 1400°C.

Table 3.4 Properties of brick specimens A and B (from Tabata et al.[49])

Type of brick specimens	Combination (wt%)		MgO grain size (mm)	Average periclase size (mm)
	MgO	C		
Specimen A	90.5	9.5	< 1	0.59
Specimen B	74	26	< 0.3	0.16

On the other hand, Zoglmeyr[38] has also found that in an oxidizing atmosphere with 14% O_2, 81% N_2, 4.8% CO_2, and 0% CO the weight loss of MgO-C brick samples increased with temperature up to 1400°C (see *Figure 3.7*), and the change in carbon content from 9% to 14% (residual carbon) did not alter this trend of weight loss with temperature, but only the extent of carbon burnout. In both Bricks A and B, the same type of magnesia grains with 99% MgO was used. His oxidation tests were also made on carbonized samples (coked at 1000°C), but not in the condition of unidirectional

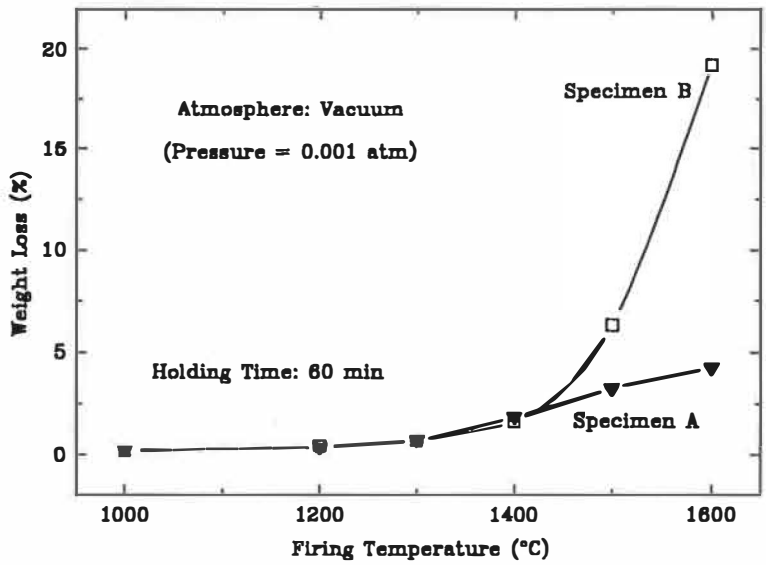

Figure 3.6 Weight loss as a function of temperature for two types of carbonized (1000°C for 1 h) brick samples after firing in vacuum for 60 min (from Tabata et al.[49]).

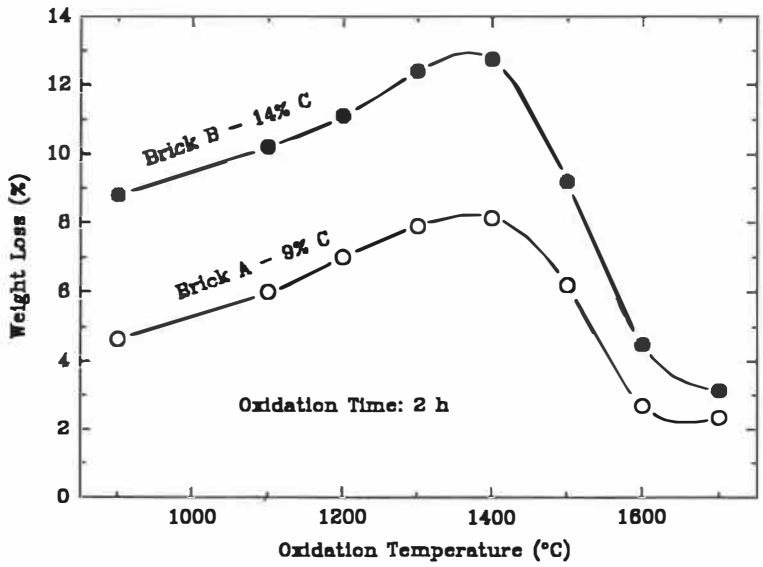

Figure 3.7 Weight loss as a function of temperature for carbonized (at 1000°C) brick samples after firing in an oxidizing atmosphere with 14% O_2 (from Zoglmeyr[38]).

oxidation, so that the oxidation results were related to the sample geometry.

The results presented in this section corroborate the above findings of the other researchers. In summary, in order to limit carbon burnout in MgO-C bricks in the temperature range $\leq 1400^{\circ}C$, suppressing Po_2 to a very low level and maintaining Pco at a high level are most effective in terms of controlling the atmosphere of the reaction system. Another effective way to hinder carbon burnout in an oxidizing atmosphere is to shorten the time of exposure to high temperatures, and a fast heating process is highly recommended. On the other hand, at a low level of Po_2, decarbonization is rather limited due to the slow reaction rate of MgO-C interaction in this temperature range.

3.3 Decarbonization at Temperatures above 1400°C

3.3.1 Experimental results

Table 3.5 lists the results of oxidation tests in air at three different temperatures, and the physical appearances of the oxidized samples (sectioned surface) are shown in *Figure 3.8*. As the temperature increases from 1400°C to 1600°C, the changes of both the weight loss and the depth of decarbonized layer do not follow the trend at lower temperatures (from 1200°C to 1400°C). By comparing the microstructural features after oxidation (*Figures 3.9* and *3.10*), significant carbon loss took place at 1400°C and the decarbonized layer became rather porous; at 1600°C, a dense MgO zone was formed at the outer face, and beneath that, the unoxidized graphite flakes were detected.

Table 3.5 Effect of temperature on decarbonization (the samples with 15 wt% graphite fired in air at given temperatures for 5 h)

Firing temperature (°C)	1200	1400	1600
Weight loss (g/cm^2)	0.29	0.35	0.32
Depth of decarbonized layer (mm)	4.3	5.8	1.6

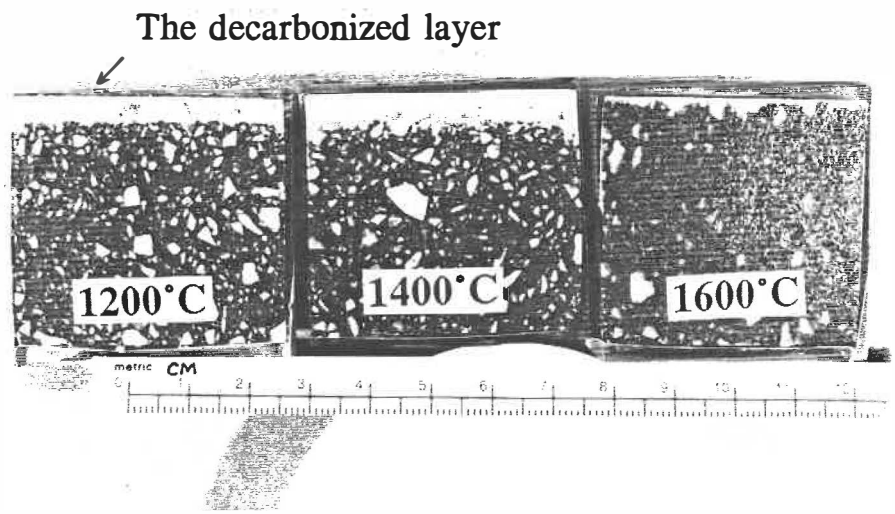

Figure 3.8 Comparison of physical appearances (sectioned surface) of oxidized samples (with 15 wt% graphite) at three different temperatures, showing the difference in the depth of decarbonized layer.

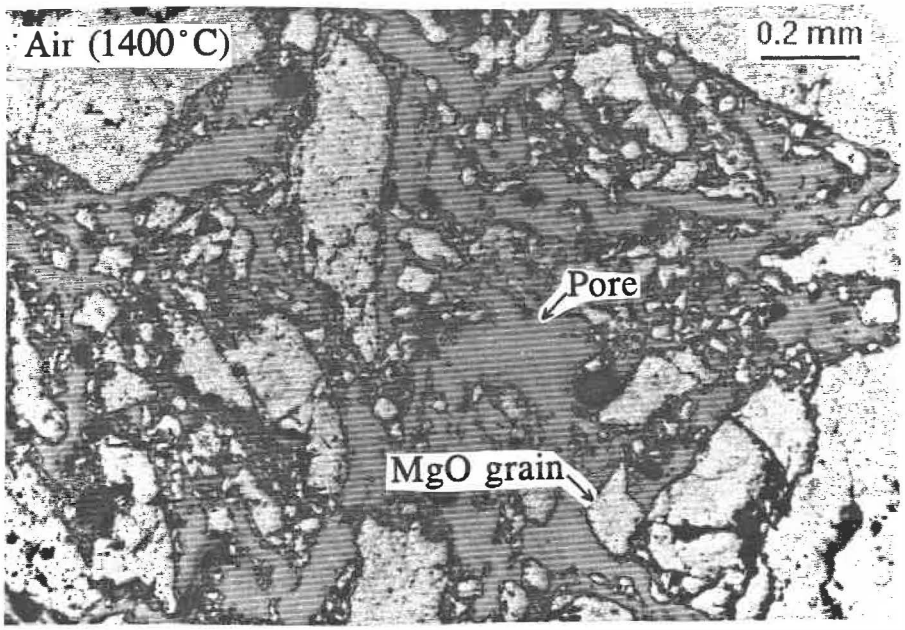

Figure 3.9 Micrograph of oxidized sample with 15 wt% graphite after oxidation for 5 h, showing neither graphite phase nor MgO dense zone in the decarbonized layer.

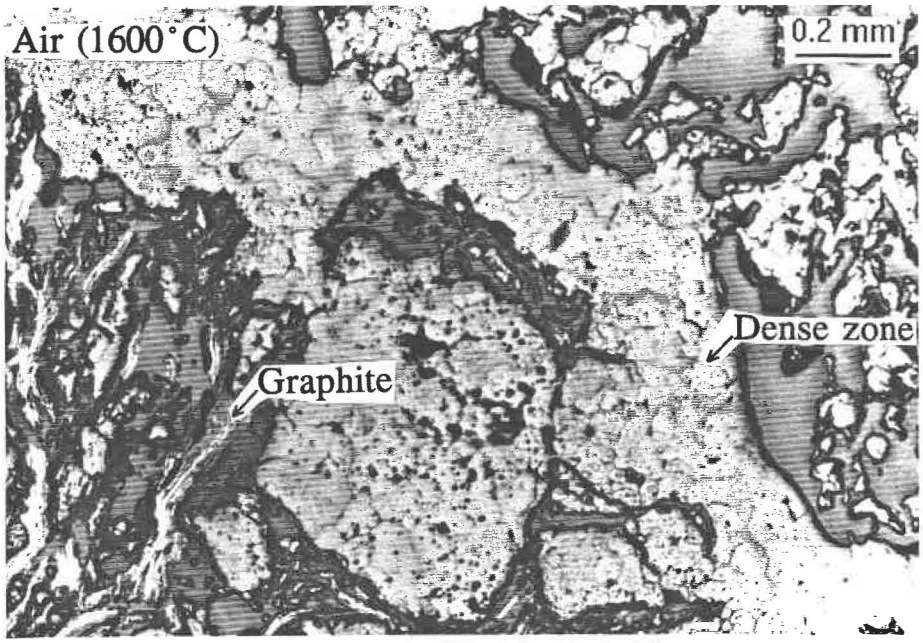

Figure 3.10 Micrograph of oxidized sample with 15 wt% graphite after oxidation for 5 h, showing a dense MgO zone and, under this zone the graphite phase is protected from oxidation.

If the atmosphere was changed from air to CO (i.e. a very low Po_2) at 1600°C, the weight loss was greatly reduced by nearly one half (see *Table 3.6*). However, the evidence of Mg vapour deposition outside the sample was observed. As shown in *Figure 3.11*, a significant amount of MgO whiskers formed on the tube of thermocouple which was pointing at the hot face of the sample. By examining the microstructure of the samples fired in CO (*Figure 3.12*), no dense zone is formed, and also no significant graphite oxidation is observed at the outer face. However, the structure of material near the outer face appears to be looser in comparison to that in the interior (*Figure 3.13*), and the formation of gaps between MgO grains and graphite flakes is observed at the outer face. These changes in microstructure are the evidence of decarbonization.

In order to study the effect of Po_2 gradient on the deposition of Mg vapour, we pre-oxidized a sample (G3-D1-B1) in air at 1000°C for 5 h to produce a decarbonized layer, and then fired it in CO at 1600°C. Its purpose was to remove the carbon phase on the outer face and to create a gradient of Po_2 from inside (lower Po_2 where carbon is present) to the outer face (higher Po_2. where carbon is not present). The result is also listed in *Table 3.6*. Although the formation of the MgO dense zone was still unable to occur in the decarbonized layer (see *Figure 3.14*), the deposition of Mg vapour now occurred directly on the outer face of the sample (see *Figure 3.15*), unlike the case of CO heat treatment alone. This result indicates that the position for Mg vapour deposition can be controlled by changing the gradient of Po_2 (i.e. carbon phase is present or not present).

Table 3.6 Effect of atmosphere on decarbonization (the brick samples D1-B1 with 15 wt% graphite fired at given temperatures for 5 h)

Atmosphere	Air	CO	Air - CO
Temperature	1600°C	1600°C	1000°C - 1600°C
Weight loss	0.32 g/cm^2	0.15 g/cm^2	0.24 - 0.14 g/cm^2
Deposition of Mg vapor	Inside the decarbonized layer	Outside the hot surface	On the hot surface

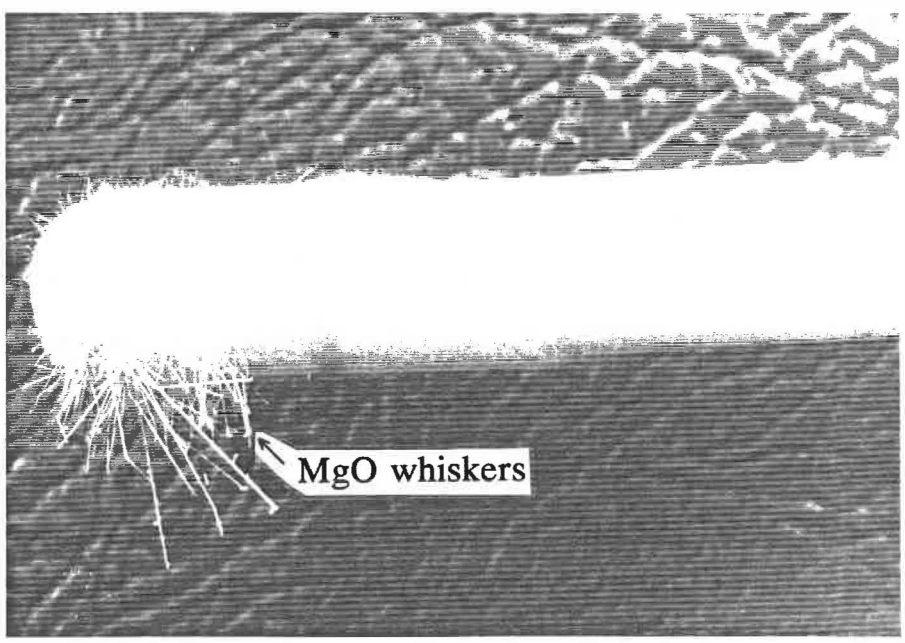

Figure 3.11 Observation of MgO whiskers formed on the thermocouple tube after firing MgO-C brick sample with 15 wt% graphite in CO at 1600°C for 5 h as a result of Mg vapour deposition.

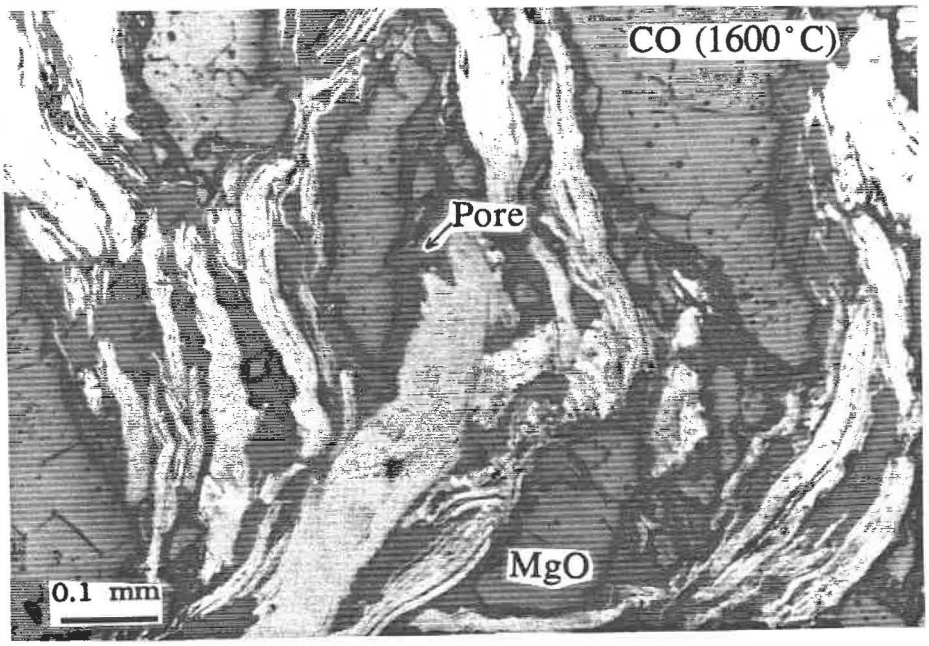

Figure 3.12 Micrograph of brick sample with 15 wt% graphite after firing in CO for 5 h, showing the gaps between MgO grains and graphite flakes at hot face.

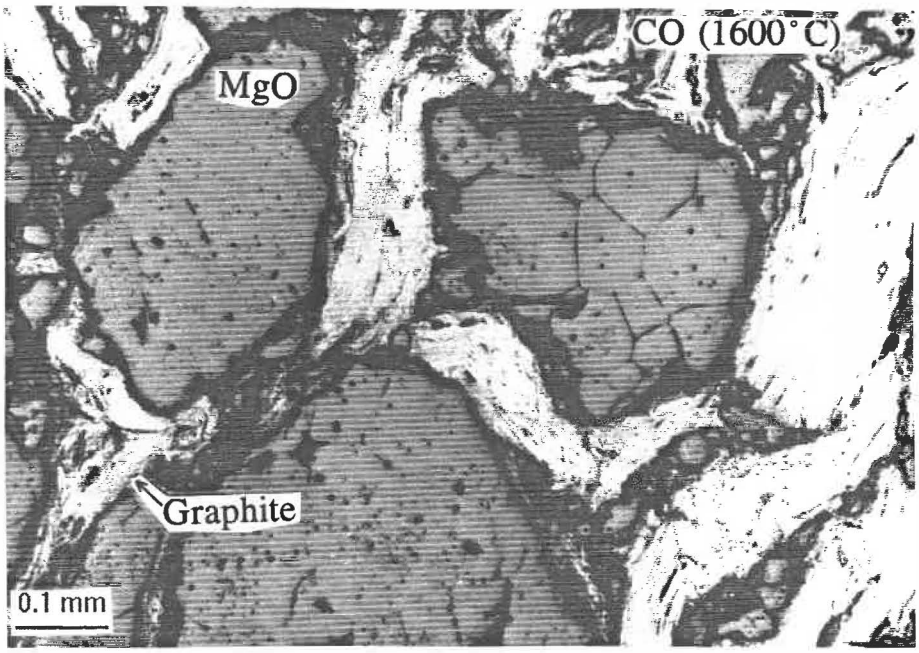

Figure 3.13 Micrograph of brick sample with 15 wt% graphite after firing in CO at 1600°C for 5 h, showing the diffference in microstructure in the interior of the sample compared to that at hot face.

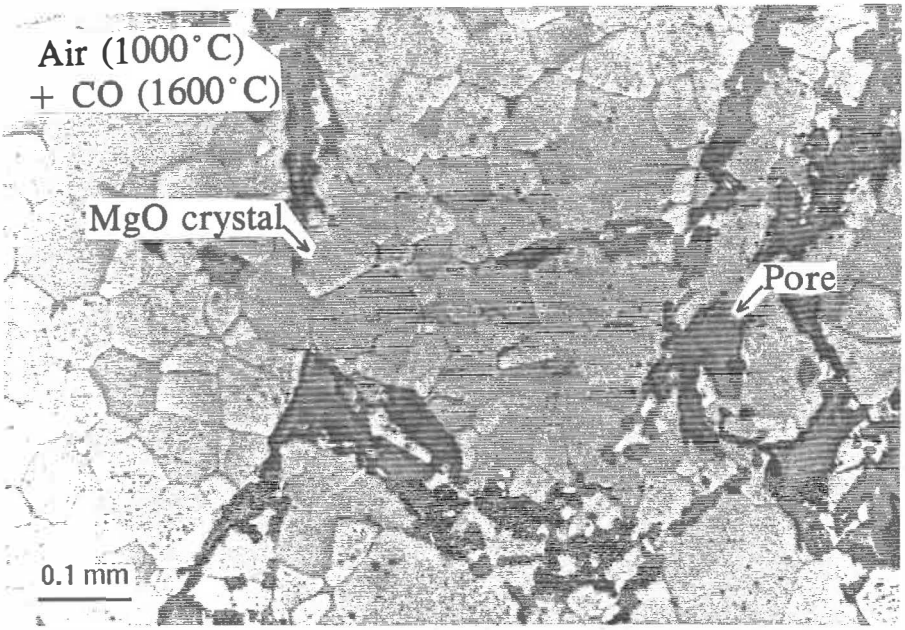

Figure 3.14 Micrograph of brick sample with 15 wt% graphite after oxidation in air for 5 h and then firing in CO for 5 h, showing the microstructure of decarbonized layer.

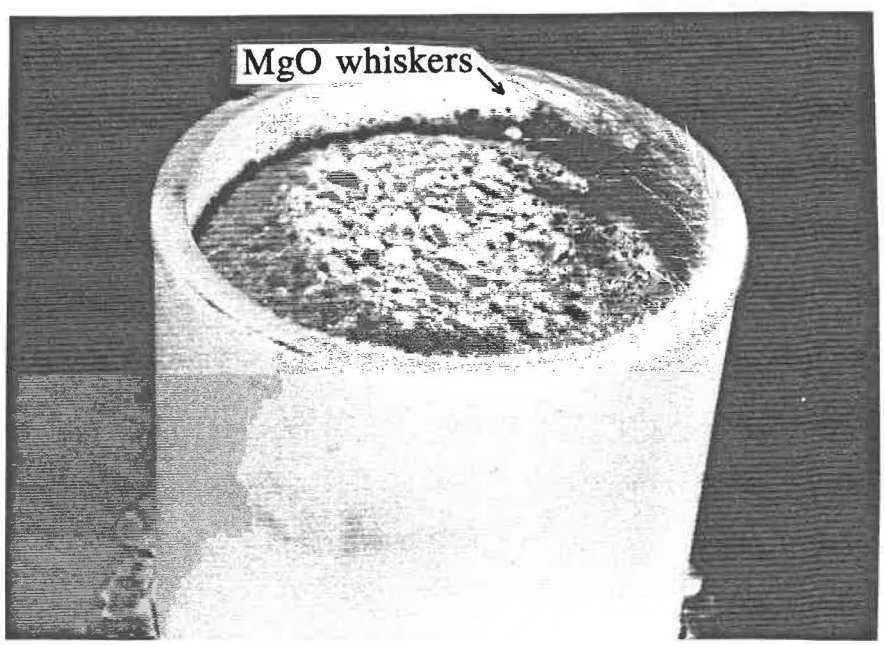

Figure 3.15 Observation of MgO whiskers formed on the hot face of brick sample with 15 wt% graphite (pre-oxidized in air at 1000°C for 5 h) after firing in CO at 1600°C for 5 h as a result of Mg vapour deposition.

3.3.2 Discussion of the results and comparison with others

The results in *Table 3.5* and *Figures 3.8*, *3.9*, and *3.10* clearly indicate the change of decarbonizing mechanisms with temperature at a high Po_2 (0.21 atm). As we know, both carbon burnout by oxygen and MgO-C interaction can contribute to the overall rate of decarbonization at 1600°C. However, both the weight loss and the depth of decarbonized layer are still lower than those at 1400°C (see *Table 3.5*). This apparent discrepancy means that decarbonization, including both carbon burnout and MgO-C interaction, is greatly hindered after the dense MgO zone forms at the outer face due mainly to the build-up of diffusion resistance. Therefore, since there is no possibility of self-protection by forming a MgO dense zone at low temperatures, decarbonization can be more serious at low rather than high temperatures if in an oxidizing atmosphere. In fact, the results of Zoglmeyr[38] and Griffin et al.[61] are in agreement with the above analysis. In *Figure 3.7* from Zoglmeyr[38], the weight loss begins to drop when the temperature is over 1400°C, very similar to our results in *Table 3.5*. Griffin et al.[61] have also found that after oxidation for 100 h, MgO-C bricks (with 6% residual carbon) fired at 1482°C had only 19.1 mm depth of decarbonized layer, compared to 57.2 mm when fired at 1204°C, almost three times lower at the higher temperature.

As we know, at high temperatures (> 1400°C), both decarbonizing mechanisms, i.e. carbon burnout by oxygen and MgO-C interaction, will occur at the beginning of the reaction process if the atmosphere is oxidizing. However, once the MgO dense zone is

formed in the decarbonized layer as a result of Mg vapour deposition, further oxygen penetration inwards is blocked and thus, carbon burnout by oxygen is greatly suppressed and MgO-C interaction will become prevailing. If the atmosphere is reducing or neutral, direct carbon burnout is then relatively insignificant due to the low level of Po_2. Therefore, MgO-C interaction is most important in this temperature range.

We propose that the process of MgO-C interaction may proceed in the following steps. When the temperature is high enough, mostly above 1400°C (according to the above thermochemical calculations), the thermal decomposition of MgO becomes significant when carbon is present. The oxygen produced by the decomposition will first react with the carbon material which is directly in contact with MgO grains. As a result, a gap between MgO grain and graphite flake forms with the proceeding of the reaction. When the carbon material loses contact with MgO grain as carbon is consumed, the gap distance between them still keeps increasing with the reaction time as shown in *Figure 3.16* from the work of Tabata et al.[49] Their measurements of gap distance were taken in the region 1 mm behind the hot face of MgO-C brick samples after firing in vacuum at 1600°C. The compositions of Specimens A and B are given in *Table 3.4*. We have also had a similar observation. In *Figure 3.12*, the gap distance can reach as high as about 25 μm after firing in CO at 1600°C for 5 h. These results indicate that the transfer and diffusion of gas species, Mg and O_2, begin to play a role on decarbonization with the proceeding of the reaction as claimed by Komarek et al.[50] From *Figure 3.17*, we can see

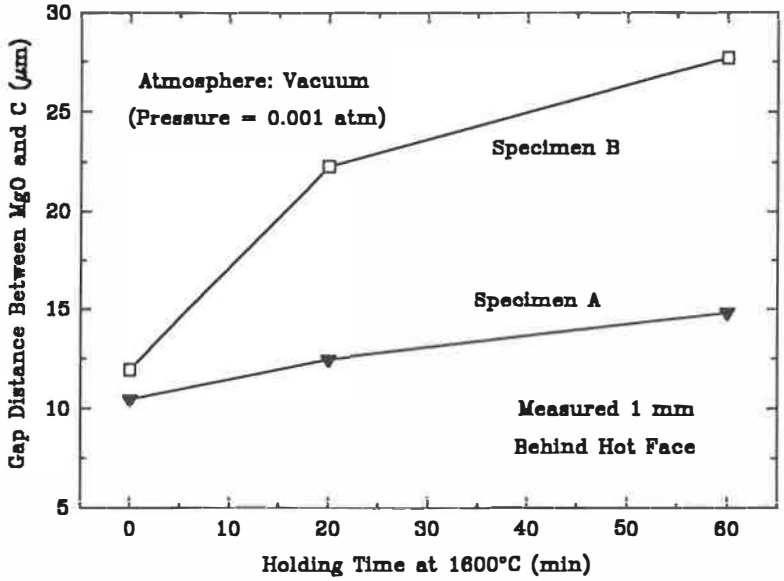

Figure 3.16 Gap distance between MgO grains and carbon phase as a function of holding time at 1600°C in vacuum (from Tabata et al.[49]).

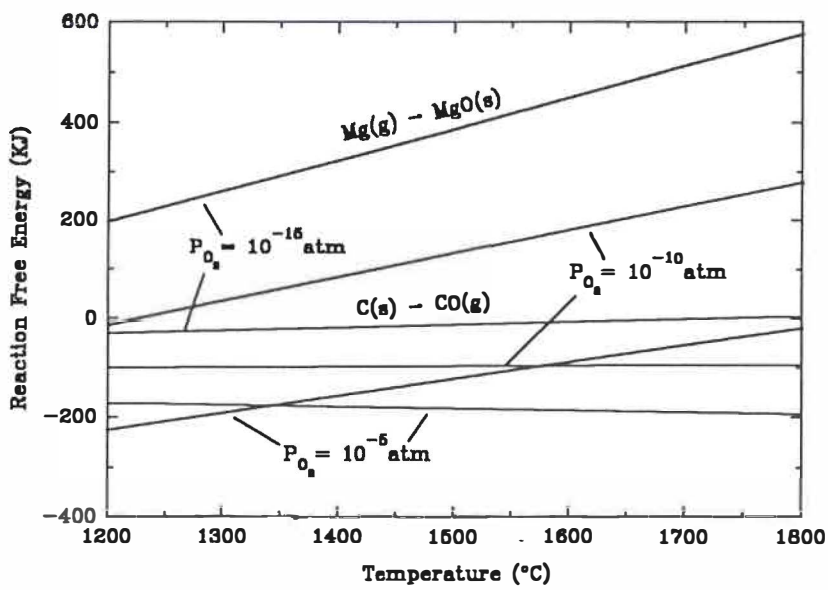

Figure 3.17 Reaction free energies for carbon oxidation and Mg vapour deposition as a function of Po_2 in the reaction system.

that, based on reaction free energy, Mg vapour is more stable than carbon at the same Po_2 and temperature. Therefore, at least from the thermochemical point of view, the oxygen released from MgO decomposition should react preferentially with carbon. As the oxygen produced by MgO decomposition is absorbed quickly by carbon, the Mg vapour is then left and diffuses outwards due to the positive pressure developed around the reaction interface. If the Mg vapour encounters the high oxygen pressure from the environment, the vapour deposition to secondary MgO occurs wherever the Po_2 meets the condition of *Reaction 3.6*. To summarize these points, MgO decomposition becomes inevitable when the temperature is high enough. The presence of carbon reduces the starting-temperature of the MgO decomposition and accelerates the decomposition rate by consuming the oxygen released from the decomposition and suppressing the Po_2 in the reaction system to a very low level. As a result, the decomposition proceeds continuously as long as carbon is not exhausted. Thus, the lower the Po_2 in the reaction system, the faster the rates of MgO decomposition and MgO-C interaction.

The results of Ishibashi et al.,[7] Ishii et al.[68] and Moore et al.,[69] which have shown that MgO-C interaction is strongly dependent on the Po_2 (although they did not well explain why), actually confirm the above analysis on the interaction mechanism. If simply based on *Reaction 3.5* itself, the increase in Pco should hinder the reaction from going further because CO is one of the reaction products as claimed by Moore et al.[69] On the contrary, the fact is that[69] a slightly higher Po_2 in the atmosphere, which could

only convert more CO to CO_2 through *Reaction 3.3* and reduce the Pco (see *Figure 3.2*), inhibits the loss of materials due to the MgO-C interaction and retards the process of decarbonization. Ishibashi et al.[7] have also observed that, when fired in CO atmosphere, the weight loss of MgO-C samples increases with temperature at a higher rate in comparison with that in Ar atmosphere (see *Figure 3.18*). This finding indicates that the decarbonization process is accelerated more rapidly with rising temperature in CO atmosphere. As we know, the reaction between carbon and oxygen will be suppressed to a very low rate in CO atmosphere because of the very low Po_2. In this case, only the decomposition of MgO could cause an appreciable weight loss. On the other hand, in an inert atmosphere where there is no restraint on the Po_2 through *Reactions 3.1* and *3.3*, both the C-O_2 reaction and MgO decomposition will release gas species and give rise to a significant weight loss collectively. Therefore, in a given time, the total weight loss in a CO atmosphere is lower than that in an Ar atmosphere. However, as the temperature rises, the situation changes. From the thermodynamic data, the reaction of C-O_2 is exothermic, but MgO decomposition is endothermic. In other words, as the temperature is increased, the driving force ($-\Delta G$) for the reaction of C-O_2 is reduced, but, in contrast, ($-\Delta G$) for MgO decomposition will be raised. In summing up these two effects, in an inert atmosphere, the overall reaction process is retarded by the reaction of C-O_2 and shows a lower increasing rate in weight loss in comparison with that in a CO atmosphere where the overall reaction rate is determined only by MgO decomposition. Consequently, as we can see from *Figure 3.18*, when the temperature reaches 1700°C, the absolute

value of weight loss in a CO atmosphere exceeds that in an Ar atmosphere. Similar results have also been obtained by Ishii et al.[68] who considered that the Po_2 in a CO atmosphere is much lower than that in an Ar atmosphere. Actually, the lower Po_2 in a CO atmosphere promotes MgO decomposition significantly when the latter becomes the rate-determining step for decarbonization at high temperatures $>1400^\circ C$.

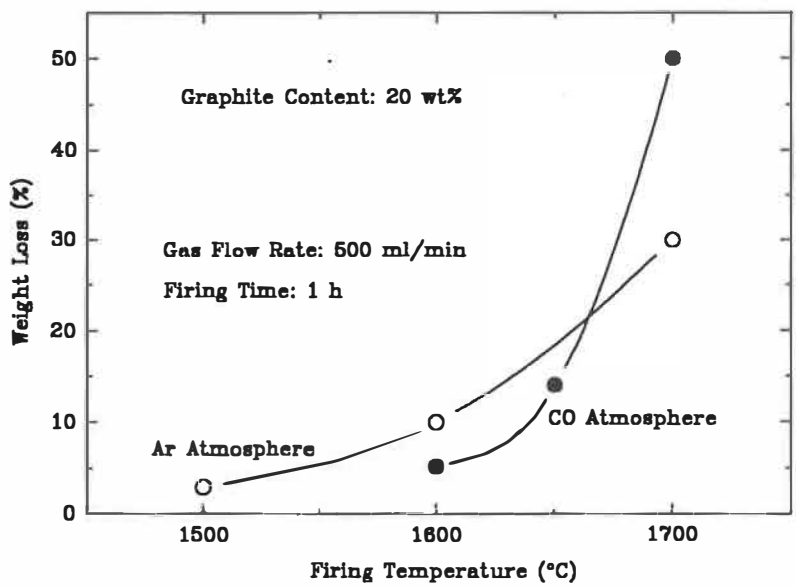

Figure 3.18 Weight loss of MgO-C samples (carbonized at 1200°C for 5 h) as a function of temperature in two different firing atmospheres (from Ishibashi et al.[7]).

From the results revealed *Table 3.6* and *Figures 3.11*, *3.12*, and *3.13*, we consider that the MgO-C interaction occurs, especially in the region where the gaseous products of Mg and CO could easily diffuse outwards (see *Figure 3.12*). In the interior

of the sample (see *Figure 3.13*), because of the difficulty in diffusion of gaseous species of reaction products, the MgO-C interaction proceeds relatively slowly. Similarly, Tabata et al.[49] have also observed that the reaction layer where gaps between MgO grains and graphite flakes form is only near the surface of brick samples, and the gap size decreases proportionately along the layer depth. As we know, the reduction of oxygen concentration through reaction with CO from the atmosphere can enhance thermal decomposition of MgO to Mg vapour and oxygen. The oxygen produced by MgO decomposition would be consumed quickly through reaction with carbon or converted to CO_2 by CO from the atmosphere wherever gas diffusion is possible. Therefore, the Po_2 in the reaction system is kept at a very low level as long as carbon is present, and the MgO-C interaction will proceed continuously. As a result, the loss of material can not be prevented. Thus, although CO atmosphere can protect carbon from oxidation by oxygen, CO cannot limit MgO decomposition and further decarbonization at high temperatures. During long-time firing at very high temperature (e.g. $\geq 1600^\circ C$) and in a very low Po_2 (e.g. CO atmosphere, $Po_2 < 10^{-15}$ atm), structure damage through MgO-C interaction will occur. The results of ours and others, as discussed above, indicate the non-protectiveness of a CO atmosphere to MgO-C bricks when MgO-C interaction becomes dominant in the process of decarbonization, or, in other words, a very low Po_2 in the reaction system can enhance decarbonization through MgO-C interaction.

When the temperature is sufficiently high, the gas phase in the interior of the

MgO-C material shifts to a CO atmosphere which is controlled by the reactions of C-O_2. Under these conditions, Mg vapour is more stable than carbon at the same Po_2 (see *Figure 3.17*). Therefore, Mg vapour deposition cannot occur as long as carbon is present, or, in other words, the MgO dense zone can only form in a decarbonized layer. *Figure 3.19* illustrates the relation between the Po_2 gradient and the position of Mg vapour deposition in our two cases of CO atmosphere firing (*Table 3.6*). As the position at which the equilibrium Po_2 for carbon oxidation (Ec) is reached moves inwards into the sample, the position at which the equilibrium Po_2 for deposition of Mg vapour (Ed) is reached also moves close to the sample. Since the formation of Mg vapour is inevitable in this temperature range (i.e. 1600°C in our cases), Mg vapour deposition occurring inside as close as possible to the hot surface is better than outside for the purpose of better protection of materials and prevention of further decarbonization. In order to allow Mg vapour to deposit inside the brick body, a decarbonized layer at the outer surface is indispensable for establishing a sufficiently high gradient of Po_2.

Examining closely the microstructure and position of the dense MgO zone formed in the decarbonized layer (see *Figure 3.20*) of our samples fired at 1600°C in air, we have observed that the periclase crystallites on the outer face of the dense zone have larger crystalline size and fewer trapped pores than those on the other side, and the dense zone is formed near, but not directly on the outer surface of the sample. Such a structure indicates that the process of dense zone development involves (1) the formation of Mg

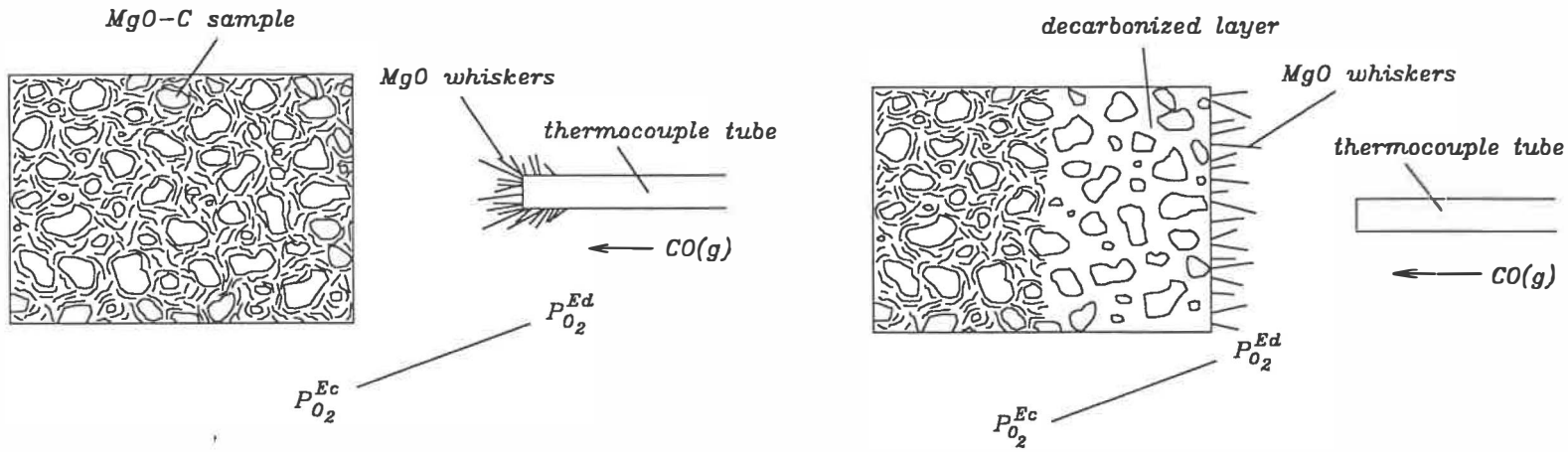

Carbon Oxidation

$$P_{O_2}^{E_c}: \quad 2\ C(s) + O_2(g) = 2\ CO(g)$$

Deposition of Mg Vapor

$$P_{O_2}^{E_d}: \quad 2\ Mg(g) + O_2(g) = 2\ MgO(s)$$

$$P_{O_2}^{E_c} < P_{O_2}^{E_d}$$

at 1600°C

Figure 3.19 Schematic illustration of the relation between the Po_2 gradient and the position of Mg vapour deposition.

vapour in the interior where MgO and C interact with each other and (2) migration of the Mg vapour to a zone in the decarbonized layer where the Mg vapour oxidizes in contact with oxygen from outside and deposits as so-called secondary periclase. The growth of this dense zone is toward the carbon side by diffusion of oxygen through the zone from outside and oxidation of Mg vapour at the interior side.

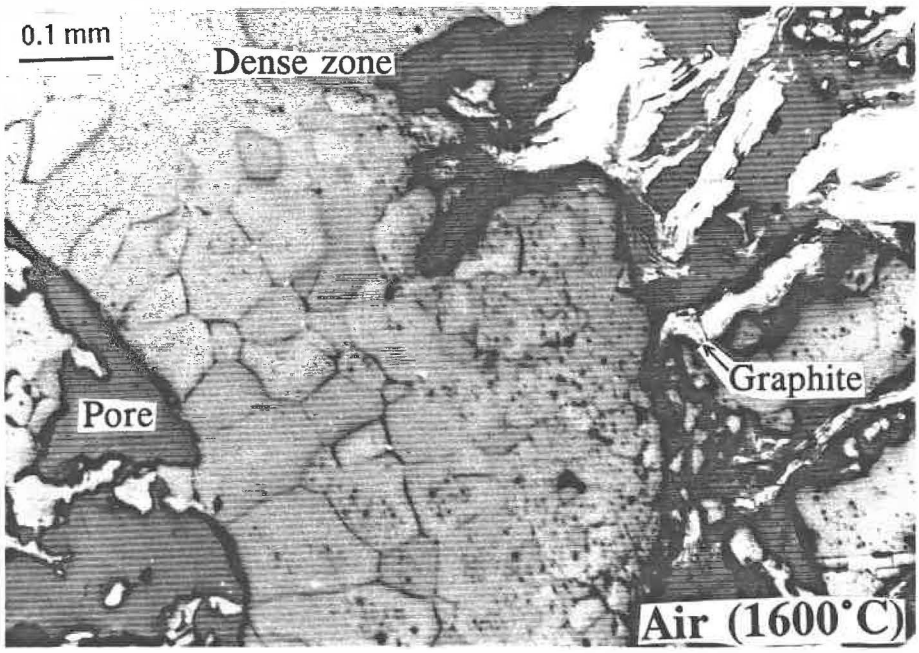

Figure 3.20 Micrograph of MgO dense zone in the brick sample with 15 wt% graphite after oxidation in air at 1600°C for 5 h.

To summarize the above discussion, although a high Po_2 is favourable for carbon burnout at low temperatures ($\leq$1400°C), the high Po_2 also has a restraining role on MgO

decomposition and a promoting role on the dense MgO zone formation when the temperature is high enough (>1400°C). Therefore, in order to limit decarbonization, careful control of Po_2 in the reaction system as the temperature rises can not only inhibit carbon burnout, but suppress MgO-C interaction. Building up the resistance to gaseous diffusion through MgO dense zone formation is very effective in hindering inward diffusion of oxygen from the atmosphere as well as outward diffusion of Mg(g) and CO(g) as the products of MgO-C interaction, and thus, retarding further decarbonization.

At temperatures above 1400°C, the extent of MgO-C interaction depends not only on the Po_2 in the atmosphere, but also on the surface areas of both MgO and C phases. As can be seen in *Figure 3.6*, increasing graphite content and reducing MgO grain size from Specimen A to Specimen B leads to a higher rise in weight loss with temperature at a low Po_2; but, in *Figure 3.7*, increasing graphite content from Brick A to Brick B results in a larger drop in weight loss with temperature at a high Po_2. We consider this trend is due to the interaction between Po_2 and material reactivity in the reaction system.

3.4 Importance of Material Reactivity during Decarbonization

In the low temperature range where the intrinsic chemical reaction of C-O_2 is rate-controlling, material reactivity is important. However, due to the low reaction rate in this stage, its significance is concealed. Once the temperature is over about 1000°C, chemical reactivity of materials becomes less important because the overall decarbonizing process

is controlled by the slowest step, i.e. the inward diffusion of oxygen through the decarbonized layer. However, as MgO-C interaction comes to control the overall process when the temperature is over 1400°C, the material reactivity will become important on decarbonization because, as discussed above, the process of MgO-C interaction is largely dependent on the rate of MgO thermal decomposition which is believed to control the main source of oxygen for decarbonization in this temperature range. Therefore, both the physical and chemical nature of MgO grains will have an evident effect on this rate. As an example, Ishii et al.[68] have found that the inclusions in MgO crystals can cause lattice deformation and promote local decomposition of MgO by forming etch pits.

If there is no chance of forming a MgO dense zone in the decarbonized layer due to the low Po_2 in the reaction system, the outward diffusion of Mg(g) and CO(g) will become less difficult. In this case, the higher chemical reactivity of materials can surely cause a higher rate of decarbonization. Wolfert et al.[65] have found that the impurities in MgO grains reduce the high temperature stability of MgO with graphite, and, between physical (bulk density and crystal size) and chemical properties (impurity), the impurity is more important in their reaction system (vacuum-tight static atmosphere). In *Figure 3.21* and *Table 3.7*, the higher the impurity in MgO grain (Grade C), the greater the weight loss during firing. Uchimura et al.[9] have also reported that the weight loss of MgO-graphite (4:1 in weight) samples increases with the impurity (SiO_2 + Fe_2O_3) level of MgO grain when fired in CO at 1660°C (see *Figure 3.22*). One mechanism[65] could

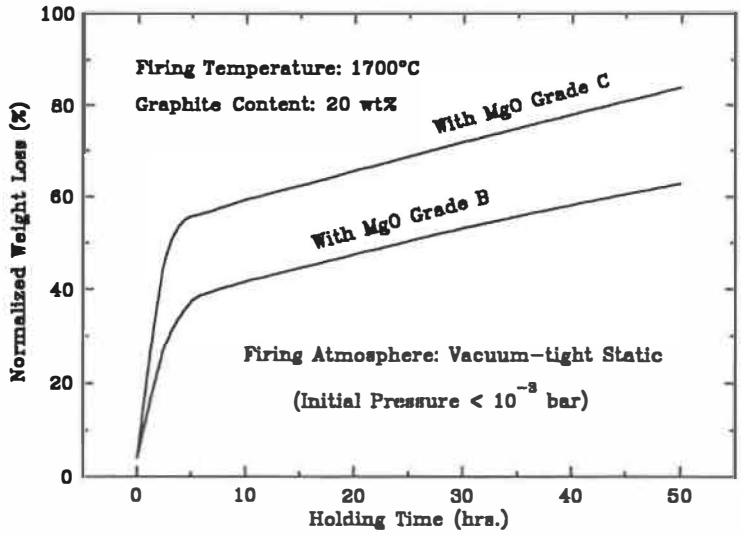

Figure 3.21 Thermogravimetric curves for MgO-C brick samples with 20 wt% graphite (from Wolfert et al.[65]).

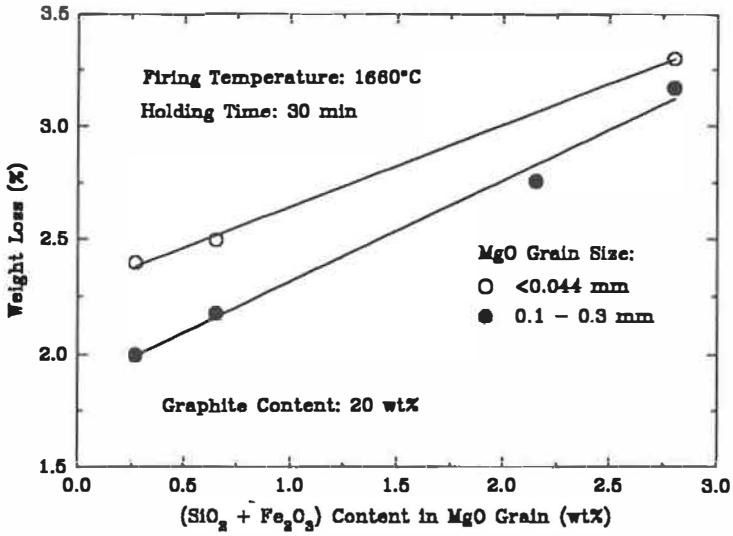

Figure 3.22 Relation between weight loss (in TGA) during firing in CO atmosphere and (SiO_2 + Fe_2O_3) content in MgO grain (from Uchimura et al.[9]).

be that MgO dissolved in the impurity phase is more reactive than the MgO which is not dissolved so that the impurity phase enhances the carbothermic reduction of MgO. Another mechanism claimed by Ishii et al.,[70] Ishibashi et al.,[7] and Uchimura et al.[9] is that the migration of impurities from the periclase crystal boundary to the MgO grain surface at high temperatures could activate the surface and promote MgO-C interaction. As a result, with the smaller-sized grain (<0.044 mm), a higher weight loss in CO atmosphere has been observed,[9] as also shown in *Figure 3.22*, because of the easier migration of impurities in the smaller grain. In addition, Moore et al.[69] have also found from the TGA measurements that the threshold temperature of MgO-C interaction (in Ar), i.e. the temperature at which a significant weight loss starts, is nearly 100°C lower because of the fine particle size of starting materials. Note that the larger surface area for reaction with smaller grain size is another important factor contributing to such a higher weight loss or a lower reaction temperature.

Table 3.7 Characteristics of MgO grains used in MgO-C bricks with 20 wt% graphite (from Wolfert et al.[65])

Magnesia grain	Chemical composition (wt%)						Bulk density (g/cm^3)	Average crystal size (μm)
	MgO	CaO	SiO_2	Al_2O_3	Fe_2O_3	B_2O_3		
Grade B	99	0.57	0.07	0.07	0.11	0.003	3.44	70
Grade C	97	1.90	0.29	0.12	0.24	0.057	3.43	80

However, if the dense MgO zone can form inside the materials, the consequence

for the effect of material reactivity will be very different. Baker et al.[8] have reported that when fired in air the dense zones formed in the samples made using standard quality (96 wt% MgO) sinter are thicker than those formed in samples made from high-purity (99 wt% MgO) quality sinter (see *Table 3.8*). As a result, a lower carbon loss, in terms of both weight loss and area of decarbonized zone, has been recorded in the samples with standard quality MgO. The results of Lin et al.[3], as shown in *Table 3.9*, also demonstrate that the MgO-graphite material with finer-grained MgO has a lower weight loss and smaller oxidized area, but a thicker MgO dense zone when fired at 1600°C in air. Apparently, the higher rate of Mg vapour formation, due to either the presence of higher impurity or the increase of surface area of MgO grains, develops a "protective" MgO dense zone sooner and better when the atmosphere is favourable (i.e. at a high Po_2), and this dense zone hinders gas diffusion and limits further decarbonization including both carbon burnout and MgO-C interaction.

3.5 Chapter Summary

The results, either from this work or previous studies, have shown that the decarbonization takes place mainly through two mechanisms: carbon burnout by oxygen or/and MgO-C interaction, depending upon both temperature and atmosphere in the reaction system. Carbon burnout is considered a process of direct oxidation due to the direct involvement of free oxygen in the reactions. During MgO-C interaction, oxygen is involved indirectly as this gas is freed from the bonding with Mg atom in MgO, so

Table 3.8 Decarbonization of MgO-C refractories with 15 wt% graphite after carbonization at 1200°C (from Baker et al.[8])

Oxidation in air 1650°C - 8 h	With standard grain	With high purity grain
Purity of grain (wt% MgO)	96	99
Weight loss (wt%)	10.47	12.47
Area of decarbonized zone (mm^2)	49.5	53.8
Thickness of dense zone (mm)	0.40	0.18

Table 3.9 Decarbonization of MgO-C samples with 10 wt% graphite after firing in air at 1600°C (from Lin et al.[3])

Type of MgO grain	Coarse		Fine	
Grain size (wt%) -65 +100 mesh -100 +200 mesh -325 mesh Calculated surface area (cm^2/g)	 45 45 148		 90 469	
Oxidation time (min)	30	90	30	90
Weight loss (wt%)	9.5	10.4	7.0	8.5
Oxidized area (% S_0)	75	100	25	42
Dense zone thickness (μm)	174	194	170	215

that this process is referred to as indirect oxidation. The process rates of both carbon burnout and MgO-C interaction are diffusion-determined, but both processes have different mechanisms. In the process of carbon burnout, inward diffusion of oxygen from the exterior is more important, and in the process of MgO-C interaction, outward diffusion of Mg and CO gaseous species from the interior is more critical. In Chapter V, these two different decarbonizing mechanisms will be discussed more broadly from a kinetic point of view.

In the lower temperature range ($\leq 1400^{\circ}C$), carbon burnout is the dominant decarbonizing reaction in an oxidizing atmosphere. Thus, in this temperature range, controlling the diffusion-affecting factors, e.g. by reduction of the Po_2 in the atmosphere, is most effective to suppression of decarbonization. At higher temperatures ($> 1400^{\circ}C$) MgO decomposition becomes inevitable, and the presence of carbon materials enhances significantly the MgO decomposition due to the very low Po_2 in the reaction system. As a result, decarbonization also takes place by the oxygen released from the MgO. The active measure to control MgO-C interaction is to reduce the reactivity between MgO and C phases because the reactivity determines directly the extent of the MgO-C interaction. Adjustment of Po_2 in the reaction system to allow Mg vapour formed during MgO-C interaction to deposit in the decarbonized layer and form a dense MgO zone can also hinder carbon burnout as well as further MgO-C interaction through obstruction of diffusion channels. A strong CO atmosphere can greatly repress carbon burnout, but can

not effectively prevent MgO-C interaction, both due to the low Po_2 in the reaction system.

This exposition represents the first time that the above argument has been put forward in the literature concerning the process of decarbonization in two different mechanisms as a function of both temperature and atmosphere in the reaction system. This argument explains clearly the strong relation of the dominant decarbonizing mechanism with changes of both temperature and atmosphere. Based on this theory, the experimental results presented earlier in this chapter, as well as the findings of previous studies (including the results of Zoglmeyr,[38] Tabata et al.,[49] Ishibashi et al.,[7] Ishii et al.,[68] Moore et al.,[69] Wolfert et al.,[65] Uchimura et al.,[9] Baker et al.,[8] Lin et al.,[3] Griffin et al.,[61] and etc.), can be fairly rationalized although some of these results were not well explained or limited to only one of the two decarbonizing mechanisms due to the specific range of temperature or atmosphere. The other experimental results which are going to be discussed in the following chapters will also be analyzed based on the premise that the process of decarbonization is a dual mechanism.

CHAPTER IV

Direct Carbon Oxidation as a Function of Brick Composition

Chapter III has explained that the decarbonization in MgO-C refractories takes place mainly through direct carbon oxidation (carbon burnout by oxygen) or/and indirect carbon oxidation (MgO-C interaction) depending on the change of both temperature and atmosphere. This chapter will focus on the role of brick composition, including graphite content, MgO grain size distribution, and amount of resin binder, on the process of carbon burnout by oxygen in air in the temperature range from 1000 to 1400°C. As described in *Section 2.1*, 9 different types of experimental bricks were prepared with four levels of graphite content, i.e. 5 (G1), 10 (G2), 15 (G3), and 20 (G4) wt%; two size distributions of MgO grains, i.e. regular size distribution (D1) and small size distribution (D2); and two levels of resin binder, i.e. 2.5 (B1) and 3.5 (B2) wt%.

4.1 Comparison of Properties before and after Carbonization

As mentioned in Chapter I, MgO-C bricks will inevitably undergo the process of carbonization during their usage as furnace lining, in which the pyrolysis of resin binder occurs. Thus, how this process affects brick properties and the later performance of lining bricks including the resistance to carbon oxidation represents a meaningful investigation.

The procedure of carbonization adopted in the present study has already been described in *Section 2.4*. To study the effect of the carbonization process, various physical properties, including pycnometric volume, weight, dimension, and cold crushing strength, were measured both before and after carbonization, and attention was paid to the changes (i.e. increments) of these properties due to the process of carbonization.

4.1.1 Effect of graphite content

The increment values of pycnometric volume, weight, and dimension due to the process of carbonization versus graphite content are illustrated in *Figure 4.1*. The cold crushing strength before and after carbonization versus graphite content is also displayed in *Figure 4.2*. As the graphite content increases, the weight loss, permanent linear expansion, and reduction in pycnometric volume all increase. The changes in cold crushing strength as a function of graphite content are very different before and after carbonization. Although a lower graphite content can improve the brick strength before carbonization, the same trend is not maintained after carbonization, and only a slight variation in strength is shown with the change of graphite content.

(1) Weight loss

Because of the low carbonizing temperature (1000°C), a well-sealed metallic retort, and usage of argon gas for protection, the loss of carbon materials during carbonization process should not be appreciable. Also, MgO grains do not release a

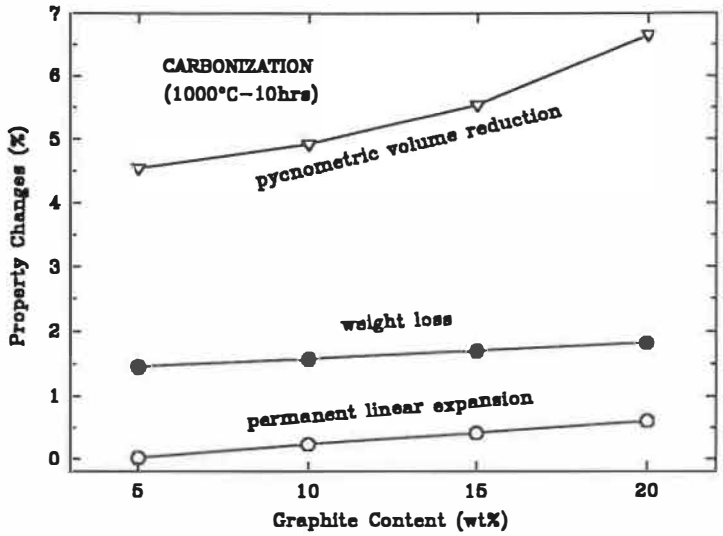

Figure 4.1 Changes of properties for brick samples (Gx-D1-B1) during carbonization (1000°C - 10 h).

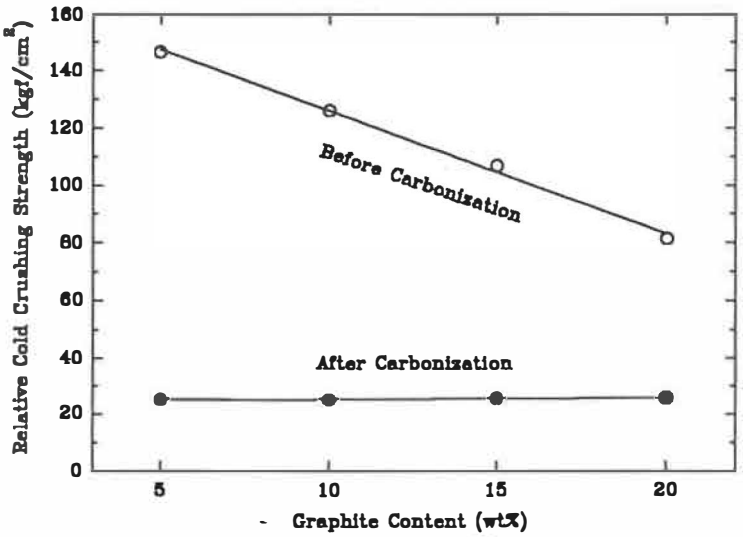

Figure 4.2 Changes in cold crushing strength before and after carbonization (1000°C - 10 h).

significant amount of volatile species at 1000°C. Therefore, the weight loss during the process of carbonization is hypothesized to be due to the removal of volatile materials from both the resin binder and graphite phase. Because the same amount of resin binder was used for all the graphite levels (only limited to the brick samples with D1 and B1 in this section), we can easily calculate the percentage of volatiles from each phase based on the relation of weight loss and graphite content.

Assume x is the volatile content in graphite phase and y is the volatile content in resin binder. Since the amount of resin binder plus hexa added is 2.6 wt% in total (B1), and the graphite content varies from 5, 10, 15, to 20 wt%, then we can have:

$$5x + 2.6y = 1.46$$

$$10x + 2.6y = 1.58$$

$$15x + 2.6y = 1.70$$

$$20x + 2.6y = 1.82$$

On the right side of above equations are the values of total weight loss (in wt%) during carbonization, which are illustrated in *Figure 4.1*. By solving the above equations, the average values of x and y are obtained as:

$$x = 2.4 \text{ wt\%}$$

$$y = 51.5 \text{ wt\%}$$

Therefore, the major weight loss results from the pyrolysis of carbon binder, or, in other words, the removal of volatile materials from the resin binder. In addition, the increase

in weight loss with graphite content, as shown in *Figure 4.1*, indicates that graphite also contains a small amount of volatile species, i.e. about 2.4 wt%; these volatiles are believed to come from the residue oil which was absorbed on the surface of graphite flakes during mineral processing.[71]

(2) Change of porosity

The change of porosity during carbonization is the result of a combination of several factors, including mainly volume contraction of the resin binder, removal of volatile species, and irreversible thermal expansion of graphite phase. Understandably, the removal of volatile materials from both resin binder and graphite flakes to the exterior of the brick can cause an increase in open porosity. In addition, after cooling from the carbonizing temperature, the graphite flake does not contract back to its initial position and shape, resulting in a formation of a gap between the basal planes. Thus, both a permanent linear expansion and an increase in porosity are expected.[64] Increasing the graphite content can make these two latter effects more significant. Consequently, as shown in *Figure 4.1*, the values of pycnometric volume reduction and permanent linear expansion increase with graphite content. Note that the reduction in pycnometric volume value for a sample after a heat treatment is relevant to the increase of its porosity, as mentioned earlier in *Section 2.7*. In fact, the results presented here are in agreement with those of Lubaba et al.[18] as shown in *Figure 4.3*, which indicates that the difference in porosity before and after firing increases with graphite content. According to their

calculations, about three quarters of the increase in porosity during carbonization is due to the volume-expansion effect of the graphite phase.

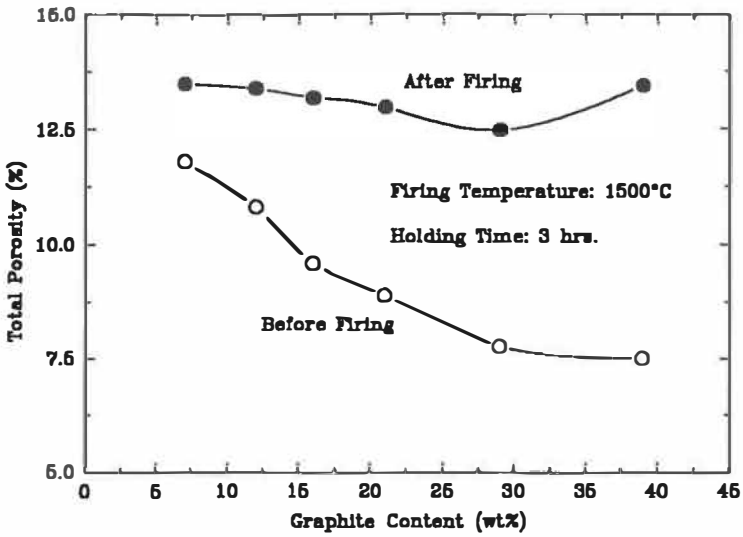

Figure 4.3 Variation of porosity with graphite content for MgO compacts before and after firing in a reducing atmosphere (from Lubaba et al.[18]).

(3) Cold crushing strength

Figure 4.2 shows that the strength value before carbonization drops down dramatically as the graphite content increases. As we know, in carbon-bonded MgO-graphite-composite material, MgO grains and graphite flakes are weakly bonded by resin binder because of the non-wettability of graphite flake surfaces; thus, cracking mostly propagates along the weak interface between graphite and resin when a load is applied to the material. An increased area of this weak interface due to an increase of graphite content will then surely result in a lower strength.

On the other hand, although the carbon bonding is rather weak, crack propagation through MgO grains was still observed on the cracked surfaces. By comparing *Figures 4.4* and *4.5*, this phenomenon is more evident with lower graphite content. This observation indicates that the resin binder can adhere to MgO grains so strongly that crack propagation along MgO grains, or the pulling-out of MgO grains hardly occurs when the grains are large enough. Therefore, the strength of carbon-bonded MgO-graphite materials before carbonization is largely dependent on the total area of weak interface between graphite flakes and binder, or that of strong interface between MgO grains and binder which is inversely proportional to the former.

After carbonization, however, the strength values and their graphite-content dependence are quite different compared to those before carbonization. The carbonizing process can create many micropores in the resin body due to the removal of volatile material and the volume shrinkage of resin body, and thus, weaken its cohesive force. As a consequence, the strength is reduced significantly (see *Figure 4.2*); and crack propagation through MgO grains is seldom observed, even at a low graphite level, after examining the cracked surfaces of samples. Furthermore, unlike the case before carbonization, there is a slight increase in strength with graphite content (see *Figure 4.2*). After carbonization (before oxidation), carbon bonding becomes the weakest phase in the composite structure, or, in other words, cracking mostly goes through the binder phase when a load is exerted so that the crushing strength does not change much with graphite

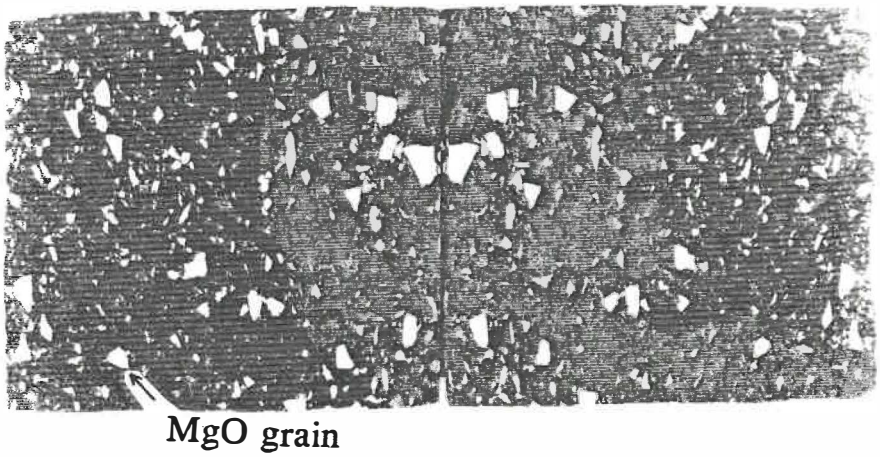

Figure 4.4 View of cracked surfaces of brick samples as-received with 5 wt% graphite after crushing test, showing crack propagation through large MgO grains.

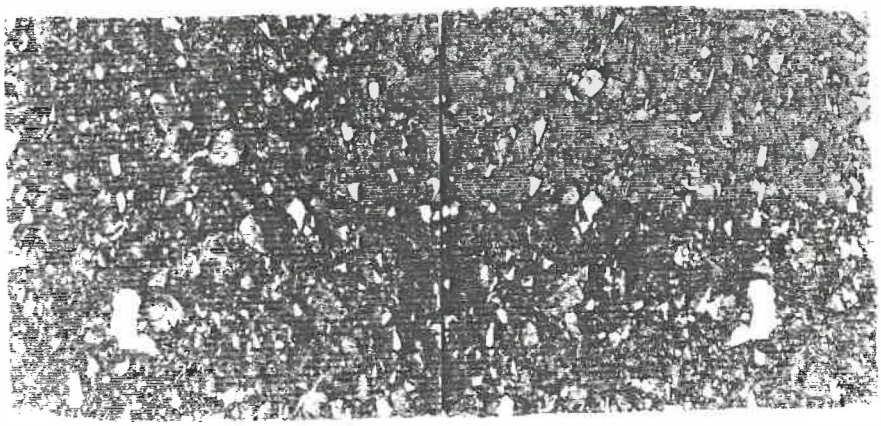

Figure 4.5 View of cracked surfaces of brick samples as-received with 20 wt% graphite after crushing test, showing crack propagation through large MgO grains.

content because of the same amount of carbon binder used in all the samples. These results demonstrate the controlling role of carbon binder on strength after carbonization. On the other hand, as claimed by Cooper et al.,[55] graphite flake can act as a kind of reinforcement in oxide-graphite composite materials as the graphite content increases. However, this effect is rather limited in our case since the increase in crushing strength with graphite content is very slight. This observation indicates that the reinforcing role is not dominant in the range of these graphite levels. The results of Lubaba et al.[72] have shown that only at a graphite level greater than 20 wt% can the strength after carbonization increase significantly (see *Figure 4.6*). Thus, they have also concluded that the bonding medium remains the major factor controlling the strength except when a sufficiently high level of flakes comes to play a reinforcing role.

4.1.2 Effect of MgO grain-size distribution

In the bricks with D1 (regular grain size distribution) or D2 (small grain size distribution), their chemical compositions are same, i.e. 15 wt% graphite (G3) and 2.5 wt% resin binder (B1). The two MgO grain-size distributions are illustrated in *Figure 2.1*. The comparison of properties for these two types of samples before and after carbonization is shown in *Table 4.1*. The changes of other properties during carbonization, i.e. weight loss, pycnometric volume reduction, and permanent linear change, are also listed in *Table 4.2*. As can be seen, the properties and their changes during carbonization are rather different for the two types of samples with either D1 or

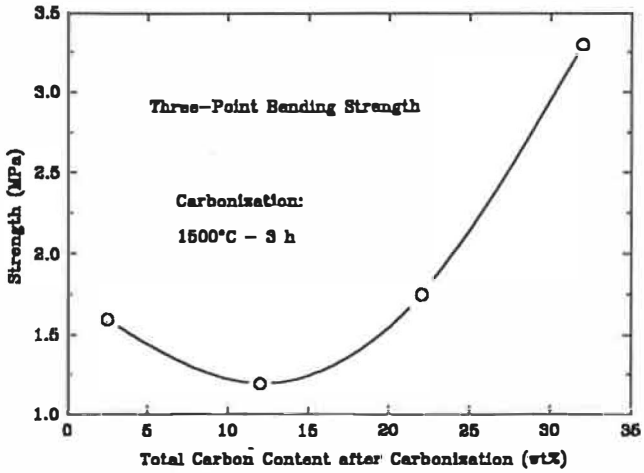

Figure 4.6 Variation of strength of MgO-graphite composites with carbon content after carbonization in a reducing atmosphere (from Lubaba et al.[72]).

Table 4.1 Comparison of properties for brick samples (15 wt% graphite) with either regular (D1) or small (D2) MgO grain size distribution before and after carbonization

Heat treatment	Before carbonization		After carbonization	
Type of brick samples	D1	D2	D1	D2
Bulk density (g/cm^3)	2.97	2.93	2.89	2.84
Open porosity (%)	3.84	4.52	10.25	11.27
Crushing strength (kgf/cm^2)	106.97	114.88	25.65	28.87

Table 4.2 Changes of properties for brick samples (15 wt% graphite) with either regular (D1) or small (D2) MgO grain size distribution due to carbonization process

Type of brick samples	D1	D2
Weight change ($\Delta W/W_0$ %)	-1.70	-1.70
Pycnometric volume change ($\Delta V/V_0$ %)	-5.54	-5.04
Permanent linear change ($\Delta L/L_0$ %)	+0.42	+0.44

D2. In the following paragraphs, a discussion of these results will be presented.

When MgO grain compact is combined with graphite, the grain-size distribution has to be adjusted in order to give the minimum porosity on compaction. Lubaba et al.[18] have found that when there are fewer fines present in the MgO-graphite mixtures, graphite flakes are not separated, but pack together quite tightly in the interstices between the medium and coarse MgO grains. In this region, the flakes deform to fill the interstices, leading to the extremely efficient packing. When the proportion of fines is relatively high, they tend to occupy the spaces between graphite flakes which are, therefore, more separated on average, and thus, the porosity is raised. Our results further confirm the significant influence of size distribution of MgO grains, particularly the proportion of grain fines, on the porosity at a fixed graphite content. As we can see from *Table 4.1*, the samples with D2 have a lower bulk density and a higher open porosity both before and after carbonization. However, although finer grains separate more flakes apart and increase the packing voids, the finer grains also reduce the number of flake aggregates and make the microstructure more homogeneous.

From *Table 4.1* we can also see that the samples with D2 have a larger increase in open porosity (6.75%) during carbonization than that of the samples with D1 (6.41%). However, the same weight loss due to carbonization was recorded for the two types of samples (see *Table 4.2*), which implies that the increase in open porosity due to the

removal of volatile species is identical in both cases. Therefore, the difference in porosity change is attributed to the difference in microstructural features. Obviously, the opening-up of more closed pores during carbonization should be a factor since before carbonization the samples with D2 have a rather low bulk density which may embody a larger amount of closed pores. Moreover, the increase in porosity due to the irreversible thermal expansion of graphite phase will be different if the positional distribution of graphite flakes is changed. In comparison with the values of permanent linear expansion (see *Table 4.2*), a larger extent of irreversible thermal expansion may take place in the samples with D2, leading to a formation of more closed pores and, thus, a contribution to the increase in pycnometric volume after carbonization. Therefore, the net reduction in pycnometric volume for the samples with D2 becomes smaller compared to that for the samples with D1.

As discussed previously, the strength before carbonization is directly proportional to the area of interface between the MgO grain and binder and inversely to the area of interface between the graphite flake and binder. When the graphite content and flake size do not change, the area of interface between graphite flake and binder should be unchanged. However, the finer MgO grain-size distribution increases the surface area of the MgO phase and, thus, the area of interface between the MgO grain and binder. As a result, the strength values of the samples with D2 both before and after carbonization are higher than those with D1. Similar results have also been reported by Lubaba et al.;[72]

their data have shown that both increasing the proportion of fines and reducing the maximum grain size can significantly increase the strength of the MgO-graphite composite materials. In this work, when the maximum MgO grain size changes from 4 mm (4-6 mesh) for the D1 distribution to 2.19 mm (8-10 mesh) for the D2 distribution, the increases in strength are about 7% and 13% for the uncarbonized and carbonized brick samples, respectively. Thus, in terms of improvement of mechanical strength the use of small MgO grain-size distribution may be beneficial. On the other hand, the fact that the samples with D2 have a higher crushing strength although their porosity is greater implies that the porosity is unlikely to be the major factor controlling the mechanical strength of MgO-graphite bricks after carbonization.

4.1.3 Effect of carbon binder content

By changing the amount of resin binder from 2.5 wt% (B1) to 3.5 wt% (B2), but keeping other compositions unchanged, i.e. a regular MgO grain size distribution (D1) and graphite content of 15 wt% (G3), the properties of the sample bricks can also vary significantly. *Table 4.3* gives some of the data of the properties before and after carbonization showing the differences of these two types of samples in both cases. The changes of other physical properties during carbonization are also listed in *Table 4.4*.

Note from *Table 4.3* that in the uncarbonized state the open porosity decreases with increasing amount of binder phase. After carbonization, however, the porosity of

Table 4.3 Comparison of properties for brick samples (15 wt% graphite) with either 2.5 wt% (B1) or 3.5 wt% (B2) resin binder before and after carbonization

Heat treatment	Before carbonization		After carbonization	
Type of brick samples	B1	B2	B1	B2
Bulk density (g/cm^3)	2.97	2.94	2.89	2.84
Open porosity (%)	3.84	3.19	10.25	11.84
Crushing strength (kgf/cm^2)	106.97	113.64	25.65	30.52

Table 4.4 Changes of properties for brick samples (15 wt% graphite) with either 2.5 wt% (B1) or 3.5 wt% (B2) resin binder before and after carbonization

Type of brick samples	B1	B2
Weight change ($\Delta W/W_0$ %)	-1.70	-2.12
Pycnometric volume change ($\Delta V/V_0$ %)	-5.54	-7.29
Permanent linear change ($\Delta L/L_0$ %)	+0.42	+0.39

the samples shows the opposite dependence on binder content, attaining a higher level at the higher binder content. As expected, the carbon binder will fill the interstices between the granular phases or seal the intergranular voidages during the process of compaction. Increasing the binder content can obviously improve these effects and, thus, reduce the porosity unless the volume fraction of binder is greater than the intergranular volume, beyond which the latter will increase. On the other hand, according to Rand et al.,[19] both the evolution of volatiles and volume shrinkage occur during the pyrolysis of phenolic resins, resulting in an increase in both true density and bulk density of the resin body. In the case of resin precursors, the evolution of volatiles causes about 50% loss of the initial weight, and the contraction can also amount to a volumetric shrinkage of 50% or so. Thus, the volumetric contraction of binder phase during carbonization leads to a formation or opening of the intergranular voidages in the MgO-graphite compact, increasing open porosity. This effect is more evident at a higher level of binder.

In addition, the ability of the binder phase to restrain the body against the tendency of irreversible thermal expansion is noticeable. As a matter of fact, a lower irreversible linear expansion was recorded in the samples with B2 (see *Table 4.4*). As reported by Lubaba et al.,[21] the resin undergoes a substantial bulk volume shrinkage during carbonization, which perhaps has a tendency for the solid carbon bond to restrain the expansion of the other phases. However, despite of the greater ability of restraining the compact body against the tendency of irreversible thermal expansion of graphite

phase due to the higher level of binder, the samples with B2 still have a greater porosity increase after carbonization (8.65% for B2 compared to 6.41% for B1), indicating that the contribution of volume reduction of binder phase to the porosity change during carbonization is prevailing.

Also, note from *Table 4.3* that increasing the amount of carbon binder improves the crushing strength, either before or after carbonization. However, the strength value does not increase to any appreciable extent, but the open porosity, which is disadvantageous to both oxidation and corrosion resistance, increases quite significantly after carbonization (an increment of 8.65%). In fact, our results are also in agreement with the findings of Lubaba et al.[21,72] As can be seen, the results in *Table 4.5* show the exact same trends for the changes of porosity and strength as ours in *Table 4.3* although the amount of resin binder which they added is higher.

In the available literature, the present study is the only one after Lubaba et al.[18,21,72] that has systematically investigated the changes of brick properties before and after carbonization process as a function of brick composition. The results of Lubaba et al. and those of this work presented in this section demonstrate strongly that the process of carbonization can bring about a significant modification in brick properties, including porosity, strength, and dimension. And this change in properties can be very different depending on the variation of brick composition, i.e. graphite content, MgO grain-size

distribution, and amount of resin binder. As expected, this change will have a great influence on the other properties in the later stage. For example, the change of porosity during carbonization should affect the resistance to carbon oxidation when oxygen becomes available. Unfortunately, this part was missing in the work of Lubaba et al.[18,21,72] In the next section, the relation of change of properties due to carbonization with carbon oxidation resistance as a variation of brick composition will be discussed.

Table 4.5 Properties of MgO-graphite (80:20 in weight) compacts as a function of resin binder content before and after firing at 1500°C for 3 h in a reducing atmosphere (from Lubaba et al.[21,72])

Parts of resin per 100 parts of MgO/graphite	Total porosity (%)		Cold strength (MPa)
	Before firing	After firing	After firing
5 wt%	6.0	13.2	1.60
11 wt%	4.7	16.8	1.75

4.2 Resistance to Direct Carbon Oxidation

This section focuses on a discussion of the decarbonizing behaviour of MgO-graphite bricks through direct carbon oxidation i.e. carbon burnout by oxygen in air, in the temperature range between 1000 and 1400°C. The properties of weight loss, porosity change, depth of decarbonized layer, and strength loss after unidirectional oxidation tests have been used to evaluate the resistance to oxidation as a function of brick composition, i.e., graphite content (G1, G2, G3, and G4), MgO grain-size distribution (D1 and D2), and amount of resin binder (B1 and B2).

4.2.1 Effect of graphite content

(1) Weight loss

The weight losses after oxidation for 5 hours in air vs graphite content at three temperatures are presented in *Figure 4.7*. In the temperature range from 1000 to 1400°C, the measured weight loss is believed to be directly related to the extent of carbon loss, including both graphite and secondary carbon pyrolysed from the resin binder. From the results shown in *Figure 4.7*, the oxidation rate (an average of weight loss over 5 hours) is proportional to the amount of graphite, or in other words, the rate is a function of the contacting area of carbon with oxygen. Since the amount of oxygen available is kept constant and sufficient, a higher amount of graphite leads to losing more carbon.

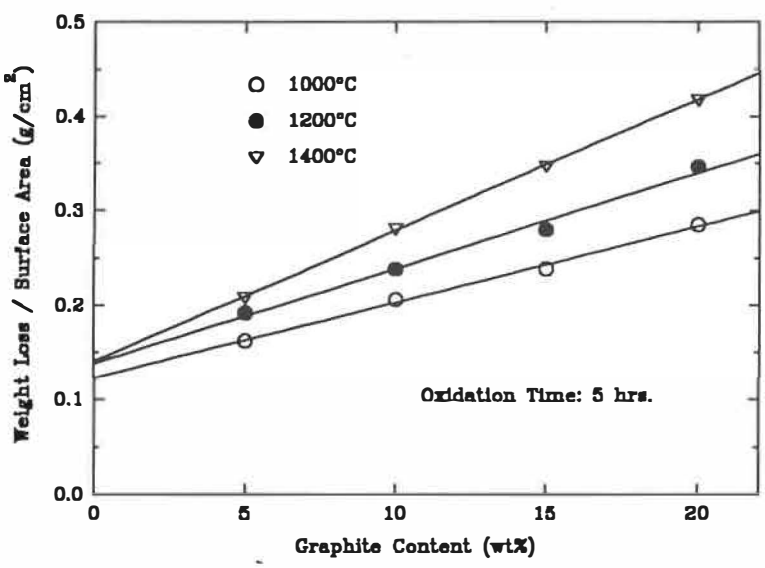

Figure 4.7 Weight loss (unidirectional oxidation) as a function of graphite content at different oxidation temperatures.

In addition, *Figure 4.7* indicates that as the graphite content changes from low

level to high level, the increase in oxidation rate is different with the temperature. At 1400°C, the weight loss appears to have the largest increase with the change of graphite content. This trend is because both the chemical reaction between carbon and oxygen and gas diffusion of product species can be promoted by increasing temperature.

Note that at the zero level of graphite, the lines in *Figure 4.7* do not go through the origin. This result implies that the oxidation of a portion of carbon binder also contributes to the overall weight loss. In our samples with four different levels of graphite, the same amount (2.5 wt%, B1) of phenolic resin was added initially, which could yield about 1.28 wt% secondary carbon after carbonization (as calculated from the results in *Section 4.1.1*). However, the contribution of secondary carbon loss during oxidation to the total weight loss varies with the proportion of graphite. For example, for the samples with 5 wt% graphite, about 21% of total weight loss is due to the loss of secondary carbon, but, for the samples with 20 wt% graphite, the portion of secondary carbon loss in the total weight loss is only about 6%.

(2) Temperature-dependence of weight loss

Figure 4.8 is obtained by plotting the weight loss against the reciprocal of temperature. As can be seen, the relation is fairly linear for each graphite content, or, in other words, the weight loss obeys the Arrhenius' law. Through linear regression, we have also found that the slope values, k_i, of the lines in *Figure 4.8* are not equal, and

they follow the order:

$$k_{20} > k_{15} > k_{10} > k_5$$

The results show that at higher graphite levels, the oxidation rate is more sensitive to the change of temperature. On the other hand, if the chemical reaction between carbon and oxygen controlled the overall rate of the decarbonizing process, the activation energies should not depend on the amount of graphite. The values of "activation energy" calculated from *Figure 4.8* increase from 11 kJ for 5 wt% graphite samples to 17 kJ for 20 wt% graphite samples. This implication is that the chemical reaction between carbon and oxygen is not rate-controlling under the present test conditions. Note that the values calculated from this type of plotting are only based on an average rate of oxidation over 5 h, and are not the true values for activation energy of the oxidation process. Even so, these values are still useful for comparison under the same conditions. In Chapter V, where the kinetics of oxidation is the theme, this issue will be considered more precisely.

(3) Change of porosity

Along with a weight loss during decarbonization, the porosity of the oxidized sample also increases. In terms of volume, the increase of porosity due to carbon loss can be calculated from the amount of total weight loss. The calculations have taken into account the weight proportions of graphite and secondary carbon after carbonization (see *Section 4.1.1*) and their densities (taking natural graphite flake as 2.29 g/cm^3 and carbonized phenolic resin as 1.55 g/cm^3). The calculated values (given in a regressed

form because of their strong linear relations with graphite content as shown in *Figure 4.7*) are displayed as the fit lines in *Figure 4.9*. The points shown in *Figure 4.9* were actually obtained from the experimental measurements of the reduction in pycnometric volume after oxidation, which should be equivalent to the volume increase of open porosity due to carbon loss if the change of close porosity is assumed to be negligible. These experimental results which are in a reasonable agreement with the fit lines indicate that after carbon burnout the measuring gas medium can gain access to the pores which were initially occupied by carbon. From another point of view, these data imply that no impervious dense MgO zone has formed during oxidation under the test conditions. The results in *Figure 4.9* also demonstrate that the porosity of the samples after oxidation increases with both graphite content and temperature because more carbon materials are burnt out in both cases.

(4) Depth of decarbonized layer

After loss of carbon, one typical structural feature is the decarbonized layer. The measured values of the depth of decarbonized layer for the different graphite contents are shown in *Figure 4.10*. The fact that the rate at which the depth of decarbonized layer decreases with graphite content suggests that the rate is inversely proportional to the area fraction of graphite phase at the interface of oxidation reaction between the graphite depleted zone and the region of unreacted graphite. Actually, more graphite is consumed as the graphite content increases (see *Figure 4.7*), creating more CO(g) to desorb, which,

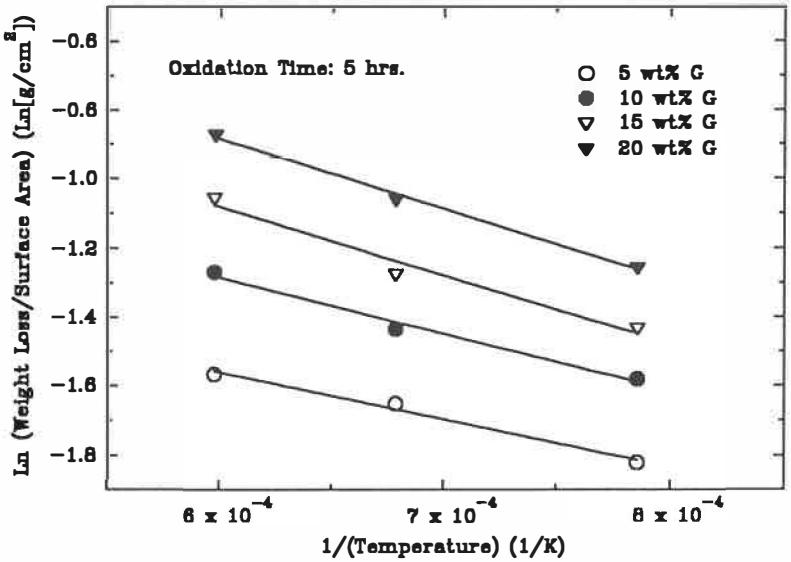

Figure 4.8 Weight loss (unidirectional oxidation) as a function of reciprocal temperature for different levels of graphite content.

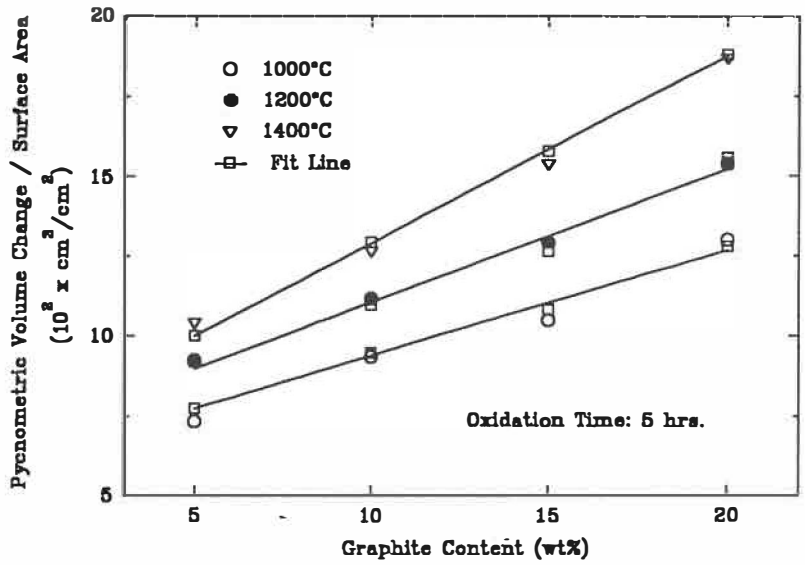

Figure 4.9 Change of porosity (unidirectional oxidation) as a function of graphite content at different oxidation temperatures.

in turn, delays graphite consumption as CO(g) acts as a gaseous antioxidant.

The fact that the depth of decarbonized layer at 1000°C is greater than the one at 1200°C is also a reflection of the CO(g) effect. CO(g) generation also occurs through the consumption of secondary carbon which is pyrolysed from resin binder. This reaction can take place at a faster rate than that for graphite due to the difference in material reactivity. As a result, the diffusion of oxygen in the pore structure leads to the disappearance of the secondary carbon at a faster rate than graphite. Because this contribution of secondary carbon to preventing deep decarbonizing penetration is greater at 1200°C, the depth of the decarbonized layer does not increase as the temperature rises from 1000 to 1200°C, but the total weight loss is increased due to the loss of a larger amount of secondary carbon. However, as the temperature reaches 1400°C, the reactivity of graphite becomes comparable to that of secondary carbon, and thus, the depth of decarbonized layer increases again with the temperature.

(5) Loss of crushing strength

Figure 4.11 shows the plots of relative cold crushing strength vs graphite content before and after oxidation (at different temperatures). The crushing strength drops greatly after oxidation because a part of the carbon bonding and graphite has been lost and, at the same time, there is almost no strength build-up in the decarbonized layer formed because the oxidation temperature is not high enough. As graphite content increases, deep

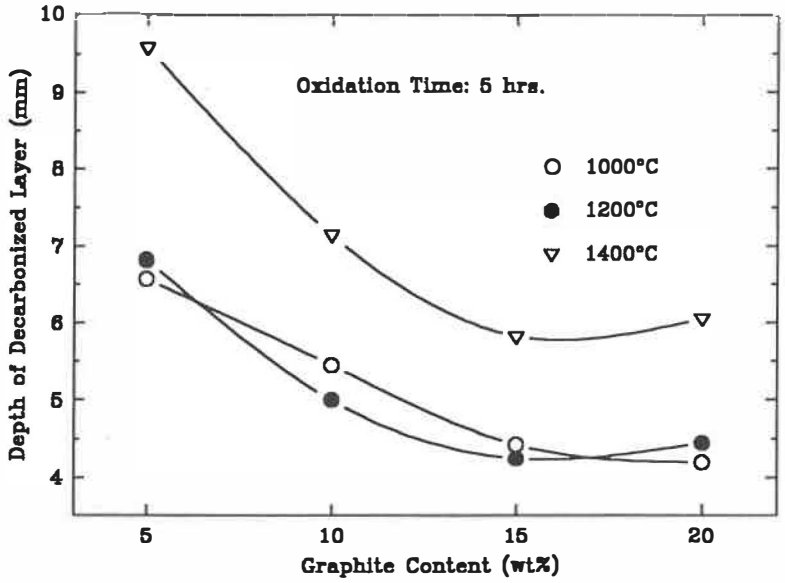

Figure 4.10 Depth of decarbonized layer (unidirectional oxidation) as a function of graphite content at different oxidation temperatures.

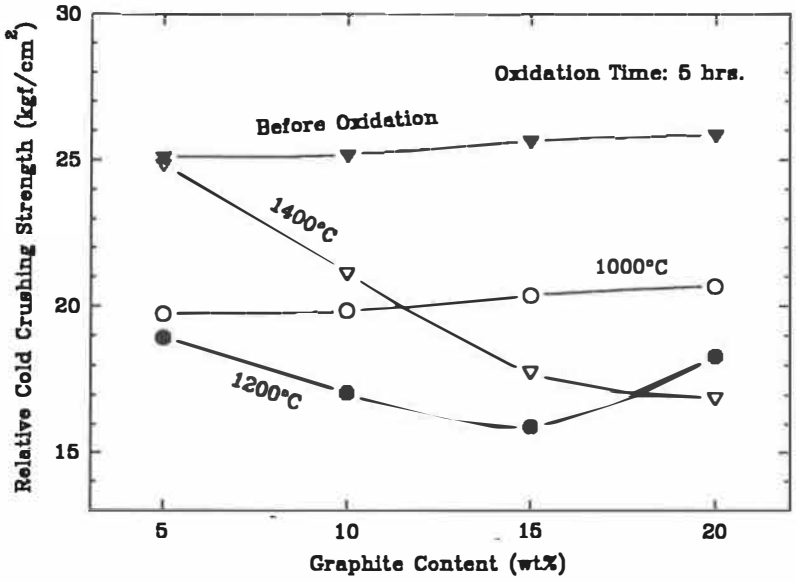

Figure 4.11 Loss of crushing strength as a function of graphite content after oxidation at different temperatures.

decarbonizing penetration is hindered, and thus, the extent of strength loss is reduced. This case is most likely at 1000°C, although the effect is not so significant.

As the oxidation temperature rises to 1200°C, the strength further decreases because the amount of carbon lost increases with temperature (see *Figure 4.7*). However, at either the low or high level of graphite content, the strength loss is relatively small. Sintering is believed to occur in the decarbonized layer; this action builds up a certain amount of strength and reduces the total strength loss. This situation occurs at 5 wt% graphite, in which a lower porosity results from graphite burnout. However, at 20 wt% graphite, the texture of the decarbonized layer is very porous, and the MgO grains are rarely in contact with each other when the graphite is burnt out, making sintering relatively difficult. In this situation, the prevention of deep decarbonizing penetration remains the prevailing factor in determining the total strength.

As a result of the temperature-enhancement of sintering effect, the strength values at 1400°C are above the ones at 1200°C except for the samples with 20 wt% graphite. For the samples with 5 wt% graphite at 1400°C, the strength loss due to oxidation is only 0.24 kgf/cm^2 compared with the value of 9.72 for the samples with 15 wt% graphite at 1200°C. These data indicate the domination of sintering over the accelerated decarbonization due to the increase of temperature. At lower levels of graphite, this influence is more obvious because of the less loose decarbonized texture. However, at

the highest level of graphite, i.e. 20 wt% of graphite, the dominant mechanism to control strength loss is still the prevention of deep decarbonizing penetration. Therefore, the strength value maintains the order: $\sigma_{1000} > \sigma_{1200} > \sigma_{1400}$.

4.2.2 Effect of MgO grain-size distribution

(1) Weight loss and the depth of decarbonized layer

By shifting the MgO grain size from the regular distribution D1 to small distribution D2 (with 15 wt% graphite, G3; and 2.5 wt% resin binder, B1), the rate of carbon burnout is significantly increased (see *Figure 4.12*). This increase is believed mainly due to the higher initial porosity in D2 (before oxidation) which promotes the diffusion of gas species and thus, accelerates decarbonization. These results confirm that the process of carbon burnout is diffusion-controlled because there is a significant increase in oxidation rate just by increasing the porosity.

In addition, note from *Figure 4.12* that, as the temperature rises, the difference of increment in weight loss for the two types of samples remains almost unchanged. These results imply that the increase in porosity due to the change of MgO grain size distribution does not alter the diffusion-controlled decarbonizing mechanism, but only accelerates the process of decarbonization. Since the difference in porosity between the samples with D1 and D2 is fixed, the increase in decarbonizing rate due to the porosity change will remain unchanged with the rise of temperature.

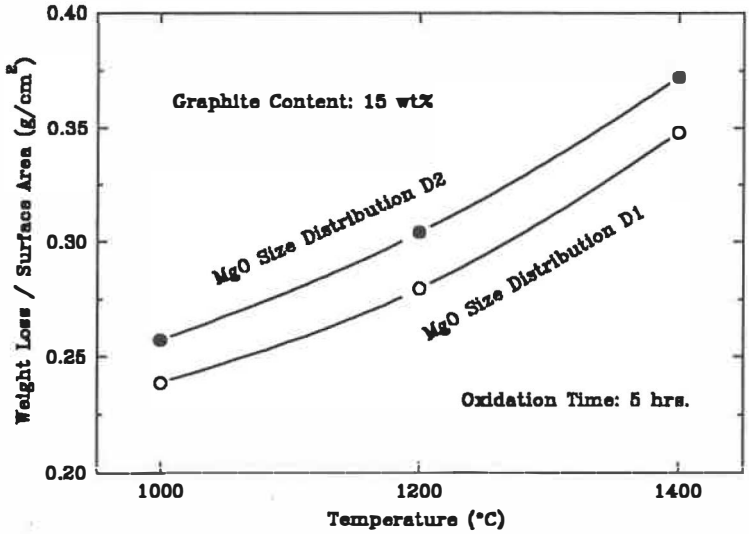

Figure 4.12 Weight loss (unidirectional oxidation) as a function of oxidation temperature for both the regular MgO grain-size distribution, D1, and the small MgO grain-size distribution, D2.

The comparison of temperature-dependence of weight loss for the two cases, as shown in *Figure 4.13*, further confirms that the decarbonizing mechanism is the same because the two lines are almost parallel to each other, or say, the temperature-dependence does not change with MgO grain size distribution.

Figure 4.14 illustrates the depth of the decarbonized layer for both cases. The depth of decarbonized layer is higher for the samples with D2 because of their higher decarbonizing rate including the losses of both graphite and secondary carbon.

(2) Change of porosity

The comparison of the changes in pycnometric volume for both cases is illustrated

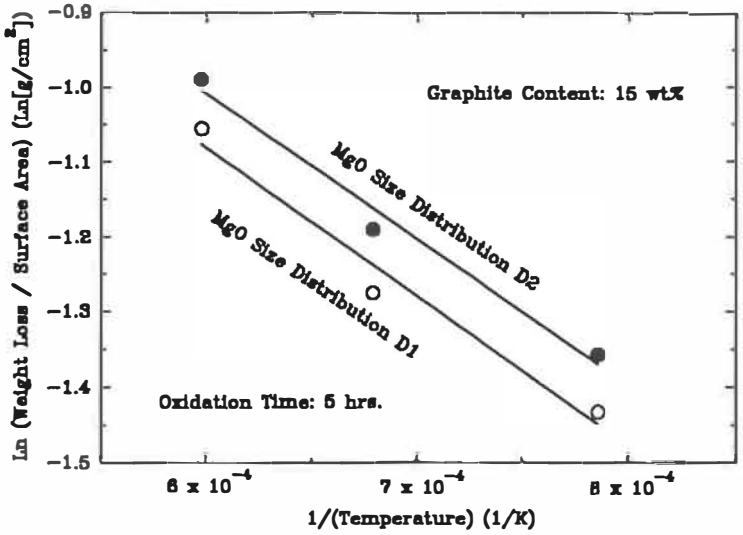

Figure 4.13 Weight loss (unidirectional oxidation) as a function of reciprocal temperature for the samples (15 wt% graphite) with either the regular MgO grain-size distribution D1 or small MgO grain-size distribution D2.

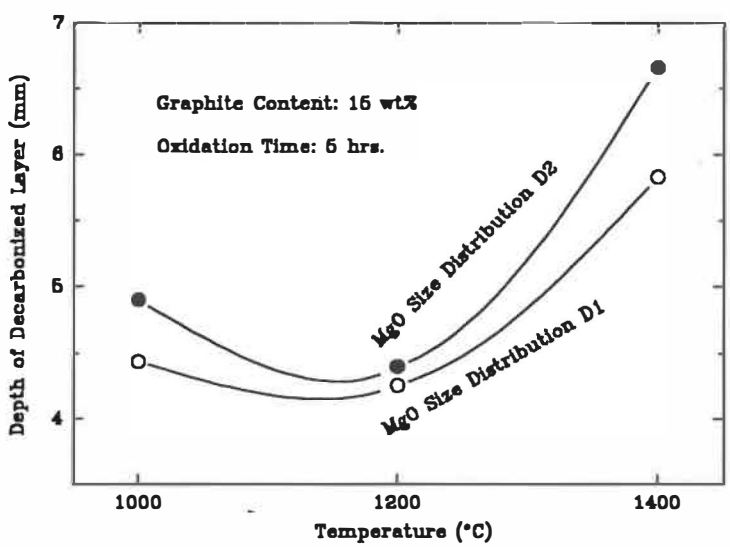

Figure 4.14 Depth of decarbonized layer as a function of oxidation temperature for the samples (15 wt% graphite) with either the regular MgO grain-size distribution, D1, or the small MgO grain-size distribution, D2.

as *Figure 4.15*. Unlike the case for D1, the reduction of the pycnometric volumes for the samples with D2 after oxidation (which represents the increase in open porosity) no longer fits the volume increase of open pores due to carbon loss (which is calculated from the total weight loss). The measured values are consistently larger than those calculated. This discrepancy is believed to exist because the samples with D2 have more closed pores initially, so that after carbon burnout these initially closed pores open up, increasing the total volume of open pores. This condition leads to an extra reduction in the pycnometric volume which is not due to carbon loss. Apparently, more closed pores become open at higher temperatures as the penetration of decarbonization. As a result, the deviation between the measurement and calculation for the samples with D2 increases with temperature.

(3) Loss of crushing strength

The values of cold crushing strength after oxidation for both the samples with D1 and D2 are plotted in *Figure 4.16* against oxidation temperature. Note that the change of MgO grain size distribution does not seem to change the trend of strength loss, i.e. the crushing strength drops considerably as the process of carbon oxidation until the temperature reaches 1400°C where the effect of sintering on strength build-up becomes significant.

Figure 4.16 also shows that although the samples with D2 have a larger extent of

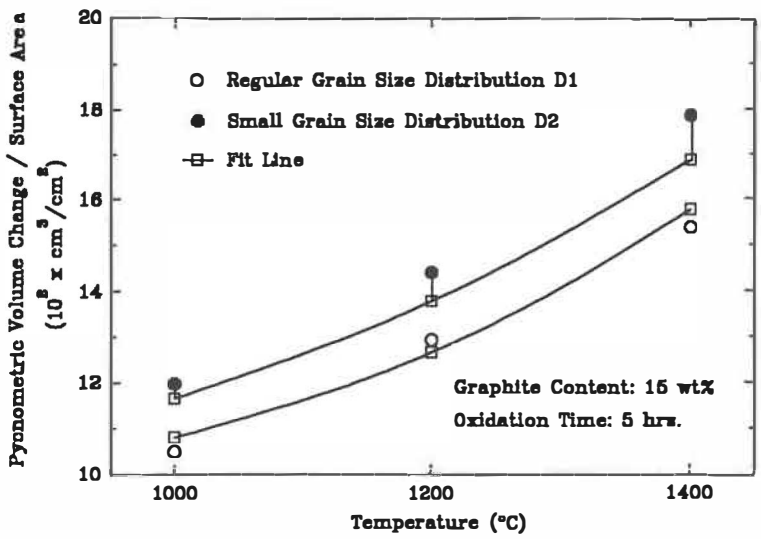

Figure 4.15 Change of porosity as a function of oxidation temperature for the samples (15 wt% graphite) with either the regular MgO grain-size distribution, D1 or the small MgO grain-size distribution, D2.

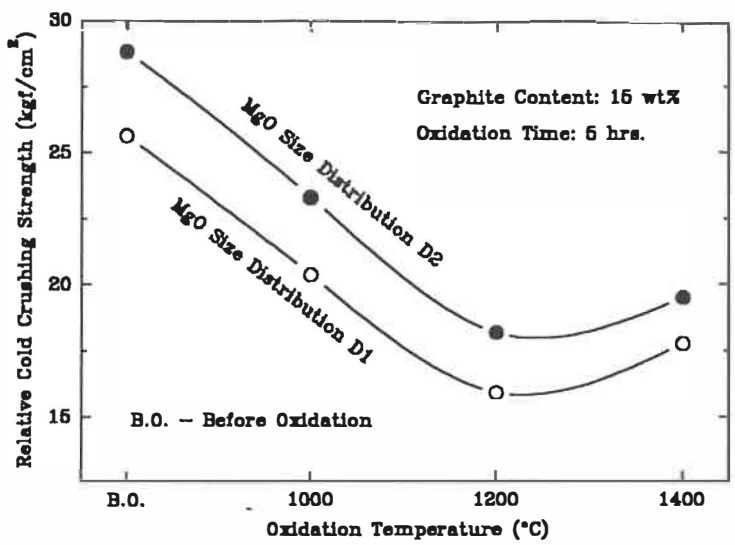

Figure 4.16 Loss of crushing strength as a function of oxidation temperature for the samples (15 wt% graphite) with either the regular MgO grain-size distribution, D1, or the small MgO grain-size distribution, D2.

carbon burnout, their strength values are consistently higher than those of the samples with D1. This trend indicates that the carbon bonding in the unoxidized part of the sample still determines its remaining strength, similar to the situation after carbonization as discussed above. However, the contribution of the difference in carbon oxidation rate to strength loss is also noticeable. As oxidation temperature rises, the samples with D2 have deeper decarbonized layers (see *Figure 4.14*) so that their strength losses are greater and the difference in strength for two cases becomes smaller. On the other hand, the increase in strength at 1400°C due to the effect of sintering also becomes more evident in the samples with D1 which have a lower porosity.

4.2.3 Effect of carbon binder content

(1) Weight loss and the depth of decarbonized layer

The comparisons of weight loss and depth of decarbonized layer as a function of oxidation temperature for the samples with either 2.5 wt% (B1) or 3.5 wt% (B2) resin binder are shown in *Figures 4.17* and *4.18*, respectively. The samples with B2 not only have a higher weight loss, but also a greater depth of decarbonized layer. Similar to the cases of D1 and D2 just discussed, the higher porosity in the samples with B2 is believed to be the major factor leading to such a higher oxidation rate. On the other hand, since the secondary carbon derived from resin binder is more reactive than graphite and thus, easier to be oxidized, the higher content of secondary carbon after carbonization in the samples with B2 also contributes to the higher weight loss besides the effect of porosity.

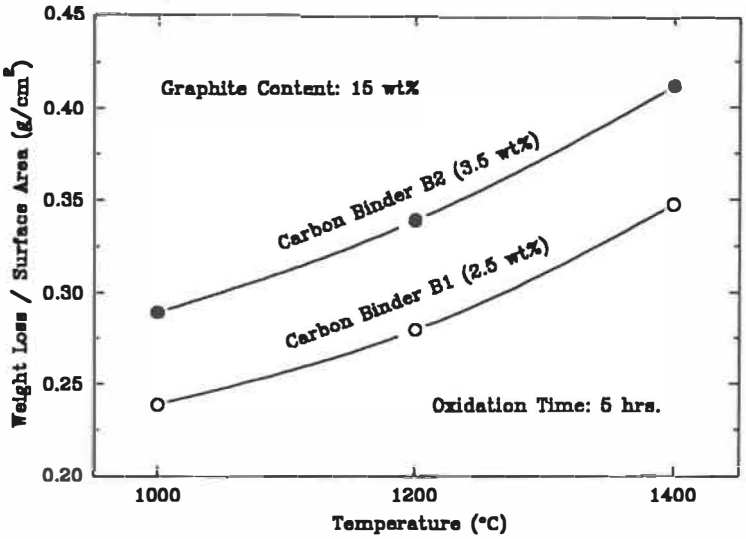

Figure 4.17 Weight loss (unidirectional oxidation) as a function of oxidation temperature for the brick samples (15 wt% graphite) with carbon binder either B1 (2.5 wt%) or B2 (3.5 wt%).

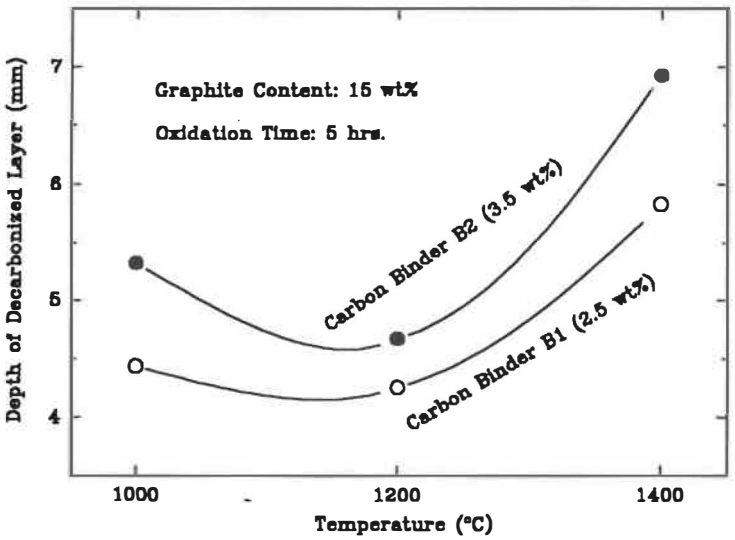

Figure 4.18 Depth of decarbonized layer as a function of oxidation temperature for the brick samples (15 wt% graphite) with carbon binder either B1 (2.5 wt%) or B2 (3.5 wt%).

These results suggest that using a large amount of carbon binder can bring about a negative effect on the resistance of carbon oxidation.

(2) Change of porosity

Figure 4.19 shows the comparison of the changes of pycnometric volumes for both the samples with B1 and B2. Since the samples with B2 lose more carbon in a given time, the resulting reduction in solid volume is larger. In addition, unlike the case of D2, the changes in pycnometric volume for the samples with B2 after oxidation fit quite well the volume loss due to oxidation of carbon which is calculated from the total weight loss. This good fit implies that there is no significant opening-up of closed pores during oxidation, or, in other words, the addition of a higher amount of carbon binder mainly results in an increase of open porosity rather than closed porosity.

(3) Loss of crushing strength

The values of cold crushing strength for the samples with B1 and B2 are plotted vs oxidation temperature in *Figure 4.20.* The difference in strength for the two types of samples becomes very small at 1400°C. This trend indicates that, besides the contribution of the difference in oxidation rate, the effect of carbon bonding on the overall strength becomes weak when the temperature is rather high. Also, because of the higher porosity in the samples with B2, the effect of reducing the loss of strength through sintering is not as obvious as that for the samples with B1 as the oxidation temperature reaches 1400°C.

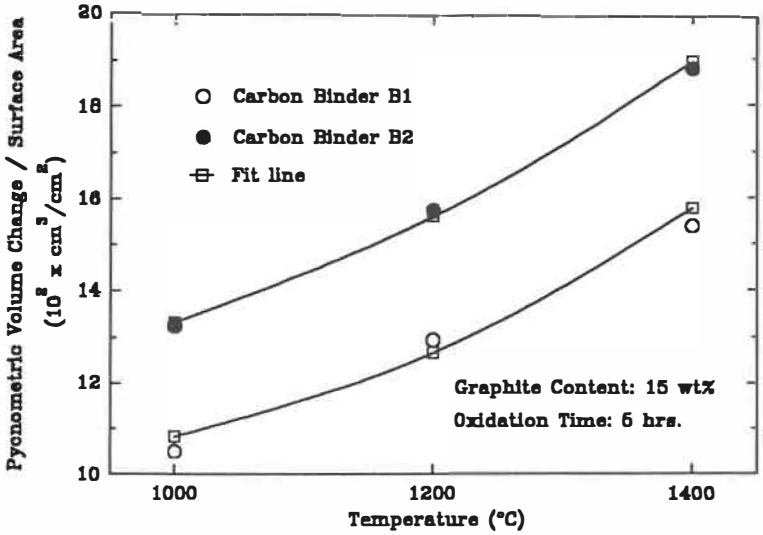

Figure 4.19 Change of porosity as a function of oxidation temperature for the brick samples (15 wt% graphite) with carbon binder either B1 (2.5 wt%) or B2 (3.5 wt%).

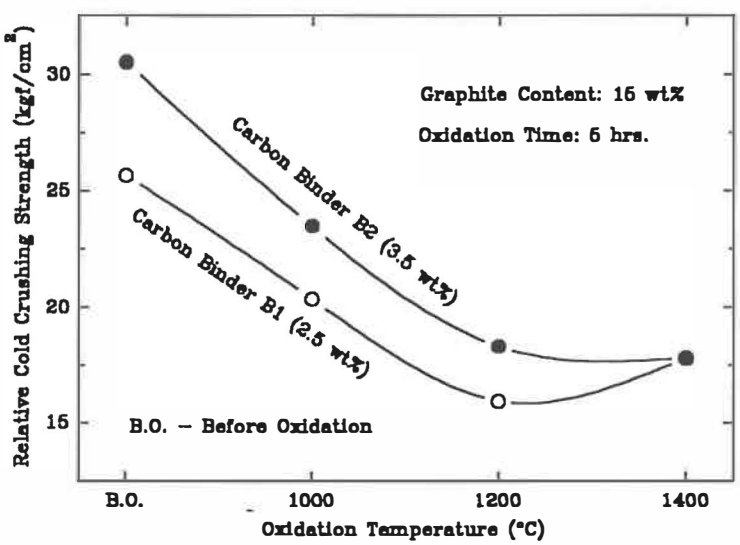

Figure 4.20 Loss of crushing strength as a function of oxidation temperature for the brick samples (15 wt% graphite) with carbon binder either B1 (2.5 wt%) or B2 (3.5 wt%).

In addition, the samples with B2 retain a higher strength until the temperature reaches 1400°C even though they have a larger extent of oxidation than the samples with B1. This fact shows that, like the cases before oxidation, the carbon bonding in the unoxidized part of the samples is still the determining factor on the overall strength of the oxidized samples when the temperature is below 1400°C.

4.3 Chapter Summary

The results presented in this chapter, which corroborate the findings of Lubaba et al.,[18,21,72] have clearly shown that the properties of MgO-C bricks change significantly during the process of carbonization, and the variations in brick composition result in noticeable differences in the changes of these properties. Among them, the difference in porosity change is most important in terms of the resistance to direct carbon oxidation. In fact, the work presented here appears to be the first research effort on correlating the changes of properties during carbonization with the resistance to direct carbon oxidation as a function of brick composition.

The results of this work (*Figure 4.1*) and those of Lubaba et al.[18] (*Figure 4.3*) have indicated that the increase of graphite content can lead to an increase in porosity after carbonization. Thus, an optimum graphite content exists in terms of the resistance to direct carbon oxidation. Although the total amount of graphite is important, the pore structure after loss of carbon, which depends on the arrangement of the MgO grains, is

also crucial. Increasing the graphite content can not only reduce the depth of decarbonized layer, or more precisely, the extent of decarbonizing penetration when the amount of oxygen available in a given time is unchanged, but also cause larger porosity increase and strength loss after loss of graphite phase. This effect will accelerate further decarbonization.

For MgO-graphite compacts, the size distribution of MgO grains is very important to the compaction. The results of this work (*Tables 4.1* and *4.2*) and those of Lubaba et al.[72] have shown that reducing the portion or size of maximum MgO grains can upset the optimum compacting and cause an increase in porosity. Although the use of more fine MgO grains can reduce the strength loss of the bricks when the oxidation temperature is not very high, the induced increase in porosity is destructive to the oxidation resistance. Thus, selection of a proper MgO grain size distribution is very important to both the mechanical strength and carbon oxidation resistance of MgO-graphite bricks and compromise has to be made in consideration of the overall performance.

The results presented in this chapter (*Figures 4.3* and *4.4*), in supplement to the findings of Lubaba et al.[21,72] (*Table 4.5*), have demonstrated that the increase of carbon binder content does not bring about a significant improvement of the strength, especially after firing at high temperatures, but the resistance to carbon burnout is really deteriorated due to the induced increase mainly in open porosity. Therefore, the amount

of binder in MgO-C refractories has to be kept to a minimum, and selection of a carbon binder with a high carbon yield, low amount of volatile materials, and small volumetric contraction during the process of pyrolysis can be beneficial.

On the other hand, in comparison with the effects of changing MgO grain-size distribution and increasing the amount of carbon binder in the present case, a major increase in open porosity due to adding more resin binder is more detrimental to oxidation resistance in terms of gaseous diffusion. Therefore, as can be expected, the samples with B2 have a deeper decarbonizing penetration than the samples with D2 under the same conditions of oxidation (see *Figure 4.21*).

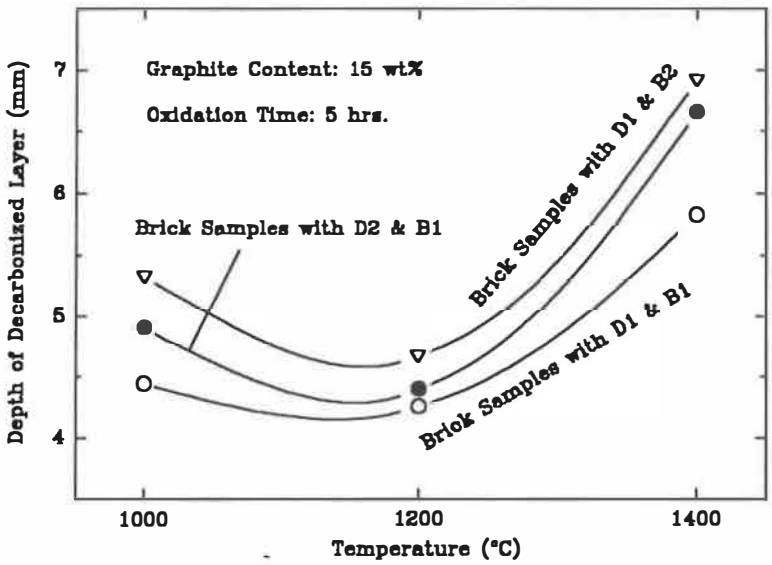

Figure 4.21 Comparison of the effect of changing either MgO grain size distribution (from D1 to D2) or amount of carbon binder (from B1 to B2) on the resistance of carbon oxidation.

As noted, Brant et al.[42] have also studied the physical properties of MgO-C bricks after carbonization at different temperatures, including bulk density, apparent porosity, pore size distribution, and permeability. However, the changes of these properties before and after carbonization as a function of brick composition have been neglected in their study, so that comparison with our results of carbonization is not made.

On the other hand, in the previous studies, Zoglmeyr,[38] Brant et al.,[42] and Velluet et al.[60] have also carried out oxidation tests in oxidizing atmosphere in the temperature range $\leq 1400^{\circ}C$, but their results are not suitable for comparison in terms of the values themselves due to the test conditions. In fact, they adopted either cubic or cylindrical samples for oxidation tests under a non-unidirectional condition, and the conditions of gas transfer of the oxidizing medium (including both convection and flow rate), which is important to the evaluation of oxidation resistance, were not well considered. Among their results, the weight loss is a relative measurement which is related to the geometry (both shape and size) of samples for testing. Although Velluet et al.[60] have also measured the depth of decarbonized layer for oxidized samples (cubes of 50-mm edge) after firing at 1200°C for 2 h in an oxidizing atmosphere, their measurements are not very meaningful because all the six faces of the cubic sample under testing are not in the same oxidation conditions in terms of gas convection, especially the bottom face of the cube.

However, in terms of the trends as a function of testing conditions, the results of

Zoglmeyr,[38] Brant et al.,[42] and Velluet et al.[60] are also in agreement with the results presented in this chapter. As already shown in *Figure 3.7*, Zoglmeyr[38] has found that the extent of carbon loss for carbonized samples at 1000°C also increases with oxidizing temperatures in the range 900~1400°C. The relations of weight loss as a function of temperature and carbon content are actually in agreement with the data presented in *Figure 4.7*. In addition, as shown in *Table 4.6*, Brant et al.[42] have reported that, after oxidizing brick samples with different carbon content at 1400°C for 10 h, the oxidized area decreases with carbon content, although the weight loss increases in the same direction. Therefore, they have also concluded that a higher amount of carbon per unit volume is oxidized for higher carbon content bricks, resulting in greater strength loss in the decarbonized area. The results presented in *Section 4.2.1* are in supplement to their above findings. Unfortunately, their samples were not carbonized before oxidation tests, so that the values of weight loss given in *Table 4.6* are composed of both loss of carbon materials and removal of volatile species.

Table 4.6 Oxidation behaviour of MgO-C bricks in air at 1400°C (from Brant et al.[42])

Chemical composition			
MgO (%)	90	85	80
Fixed C (%)	8	13	18
Oxidation 1400°C - 10 h			
Weight loss (wt%)	7.8	12.8	14.9
Oxidized area (%)	89	82	76

As a matter of fact, the test procedure for unidirectional oxidation developed

during this work has taken into consideration both the gas flow rate and direction of the oxidizing medium. The results obtained from measurements can be easily normalized and are better for characterizing and comparing brick properties because they reflect more directly the resistance to carbon oxidation for the bricks. The next chapter will show how meaningful these unidirectional oxidation tests are to the evaluation of oxidation kinetics.

CHAPTER V

Decarbonizing Kinetics in Direct Carbon Oxidation

Although the behaviour of decarbonization in MgO-C materials has been investigated intensively for the last decade, only a few researchers[48,49] have attempted to derive equations to describe the kinetic process. These studies were carried out in the range of temperature and atmosphere where the MgO-C interaction is dominant. Ozgen et al.[66,67] are the only researchers who have studied the kinetics of carbon burnout by oxygen, but in Al_2O_3-C materials. They followed the oxidation rate of graphite phase in the materials gravimetrically and isothermally at temperatures from 700 to 1200°C in air. In this work, the direct carbon oxidation was approached kinetically in MgO-C materials, but in a different way. The amount of CO_2 formed during oxidation in a given time was adopted as an indicator of carbon burnout rate. Also, unidirectional oxidation tests in air was carried out in a higher temperature range and under a controlled convection. The related experimental procedure has already been described in Chapter II. In this chapter, a presentation will be made of a diffusion-limited model for kinetics of direct carbon oxidation (i.e. carbon burnout in air), wherein the rate of diffusion-in of oxygen from the exterior is controlling. The important factors which affect significantly the overall reaction process of direct oxidation will be considered when developing the kinetic model. Then, the experimental fitness for our oxidation kinetic model will be discussed.

5.1 Kinetic Considerations of Decarbonizing Process

In this section, we are going to present our understanding of the decarbonizing process from a kinetic point of view, in the temperature range where both direct and indirect carbon oxidation may take place by control of either chemical reaction or diffusion. This understanding is based on the work of Lewis[73] concerning the oxidation of graphite materials and the experimental observations made during this work on the decarbonization of MgO-graphite bricks as a function of temperature and reaction time.

At the beginning of the decarbonizing process, the external surface of the original MgO-C brick is in direct contact with the atmosphere, and sufficient oxygen for oxidation is available if the atmosphere is oxidizing. When the temperature is still low, the intrinsic reactivity of carbon materials, especially the graphite, is low. Thus, although chemical reaction of C-O_2 occurs along with diffusion, the overall rate should be controlled by the intrinsic chemical reaction since the diffusion of the oxidant is relatively rapid so as to present a negligible resistance to the progress of decarbonization. On the other hand, due to the low chemical reaction rate, some of the oxygen could penetrate into a certain depth of MgO-C solid before reacting with carbon. However, MgO-C brick is initially rather nonporous, and deep penetration of oxygen into the compact structure is difficult. Therefore, oxidation can be considered to occur uniformly in a certain layer starting from the external surface. The activation energy of the overall process at this stage should be the same as the intrinsic value and is not dependent on physical

properties of the material. As a matter of fact, both Ozgen et al.[66] and we have observed that, after oxidation at 700°C in air, partially oxidized flakes are distributed uniformly in a layer at a certain depth into the surface of the graphitic materials (either Al_2O_3-C or MgO-C compacts), which confirms the above interpretation.

As the decarbonizing process continues, carbon will be consumed at the surface. Once a porous decarbonized layer forms at the external surface after carbon removal, decarbonization may proceed in the following steps:

1) external mass transport of reactant oxygen to the outer face of MgO-C material solid;
2) diffusion of oxygen through the pores in the decarbonized layer to reach the reaction interface;
3) chemical reaction between carbon solid and oxygen gas at reaction interface to form gaseous product;
4) diffusion of the gaseous product through the decarbonized layer to the outer face;
5) mass transfer of the gaseous product from external surface into the surrounding atmosphere.

As the thickness of the decarbonized layer increases, diffusion will exert a greater influence on the progress of decarbonization, and then the rate of chemical reaction will compete with that of diffusion. Due to the combination of increasing the reactivity of carbon and the resistance of gaseous diffusion with temperature and reaction time, there

will be a gradual transition from chemical-reaction control to diffusion control. When the intrinsic reactivity of carbon becomes so high that the gaseous reactant will react immediately with the carbon, the probability of oxygen molecules penetrating deeply into the original material before reacting with carbon becomes very small, and, consequently, the chemical reaction will occur at a macroscopic sharp boundary between the unreacted and the completely reacted layers. At this boundary, the gaseous reactant concentration drops to a very small value (or takes on its equilibrium value in the case of a reversible reaction). Meanwhile, only diffusion and reactions among gaseous species occur in the decarbonized layer because carbon solid reactant has already been completely consumed.

As the reaction interface moves inwards deeply, the pore diffusion gradually becomes the major resistance to the overall process. Meanwhile, the elevated temperature makes the chemical reaction step present a negligible resistance to the progress of decarbonization in comparison with the resistance due to pore diffusion. Consequently, the diffusion step becomes the slowest step and rate-determining. As discussed in Chapter III, in the diffusion-control stage during the process of decarbonization, there are two different dominant mechanisms of decarbonization, i.e. carbon burnout by oxygen (direct oxidation) and MgO-C interaction (indirect oxidation), depending on both temperature and atmosphere in the reaction system. In the range of low temperatures, inward diffusion of oxygen determines the rate of overall process when carbon burnout is dominant, while outward diffusion of Mg and CO vapours becomes controlling when

MgO-C interaction is prevailing in the range of high temperatures.

5.2 Important Parameters Affecting Kinetics of Direct Oxidation

Once the decarbonizing process is in the diffusion-controlled stage, the rate of carbon burnout by oxygen is largely dependent on the amount of carbon available to react (carbon content and distribution, graphite orientation, and carbon reactivity) and the amount of oxygen arriving at the reaction interface in a given time. The amount of oxygen arriving at the reaction interface is related to two factors: 1) the difference in Po_2 between the outer surface and reaction interface (the driving force of gaseous diffusion), and 2) the resistance to gaseous diffusion in the decarbonized layer which depends on the permeability or open porosity, the thickness of decarbonized layer, and the counter-diffusion of gaseous products. The Po_2 at the outer surface is a function of the gas composition (e.g. pure oxygen, air, neutral gas) and the condition of gas flow (including flow rate, direction of gas flow, and furnace configuration). The Po_2 at reaction interface could be considered as the equilibrium partial pressure of the reaction system at a given temperature because the rate of carbon oxidation is so fast that accumulation of oxygen at the interface is almost impossible. Of the above parameters, the amount of carbon available to react, the resistance to gaseous diffusion in the decarbonized layer, and the Po_2 at reaction interface are the characteristics of oxidation resistance of MgO-C materials. The Po_2 at the outer surface and reaction temperature belong to the external factors.

According to the above analysis, the overall rate of the process of direct carbon oxidation is considered to have three parallel components, namely:

1) the rate of gas phase mass transfer;
2) the rate of gaseous diffusion through the porous decarbonized layer;
3) the rate of chemical reaction occurring at the boundary separating the decarbonized and undecarbonized regions (reaction interface).

The rate of oxygen diffusion through the porous decarbonized layer is considered to be the most important element because the overall process is dependent on the slowest step.

In fact, the experimental data have shown that the change in Po_2 at the outer face of the oxidizing sample, which determines the driving force of the inward diffusion of oxygen, can significantly affect the rate of overall process of carbon burnout. As first evidence, the results in *Tables 3.2* and *3.3* of Chapter III have shown how greatly the change of oxygen concentration in the external atmosphere (all at the same flow rate) influences the rate of carbon burnout. The results in *Tables 5.1* and *5.2* also indicate the considerable effects of both the rate and direction of air flow, which are also related to the Po_2 at the outer surface of the oxidizing sample through the gas phase mass transfer. During oxidation on the front surface, the oxidizing face is frontly exposed to the air flow, while the oxidizing surface is rearly exposed to the air flow during oxidation on the back surface. As can be seen, such a change in orientation of the oxidizing surface with the direction of air flow has modified the rate of carbon burnout significantly.

Table 5.1 Effect of air flow rate on carbon burnout

Oxidation in air 1200°C - 10 h	At flow rate 500 ml/min	At flow rate 300 ml/min
Weight loss (g/cm^2)	0.52	0.41
Depth of decarbonized layer (mm)	8.80	6.93

Table 5.2 Effect of air flow direction (at the same flow rate) on carbon burnout

Oxidation in air 1200°C - 10 h	Oxidation on the front surface	Oxidation on the back surface
Weight loss (g/cm^2)	0.52	0.43
Depth of decarbonized layer (mm)	8.80	7.16

The difference in chemical reactivity for the two types of carbons in the bricks, i.e. secondary carbon and graphite flakes, can also influence the overall rate of the decarbonizing process. However, a review of the literature indicates that nobody has ever effectively measured the oxidation rates of both secondary carbon and graphite flakes in the bricks at the same time and then differentiated the contribution of secondary carbon to the overall rate of decarbonization from that of graphite flakes. Since the current work was unable to solve this problem either (after many trials), the issue was intentionally avoided by taking the step of pre-oxidation (as described in *Section 2.5* of Chapter II), and only the oxidation of the graphite phase in the bricks was considered.

5.3 Derivation of Mathematical Equations for Kinetics

Based on the above understanding of the process of direct carbon oxidation and the important parameters affecting the overall process rate, a mathematical model (as presented in this section) has been developed for oxidation kinetics of a planar surface (unidirectional oxidation) in the temperature range from 1000 to 1400°C, where the dominant mechanism of decarbonization, i.e. carbon burnout by oxygen, is determined by the inward diffusion of oxygen from the external atmosphere.

The time for the reaction-controlled stage is generally very short in the temperature range considered in our case and can usually be neglected. Thus, the following three main kinetic steps for the oxidation process have been considered: 1) mass transfer of oxygen in a gas flow (determining the oxygen concentration at the outer surface), 2) oxygen diffusion through the decarbonized layer (determining the amount of oxygen arriving at reaction interface in a given time), and 3) the intrinsic chemical reaction between graphite and oxygen at the reaction interface. *Figure 5.1* illustrates the general model showing all these three kinetic steps and lists the variables for the whole process of reaction.

5.3.1 Mass transfer of oxygen through gas flow

During the process of mass transfer of oxygen through gas flow, we assume that:

1) the air flows through the furnace tube (d = 70 mm) without friction;
2) the air flow is heated up from ambient temperature at the gas inlet T_1 to the

testing temperature at the outer surface of the oxidizing samples T_2;

3) the air flow obeys ideal gas law.

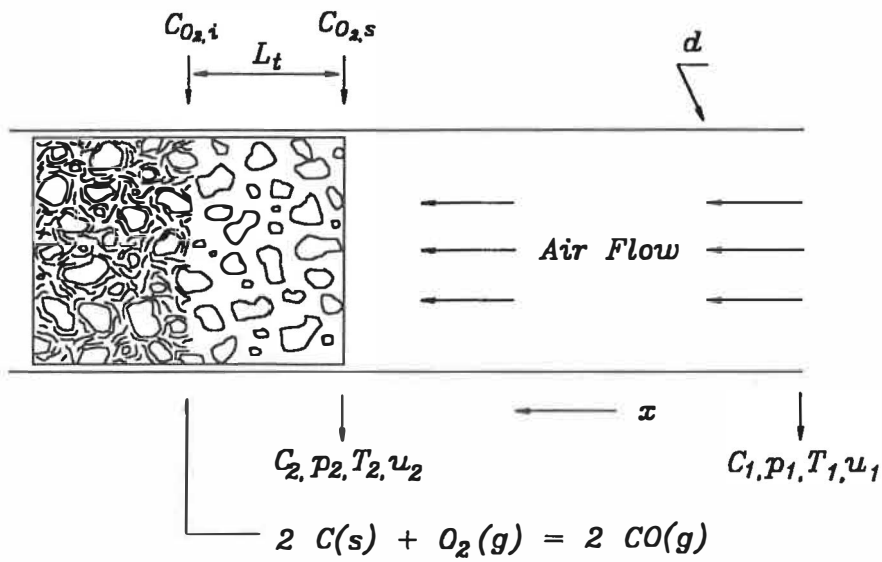

Figure 5.1 Schematic of the diffusion-controlled kinetic model for graphite oxidation in MgO-C refractories.

According to the above assumptions, the following governing equations can be derived based on the principles of fluid mechanics:

1) continuity equation

$$\frac{d}{dx}(Cu) = 0 \tag{5.1}$$

2) momentum equation

$$\frac{d}{dx}(Cu^2) + \frac{dp}{dx} = 0 \tag{5.2}$$

where C and p are the oxygen concentration and partial pressure, respectively, in the air

flow; u, the air flow velocity; and x, the distance of flow movement. The variations of u and p with temperature can be expressed as below:

$$u = M\sqrt{\gamma RT} \tag{5.3}$$

$$p = CRT \tag{5.4}$$

where M is March number, i.e. the ratio between flow velocity and sonic velocity; γ, adiabatic exponent, i.e. the ratio of the two specific heats of the gas, that at constant pressure, C_p, to that at constant volume, C_v (for air, $\gamma = 1.4$); R, gas constant; and T, absolute temperature. By solving *Equations 5.1* and *5.2* together with *Equations 5.3* and *5.4* (see Appendix II), we can have:

$$T_1 \left(\frac{1}{M_1} + \gamma M_1\right)^2 = T_2 \left(\frac{1}{M_2} + \gamma M_2\right)^2 \tag{5.5}$$

$$p_1 (1 + \gamma M_1^2) = p_2 (1 + \gamma M_2^2) \tag{5.6}$$

From the above two equations, the oxygen concentration arriving at the outer surface of an oxidizing sample through gas flow can then be obtained:

$$C_2 = \frac{p_2}{RT_2} \tag{5.7}$$

The known variables for the process of gaseous mass transfer in the present study are listed as below:

$p_1 = 0.21$ atm (Po_2 in air)

T_1 = 25°C (ambient temperature)

$u_1 = Q_1$ (500 ml/min) / A_1 (π(70 mm)^2/4)

Based on the above model of gaseous mass transfer, the C_2 (i.e. the oxygen concentration at the outer surface of an oxidizing sample) at a given testing temperature, T_2, can be calculated and the results are listed in *Table 5.3*.

Table 5.3 Oxygen concentrations at the outer surface of an oxidizing sample at different temperatures of oxidation through gaseous mass transfer of air flow

Temperature (°C)	1000	1100	1200	1300	1400
$C_{O2,s}$ (mole/m^3)	2.0104	1.8640	1.7374	1.6270	1.5297

5.3.2 Diffusion of oxygen through the decarbonized layer

Assuming that the process of diffusion is in steady state because the slow movement of the reaction interface makes the concentration of oxygen nearly independent of time and follows Fick's first law, the amount of oxygen diffusing from the outer surface to the reaction interface can be given by

$$\Phi_{O_2} = D_{eff} (C_{O_2,s} - C_{O_2,i})/L \qquad (5.8)$$

where Φ_{O2} is the mass flux density in mole/min/cm^2; D_{eff}, the effective diffusion coefficient of oxygen in cm^2/min; L, the thickness of the decarbonized layer in cm; ($C_{O2,s}$ - $C_{O2,i}$), the difference in oxygen concentration from the outer surface to the reaction interface. Here, only the case of diffusion without a temperature gradient is considered.

5.3.3 Chemical reaction rate

Assume the reaction of graphite oxidation which takes place at the interface proceeds according to

$$2\ C(s) + O_2(g) = 2\ CO(g) \tag{5.9}$$

If the oxidation is of first order with respect to gaseous reactants and products only, and the solid reactant, carbon, remains sufficient throughout the entire process of reaction, then the reaction rate can be expressed as the rate of disappearance of oxygen at the interface by chemical reaction as (see Appendix II)

$$R_{O_2} = k_c\ (C_{O_2,i} - \frac{C_{CO,i}}{K_E}) \tag{5.10}$$

where $\mathbf{R}_{O2}$ is the rate of chemical reaction of graphite oxidation, in moles of oxygen per unit time per unit surface area of MgO-C solid; k_c, the rate constant of chemical reaction; K_E, the equilibrium constant; and $C_{O2,i}$ and $C_{CO,i}$ denote the concentrations of gaseous reactant O_2 and product CO, respectively, at the reaction interface. The oxidation reaction is considered irreversible, i.e. K_E is large enough so that the term $C_{CO,i}/K_E$ tends to be zero; thus

$$R_{O_2} = k_c \cdot C_{O_2,i} \tag{5.11}$$

where $\mathbf{R}_{O2}$ is in mole/min/cm^2; k_c,- cm/min; and $C_{O2,i}$, mole/cm^3.

The rate of oxidation reaction may also be equated to the rate of disappearance

of solid carbon (in mole per time per area due to oxidation on the planar face), i.e.:

$$R_C = \frac{dn_C}{dt} \cdot \frac{1}{S} \tag{5.12}$$

$$= \frac{dW}{M_C dt} \cdot \frac{1}{S} \tag{5.13}$$

$$= \rho_m \cdot \frac{dL}{dt} \tag{5.14}$$

where ρ_m is the molar density of carbon in the solid MgO-graphite compact (mole/cm^3). Here assume that no structural change occurs in the decarbonized layer, and also, the weight change only corresponds to the burnout of the graphite.

According to the reaction of carbon oxidation *Equation 5.9*, we can have

$$R_C = 2R_{O_2} \tag{5.15}$$

or

$$\rho_m \cdot \frac{dL}{dt} = 2k_c \cdot C_{O_2,i} \tag{5.16}$$

5.3.4 Controlling step of the overall process

Assume that the overall process is limited by the slowest step, i.e. the diffusion of oxygen from the outer surface to the reaction interface, so that, as soon as the oxygen molecules arrive at the interface, they are consumed very quickly through chemical

reaction with graphite, and there is no accumulation of oxygen at the reaction interface. Then we have

$$\Phi_{O_2} = R_{O_2} \tag{5.17}$$

or

$$D_{eff}(C_{O_2,s} - C_{O_2,i})/L = k_c \cdot C_{O_2,i} \tag{5.18}$$

so we can solve

$$C_{O_2,i} = \frac{D_{eff}\, C_{O_2,s}}{D_{eff} + k_c L} \tag{5.19}$$

Combining *Equations 5.16* and *5.19*

$$\rho_m \cdot \frac{dL}{dt} = \frac{2k_c\, D_{eff}\, C_{O_2,s}}{D_{eff} + k_c L} \tag{5.20}$$

and then by integrating on both sides of the above equation after arrangement

$$\int_0^{L_t} \rho_m (k_c L + D_{eff}) dL = \int_0^t 2k_c\, D_{eff}\, C_{O_2,s}\, dt \tag{5.21}$$

the kinetic equation is finally stated as

$$\frac{\rho_m}{4D_{eff}\, C_{O_2,s}} L_t^2 + \frac{\rho_m}{2k_c\, C_{O_2,s}} L_t = t \tag{5.22}$$

Note that the advancement of the reaction interface during the process of oxidation obeys a parabolic law with reaction time according to the above kinetic model.

5.4 Experimental Results and Their Fit with Kinetic Modelling

In order to compare the kinetic model with experimental observations, another series of oxidation tests were conducted. So far, only the samples (D1-B1) with one level of graphite content, i.e. 15 wt%, were selected. To minimize the effect of secondary carbon, the samples were pre-oxidized in air at 400°C for 50 h after carbonization at 1000°C for 10 h in a CO atmosphere. This step was for the purpose of removing as much as possible secondary carbon, but keeping the graphite phase unreacted at the same time. The oxidation tests were carried out isothermally (in the temperature range from 1000 to 1400°C) and unidirectionally in a fixed air flow (dry air, $H_2O \leq 3$ ppm, CO_2 free) of 500 ml/min for 20 h. During the process of either heating-up or cooling-down, Ar gas (ultra high purity, >99.999%, $O_2 < 1$ ppm, $H_2O < 1$ ppm), instead of air, was circulated to prevent possible carbon loss. The volumetric concentrations of CO and CO_2 in the composition of the exhaust gas during oxidation were measured continuously. The weight losses of the oxidized samples were also measured after oxidation tests on a discontinuous basis. For other related details of the experimental procedure, Chapter II has a full description and illustrated schematics.

The measured bulk density and open porosity of brick samples with 15 wt% graphite before oxidation (after pre-oxidation) are 2.85 g/cm^3 and 12.67 vol%, respectively. According to the experimental data presented in Chapter IV, the graphite content before oxidation (after carbonization and then removal of secondary carbon) is

calculated as 15.08 wt%. Thus, the molar density of carbon in the samples for oxidation tests, ρ_m, is 0.0358 mole (C)/cm^3 (MgO-C). If graphite (natural flake) true density[74] is 2.29 g/cm^3, the graphite volume percentage in the samples approximates 18.77%.

5.4.1 Relations of thickness of decarbonized layer with reaction time

According to *Equation 5.9*, CO should be the only gaseous product released during carbon oxidation. The recorded CO and O_2 concentrations in the exhaust gas flow during oxidation are shown in *Figure 5.2*. At about 500°C, both CO and O_2 levels start to drop, and the CO concentration becomes almost zero when the temperature reaches 800°C. Based on this observation, a theory is proposed that once CO is generated at the reaction interface, CO diffuses outwards and reacts with oxygen from the air flow:

$$2\ CO(g) + O_2(g) = 2\ CO_2(g) \qquad (5.23)$$

This reaction converts CO to CO_2 by consuming O_2. Therefore, when the temperature rises above 800°C, the CO generated through carbon oxidation is converted totally to CO_2 so that the concentration of CO_2 represents directly the amount of carbon oxidized. However, during the diffusion of CO out of the decarbonized layer, the conversion of CO to CO_2 may consume a certain amount of oxygen and change its concentration profile in the decarbonized layer. This work assumes that the gas flow of CO is very strong so that the majority of conversion will occur outside the decarbonized layer. Thus, this effect of changing oxygen concentration profile in the decarbonized layer on the process of carbon oxidation can be neglected.

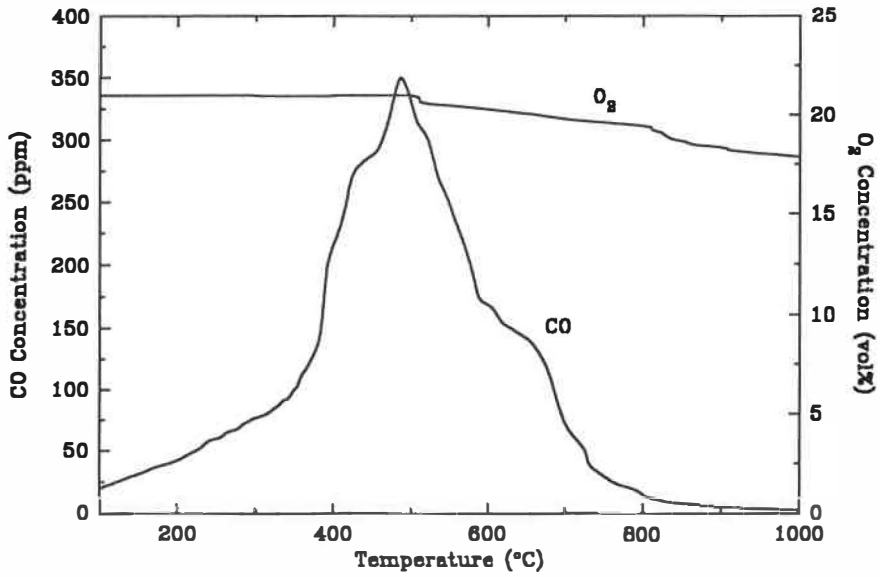

Figure 5.2 CO and O_2 concentrations in the exhausting gas flow during oxidation as a function of oxidation temperature.

Figure 5.3 shows the profiles of CO_2 concentration in volume percentage with the proceeding of oxidation, $CO_2vol\%(t)$, at temperatures 1000, 1200, and 1400°C. Since the total amount of CO_2 gas released from oxidation represents the total amount of burned carbon, the total weight loss, ΔW, which indicates the amount of burned carbon, after a given time, t, can be obtained:

$$\Delta W_t = \frac{QM_C}{V_M}\int_0^t CO_2vol\%(t)\ dt \qquad (5.24)$$

where Q is the volumetric flow rate of air; V_M, the molar volume of CO_2 gas; M_C, the molecular weight of carbon. Because this equation can not be integrated analytically, ΔW_t is calculated using the method of graphical integration:

$$\Delta W_t = \frac{QM_C}{V_M} \sum_{i=0}^{i=n} \frac{CO_2vol\%(t_i) + CO_2vol\%(t_{i+1})}{2}(t_{i+1} - t_i) \qquad (5.25)$$

The depth of the decarbonized layer, L_t, can be then calculated from ΔW_t, assuming that there is no structural change occurring in the decarbonized layer:

$$L_t = \frac{\Delta W_t}{\rho_m S M_C} \qquad (5.26)$$

where S is the original exposed surface area of the oxidizing sample during unidirectional oxidation. Combining *Equations 5.25* and *5.26* gives:

$$L_t = \frac{Q}{\rho_m S V_M} \sum_{i=0}^{i=n} \frac{CO_2vol\%(t_i) + CO_2vol\%(t_{i+1})}{2}(t_{i+1} - t_i) \qquad (5.27)$$

Figure 5.4 shows three curves of the L_t - t relations at 1000, 1200, and 1400°C, respectively, which are calculated from the results of CO_2 concentration profiles using the above equation.

We have adopted the method of nonlinear curve fitting to find out the values of coefficients A and B in the following equation from the L_t-t curves:

$$A\ L_t^2 + B\ L_t = t \qquad (5.28)$$

The Marquardt-Levenberg algorithm is used to determine the parameters A and B that minimize the sum of squares of differences between the dependent variable, t, for a given L_t and the experimental measurements at the tolerance 0.0001. The results of calculation for the values of A and B and their coefficients of variation CV% (i.e. the asymptotic

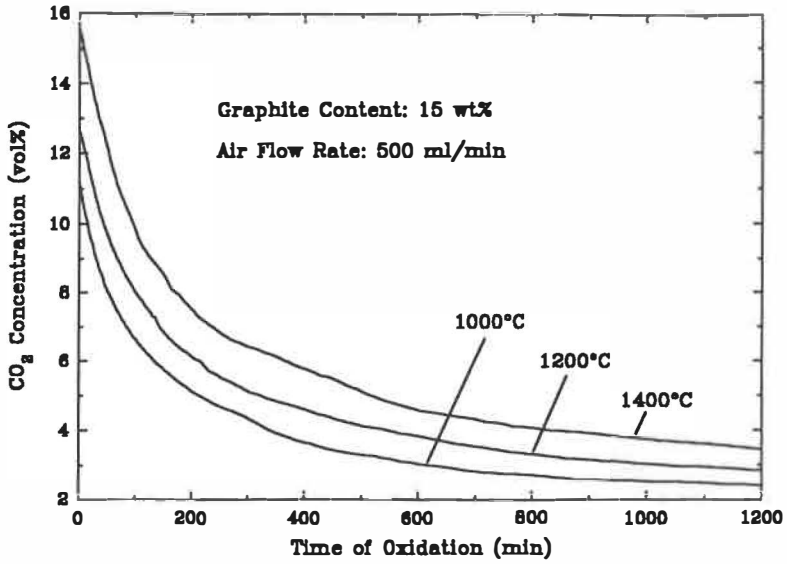

Figure 5.3 Variation of CO_2 concentration with reaction time as a function of oxidation temperatures.

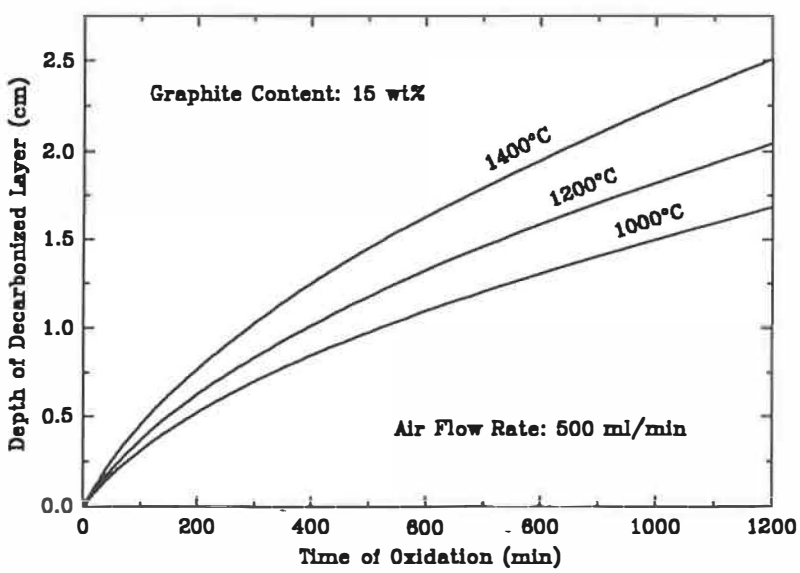

Figure 5.4 Variation of depth of decarbonized layer with reaction time as a function of oxidation temperatures.

standard error of the parameter divided by the parameter value and expressed as a percentage) are listed in *Table 5.4*. As can be seen, the experimental results fit rather well the parabolic laws, or say, the kinetic *Equation 5.22*.

Table 5.4 Values of coefficients A and B in *Equation 5.28* and their coefficients of variation, CV%, at different temperatures

Temperature (°C)	A (min/cm^2)	CV% for A	B (min/cm)	CV% for B
1000	288.9300	0.2329	228.8363	0.3374
1100	235.9286	0.2053	202.1401	0.3074
1200	189.3831	0.0818	200.7467	0.1097
1300	156.6613	0.0911	176.2848	0.1283
1400	126.4756	0.0982	161.4572	0.1336

5.4.2 Evaluation of D_{eff} and k_c

(1) Calculation of D_{eff} and k_c from experimental data

According to the kinetic *Equation 5.22*, the effective diffusion coefficient and rate constant of chemical reaction at a given temperature can be calculated from the coefficients of the quadratic and linear terms, respectively. The experimental values of the coefficients, i.e. A and B in *Equation 5.28*, are listed in *Table 5.4*. The oxygen concentrations at the surface, $C_{O2,s}$, of the oxidizing samples at different temperatures are given in *Table 5.3*. The carbon molar density of MgO-C samples, ρ_m, equals 0.0358. The results of calculation in the temperature range of 1000 to 1400°C are listed in *Table 5.5*.

Table 5.5 Values of the effective diffusion coefficients, D_{eff}, and rate constants of chemical reaction, k_c, at different temperatures (calculated from experimental data)

Temperature (°C)	1000	1100	1200	1300	1400
D_{eff} (cm^2/min)	15.4016	20.3430	27.1895	35.0989	46.2412
k_c (cm/min)	38.8924	47.4869	51.3008	62.3835	72.4450

(2) Theoretical prediction of gaseous effective diffusivity

Prediction of diffusivity for oxygen in CO

During the process of carbon oxidation, N_2 from air will not be involved in the oxidation reaction. We assume that N_2 diffuses from the outer face through the decarbonized layer to the reaction interface along with O_2, until the difference in concentration on both sides reaches zero, i.e. $\Delta C = 0$. On the other hand, CO gas generated from oxidation at the reaction interface will diffuse outwards through the decarbonized layer which is believed to be a major resistance to the inward diffusion of oxygen by counter-diffusion. Therefore, O_2 and CO molecules are chosen as the diffusion-gas-pair in the reaction system. Since both O_2 and CO are nonpolar gases, the Chapman-Enskog equation along with the Lennard-Jones constants (see Appendix II) may be used to predict the molecular diffusion coefficients for O_2 in CO, i.e. $D_{O2\text{-}CO}$, at the atmospheric pressure (P = 1 atm). The results of calculations for different temperatures are listed in *Table 5.6*.

Table 5.6 Theoretical prediction of diffusivity for oxygen in CO and in the porous decarbonized layer of brick samples with 15 wt% graphite at different temperatures

Temperature (°C)	1000	1100	1200	1300	1400
$D_{O2\text{-}CO}$ (cm^2/min)	143.71	162.92	183.06	204.11	226.06
D_{eff} (cm^2/min)	14.21	16.10	18.09	20.18	22.35

Diffusive mechanism in the porous decarbonized layer

Gas diffusion through porous materials occurs typically by one or more of three mechanisms: molecular (bulk, ordinary) diffusion, Knudsen diffusion, and surface diffusion. Molecular diffusion takes place when the pores of material are large enough so that the mean free path of the molecules of the gas becomes negligibly small. Molecular transport through the pores which are quite small so that the molecules of the gas collide with the pore walls much more frequently than with each other is described as Knudsen diffusion. In surface diffusion, the molecules of the gas are absorbed on the surface of the material and are subsequently transported from one site to another in the direction of decreasing concentration.

Szekely et al.[75] have indicated that once the molecular diffusion becomes predominant, the gaseous diffusivity through the porous media will be independent of the pore size. In MgO-C bricks, especially after oxidation, the structure of the decarbonized layer becomes very porous, and the pores are the size of graphite flakes or even larger due to the presence of flake aggregates. The results of Nacamu et al.[76] have confirmed

that the rate of carbon oxidation in MgO-C bricks is dependent on the volume of space available for diffusion (apparent porosity) and not on the nature of diffusion path (pore size distribution). This statement implies that molecular diffusion is predominant during the oxidation process. In addition, since the number of gas molecular collision increases as the temperature rises, Knudsen diffusion will become less important in the present case where the reaction of carbon oxidation takes place at high temperatures. Therefore, the approach taken here is to assume that the laws of molecular diffusion are obeyed in the porous decarbonized layer.

Tortuosity

In MgO-C materials, the pores are not an array of cylinders parallel to the diffusion path. Thus, the length of the tortuous diffusion path in real pores is greater than the distance along a straight line in the mean direction of diffusion. Moreover, the channels through which diffusion occurs are of irregular shape and of varying cross section. Both factors cause the flux to be less than would be possible in a uniform pore of the same length and mean radius. In such a case, an effective diffusion coefficient is defined which relates the flux per unit of face area of pores at any intersecting plane by using a single factor, which is termed the tortuosity factor, to allow for both varying direction of diffusion and varying pore cross section, i.e.:

$$D_{eff} = D_{O_2\text{-}CO} \frac{\varepsilon}{\tau} \tag{5.29}$$

where $D_{O2\text{-}CO}$ is the bulk gas phase molecular diffusivity of oxygen in CO; ε, the

porosity; and τ, the tortuosity of pore structure. Since the value of the factor, τ, is difficult to determine experimentally, Regan[77] has suggested that the τ value can be approximated by the term ε^{-1} giving:

$$D_{eff} = D_{O_2\text{-}CO}\ \varepsilon^2 \tag{5.30}$$

In the present case, the open porosity of the samples before oxidation is 12.67%, and the volume percentage of graphite phase is 18.77%; thus, the total porosity in the decarbonized layer is approximately 31.44% if the volume portion of closed porosity of the samples before oxidation is neglected. Taking the values of the bulk molecular diffusivity, $D_{O2\text{-}CO}$, at different temperatures (see *Table 5.6*), the values of D_{eff} can then be estimated based on the above theoretical prediction. The calculated results are also listed in *Table 5.6*.

(3) Comparison of theoretical prediction of D_{eff} with experimental values

The comparison of D_{eff} values from both experimental measurement and theoretical estimation is shown in *Figure 5.5*. As we can see, the experimental and calculated values are close at low temperatures. If the effect of closed porosity during calculating the theoretical D_{eff} from *Equation 5.30* is included, say there is 5% of initial closed porosity before oxidation, the total porosity after oxidation is then increased to about 36%, and the calculated D_{eff} is also raised. However, the difference between the experimental and calculated values becomes larger as the temperature rises. This divergence means that these two types of values have different temperature dependencies.

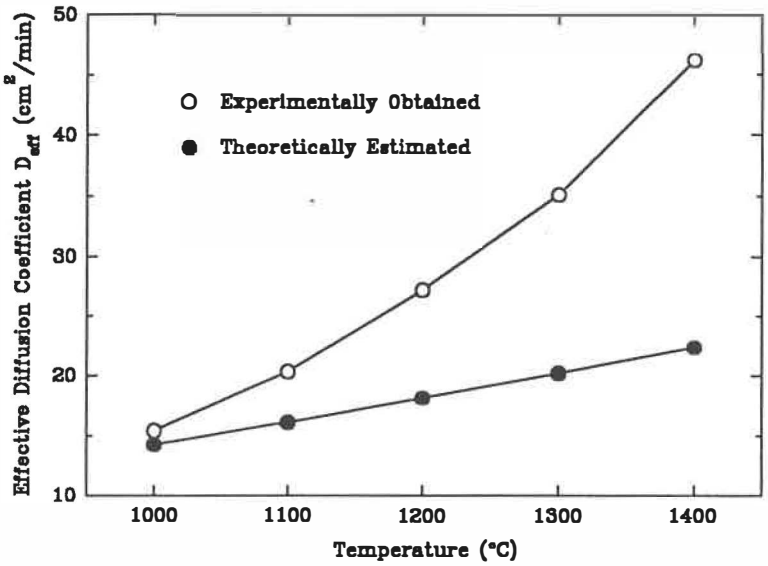

Figure 5.5 Comparison of effective diffusion coefficients obtained from either experimental measurement or theoretical estimation.

(4) Significance of k_c values

The values of k_c, representing the chemical reactivity of graphite, depend on both the physical (flake size) and chemical (impurity) properties of graphite, as well as the orientation of graphite flakes with respect to the direction of oxidation. The values obtained in the present study under the condition of unidirectional oxidation are the surface reaction rate constants (in the unit of cm/min), which are not comparable to the volume reaction rate constants (in the unit of min^{-1} or sec^{-1}) mostly obtained from non-unidirectional oxidation through thermogravimetric analysis. For example, the equation for the first-order rate constant for graphite oxidation in O_2 from Lewis[73] is 112 x 10^{14} exp (-60,000/RT) sec^{-1}; in this equation, R is in the unit of $Cal \cdot K^{-1} \cdot mole^{-1}$.

5.4.3 Temperature dependence of the oxidation process

The plots of both D_{eff} and k_c against the reciprocal of temperature are shown in *Figure 5.6*. By using an Arrhenius-type relationship, the values of activation energy for both D_{eff} and k_c are obtained through linear regression as bellow:

$$\Delta E\ (\ln k_c \sim 1/T) = 6.39 \text{ kcal/mole } (26.75 \text{ kJ/mole})$$

$$\Delta E\ (\ln D_{eff} \sim 1/T) = 11.58 \text{ kcal/mole } (48.46 \text{ kJ/mole})$$

According to Lewis,[73] for graphites containing less than 5 ppm impurities, the overall activation energy for the reaction with oxygen (at Po_2 = 1 atm) is between 60 and 62 kcal/mole, while for graphites containing about 150 ppm of impurities, the overall activation energy lies between 40 and 45 kcal/mole. In the present case, the graphite used is natural flakes with ash content as high as about 8 wt% (in the magnitude of 8×10^4 ppm), and the oxidizing agent is air with only 21% of oxygen. Therefore, the apparent activation energy for the chemical reaction with oxygen could drop to only 6.39 kcal/mole. These results also indicate that due to the presence of a large quantity of impurities, graphite can be very reactive, and its oxidation will become less temperature-dependent (i.e. its oxidation rate changes less with temperature). On the other hand, the smaller change in the k_c values with the increase of temperature in the present reaction system further supports the assumption that the rate of chemical reaction of graphite oxidation is largely limited by the slow rate of oxygen diffusion through decarbonized layer because the diffusion-controlled process has a lower activation energy than that of the chemical reaction-controlled process.[73]

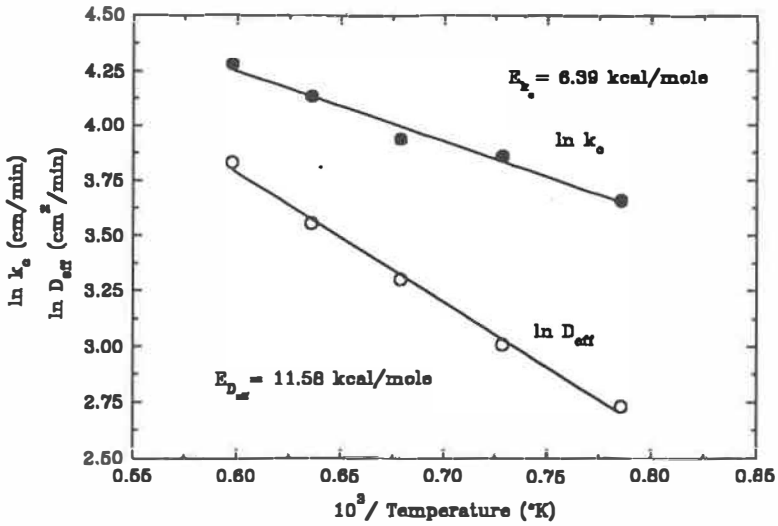

Figure 5.6 Arrhenius plots for the effective diffusion coefficients, D_{eff}, and chemical reaction rate constants, k_c.

From the theoretical calculation, during the process in which only diffusion takes place, the D_{eff} values are less temperature-dependent (*Figure 5.5*), and the calculated activation energy is only 4.79 kcal/mole. However, in this reaction system where both chemical reaction and diffusion occur concurrently, a higher activation energy for D_{eff} is obtained (11.58 kcal/mole). This higher value may be a result of the contribution of MgO-C interaction to the overall process as temperature increases. As discussed in Chapter III, the oxygen released through MgO decomposition can also oxidize carbon, giving off an extra amount of CO gas besides those from the reaction of carbon burnout. This MgO-C interaction will obviously accelerate the process of decarbonization. In fact, Tabata et al.[49] have reported that the value of activation energy for the process of decarbonization in which MgO-C interaction is rate-controlling (in the temperature range of 1300 to 1600°C in vacuum of 0.001 atm) is 35 kcal/mole for the samples with 10

wt% graphite. This value is greater than the one obtained in this case where decarbonization is mainly through direct oxidation. The activation energy from this case would be expected to increase as reaction temperature exceeds 1400°C due to the increasing contribution of the MgO-C interaction.

5.5 Chapter Summary

The kinetic model presented here is believed to be the first one to combine together the effects of mass transfer of gas flow, gaseous diffusion in porous media, and chemical reaction of carbon and oxygen for the process of carbon burnout in MgO-C materials. The kinetic model of oxidation of the graphite phase in Al_2O_3-C materials from Ozgen et al.[66,67] is expressed by the equation

$$f(\alpha) = 2k \frac{1}{F} \left(\frac{A}{V}\right)^2 \cdot t \tag{5.31}$$

where α is the fraction of graphite oxidized; F, a geometric factor; A, the external surface area of the material; V, its volume; and t, the reaction time. For an infinite slab of thickness, x_0, reacting on one face, $F = 1$, $(A/V)^2 = x_0^{-2}$, and $f(\alpha) = \alpha^2$; whereas for long cylinders of radius r_0, $F = 2$, $(A/V)^2 = 4r_0^{-2}$ and $f(\alpha) = \alpha + (1-\alpha)\cdot\ln(1-\alpha)$. The rate constant, k, is given by

$$k = \frac{2\, D_e C_{O_2}}{\theta_g\, \rho_m} \tag{5.32}$$

where D_e is the effective diffusivity of oxygen through the pore structure of the

decarbonized layer; C_{O2}, the oxygen concentration in the gas phase at the oxidizing surface; θ_g, the volume fraction of graphite in the material; and ρ_m, the molar density of the graphite phase. As can be seen, their kinetic model is rather different from the one developed in this work. In their equation, the fraction of graphite oxidized, α, is used as a variable to describe the extent of reaction, but the depth of decarbonized layer, L, is adopted in *Equation 5.22*. Note that α is a relative value depending on the total content of graphite and can only be calculated from the measurement of weight loss. As a result, their model is suitable for thermogravimetric analysis (as they used in their study) whose accuracy of measurement is greatly influenced by the gas flow. On the other hand, in their model, there is no equation developed to estimate the C_{O2} value which is strongly dependent on the mass transfer of the gas phase (e.g. flow rate, flow direction, and furnace geometry). As a matter of fact, the effects of these important factors have been neglected in their study. Furthermore, unlike the variable α, L is a structure-sensitive parameter and, thus, more meaningful to the description of a diffusion-controlled process in which the structure of diffusion path is crucial.

As presented in this chapter, the experimental results fit rather well with the rate equation of carbon burnout derived from the proposed model (i.e. *Equation 5.22*). On the other hand, note that the experimental values of D_{eff} from this work are close to those for oxidation of Al_2O_3-C materials in air, as obtained by Ozgen et al.[66,67] For their Al_2O_3-C compacts with 36 wt% graphite, the apparent effective diffusivity at 1000°C is 21

cm^2/min, compared to 15 cm^2/min for MgO-C samples with 15 wt% graphite in the present study. These two values are actually consistent considering the porosity in the decarbonized layer as a function of volume fraction of graphite phase. Moreover, as Ozgen et al. reported,[66,67] a value of 32.5 kcal/mole (136 kJ/mole) was obtained for the activation energy of D_{eff} in the temperature range $\leq 900^\circ C$. And once the temperature was over 950°C, the value became almost zero (no value was given). In the present study, the activation energy obtained is 12 kcal/mole in the temperature range 1000 ~ 1400°C. Since the rate constant, k, in *Equation 5.32* has a different physical meaning (in the unit of cm^2/min) from the k_c for this study (in the unit of cm/min), further comparison will not make sense.

Besides measuring CO_2 concentration, the conventional method, i.e. weight-loss measurement, was also used for comparison. Under the same conditions of unidirectional oxidation, the total weight losses of samples after oxidation were measured on a discontinuous basis. The values of depth of the decarbonized layer based on the measurement of either CO_2 concentration or total weight loss are shown in *Figure 5.7* for the case of 1200°C. Note that the depth values from these two different measurements are rather close at the beginning, and their difference becomes larger as oxidation proceeds. This divergence is mainly due to the uncertainty of the value of CO_2 molar volume V_M in the real case. In this work, the exhausting gas from oxidation is assumed to obey the ideal gas law; thus, the value of V_M is 22.41 l/mole at 0°C and

24.47 l/mole at 25°C. Based on the latter value, the total amount of carbon loss is then calculated by using *Equation 5.24*. Obviously, selecting a bigger value of V_M for calculation, the corresponding amount of carbon burnout from CO_2 vol% will be decreased, and this kind of decrease will be greater as reaction time increases.

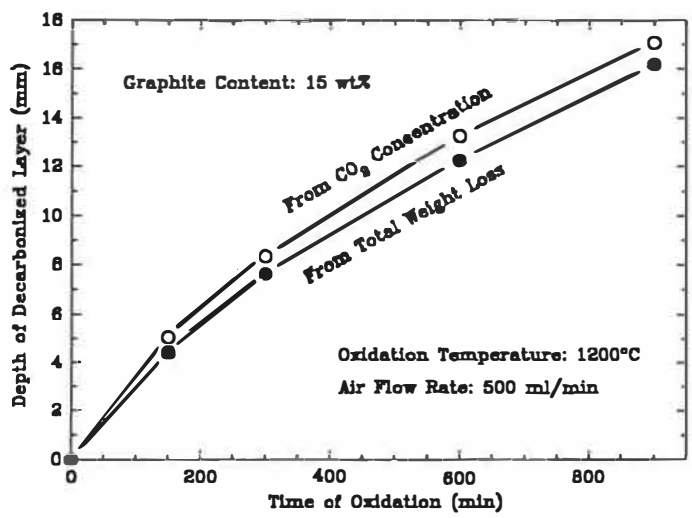

Figure 5.7 Values of depth of the decarbonized layer obtained from the measurement of either CO_2 concentration or total weight loss.

As can be seen, the kinetic model presented in this chapter is still rather crude and may be over-simplified to some extent. Apparently, further modifications are needed in order to better describe the overall rate of decarbonizing process in the real system. Using a numerical method to solve the unsteady state diffusion equation (Fick's second law) is one of the approaching directions. Also, both the graphite reactivity and orientation should be included in the parameter k_c. The theoretical calculation of D_{eff} should also be modified to meet the temperature-dependence of the experimental results from this work in consideration of the effect of chemical reaction.

On the other hand, decarbonization through MgO-C interaction has not been considered yet in the present kinetic model. As discussed in Chapter III, the material reactivity, especially MgO grains, determines largely the amount of Mg and CO vapours formed in a given time during the MgO-C interaction. Po_2 in the reaction system is also crucial because it not only affects the rate of MgO decomposition which provides the source of oxygen for decarbonization, but also controls the forming rate of MgO dense zone which limits the outward diffusion of Mg and CO vapours. Carniglia[48] and Ishibashi et al.[7] have realized, based on theoretical calculations and experimental results, respectively, that the MgO-C interaction has a higher activation energy in CO atmosphere than that in an inert atmosphere, although both of them did not explain clearly this difference. The evidence from this work suggests that this fact is due to the difference of Po_2 in the reaction system for these two cases; the lower Po_2 in CO atmosphere promotes the MgO-C interaction. As the temperature increases, the MgO-C interaction is greatly accelerated in CO atmosphere which shows a stronger dependence on the change of temperature. Therefore, extending the proposed kinetic model to a higher temperature range ($>1400^\circ C$) is necessary in order to cover both the decarbonizing mechanisms of carbon burnout and MgO-C interaction in consideration of the effects of material reactivity, Po_2 in the reaction system, and gaseous diffusion. The bias between the predictions from the extended model with the experimental data based on the measurement of CO_2 concentration also needs to be evaluated.

CHAPTER VI

Roles of Antioxidants (Al, Si, and SiC) on Carbon Protection

Although the addition of antioxidants is widely adopted as a means of improving the performance of MgO-C refractories in service, the roles of antioxidants on carbon protection are still not very clear. This chapter is intended to provide a new insight of how the antioxidants evolve during the process of decarbonization. Based on the understanding of the mechanisms of decarbonization with the changes of both temperature and atmosphere (as discussed in Chapter III) and the important parameters controlling the overall rate of decarbonization (as discussed in Chapters III, IV, and V), the roles of single antioxidants (Al, Si, and SiC, all at 4 wt%, added individually) are addressed along with the discussion of previous studies. As will be seen, the antioxidants do not always behave positively in protecting the carbon materials in MgO-C refractories.

6.1 Changes of Properties due to Reactions during Carbonization

Because of the importance of the carbonization process as discussed in Chapter IV, the reactions of antioxidants with both brick constituents and the atmosphere in the reaction system during carbonization and the changes of properties which result from these reactions have been investigated in the present study. The changes in both weight and pycnometric volume of brick samples with or without antioxidants due to the process

of carbonization are listed in *Table 6.1*. As can be seen, in comparison to the case without additives, the changes in both weight and pycnometric volume are not the same if the antioxidants are present. The phases identified through the x-ray diffraction (XRD) analysis in the samples after carbonization are listed in *Table 6.2*. In fact, the difference in the changes of properties as shown in *Table 6.1* is a reflection of the formation of new phases, i.e. Al_4C_3, $MgAl_2O_4$, SiC, and Mg_2SiO_4 in the samples with antioxidants (see *Table 6.2*), indicating that the reactions of antioxidants have already taken place in the interior of samples. In the following, explanations of what reactions could occur and how these reactions affect the changes of sample weight and volume during carbonization will be presented.

Table 6.1 Comparison of the changes in the weight and volume of samples due to the process of carbonization at 1000°C for 10 h with or without antioxidants

Type of antioxidant	No additive	With Al	With Si	With SiC
Weight change ($\Delta W/W_0$ %)	-1.70	-1.57	-1.62	-1.67
Pycnometric volume change ($\Delta V/V_0$ %)	-5.54	-6.12	-4.92	-5.40

During the compaction process, a certain amount of air or oxygen is trapped in the pores of bricks. As the temperature rises during carbonization, this small amount of oxygen is quickly consumed to establish an equilibrium of C-O_2-CO-CO_2 within the material. From the thermochemical calculations shown in *Figure 3.1*, CO gas will be

prevailing at such an equilibrium when the temperature reaches above 700°C. Under such a strong CO atmosphere, antioxidants become unstable and can be transferred to their oxides. *Figures 6.1* and *6.2* show the results of our thermochemical calculations for the equilibrium Pco at which $MgO \cdot Al_2O_3$ (MA) or $2MgO \cdot SiO_2$ (M_2S) is formed, assuming that the activity of all solids in the reaction system is unity. The top line represents the equilibrium Pco for the C-O_2-CO-CO_2 system. As can be seen, the minimum Pco required to further oxidize Al and Al_4C_3 to MA, or Si and SiC to M_2S are much lower than that generated by the equilibrium of C-O_2-CO-CO_2 at the same temperature (at a total pressure of 1 atm). Therefore, thermochemically, both Al and Al_4C_3 (if there is any formed), or Si and SiC, can not coexist with carbon because of the high Pco generated in the reaction system; or kinetically speaking, as long as the reaction time is long enough or the temperature is high enough, more and more oxides can form in the interior of bricks by the antioxidants added. The possible reactions for Al, Si, and SiC additions will be discussed respectively in the following.

Table 6.2 Results of XRD analysis on antioxidant-containing samples after carbonization at 1000°C for 10 h

Phases detected (listed in descending order of peak height)		
With Al addition	With Si addition	With SiC addition
MgO Graphite Al_4C_3 $MgAl_2O_4$	MgO Graphite Si SiC Mg_2SiO_4	MgO Graphite SiC

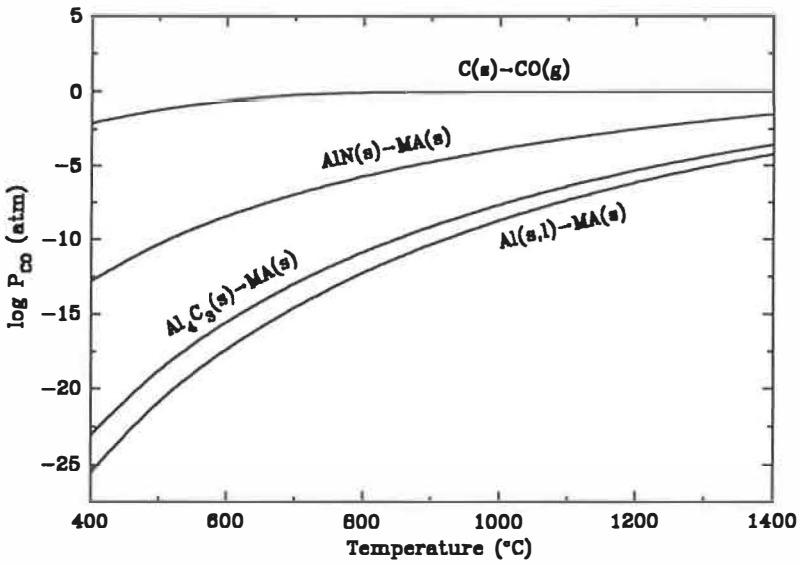

Figure 6.1 Equilibrium partial pressures of CO for the reactions forming spinel, $MgO \cdot Al_2O_3$ (MA), or for carbon oxidation at different temperatures.

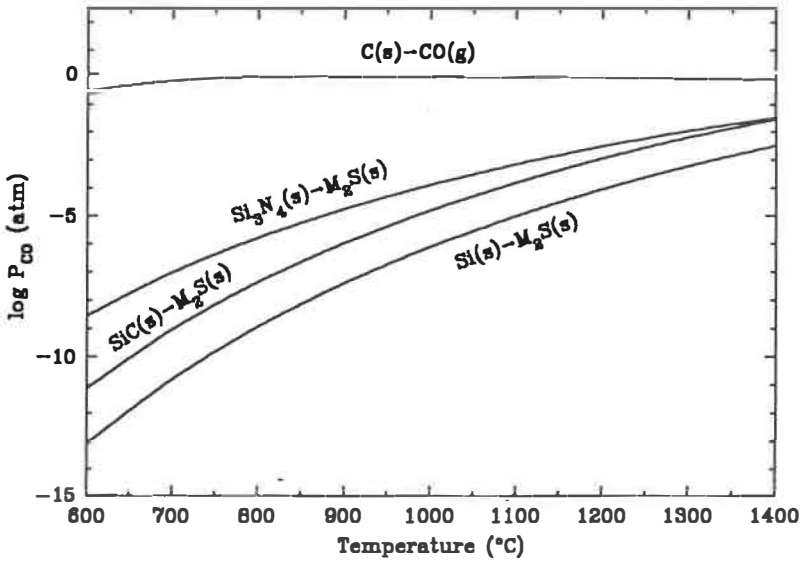

Figure 6.2 Equilibrium partial pressures of CO for the reactions forming forsterite, $2MgO \cdot SiO_2$ (M_2S), or for carbon oxidation at different temperatures.

Addition of Al

According to Yamaguchi,[78] as the temperature rises to above 700°C, Al metal, mostly in the liquid state (the melting point is 660°C), will first react with carbon to form Al_4C_3 if there is carbon in direct contact:

$4\ Al(l) + 3\ C(s) = Al_4C_3(s)$ $(\Delta G^\circ_{1000^\circ C} = -155\ kJ)$

If there is no carbon nearby, Al metal may be converted directly to Al_2O_3, or further to spinel MA, when an enough Pco is established in the system by the carbon materials at a higher temperature:

$2\ Al(l) + 3\ CO(g) = Al_2O_3(s) + 3\ C(s)$ $(\Delta G^\circ_{1000^\circ C} = -598\ kJ)$

$2\ Al(l) + MgO(s) + 3\ CO(g) = MgAl_2O_4(s) + 3\ C(s)$ $(\Delta G^\circ_{1000^\circ C} = -635\ kJ)$

Brant et al. have reported[79] that MA starts to form at temperature as low as 900°C where CO begins to reach its maximum pressure, thermochemically, in the $C\text{-}O_2\text{-}CO\text{-}CO_2$ system (see *Figure 3.1*). As the Pco increases with temperature, the Al_4C_3 formed will also become unstable due to the reactions:

$Al_4C_3(s) + 6\ CO(g) = 2\ Al_2O_3(s) + 9\ C(s)$ $(\Delta G^\circ_{1000^\circ C} = -1040\ kJ)$

$Al_4C_3(s) + 6\ CO(g) + 2\ MgO(s) = 2\ MgAl_2O_4(s) + 9\ C(s)$ $(\Delta G^\circ_{1000^\circ C} = -1114\ kJ)$

On the other hand, if the vapour species Al(g) or/and C(g) are present, as claimed by Yamaguchi,[78,80] Al and C may not necessarily have to be in contact with each other in order to form Al_4C_3 due to the following reactions:

$4\ Al(g) + 3\ C(s) = Al_4C_3(s)$ $(\Delta G^\circ_{1000^\circ C} = -805\ kJ)$

$4\ Al\ (l) + 3\ C(g) = Al_4C_3(s)$ $(\Delta G^\circ_{1000^\circ C} = -1709\ kJ)$

$4\ Al(g) + 3\ C(g) = Al_4C_3(s)$ $(\Delta G^\circ_{1000^\circ C} = -2359\ kJ)$

However, the above reactions appear to be not significant because of the low partial pressures of Al(g) or/and C(g) when the temperature is still rather low. For example, at 1000°C, $P_{Al} = 2.143 \times 10^{-7}$ atm and $P_C = 5.803 \times 10^{-22}$ atm. In addition, the transportation of Al liquid to the position of carbon seems to be also a rather limited possibility because of the dense structure of MgO-C bricks. Thus, the chance of forming Al_4C_3 by either gas or liquid diffusion should be very small, and its formation is mostly limited to the local regions where Al and carbon is in direct contact. These factors increase the possibility of direct oxidation of Al metal by CO gas. As a result, a rather large amount of spinel is formed in the samples with Al addition after carbonization at 1000°C.

However, if the temperature of carbonization becomes relatively high, say 1600°C as used by Brant et al.,[14] the role of Al(g) may not be neglected because Al(g) is the most volatile vapour species for Al metal, and its partial pressure can reach an ineligible level (at the level of above $\sim 10^{-8}$ atm, in terms of thermogravimetric analysis[81]) when the temperature is high enough (see *Table 6.3*). In this case, the following reactions may occur through Al vapour:

$4\ Al(g) + 3\ C(s) = Al_4C_3(s)$ $(\Delta G^\circ_{1000^\circ C} = -805\ kJ)$

$2\ Al(g) + MgO(s) + 3\ CO(g) = MgAl_2O_4(s) + 3\ C(s)$ $(\Delta G^\circ_{1000^\circ C} = -798\ kJ)$

Table 6.3 Change of Al vapour pressure as a function of temperature

Reaction	Al(l) = Al(g)			
Temperature (°C)	1000	1200	1400	1600
Equilibrium P_{Al} (atm)	2.143×10^{-7}	1.087×10^{-5}	2.112×10^{-4}	2.141×10^{-3}

Addition of Si

When the temperature is high enough (about 900°C according to Brant et al.[79]), the in-situ SiC can form by direct reaction of silicon and carbon which are in intimate contact in the brick matrix:

$Si(s) + C(s) = SiC(s)$ $(\Delta G^{\circ}_{1000^{\circ}C} = -63\ kJ)$

Besides, the high Pco generated in the presence of carbon can also transform Si and in-situ formed SiC to forsterite (M_2S) by the reactions:

$Si(s) + 2\ MgO(s) + 2\ CO(g) = Mg_2SiO_4(s) + 2\ C(s)$ $(\Delta G^{\circ}_{1000^{\circ}C} = -296\ kJ)$

$SiC(s) + 2\ MgO(s) + 2\ CO(g) = Mg_2SiO_4(s) + 3\ C(s)$ $(\Delta G^{\circ}_{1000^{\circ}C} = -233\ kJ)$

According to these reactions, a higher Pco is more thermochemically favourable for the formation of M_2S, and at a lower Pco SiC is formed more easily.

At a sufficient Pco and temperature, SiO(g) could be generated at the Si grain surface through the reaction:

$Si(s) + CO(g) = SiO(g) + C(s)$ $(\Delta G^{\circ}_{1000^{\circ}C} = +15\ kJ)$

The SiO vapor formed will diffuse away from Si grains and react with either C or MgO:

$SiO(g) + 2\ C(s) = SiC(s) + CO(g)$ $(\Delta G^{\circ}_{1000^{\circ}C} = -78\ kJ)$

$SiO(g) + 2\ MgO(s) + CO(g) = Mg_2SiO_4(s) + C(s)$ $(\Delta G^\circ_{1000^\circ C} = -311\ kJ)$

However, during carbonization at 1000°C, the formation of SiO vapour would not expect to be significant because its vapour pressure is very low.

Addition of SiC

Although SiC is also thermochemically unstable during carbonization at 1000°C, the oxidation of SiC through the reaction:

$SiC(s) + 2\ MgO(s) + 2\ CO(g) = Mg_2SiO_4(s) + 3\ C(s)$ $(\Delta G^\circ_{1000^\circ C} = -233\ kJ)$

or even the reactions:

$SiC(s) + CO(g) = SiO(g) + 2\ C(s)$ $(\Delta G^\circ_{1000^\circ C} = +78\ kJ)$

$SiO(g) + 2\ MgO(s) + CO(g) = Mg_2SiO_4(s) + C(s)$ $(\Delta G^\circ_{1000^\circ C} = -311\ kJ)$

actually proceeds very slowly because of the kinetic factors (e.g. chemical reactivity).

In fact, the experimental results in *Tables 6.1* and *6.2* have shown both the physical and chemical evidences of above oxidation reactions of antioxidants. From the results of XRD analysis after carbonization, both Al_4C_3 and MA were present in the samples with Al additive, and SiC and M_2S were also identified in the samples with Si additive. Because the antioxidants are oxidized by absorbing the gaseous species, CO, from the atmosphere, a weight gain is added to the samples, which contributes to a less total weight loss after carbonization in comparison with the samples without additive. Thus the more antioxidant that is oxidized, the lower is the total weight loss. In the case

of SiC addition, only a small weight gain contribution was recorded, but the amount of M_2S formed was not enough to be detected by the XRD analysis.

In the case of no additive, the reduction of pycnometric volume is mainly due to the increase of porosity by the removal of volatile species during carbonization and the effect of graphite irreversible expansion. When antioxidants are present, the formation of oxides, either MA or M_2S, during carbonization can result in an increase of solid volume, reducing the apparent porosity by a mechanism of pore filling. As shown in *Table 6.2*, this situation is typical in the case of Si addition, i.e. a smaller reduction in pycnometric volume. Since the difference in weight loss is relatively small when SiC is present, the reduction of porosity due to the oxidation of SiC is also not significant. However, when the expansion of solid volume due to the formation of new solid phases can not be accommodated by the pore structure because of a large amount of reaction, an increase in porosity is expected as in the case with Al addition.

When the carbonized (at 1000°C for 10 h) samples are fired again at 1200°C in CO atmosphere for another 5 h (further carbonization), the results in *Table 6.4* indicate that the weight loss due to carbon oxidation is rather small in the samples without any additive. This situation is because the amount of measured weight loss also includes the further loss of volatile species after firing at 1200°C (the samples were initially carbonized only at a lower temperature, i.e. 1000°C). For the samples with antioxidants,

however, a considerable weight gain was recorded; the samples with Al addition having the highest one. These weight gains are believed to be due to the oxidation of additives by CO gas from the atmosphere or generated inside the samples. For example, in the samples with Si addition both the amounts of M_2S and SiC are increased while that of Si is reduced after further firing in CO (see *Figure 6.3*, the XRD results). As a result of oxidation of additives, the sample volumes are further expanded (see *Table 6.4*). In addition, the amounts of both weight gain and volume expansion follow exactly the order of chemical reactivity of the additives during oxidation, i.e. Al > Si > SiC.

In practice, most MgO-C lining bricks will undergo the process of carbonization inevitably through thermal cycling before they become the surface of furnace lining where they are exposed directly to an oxidizing atmosphere. As discussed above, reactions of antioxidants with other brick components or the gases in the reaction system occur during this process, changing the forms of antioxidants and also the properties of bricks. Obviously, these changes will have a great influence on their roles on carbon protection in the later stage when the oxygen invades from the exterior. This subject will be discussed in the next section.

6.2 Effect of Antioxidants on Direct Carbon Oxidation

In this section, the experimental results of oxidation in air in the temperature range, 1000 ~ 1400°C, will be presented first in *Section 6.2.1*, which will be followed by

Table 6.4 Comparison of the changes in weight and volume of carbonized (at 1000°C for 10 h) samples after firing in CO at 1200°C for 5 h

Type of antioxidant	No additive	With Al	With Si	With SiC
Weight change ($\Delta W/W_0$ %)	-0.02	+2.51	+2.12	+0.30
Pycnometric volume change ($\Delta V/V_0$ %)	+0.05	+3.20	+2.21	+1.17

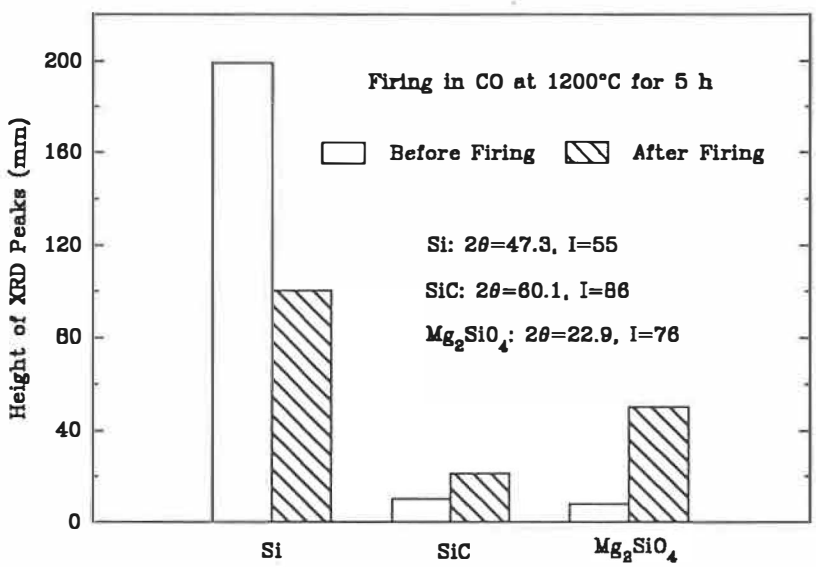

Figure 6.3 Comparison of results of XRD analysis (relative intensities of peaks) for the carbonized (at 1000°C for 10 h) samples with Si addition before and after firing in CO atmosphere.

the discussion of these results in *Sections 6.2.2*, *6.2.3* and *6.2.4*, considering both the physical and chemical roles of antioxidants and also the effect of N_2 in air.

6.2.1 Changes of properties during oxidation

A series of oxidation tests were carried out on the carbonized (at 1000°C for 10 h) samples containing different antioxidants. After oxidation in air for 5 h at 1000, 1200, and 1400°C, respectively, the depth of the decarbonized layer for each sample was measured, and their values are listed in *Table 6.5* in comparison with the samples without additive. The results indicate that the addition of Al metal does not reduce significantly the depth of the decarbonized layer, although a better result (smaller depth of the decarbonized layer) was achieved at the lower temperatures. The presence of Si metal or SiC powder considerably hindered the decarbonizing penetration only when the temperature reached 1400°C.

The comparisons of weight and pycnometric volume changes before and after oxidation process are also given in *Tables 6.6* and *6.7*, respectively. In the case of Al addition, the weight losses are much lower than those of samples without additive, although their depths of the decarbonized layer are quite close (see *Table 6.5*). The tendency for the changes of pycnometric volume is also similar. Note that for the samples with Si addition the overall weight change after oxidation at 1400°C is a weight gain although loss of carbon does take place.

Table 6.5 Comparison of the decarbonized layer depths (mm) of carbonized samples after oxidation in air at given temperatures for 5 h

Temperature (°C)	No Additive	With Al	With Si	With SiC
1000	4.44	4.31	4.38	4.43
1200	4.26	4.20	4.13	4.23
1400	5.83	5.82	4.53	5.10

Table 6.6 Comparison of weight changes ($\Delta W/W_0$ %) of carbonized samples after oxidation in air at given temperatures for 5 h

Temperature (°C)	No Additive	With Al	With Si	With SiC
1000	-2.09	-0.92	-1.55	-2.05
1200	-2.47	-0.44	-0.27	-2.12
1400	-3.00	-0.37	+0.28	-0.87

Table 6.7 Comparison of pycnometric volume changes ($\Delta V/V_0$ %) of carbonized samples after oxidation in air at given temperatures for 5 h

Temperature (°C)	No Additive	With Al	With Si	With SiC
1000	-2.82	-2.05	-2.51	-2.79
1200	-3.39	-0.79	-0.46	-2.15
1400	-4.28	-1.42	-0.17	-0.33

The phases present in both the decarbonized and undecarbonized layers after oxidation were examined by the XRD analysis. The results are listed in *Tables 6.8*, *6.9* and *6.10*, respectively. Generally speaking, because of the oxidation of antioxidants by either O_2 or CO, depending on the region where they are located, i.e. either decarbonized (in O_2) or undecarbonized (in CO) region, the amount of oxides is increased as the oxidation temperature rises. AlN is formed only in the undecarbonized layer where the amount of Al_4C_3 is reduced and MA is increased with temperature. At 1400°C, all Si and SiC (either formerly added or formed later) are converted to M_2S in the decarbonized layer since no Si or SiC can be detected (see *Tables 6.9* and *6.10*).

In order to study the effect of the carbonization process on the oxidation of antioxidants, another series of oxidation tests were carried out, for comparison, on the samples from as-received bricks. Direct oxidation of the uncarbonized samples with and without antioxidants was conducted at 1200° for 10 h. Instead of changing CO (during heating) to air (during oxidation) and then back to CO (during cooling), air was circulated throughout the entire process of direct oxidation. The results of direct oxidation on the as-received brick samples, as listed in *Table 6.11*, clearly show the improvement of oxidation resistance, i.e. significant decrease in the depth of the decarbonized layer in the presence of antioxidants, compared to the results in *Table 6.5*. This information provides a new insight on how the evolution of antioxidants during carbonization affects their roles on carbon protection in the later stage.

Table 6.8 Results of XRD analysis on oxidized samples with Al addition in the regions of both decarbonized layer (D.L.) and undecarbonized layer (U.L.)

	Relative height of the peak (mm)					
Oxidation in air for 5 h	1000°C		1200°C		1400°C	
Phase	D.L.	U.L.	D.L.	U.L.	D.L.	U.L.
Al_4C_3 $2\theta = 40.1$ $I = 83$	10	27	4	15	0	11
$MgAl_2O_4$ $2\theta = 19.0$ $I = 35$	35	29	46	32	77	37
AlN $2\theta = 33.1$ $I = 100$	0	5	0	11	0	32

Table 6.9 Results of XRD analysis on oxidized samples with Si addition in the regions of both decarbonized layer (D.L.) and undecarbonized layer (U.L.)

	Relative height of the peak (mm)					
Oxidation in air for 5 h	1000°C		1200°C		1400°C	
Phase	D.L.	U.L.	D.L.	U.L.	D.L.	U.L.
Si $2\theta = 47.3$ $I = 55$	128	172	58	94	0	5
SiC $2\theta = 60.1$ $I = 86$	5	15	3	26	0	35
Mg_2SiO_4 $2\theta = 22.9$ $I = 76$	20	12	108	41	175	71

Table 6.10 Results of XRD analysis on oxidized samples with SiC addition in the regions of both decarbonized layer (D.L.) and undecarbonized layer (U.L.)

	Relative height of the peak (mm)					
Oxidation in air for 5 h	1000°C		1200°C		1400°C	
Phase	D.L.	U.L.	D.L.	U.L.	D.L.	U.L.
SiC $2\theta = 60.1$ I = 86	31	36	17	22	0	14
Mg_2SiO_4 $2\theta = 22.9$ I = 76	9	0	20	15	87	43

Table 6.11 Effects of antioxidants on direct oxidation of uncarbonized brick samples (as-received) with 15 wt% graphite in air at 1200°C for 10 h

Direct oxidation in air (1200°C x 10 h)	Without additive	With Al addition	With Si addition	With SiC addition
Depth of decarbonized layer (mm)	10.14	7.56	8.86	9.08
Total weight loss (%)	7.16	3.89	4.49	5.46

To summarize, during the process of oxidation, chemical reactions of antioxidants take place in both the decarbonized and undecarbonized layers which lead to great changes in both physical properties and phase compositions as a function of temperature. As a result, the antioxidants play both chemical and physical roles on carbon protection.

6.2.2 Chemical roles of antioxidants

(1) Oxidation of antioxidants by oxygen

As discussed in Chapter III, in the temperature range where direct carbon oxidation is dominant ($\leq 1400^{\circ}C$), carbon burnout can be significantly suppressed by reducing the Po_2 or/and increasing the Pco in the reaction system. Thus, from the chemical point of view, the desirable situation for the addition of antioxidants is that, when carbon is about to be attacked by oxygen, the antioxidants as well as their carbides formed during carbonization will preferentially react with oxygen and produce CO, i.e.:

$$4\ Al(s,l) + 2\ MgO(s) + 3\ O_2(g) = 2\ MgAl_2O_4(s)$$

$$Al_4C_3(s) + 2\ MgO(s) + 3\ O_2(g) = 2\ MgAl_2O_4(s) + 3\ C(s)$$

$$Si(s) + 2\ MgO(s) + O_2(g) = Mg_2SiO_4(s)$$

$$SiC(s) + 2\ MgO(s) + O_2(g) = Mg_2SiO_4(s) + C(s)$$

or further

$$2\ Al_4C_3(s) + 4\ MgO(s) + 9\ O_2(g) = 4\ MgAl_2O_4(s) + 6\ CO(g)$$

$$2\ SiC(s) + 4\ MgO(s) + 3\ O_2(g) = 2\ Mg_2SiO_4(s) + 2\ CO(g)$$

Through decreasing Po_2 and increasing Pco in the reaction system, these reactions can

reduce the chance for carbon to react with oxygen, and eventually, retard carbon oxidation in the refractories.

When the newly-made bricks containing antioxidants are heated the first time in an oxidizing atmosphere, the above chemical reactions are expected to occur at the hot face of the bricks. The results in *Table 6.11* clearly show that, due to these reactions, the rate of carbon oxidation is retarded. However, the difference of oxidation resistance with and without antioxidants in our results is not as significant as what was claimed by Griffin et al,[61] or, in other words, the effectiveness of the above reactions has certain limits in our cases. In fact, after direct oxidation in air at 1204°C for 100 h, they obtained 57.2 mm depth of decarbonized layer in MgO-C bricks with 5 wt% graphite, but almost 0 mm in MgO-C bricks with the same amount of graphite and 3 wt% Mg metal. This divergence is believed to be due mainly to the kinetic factors involved. Although the antioxidants have, thermochemically speaking, a higher oxygen affinity than carbon, the chemical reactions of carbon with oxygen are actually much faster than those of the antioxidants. The difference in their reaction rates is also dependent on the type and size of antioxidants added. As a matter of fact, after direct oxidation of the as-received brick samples, a considerable amount of antioxidants, unoxidized or only partially oxidized, was observed remaining in the decarbonized layer where the graphite flakes had already been burned out (see *Figure 6.4* for the case of Al addition and *Figure 6.5* for the case of SiC addition). Since Al metal has the highest reactivity compared to

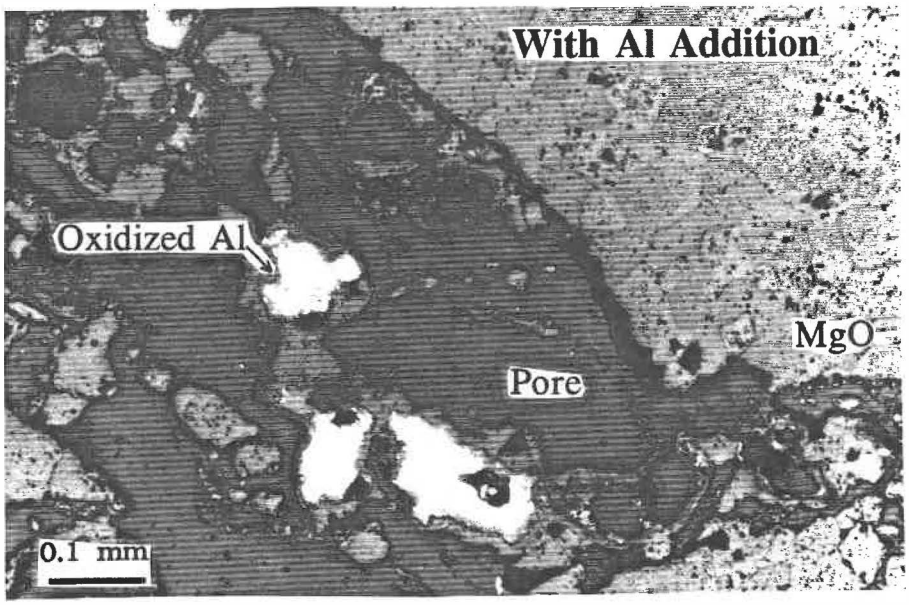

Figure 6.4 Micrograph of as-received brick sample (15 wt% graphite) after direct oxidation in air at 1200°C for 10 h, showing partially oxidized Al particles left in the decarbonized layer.

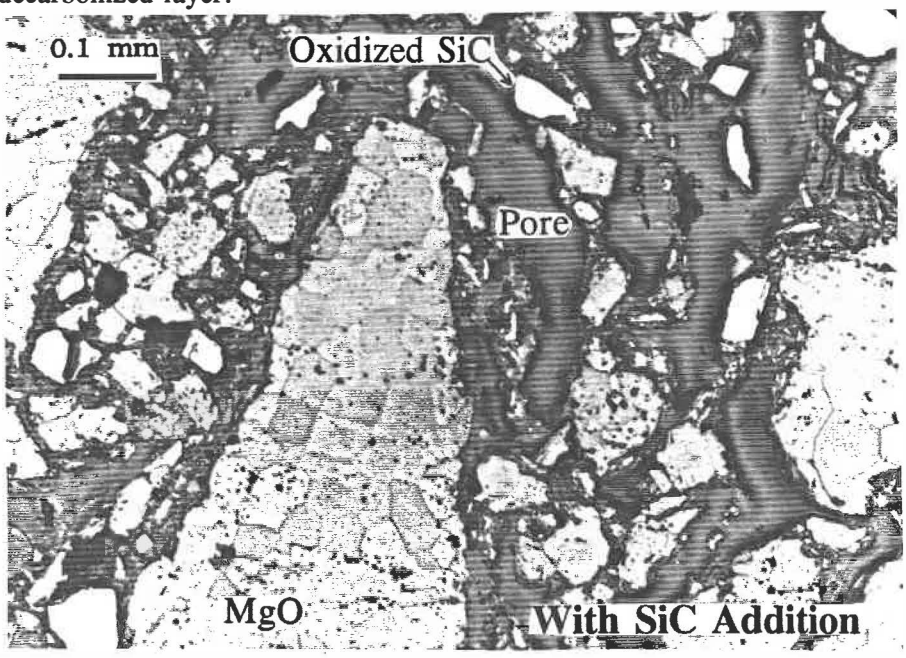

Figure 6.5 Micrograph of as-received brick sample (15 wt% graphite) after direct oxidation in air at 1200°C for 10 h, showing partially oxidized SiC particles left in the decarbonized layer.

the other two additives, Si and SiC, in this case, the best result for oxidation resistance improvement is obtained from the samples with Al addition (see *Table 6.11*). On the other hand, observations have indicated that as the temperature increases, the antioxidants left in the decarbonized layer without oxidation reduce in quantity and finally disappear at 1400°C. Thus, kinetically speaking, oxidation of antioxidants by oxygen actually needs longer time or higher temperature in our cases in comparison with carbon oxidation.

(2) Oxidation of antioxidants by CO

As shown in *Figure 3.1*, CO gas will be the prevailing gas phase in the C-O_2-CO-CO_2 system when the temperature approaches about 700°C. Under such a strong CO atmosphere, carbon materials can remain stable, but the antioxidants will become unstable and the following reactions can take place:

$$2\ Al(s,l) + 3\ CO(g) + MgO(s) = MgAl_2O_4(s) + 3\ C(s)$$

$$Al_4C_3(s) + 6\ CO(g) + 2\ MgO(s) = 2\ MgAl_2O_4(s) + 9\ C(s)$$

$$Si(s) + 2\ CO(g) + 2\ MgO(s) = Mg_2SiO_4(s) + 2\ C(s)$$

$$SiC(s) + 2\ CO(g) + 2\ MgO(s) = Mg_2SiO_4(s) + 3\ C(s)$$

In fact, the experimental results in *Table 6.4* and *Figure 6.3* have shown the evidence of these oxidation reactions occurring in CO atmosphere. These reactions can bring down the Pco and make the reaction system reach a new equilibrium of C-O_2-CO-CO_2 by consuming more carbon; this process is not helpful to the suppression of carbon oxidation if we consider that the reactions of C-O_2-CO-CO_2 control the atmosphere of the system.

Also, the transformation of carbon materials in the refractories to either CO or the carbides and then to amorphous carbon (as identified by Yamaguchi et al.[82]) through the above reactions can only increase the chemical reactivity of carbon and promote decarbonization whenever oxygen becomes available.

Based on these points, the mechanism claimed by Yamaguchi et al.,[82] i.e., the non-oxides, including both metals and their carbides, reduce CO gas to amorphous carbon and thus delay the oxidation of graphite, is felt to be rather weak. In fact, in the CO atmosphere, carbon materials are under good protection rather than under attack in the medium temperature range (as discussed in Chapter III), so that adding antioxidants to depress Pco is not meaningful. The CO atmosphere can protect carbon materials from burning out, but also damages the antioxidants at the same time. As a result of oxidation by CO gas, the antioxidants will eventually lose their chemical roles on carbon protection (as described in the former section *6.2.2 (1)*) as all antioxidants are transformed to their oxides and can no longer act as oxygen getters. At lower temperatures, the effect of carbon protection is better (see the results in *Table 6.5* for the typical case of Al addition) because the oxidation of antioxidants by CO takes place more slowly so that less amount of antioxidant is lost in a given time and more is left to react with oxygen directly during the later process of oxidation.

In practice, only the surface of brick linings is exposed to the oxidizing

atmosphere immediately; other parts of the bricks will undergo thermal cycling under CO atmosphere until the surface is worn out. During this period, the oxidation of antioxidants by CO continues in the interior. As a result, the deeper the part of a brick, the longer heat history it goes through, and the less amount of antioxidants is left without being oxidized. When that part eventually becomes the surface after progressive wearing, the antioxidants may be all transformed to their corresponding oxides. That is why fewer and fewer antioxidants are found inside the bricks after many thermal cycles in practice. Because the oxidation of antioxidants takes place inside the bricks before carbon oxidation really starts, the oxidation resistance of the bricks will not be expected to show a significant improvement. The results of oxidation tests on both carbonized and uncarbonized (as-received) brick samples (see *Tables 6.5* and *6.11*) supports the above analysis. After carbonization at 1000°C for 10 h, the improvement of oxidation resistance for the carbonized samples was not as significant as the ones without the treatment of carbonization because most of the initially added antioxidants had already been oxidized before carbon oxidation really started (see *Tables 6.8*, *6.9*, and *6.10*).

(3) Oxidation of gaseous species

Besides the above oxidation reactions just discussed, the antioxidants can also form volatile species which diffuse outwards and then are oxidized. The partial pressures of major vapour species (the most volatile gaseous species) for the systems Al-C-O and Si-C-O at different temperatures are given in the volatility diagrams of *Figures 6.6* and

6.7 if both Pco and Po_2 in the reaction system are considered to be controlled mainly by the reaction of carbon oxidation. Since CO atmosphere becomes prevailing in the interior of the bricks when the temperature is high enough, the most possible reactions to form gaseous species are:

$Al(s,l) = Al(g)$

$2\ Al(s,l) + CO(g) = Al_2O(g) + C(s)$

$Si(s) + CO(g) = SiO(g) + C(s)$

$SiC(s) + CO(g) = SiO(g) + 2\ C(s)$

From the volatility diagrams, note that, when P_{CO} approaches 1 atm, the most stable solid phases are the oxides rather than the carbides, and the major components of vapour phase are Al(g) and SiO(g) for the systems of Al-C-O and Si-C-O, respectively; however, P_{SiO} is much higher than P_{Al} at any given temperature.

After their formation, the gaseous species will diffuse away from where they are generated and have two possible ways to be oxidized in CO atmosphere. At higher P_{CO}, the oxidation reactions are:

$2\ Al(g) + MgO(s) + 3\ CO(g) = MgAl_2O_4(s) + 3\ C(s)$

$Al_2O(g) + MgO(s) + 2\ CO(g) = MgAl_2O_4(s) + 2\ C(s)$

$SiO(g) + 2\ MgO(s) + CO(g) = Mg_2SiO_4(s) + C(s)$

These reactions can accelerate the oxidation of antioxidants by CO through fast mass transfer of gaseous phase. However, at lower P_{CO}, the following reactions can take place:

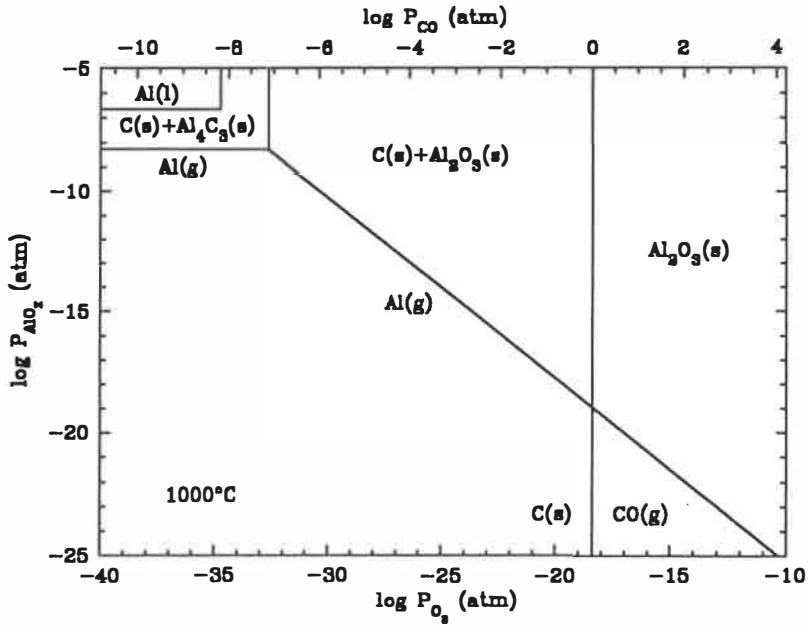

Figure 6.6 (a) Volatility diagram of the system Al-C-O at 1000°C.

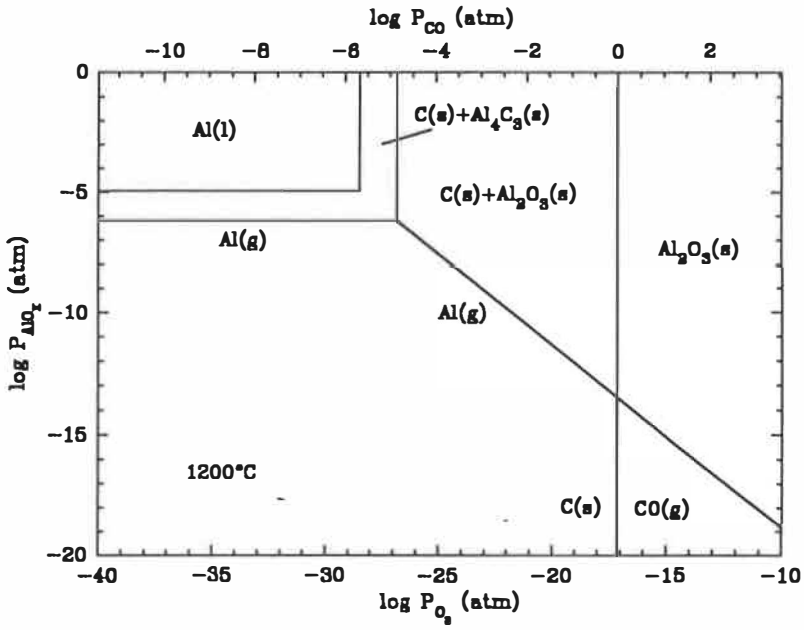

Figure 6.6 (b) Volatility diagram of the system Al-C-O at 1200°C.

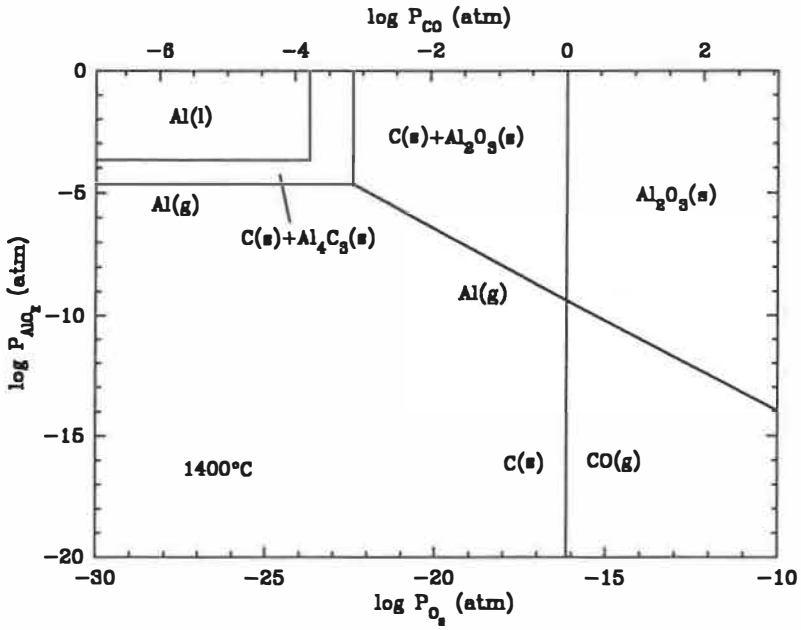

Figure 6.6 (c) Volatility diagram of the system Al-C-O at 1400°C.

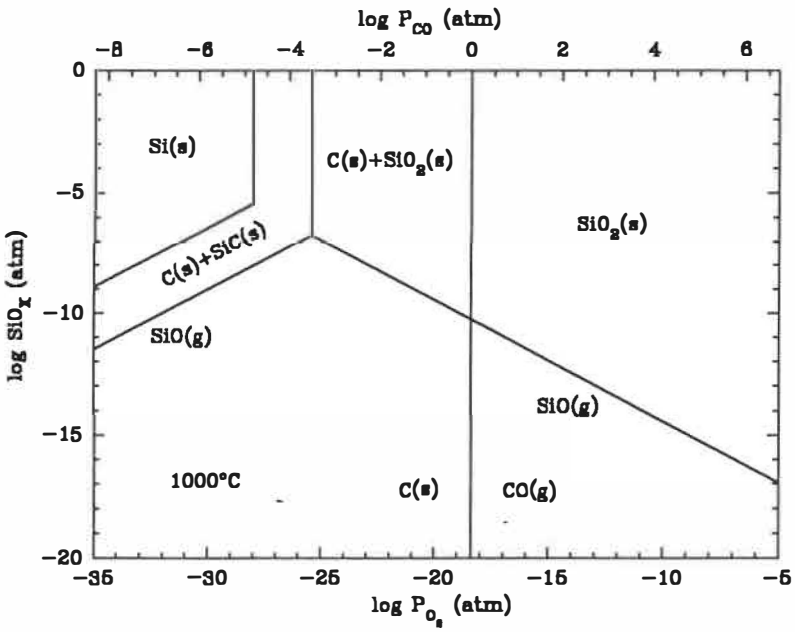

Figure 6.7 (a) Volatility diagram of the system Si-C-O at 1000°C.

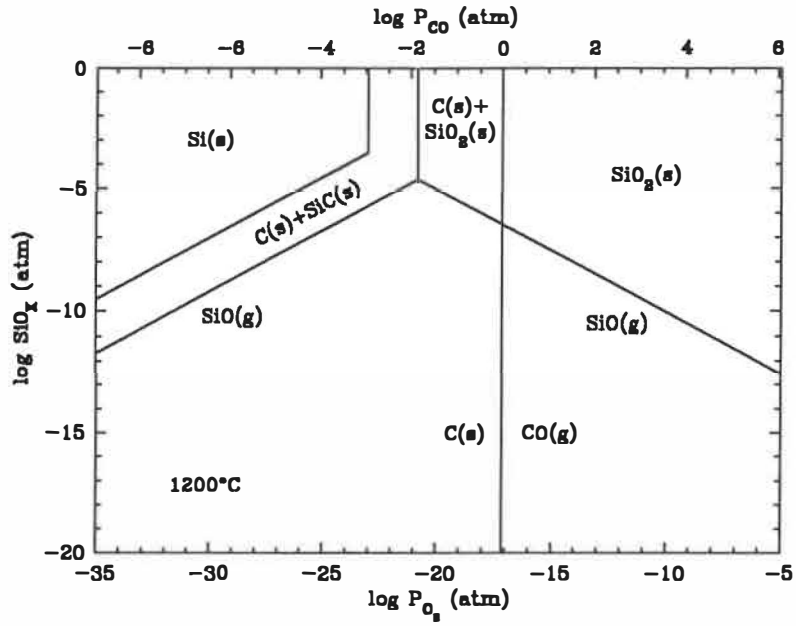

Figure 6.7 (b) Volatility diagram of the system Si-C-O at 1200°C.

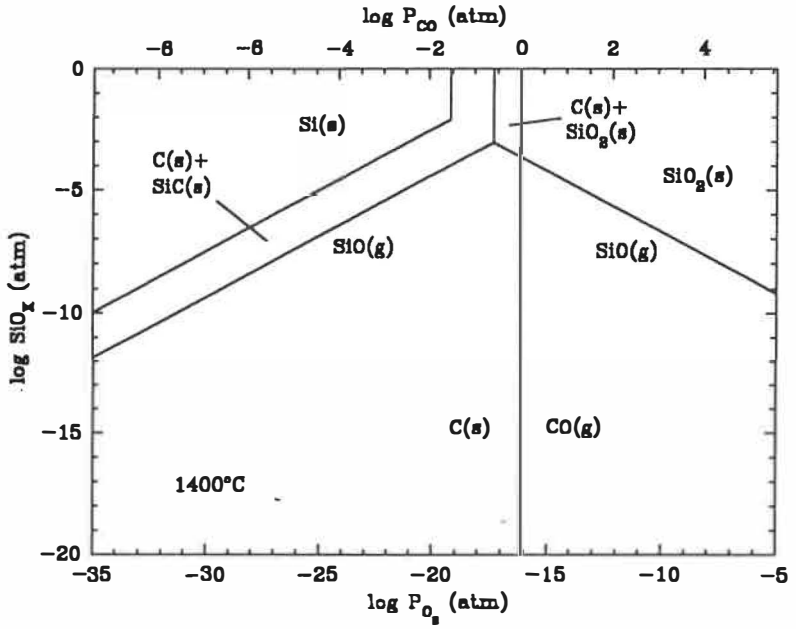

Figure 6.7 (c) Volatility diagram of the system Si-C-O at 1400°C.

$4\ Al(g) + 3\ C(s) = Al_4C_3(s)$

$2\ Al_2O(g) + 5\ C(s) = Al_4C_3(s) + 2\ CO(g)$

$SiO(g) + 2\ C(s) = SiC(s) + CO(g)$

These reactions enhance the formation of carbides also by fast gaseous transfer and will help to improve the oxidation resistance when the material is attacked by oxygen later. On the other hand, if the gaseous species diffuse outwards and encounter the oxygen from the exterior, the following oxidation can take place:

$4\ Al(g) + 2\ MgO(s) + 3\ O_2(g) = 2\ MgAl_2O_4(s)$

$Al_2O(g) + MgO(s) + O_2(g) = MgAl_2O_4(s)$

$2\ SiO(g) + 4\ MgO(s) + O_2(g) = 2\ Mg_2SiO_4(s)$

The other positive function of antioxidants involves the formation of gaseous species in the interior of the brick and migration of these gases to the zone just adjacent to the decarbonized layer where the gases oxidize in contact with various sources of oxygen to form secondary oxides. Selection of antioxidants with high volatility can enhance this role of carbon protection. In this study, the addition of Si or SiC would have better results in this aspect because P_{SiO} can become significantly high as the temperature increases.

However, due to the limit of chemical reactivity, no significant evidence was observed for the mass migration through gaseous species, i.e. Al or SiO, to the outer face during oxidation at high temperatures up to 1600°C, unlike the case of B_4C addition[83] in which significant vapour migration did occur due to the high volatility of

boron compounds, leading to a loose and porous structure in the depleted zone of the oxidized brick samples. In the case of Al addition, another reason is that the majority of Al metal may have been oxidized already by CO gas due to its high reactivity before the formation of its gaseous species becomes significant. On the other hand, unlike the case of Al addition, an appreciable amount of newly formed glassy phase has formed between MgO grains in the decarbonized layer in the case of either Si or SiC addition after firing at 1400°C (see *Figures 6.8* and *6.9*). The possibility of the migration of SiO vapour from the interior to the outer face and being then oxidized to form a glassy phase at the outer face can not be excluded when the temperature is high enough. As a matter of fact, this finding is in agreement with the results (the smaller depths of the decarbonized layer) achieved on oxidation resistance (see *Table 6.5*).

(4) Possible advantages of alloy antioxidants

Since antioxidants have the possibility to be oxidized in CO atmosphere, one of the benefits of using alloys may be due to their lower reactivity in CO gas. For example, the use of Mg-Al alloy rather than Al metal itself may retard the reaction of Al with CO generated inside the bricks or increase the reaction temperature with CO gas, so that there are more Al and Al_4C_3 left to react with oxygen when it invades. Perhaps, this explanation is one of the reasons why alloys act more effectively as a carbon protector than the metals themselves.[31,84]

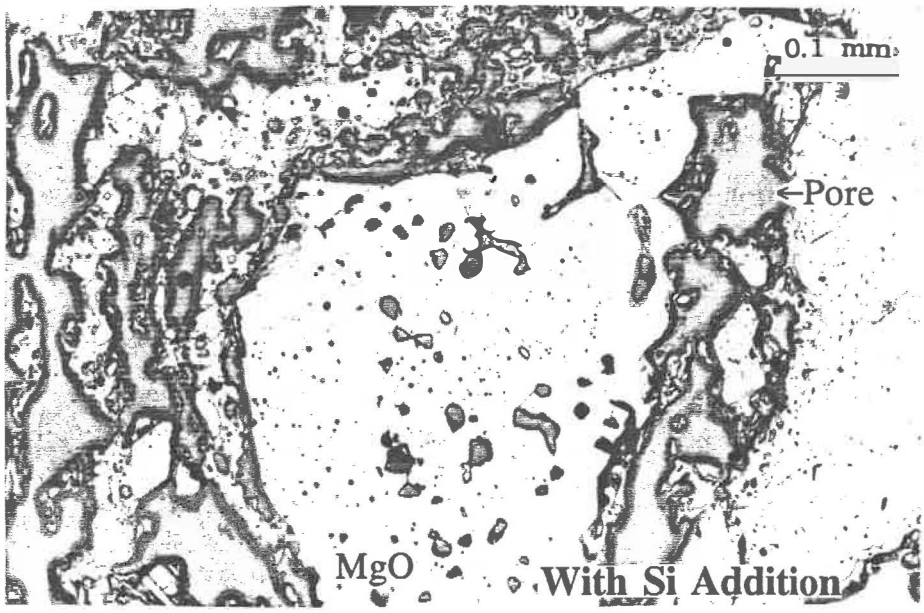

Figure 6.8 Micrograph of carbonized brick sample (15 wt% graphite) after oxidation in air at 1400°C for 5 h, showing the newly formed glassy phase between MgO grains in the decarbonized layer.

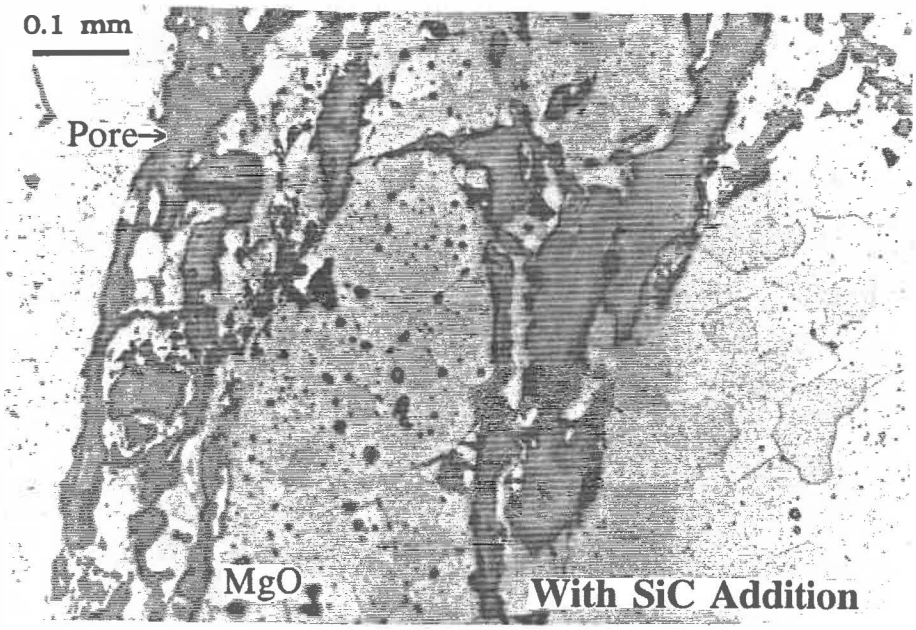

Figure 6.9 Micrograph of carbonized brick sample (15 wt% graphite) after oxidation in air at 1400°C for 5 h, showing the newly formed glassy phase between MgO grains in the decarbonized layer.

Another possible advantage of using alloy antioxidants may be due to the thermochemical stabilities of available antioxidants over a wide temperature range. As analyzed thermochemically by Yamaguchi et al.,[85] when two kinds of metals are present, one will be preferentially oxidized by the prevailing CO gas in MgO-C bricks as the temperature rises. For instance, in the case of addition of Mg-Al alloy, Al_4C_3 contributes mainly to suppressing carbon oxidation after Mg changes to MgO. In the case of Al-Si alloy, SiC comes into effect after Al and Al_4C_3 transform to the oxides. As a consequence, carbon is under better protection because of the availability of antioxidants (either in the form of metal or carbide) in a wider range of temperatures.

6.2.3 Physical roles of antioxidants

Besides the preferentiality of antioxidants in the reactions with oxygen as discussed in *Section 6.2.2*, the reactions of antioxidants can also bring about a considerable reduction in the porosity of MgO-C bricks and help to prevent the inward diffusion of oxygen and thus, to hinder direct carbon oxidation because the process of oxidation is diffusion-controlled.

(1) Volume expansion

In the presence of Al metal, formation of spinel is expected, leading to a volume expansion by about 0.86 times the initial volume according to the reaction:

$$2\ Al(s) + MgO(s) + 3\ CO(g) = MgAl_2O_4(s) + 3\ C(s)$$

Here, we assume that 2 moles of Al (d = 2.70) reacts with 1 mole of MgO (d = 3.58) and 3 moles of CO (from the atmosphere) to form 1 mole of MA (d = 3.60) and 3 moles of amorphous carbon (d = 1.95), then we have $\Delta V/V_0 = 0.86$. By analogy with that, if the reactions

$$Si(s) + 2\ MgO(s) + 2\ CO(g) = Mg_2SiO_4(s) + 2\ C(s)$$

$$SiC(s) + 2\ MgO(s) + 2\ CO(g) = Mg_2SiO_4(s) + 3\ C(s)$$

take place in the cases of Si and SiC addition, the induced volume increases are 0.62 and 0.78 times of the initial volume, respectively. On a weight basis, the volume expansion is 1.59, 2.21, and 1.95 times per 100 g of Al, Si, and SiC respectively. However, if the antioxidants are oxidized by the following reactions

$$4\ Al(s) + 2\ MgO(s) + 3\ O_2(g) = 2\ MgAl_2O_4(s)$$

$$Si(s) + 2\ MgO(s) + O_2(g) = Mg_2SiO_4(s)$$

$$SiC(s) + 2\ MgO(s) + O_2(g) = Mg_2SiO_4(s) + C(s)$$

then the induced volume increases are 0.27, 0.27, and 0.43 times of the initial volume, respectively. According to the above calculations, no matter what reactions occur, the conversion of antioxidants to their corresponding oxides will lead to a volume expansion in the materials.

The changes of pycnometric volume after firing in CO at 1200°C for 5 h are given in *Table 6.4*. As can be seen, the volume increase is very significant in the samples with additives, while the volume of the samples without addition only increases slightly

due to the irreversible thermal expansion of the graphite phase. However, note that the volume increase does not follow the order of Si (2.21) > SiC (1.95) > Al (1.59) as calculated above (on a weight basis) in the case of oxidation by CO, which indicates again the dominance of kinetic factors due to different chemical reactivity.

When the temperature is below about 1400°C, the process of carbon oxidation is rate-controlled by gas diffusion. In this temperature range, the transformation of antioxidants to oxides can take place considerably in the interior of bricks due to the strong CO atmosphere, and the induced volume expansion will squeeze pore channels of gas diffusion or even block the pores through filling, which can be beneficial to carbon protection when carbon is attacked later. Similarly, if the oxidation of antioxidants takes place during carbon oxidation, the induced volume expansion can also be beneficial to the prevention of oxidation through reducing the porosity of the decarbonized layer. However, an excess of volume expansion may damage the structure of brick samples and cause a contribution of porosity increase rather than a decrease overall. In fact, this effect was found in the case of Al addition after carbonization (see *Table 6.1*), where the reduction in pycnometric volume is greater compared to that without additive.

As discussed in *Section 6.2.2*, a certain amount of antioxidants still remained in the decarbonized layer without being oxidized, especially in the case of SiC addition due to its low chemical reactivity. As carbon oxidation continues, the oxidation of these

unoxidized antioxidants can also decrease the porosity of decarbonized layer and hinder gas diffusion through it. However, since the decarbonized layer is rather porous after removal of the graphite phase, the increase in solid volume after transformation to M_2S is still not enough to inhibit the diffusion of gaseous species significantly. This effect is typical in the case of SiC addition at 1000 and 1200°C in which oxidation resistance is not significantly improved.

(2) Formation of liquid phase

Besides the mechanism of inhibiting oxidation through volume expansion, the effect of hindering gas diffusion by forming a liquid phase and densifying the decarbonized layer is also believed very important. In the case of Al addition, the effect of liquid phase formation is not so obvious because, when carbon oxidation really begins, most of Al(l) has already reacted with carbon to form Al_4C_3, and, at high temperatures, the most stable compound formed is spinel which has a high melting point (2135°C) and also a possibility of forming solid solution with MgO. However, in the case of Si or SiC addition, the situation is different. After the transformation from metal or carbide to oxide, the forsterite formed, if combining with other impurities from both graphite flakes and MgO grains, could form a considerable amount of liquid phase when the temperature is high enough. *Figures 6.8* and *6.9* have clearly shown that, after firing at 1400°C, MgO grains in the decarbonized layer are joined together by a glassy phase. As a result of blocking the pores and densifying the decarbonized layer through the formation of a

liquid phase, carbon loss is greatly inhibited. From *Table 6.5*, the addition of Si or SiC is seen to correlate to a significant decrease in the depth of decarbonized layer at 1400°C. Based on this point, the additives which can react with MgO grains to form a significant amount of liquid phase before carbon oxidation starts is believed to be able to prevent very effectively carbon loss through direct oxidation.

(3) Counter-diffusion of gaseous species

Once there is a significant amount of gaseous species formed as the temperature rises, the gas phase can cause a positive pressure in the interior or a counter-diffusion to oxygen, and this action can also hinder direct carbon oxidation. However, the oxidation of antioxidants in CO atmosphere can reduce the Pco in the reaction system and weaken the positive effect of CO gas in counter-diffusion to oxygen.

On the other hand, the process of formation of gaseous species from antioxidants in the interior of bricks and then migration of these vapours to the hot surface, where they encounter a higher Po_2 and condense to secondary oxides, can concentrate more low melting-point compounds at the hot surface and block the pores more quickly.

6.2.4 Stability and roles of nitrides

(1) Stability of nitrides

Figures 6.10 and *6.11* show the reaction free energy for the formation of nitrides

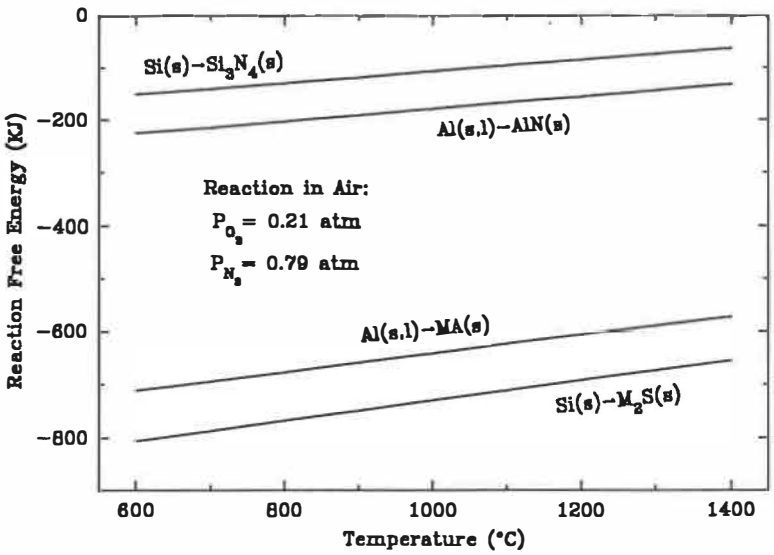

Figure 6.10 Reaction free energy for the formation of nitrides (AlN or Si_3N_4) and oxides (MA or M_2S) from Al or Si in air as a function of temperature.

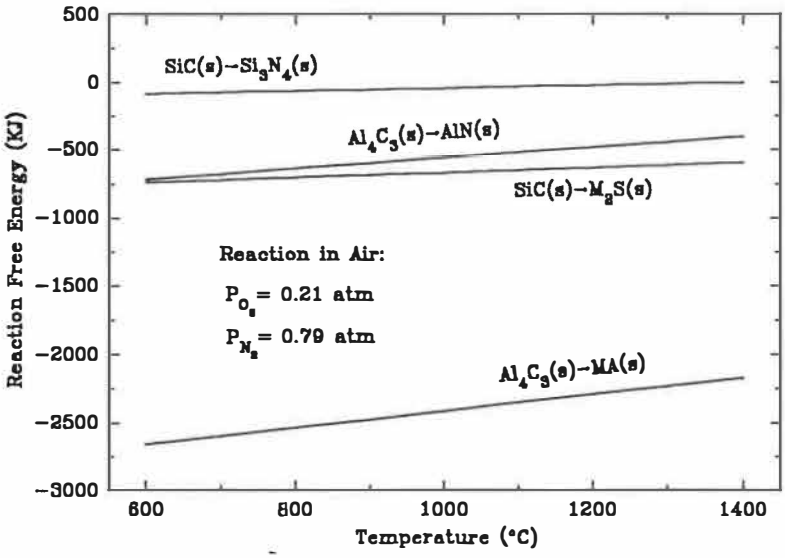

Figure 6.11 Reaction free energy for the formation of nitrides (AlN or Si_3N_4) and oxides (MA or M_2S) from Al_4C_3 or SiC in air as a function of temperature.

and oxides from Al and Si or Al_4C_3 and SiC in air (O_2 0.21 atm, N_2 0.79 atm) as a function of temperature. As can be seen from *Figure 6.10*, in a given amount (1 mole) of Al or Si, the oxides are more stable (lower reaction free energy) than nitrides if the MgO-C brick with antioxidant Al or Si is directly exposed to air; in other words, the oxides can form preferentially. Even existing in the form of carbides, the nitrides are still more unstable to form than the oxides (see *Figure 6.11*). Based on this point, both AlN and Si_3N_4 can not exist at any temperatures either at the outer surface or in the decarbonized layer where the atmosphere is air. The results of the XRD analysis from *Tables 6.8*, *6.9*, and *6.10*, and Yamaguchi's[78] support this analysis.

At the reaction interface where carbon oxidation takes place, the oxygen from air can be consumed very quickly by reacting with carbon to form mainly CO gas, and N_2 is left without any reactions. Consequently, the region just behind the reaction interface is mainly in an atmosphere of gas mixture of CO and N_2 if carbon is not exhausted. In this case, the partial pressures of CO and N_2 can be calculated based on the assumption that 1 mole of oxygen produces 2 moles of CO gas during oxidation:

$$2\ C(s) + O_2(g) = 2\ CO(g)$$

Thus, $P_{CO} = 0.35$ atm and $P_{N2} = 0.65$ atm if the total pressure in the reaction system remains at 1 atm. Note from the predominance diagrams of *Figure 6.12* that the stability of AlN in the system increases with temperature. At 1600°C, AlN is stable, and Al_2O_3 becomes unstable if the atmosphere of 0.35% CO and 0.65% N_2 (point B) is maintained.

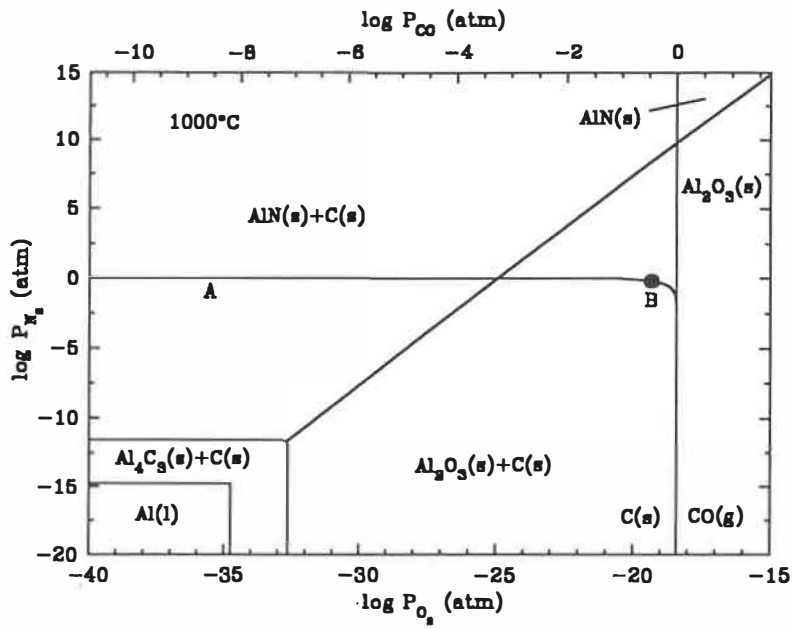

Figure 6.12 (a) Predominance diagram of Al-C-O-N system at 1000°C.

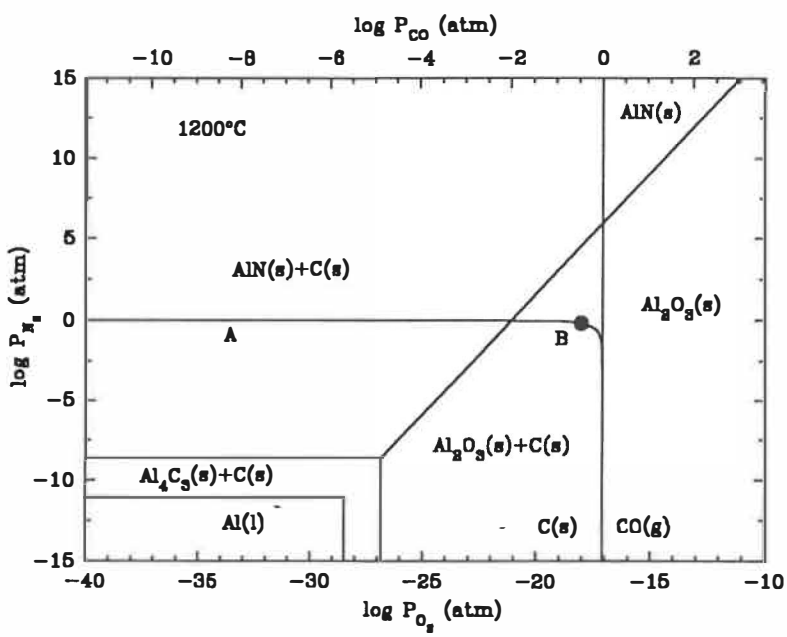

Figure 6.12 (b) Predominance diagram of Al-C-O-N system at 1200°C.

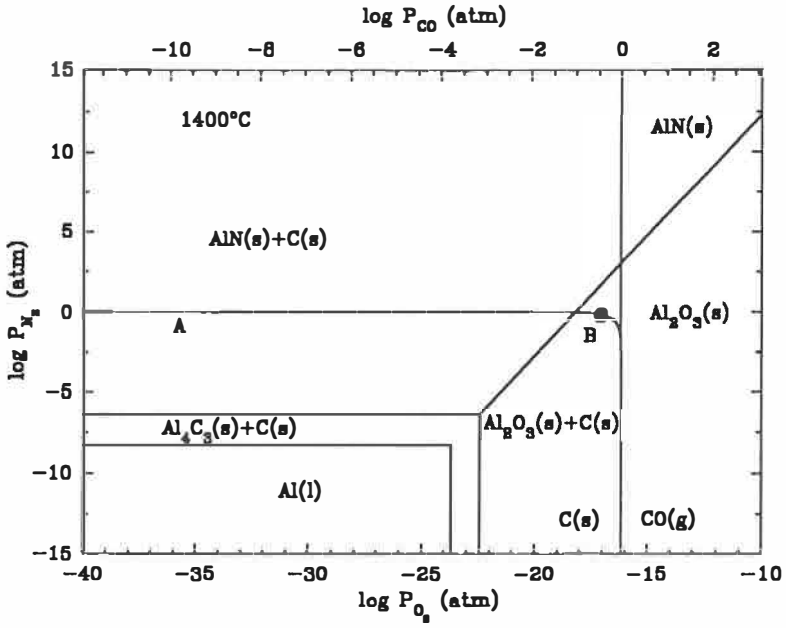

Figure 6.12 (c) Predominance diagram of Al-C-O-N system at 1400°C.

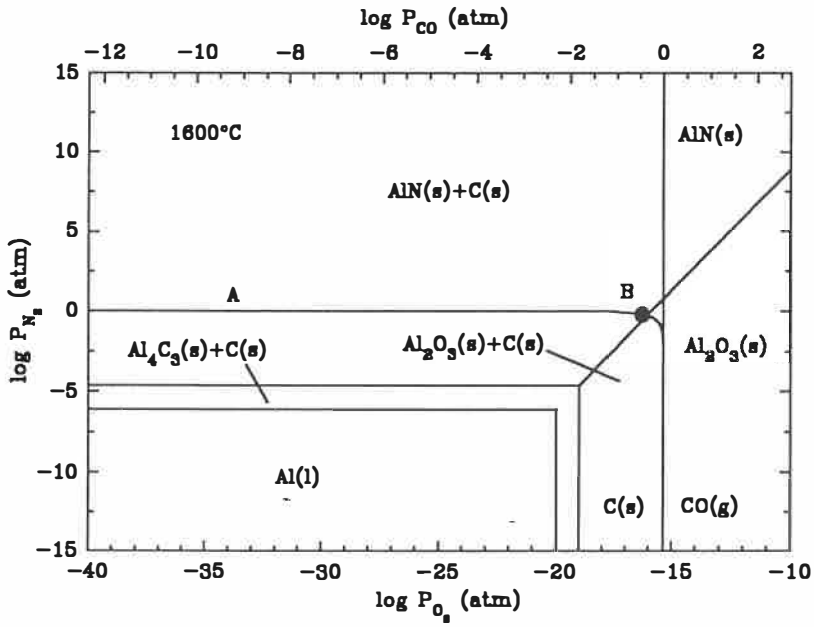

Figure 6.12 (d) Predominance diagram of Al-C-O-N system at 1600°C.

On the other hand, the oxidation of antioxidants in CO can take place in the interior of MgO-C brick, which will result in a reduction of Pco locally and thus, a rise of N_2 relative pressure nearby. The line A in *Figure 6.12* represents the change in the relative partial pressures of CO and N_2 at 1 atm, showing that the line is in the domain of nitrides as P_{N2} rises and approaches 1 atm. Therefore, the presence of AlN would not be surprising somewhere in the area near the C-O_2 reaction interface as the temperature is close to 1560°C which is the critical temperature for the AlN phase to be stable under such a condition. In this study, a considerable amount of AlN was found in the undecarbonized zone of the samples after oxidation in air at 1400°C (see *Table 6.8*).

In the case of Si or SiC addition, the situation is rather similar to that of Al, in terms of thermochemical stability of Si_3N_4 in the undecarbonized layer (see *Figure 6.13*). However, by comparing *Figure 6.13* with *6.12*, at any given level of N_2, AlN can be stable in a lower temperature range than Si_3N_4. Because of the chemical reactivity, Si_3N_4 has not been found in the samples at temperatures up to 1400°C. Another possible reason is that the liquid phase formed in the decarbonized layer could greatly hinder the penetration of N_2 from outside and thus, retard formation of Si_3N_4.

The formation of AlN or Si_3N_4 is controlled by the diffusion of N_2 and the availability of Al and Al_4C_3 or Si and SiC along its diffusing path. Going deeper from the reaction interface, the N_2 pressure will drop down quickly because of the difficulty

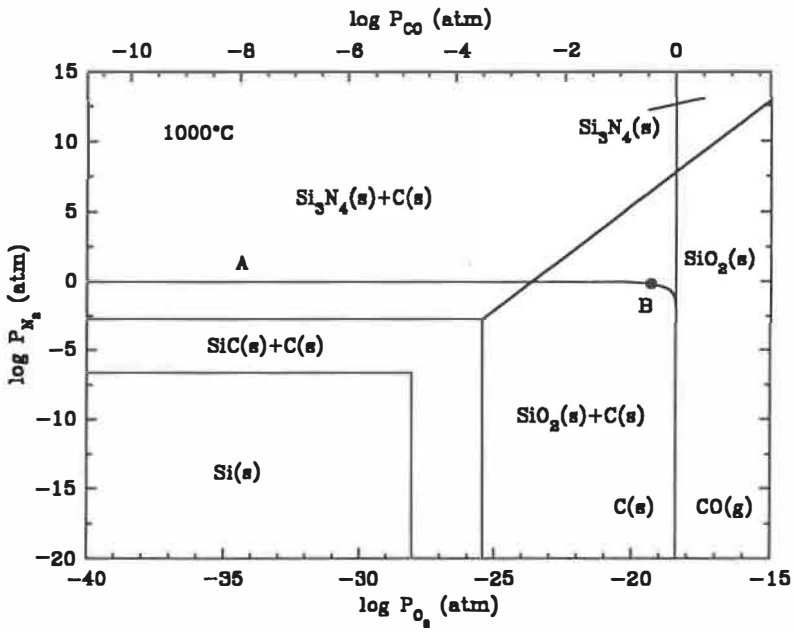

Figure 6.13 (a) Predominance diagram of Si-C-O-N system at 1000°C.

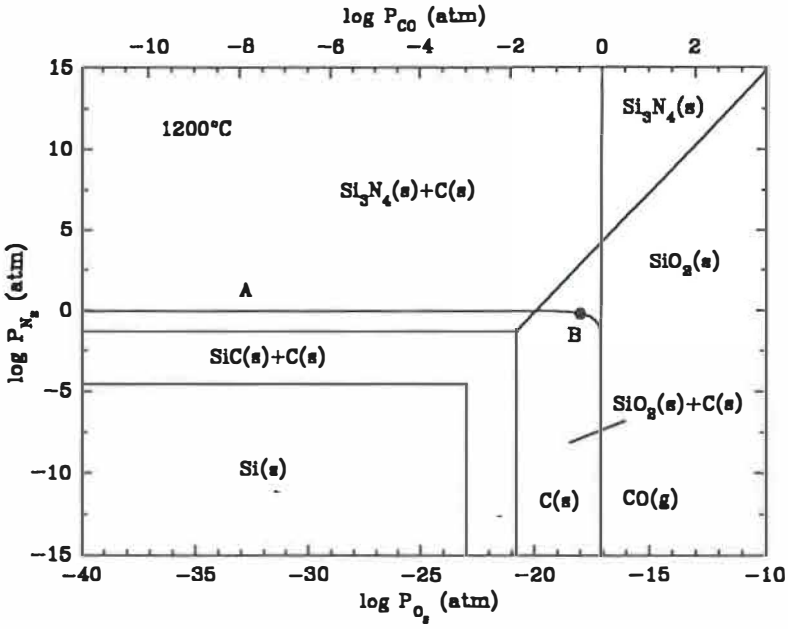

Figure 6.13 (b) Predominance diagram of Si-C-O-N system at 1200°C.

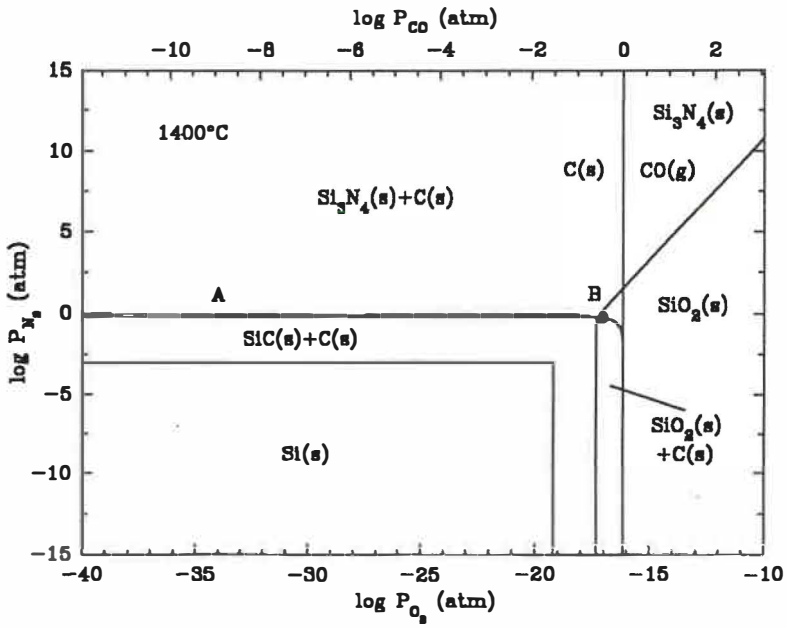

Figure 6.13 (c) Predominance diagram of Si-C-O-N system at 1400°C.

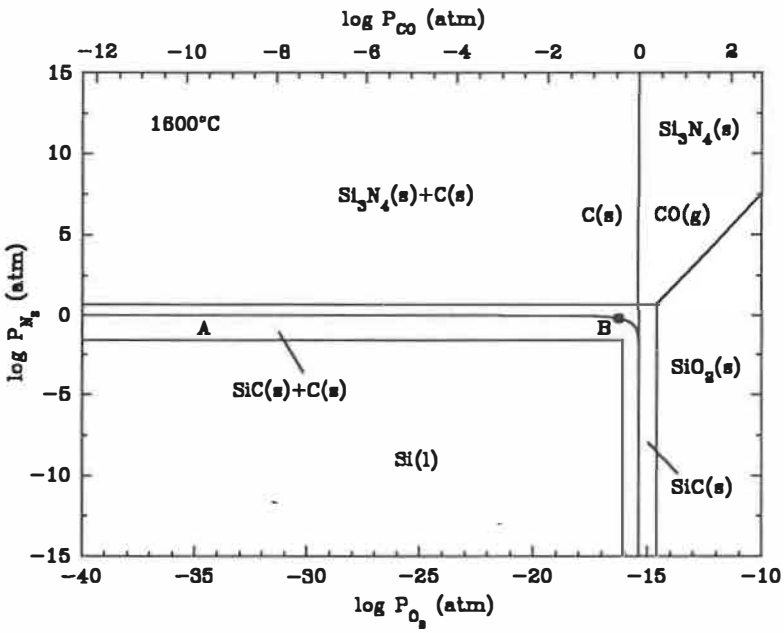

Figure 6.13 (d) Predominance diagram of Si-C-O-N system at 1600°C.

in diffusion. Thus, during oxidation in air, the formation of nitrides can only possibly take place in the region near and behind the reaction interface of C-O_2, which is directly adjacent to the decarbonized layer.

(2) Roles of nitrides

Since there is a possibility of forming nitrides during oxidation in air, their roles on carbon protection needs to be examined. *Figure 6.14* shows that in a given amount (1 mole) of oxygen the oxidation of AlN(s) or Si_3N_4(s) needs a lower reaction energy than that of carbon when the temperature is below about 1680˚C, or in other words, when coexisting with carbon, the nitrides will be oxidized preferentially whenever oxygen is available:

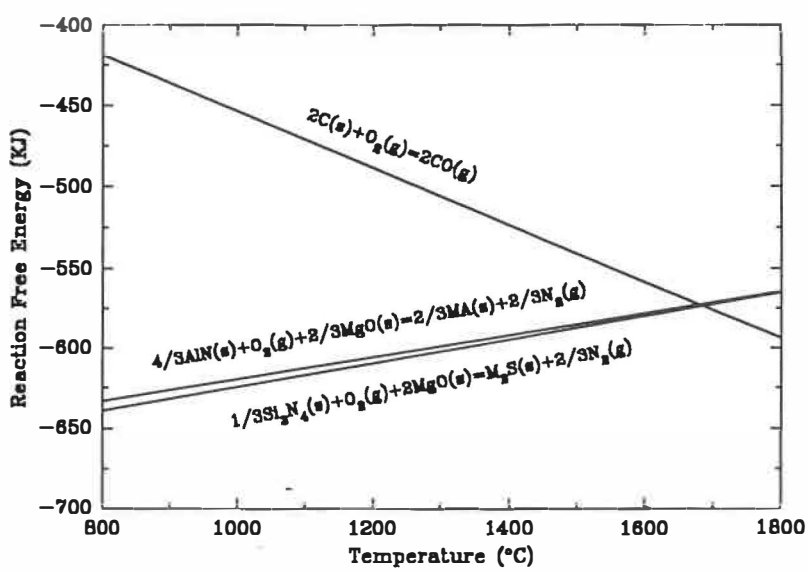

Figure 6.14 Reaction free energy for the oxidation of nitrides (AlN or Si_3N_4) or carbon as a function of temperature.

$$4\ AlN(s) + 2\ MgO(s) + 3\ O_2(g) = 2\ MgAl_2O_4(s) + 2\ N_2(g)$$

$$Si_3N_4(s) + 6\ MgO(s) + 3\ O_2(g) = 3\ Mg_2SiO_4(s) + 2\ N_2(g)$$

Accompanied by the above reactions, a volume expansion of 0.09 and 0.21 times of initial volume can occur, respectively. These reactions will be helpful in inhibiting carbon oxidation by snatching oxygen from carbon, count-diffusing of N_2 released from these reactions, and reducing the porosity through volume expansion.

On the other hand, note from *Figures 6.1* and *6.2* that a higher Pco is needed in order to transform the nitrides, AlN or Si_3N_4, to the corresponding oxides in comparison with Al and Al_4C_3 or Si and SiC. Accordingly, the transformation to nitrides can increase the temperature of stability of antioxidants in a CO atmosphere and protect more antioxidants to higher temperatures. This effect can help to retard carbon oxidation in a higher temperature range or during a longer heating period. Therefore, at least from a thermochemical standpoint, the nitrides should be more effective than their corresponding carbides or metals in protecting carbon over a wider temperature range. The fact that the presence of nitrides in the undecarbonized zone, but not in the decarbonized zone during oxidation in air, as found in this case (see *Table 6.8*), confirms the positive effect of nitrides on carbon protection.

6.3 Effect of Antioxidants on Indirect Carbon Oxidation

As discussed in *Sections 6.1* and *6.2*, the antioxidants have a tendency to

transform to their corresponding oxides in the interior of materials before the temperature reaches about 1600°C where the MgO-C interaction becomes important. However, if the firing time is not very long, especially in the case of laboratory tests, the transformations may not be completed due to kinetic factors, so that a mixture of metal, carbide and nitride (if exposed to air during heating) could be obtained at temperature ~1600°C.

Figure 6.15 shows the results of the thermochemical calculations on the equilibrium Mg vapour pressures in the MgO-C systems in or not in the presence of one of Al compounds (assuming the Pco in the reaction system is maintained at 1 atm). The reactions which are considered for calculation are listed as follows:

$MgO(s) + C(s) = Mg(g) + CO(g)$

$2\ Al(l) + 5\ MgO(s) + C(s) = MgAl_2O_4(s) + 4\ Mg(g) + CO(g)$

$Al_4C_3(s) + 12\ MgO(s) + C(s) = 2\ MgAl_2O_4(s) + 10\ Mg(g) + 4\ CO(g)$

$2\ AlN(s) + 5\ MgO(s) + C(s) = MgAl_2O_4(s) + 4\ Mg(g) + N_2(g) + CO(g)$

The presence of Al(l), $Al_4C_3(s)$, or AlN(s) can increase the equilibrium Mg vapour pressure considerably in comparison with the condition without antioxidants, especially at lower temperatures. In other words, the addition of Al metal, which transforms to another compounds later, can significantly enhance the interaction between MgO and C, and this enhancement is more significant in the lower temperature range. As shown in *Figure 6.16*, in the presence of Si(s or l), SiC(s) and $Si_3N_4(s)$, similar results, i.e. an increase of the equilibrium P_{Mg} in the system, can be attained when the reactions follow:

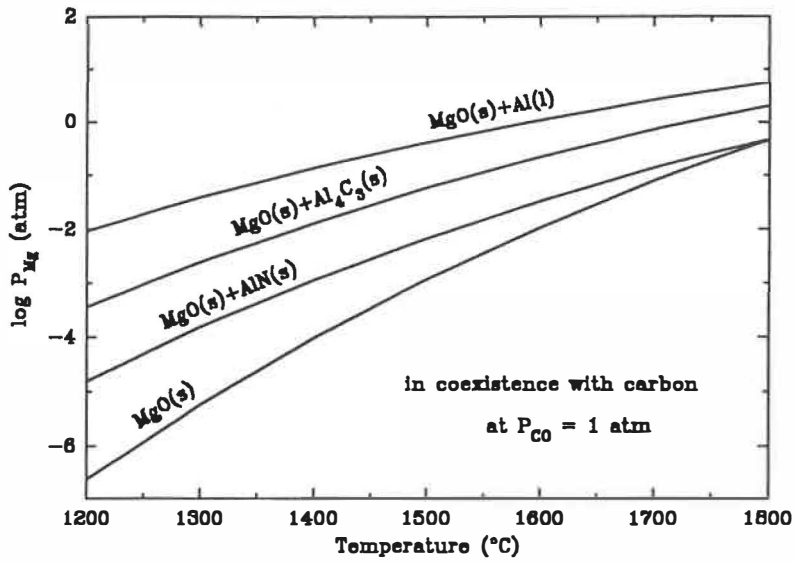

Figure 6.15 Equilibrium Mg partial pressures in the MgO-C systems in or not in the presence of Al compound as a function of temperature.

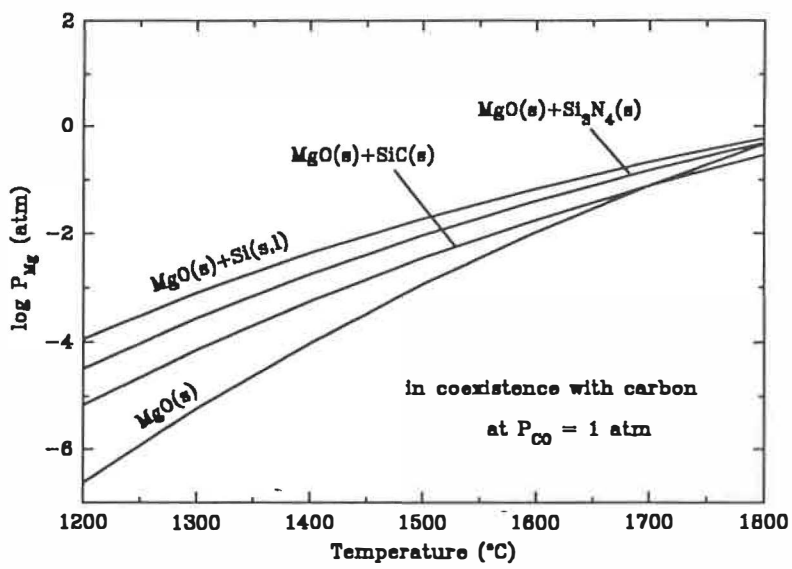

Figure 6.16 Equilibrium Mg partial pressures in the MgO-C systems in or not in the presence of Si compound as a function of temperature.

$$Si(s,l) + 5\ MgO(s) + C(s) = Mg_2SiO_4(s) + 3\ Mg(g) + CO(g)$$

$$SiC(s) + 6\ MgO(s) + C(s) = Mg_2SiO_4(s) + 4\ Mg(g) + 2\ CO(g)$$

$$Si_3N_4(s) + 13\ MgO(s) + C(s) = 3\ Mg_2SiO_4(s) + 7\ Mg(g) + 2\ N_2(g) + CO(g)$$

Moreover, note by comparing *Figure 6.15* with *Figure 6.16* that Al compounds have a better effect on the promotion of MgO-C interaction than Si compounds. When the temperature is above 1700°C, SiC(s) does not promote MgO-C interaction any more.

The acceleration of MgO-C interaction by adding antioxidants can be either positive or negative to the protection of carbon, depending upon the Po_2 in the reaction system. If the Po_2 meets the condition of MgO dense zone formation (as discussed in Chapter III), the antioxidants can enhance the role of MgO dense zone on preventing further decarbonization, i.e. forming the MgO dense zone more quickly or at a lower temperature. However, if the Po_2 is not high enough to allow Mg vapour generated by the interaction of MgO-C-antioxidants to deposit inside the brick, then more material losses can be expected due to the continuous giving-off of Mg vapour to the exterior. This action is obviously structure destructive and can only promote decarbonization.

In fact, the above analysis is in agreement with the experimental findings obtained by both Baker et al. and Moore et al. Baker et al.[8] have found that the presence of metallic additives Mg, Al, and Si not only decreases the starting temperature of MgO reduction, but also increases the formation rate of Mg vapour. As a result, when the

samples are fired in air (at a high Po_2), significant differences have been observed in the thickness and quality of MgO dense zones when changing the types of metals or varying the metal levels (see *Table 6.12*). Because of the formation of a MgO dense zone at a lower temperature, or, at a higher rate, due to the presence of these metallic additives, hinderance of further decarbonization in MgO-C bricks is enhanced in comparison with the samples without additives. On the other hand, from the experimental measurements with a thermal analysis (DTA/TGA) apparatus, Moore et al.[69] have observed that in the presence of carbon MgO can be reduced by metallic Al at temperatures as low as 900°C in an argon atmosphere (at a low Po_2) through the reaction:

$$MgO(s) + Al(l) \Leftrightarrow MgAl_2O_4(s) + Mg_xAl_{1-x}(g)$$

which leads to a large exothermic peak coupled with a large weight loss. However, they considered that the gaseous product of the above reaction is Mg_xAl_{1-x} rather than Mg vapour because of its thermochemical instability under such a condition. From *Figure 6.15* it is understandable that as long as the kinetic factors are favourable, the enhancement of the MgO-C interaction through the addition of Al metal can take place at a rather low temperature.

On the other hand, after having been transformed to the corresponding oxides at high temperatures, the oxides of antioxidants may also interact with carbon to form their own gaseous species, e.g.:

$$MgAl_2O_4(s) + 4\ C(s) = 2\ Al(g) + Mg(g) + 4\ CO(g)$$

Table 6.12 Effects of metal additions on dense zone formation and carbon protection in MgO-C bricks with 96% MgO quality grain and 15 wt% graphite (from Baker et al.[8])

Oxidation in air 1650°C - 8 h	No metal	Al metal		Si metal	
		3 wt%	5 wt%	3 wt%	5 wt%
Thickness of dense zone (mm)	0.40	0.55	1.10	0.50	0.50
Area of decarbonized layer (mm^2)	50.3	40.1	24.1	37.5	29.6

$$Mg_2SiO_4(s) + 3\ C(s) = SiO(g) + 2\ Mg(g) + 3\ CO(g)$$

Apparently, these gaseous species, i.e. Al(g) and SiO(g), will have same effects as Mg vapour, i.e. either positive (enhancing MgO dense zone formation) or negative (promoting carbothermic reduction), in terms of carbon protection. Moreover, since $P_{SiO} > P_{Al}$ at a given temperature (see *Figures 6.6* and *6.7*), there is reason to believe that in the case of Si additive the amount of gaseous species formed is greater and also the effect of interaction between the oxides of antioxidants and carbon. Thus, the volatility of an additive and its corresponding oxide are also important when selecting antioxidants.

If there is a slag layer present at the hot surface of the brick, the MgO dense zone is difficult to form due to the low Po_2 in the reaction system. In this case, the presence of antioxidants is mainly helpless to the resistance of bricks to decarbonization in terms of the MgO-C interaction, except for the effect of liquid formation at high temperatures which can help to inhibit the outward diffusion of gaseous product species of MgO-C interaction.

6.4 Effect of Antioxidants on Mechanical Strength

The fact that the addition of antioxidants to MgO-C bricks can significantly improve their mechanical strength has been well documented. However, the mechanism of strength improvement has not been well discussed in the literature. In this section, the understanding of the effect of antioxidants on mechanical strength will be expanded.

6.4.1 Comparison of strength before and after carbonization

The comparison of relative cold crushing strength before and after carbonization is illustrated in *Figure 6.17* and shows a great difference in strength due to the addition of antioxidants.

Before carbonization, the difference in crushing strength for the brick samples with or without additive depends mainly upon the adhesion between resin binder and the additive particles. If the adhesive force is larger than that between resin binder and MgO grains, the strength is increased compared to that without additive, as in the case of Al or Si addition. Otherwise, the strength is lower, like the case of SiC addition. The difference in porosity may also have a contribution to the lower strength since the as-received experimental bricks with SiC addition have a lower bulk density (see *Table 2.3*).

The main reason for strength improvement over no additives after carbonization is obviously due to the bonding effect of reaction products formed. As discussed in

Chapter IV, the bonding strength of resin binder is greatly reduced after pyrolysis. However, in the case of Al addition, the entire Al metal phase has been transformed to either Al_4C_3 or spinel after carbonization (see *Table 6.2*) which significantly reinforces the existing carbon bonding. The formation of M_2S and SiC takes place in the samples with Si additive and also enhances the carbon bonding in the materials. In the case of SiC addition, no M_2S was detected after carbonization by the XRD analysis (see *Table 6.2*) although the changes in weight and volume were slightly different from those without additive (see *Table 6.1*). These results support the fact that the improvement on the crushing strength after carbonization is not obvious (see *Figure 6.17*).

6.4.2 Comparison of strength after firing in CO at 1200°C

After carbonization at 1000°C for 10 h, the carbonized samples were fired in a CO atmosphere at 1200°C for another 5 h, and then their cold crushing strength were measured. The changes in strength values due to this heat treatment are illustrated in *Figure 6.18*. As can be seen, although carbon bonding becomes slightly weaker after further pyrolysis at a higher temperature, as shown in the samples without additive, the effect of reinforcement of ceramic bonding by the antioxidants gets greater since more reaction products are formed due to either carbonization (forming carbides) or oxidation in CO atmosphere (forming oxides), especially in the case of Si addition (see *Figure 6.3*). On the other hand, although the increase in strength is minor in both the cases of Al or SiC addition, the situations are rather different; in the case of Al addition, most Al metal

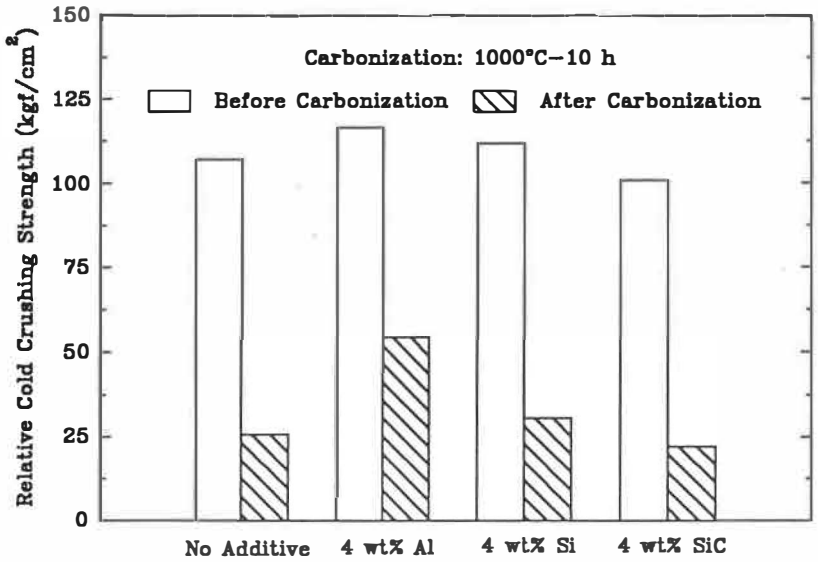

Figure 6.17 Comparison of crushing strength before and after carbonization for the as-received brick samples (15 wt% graphite) with or without antioxidant.

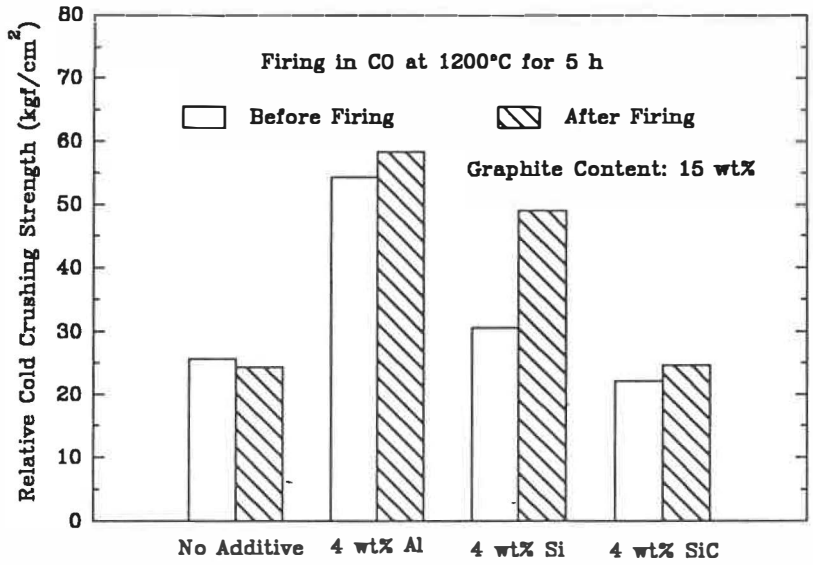

Figure 6.18 Comparison of crushing strength before and after firing in CO for the carbonized (at 1000°C for 10 h) samples with or without antioxidant.

has already been consumed to form Al_4C_3 and spinel, while no significant reaction has taken place at 1200°C in the case of SiC addition.

Based on the above results, as the firing temperature rises, the hot strength is expected to keep increasing as the formation of reaction products until a considerable amount of glassy liquid phase is formed due to the interaction of reaction products formed and the impurities existing in the raw materials. In other words, in the medium temperature range, where the impact of liquid phase does not become the major concern, enhancing the ceramic bonding by adding antioxidants can effectively improve the weak carbon bonding. In fact, the improvement on hot strength due to the addition of antioxidants in the medium temperature range ($\leq$1500°C) in various atmospheres has been frequently reported in the literature.[14,86,87] *Table 6.13*, as a typical example, lists the results of Tammermann et al.[87] on hot mechanical strength at temperatures 1200 and 1500°C, respectively, measured in Ar atmosphere. The results show an increase in hot modulus of rupture in the presence of Al metal.

Table 6.13 Hot modulus of rupture measured in argon atmosphere for MgO-C bricks with or without Al metal addition (from Tammermann et al.[87])

Type of bricks	MgO-C bricks		MgO-C bricks with Al	
Testing temperature (°C)	1200	1500	1200	1500
Hot modulus of rupture (MPa)	3.45	1.93	7.41	4.49

6.4.3 Comparison of strength before and after oxidation

The changes in cold crushing strength with oxidizing temperature are illustrated in *Figure 6.19* for the cases of Al, Si, or SiC addition. The strength changes during oxidation are attributed to the combination of two opposite factors:

1) the oxidation of the carbon phase in the decarbonized layer and further pyrolysis of the resin binder in the undecarbonized region weakens the carbon bonding;
2) the formation of more products due to the reactions of antioxidants in both decarbonized and undecarbonized regions strengthens the ceramic bonding.

Decarbonization can cause severe damage to the brick strength by burning-out the secondary carbon which is the only phase to hold the materials together and establish cohesive force. Therefore, the strength loss should be hindered as long as the carbon phase is protected by antioxidants. However, *Table 6.5* shows that the oxidation rate is not significantly reduced, and the depths of decarbonized layer are almost the same in the case of Al addition. In the case of Si or SiC addition, the significant improvement of oxidation resistance only occurs at 1400°C. Thus, there are reasons to believe that the improvement of strength is mainly due to the contribution of ceramic bonding reinforcement, rather than hinderance of carbon oxidation. At a higher oxidation temperature, the carbon bonding disappears more quickly, but the ceramic bonding between MgO grains becomes more significant, especially in the region of the decarbonized layer. In the case of Al addition, since most of Al_4C_3 and spinel have

already formed before the process of oxidation starts, the rise of oxidation temperature does not increase the strength much. In the cases of Si or SiC addition, although carbon oxidation weakens carbon bonding as oxidation temperature rises, the formation of large amounts of oxides from antioxidants during oxidation still improves the overall strength.

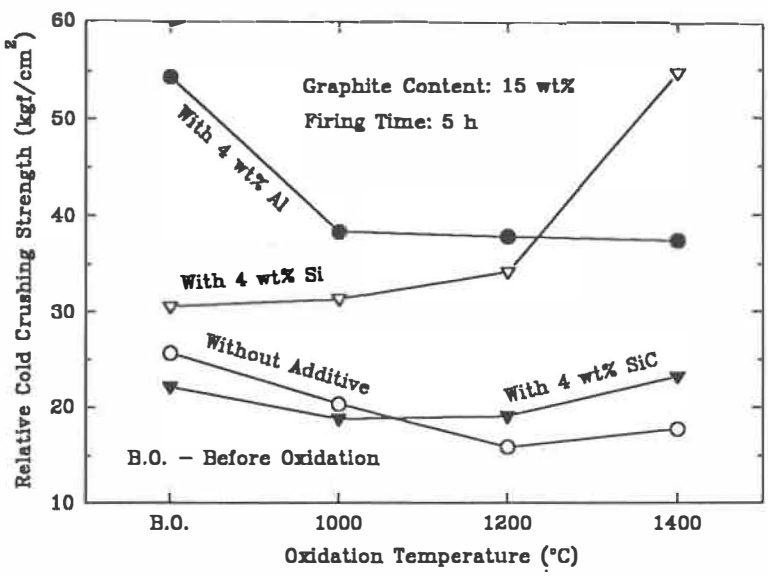

Figure 6.19 Changes of crushing strength before and after oxidation with temperature for carbonized (at 1000°C for 10 h) samples with or without antioxidant.

However, the increase of cold strength, as mentioned above, may not necessarily mean that the hot strength is also improved, especially for the Si addition. Because of the low melting point for the corresponding oxides of silicon, the hot strength could be rather low while the cold strength is shown to increase consistently with firing temperature.

6.4.4 Negative roles of antioxidants on strength

Although the improvement of strength by adding antioxidants is quite evident,

their roles on strength are not always positive as temperature rises. As discussed above, the dominant role of antioxidants on strength improvement is to reinforce the ceramic bonding which can be affected greatly above certain temperatures. The temperature limits for strength improvement will vary with both the type of additives and their amount added as a result of the different ceramic bonding formed.

Obviously, in terms of chemical composition, the addition of Mg metal would not damage the strength at high temperatures. Al addition can behave similarly since the final product is spinel which also has a very high hot strength. As reported by Troell et al.[37] (see *Table 6.14*), with the addition of Al, the strength is still higher than that without Al additive at temperature as high as 1540°C in a reducing atmosphere. However, the presence of silica due to the addition of Si metal can certainly be harmful to hot strength since silica easily forms large amounts of low-melting compounds with other impurities. The results of Troell et al.[37] in *Table 6.15* have already shown the reverse relation between hot strength at 1540°C in a reducing atmosphere and the amount of Si additive, i.e., when Si is added, the strength value decreases with the increasing amount of Si addition, the samples with no Si addition exhibiting the highest strength.

Table 6.14 Effect of Al metal addition on hot crushing strength in a reducing atmosphere for MgO-C bricks with 20 wt% carbon (from Troell et al.[37])

Addition of Al metal	No	Yes
Crushing strength at 1540°C (N/mm^2)	18.5	23.2

Table 6.15 Effect of Si additions on hot crushing strength in a reducing atmosphere for MgO-C bricks with 20 wt% carbon (from Troell et al.[37])

Content of Si additive (wt%)	0	1	2	3
Crushing strength at 1540°C (N/mm^2)	16.6	14.1	10.5	10.3

Combined with the impurities in the brick constituents, the negative impact of antioxidants on hot strength becomes more dramatic. The reactions between the impurities in either MgO grain or graphite and the oxides of the antioxidants deteriorate the hot strength because they not only reduce the forming temperature and viscosity of glassy flux, but also increase the amount of glassy flux. Using high purity raw materials, Troell et al.[37] have found that the hot crushing strength at 1540°C is greatly increased, being twice as strong, with the addition of Al metal. With the standard purity composition, the strength improvement is not so significant at the same temperature. If Si metal is added, the negative impact of forming low-melting compounds is even greater so that precautions have to be taken.

In addition, note that the transformation of antioxidants to their corresponding oxides can bring about a significant amount of volume expansion. For the unrestrained brick samples, the possibility of crack formation due to free expansion may also weaken the effect of strength improvement.

Based on the above discussion in *Section 6.4*, unless there is a tremendous

demand for hot strength in the medium temperature range where carbon bonding becomes rather weak, the usage of antioxidants should be cautious because of the possible negative aspects associated with hot strength at high temperatures in service, i.e. 1600°C.

6.5 Further Discussion on Antioxidants

6.5.1 Confusions in oxidation resistance evaluation

Characterizing the resistance to carbon oxidation for the bricks with antioxidants is tricky. The measurement of total weight loss may be misleading because the weight loss does not necessarily correspond to the total amount of carbon loss. For instance, the addition of same amount (in mole) of β-SiC and Si-C mix to MgO-C materials might yield an improper conclusion concerning their effectiveness on anti-oxidation if the conclusion is only based on the measurements of total weight loss.[88] At high temperatures the in-situ formed SiC through adding the Si-C mix is more chemically reactive than β-SiC added initially, so that the former is more easily oxidized or is oxidized faster. This action causes a higher weight gain in a given time by either of the following reactions:

$$SiC(s) + 2\ CO(g) = SiO_2(s) + 3\ C(s)$$

$$SiC(s) + O_2(g) = SiO_2(s) + C(s)$$

and contributes to reduction in the total weight loss if there is certain amount of carbon oxidized simultaneously. Therefore, in such a case, a lower total weight loss in a given time does not necessarily indicate that the amount of carbon oxidized in the materials is smaller. The exact conversion ratio of SiC to SiO_2 in the materials has to be determined

in order to calculate the amount of lost carbon and to evaluate the oxidation rate.

The same situation prevails when other antioxidants, such as metals, Mg, Al, or Si,[8] alloys, Mg-Al or Al-Si,[31] or the carbide, B_4C,[89] are used. For example, for Al addition, a mixture of Al_4C_3 and spinel was found in the carbonized samples and also in the unoxidized part of the samples after oxidation (see *Tables 6.2* and *6.8*). Since the exact amount of Al_4C_3 that has been oxidized to spinel in the unoxidized part of the samples during oxidation tests is difficult to measure, it is impossible to use the absolute values of weight change to evaluate oxidation resistance. Therefore, when antioxidants are present, the measurement of the depth of the decarbonized layer is considered to have a more meaningful value in the evaluation of carbon oxidation resistance.

6.5.2 Hydration of Al_4C_3

The addition of Al metal could cause another problem, i.e. the easy hydration of the intermediate compound, Al_4C_3. It has been reported in the literature[37,90] and also observed during the tests that after heat treatment at high temperatures, extensive cracking and bloating can occur in the samples with Al metal addition when exposed to ambient moist air for a certain time. Eventually, the sample compact disintegrates to a loose pile of powder. This degradation is due to the hydration of Al_4C_3 which is formed during the process of carbonization. According to Troell et al.,[37] Al_4C_3, once it forms, can easily hydrolyse by the reaction:

$$Al_4C_3(s) + 12\ H_2O(g) = 4\ Al(OH)_3(s) + 3\ CH_4(g)$$

This reaction is followed by a considerable volume expansion, and, as a result, cracking and bloating occur.

From the XRD results on the hydrated samples, no peaks for $Al(OH)_3$ have been identified, implying that $Al(OH)_3$ may be present in an amorphous form. However, in comparison with the XRD results on newly carbonized samples (see *Table 6.16*), the relative intensities of Al_4C_3 peaks are lower for the hydrated samples, which indicates the loss of Al_4C_3 during the process of hydration.

During the experimental work, in order to avoid contact with moist air, the samples containing Al additive were kept in a desiccator loaded with silica gel or anhydrous $CaSO_4$. $CaSO_4$ proved to be a better desiccant than silica gel due to the sensitivity to moisture. However, in spite of this, the Al-samples still tended to crack and bloat after several weeks. This fact indicates that Al_4C_3 is even more readily hydrated than the desiccants we used. Due to this fact, oxidation tests and the various subsequent measurements were taken as soon as possible, once the Al-samples were carbonized. Experience also gained during this work that hydration of samples can be significantly retarded simply by coating the fired samples with wax.

Since the hydration problem results from the presence of Al_4C_3, the seriousness

of cracking and bloating is strongly related to the amount of Al_4C_3 formed in the bricks. Comparing the physical appearances (see *Figure 6.20*) of the samples after oxidation at 1000, 1200, and 1400°C and then left in moist air for several days indicates that the lower the firing temperature, the more seriously the sample cracked and bloated. This effect is because the amount of Al_4C_3 present in the fired samples decreases as the carbide is transformed to spinel at higher oxidation temperature. On the other hand, although Al_4C_3 can only be stable up to 1400°C, there was no surprise to observe that the samples fired at 1600°C for 5 h and then left in moist air still had a tendency to crack and bloat. This fact indicates that the oxidation of Al_4C_3 to spinel does take time, especially in the interior of brick body.

Because of the possibility of Al_4C_3 hydration, intermittent operations of the furnaces in practice may have a risk of damaging brick linings. On the other hand, since less and less Al_4C_3 is left without being oxidized as the temperature increases, the damage caused by hydration would be more serious at the cold face than at the hot face because of the lower temperatures it is exposed to. Therefore, precautions must be taken to guard against hydration on the hot face as well as the cold face.

6.6 Chapter Summary

In this chapter, the roles of antioxidants on carbon protection have been clarified based on their physical and chemical aspects in relation of two different decarbonizing

Table 6.16 Comparison of the results of XRD analysis on carbonized samples with Al addition before and after hydration (exposed to ambient moist air)

	Relative height of the peak (mm)	
Phase	Before hydration	After hydration
Al_4C_3 $2\theta = 40.1$ $I = 83$	37	17
$MgAl_2O_4$ $2\theta = 19.0$ $I = 35$	24	25

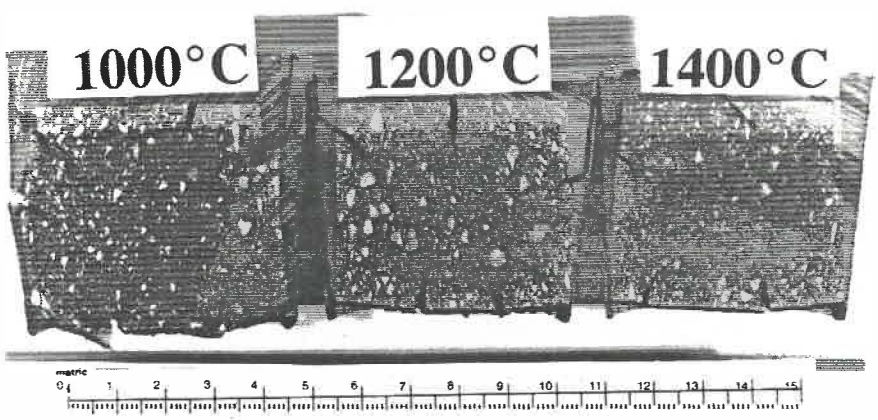

Figure 6.20 Physical appearances of oxidized samples (fired at three temperatures) with Al addition after exposure to ambient moist atmosphere.

regimes (direct and indirect carbon oxidation) in two different temperature ranges ($T \leq 1400^\circ C$ and $T > 1400^\circ C$). Also, this study is the first to point out the difference of oxidation of antioxidants by CO and O_2 and its impact on the roles of antioxidants on carbon protection. Besides the protection of carbon, another important feature of antioxidants is their effects on strength improvement. As discussed in this chapter, reactions of antioxidants take place as the heating process proceeds, changing their forms as well as their roles on carbon protection and strength improvement.

Both Chapters III and IV have discussed that carbon burnout can be greatly repressed through reduction of Po_2 in the reaction system or/and porosity in the materials. In the presence of antioxidants, depressing Po_2 occurs through either solid or vapour phase (chemical roles) only at the beginning when antioxidants have not been transformed to their corresponding oxides in a CO atmosphere. Increasing the resistance to diffusion-in of oxygen through reduction of material porosity or counter-diffusion of gaseous product species in the opposite direction (physical roles) takes place once reactions of antioxidants start.

Among the antioxidants used, Al metal had the best effect at the beginning in terms of the chemical roles. However, the results of oxidation tests at 1400°C showed that the physical roles are more effective in hindering oxidation in the cases of Si or SiC addition where a significant amount of glassy phase has formed. Apparently, the addition

of low melting-point compounds, such as the boron-containing compounds, B_4C and ZrB_2, can enhance their physical roles on carbon protection because they are very volatile, and the boron oxides formed after transformation can react quickly with the impurities from both MgO grains and graphite flakes to form a large amount of glassy phase at low temperatures, which helps to inhibit oxygen diffusion effectively.

Antioxidants can react with CO gas generated by the carbon-containing material system and form their corresponding oxides eventually. These reactions will weaken the chemical roles of antioxidants for carbon protection because the oxides formed are not able to act as an oxygen getter any more. These reactions could also bring down locally the Pco in the interior of materials and transform carbon materials in the bricks to reactive amorphous carbon, which is not helpful to the protection of carbon either. Therefore, the physical roles of antioxidants will become more significant than their chemical roles if they have been oxidized by CO atmosphere in the interior of bricks before being exposed eventually to an oxidizing atmosphere. This situation no doubt occurs under service conditions.

At high temperatures, the negative aspects of using antioxidants become more significant because they not only enhance the MgO-C interaction, but also deteriorate hot strength. Thus, unless carbon burnout in the low temperature range is the major concern or the Po_2 in the reaction system meets the condition of the MgO dense zone formation,

the addition of antioxidants should be cautious as a means of hindering decarbonization because of its possible negative impact on the overall performance of bricks.

According to the results presented in this chapter and from previous studies, the possible mechanisms for strength improvement in the presence of antioxidants are believed as follows:

1) the weak carbon bonding between the particles is reinforced by the formation of carbides, nitrides, and oxides;
2) carbon loss is hindered due to the effect of carbon protection;
3) the formation of the MgO dense zone is enhanced in the presence of antioxidants.

However, the results from this work have indicated that the strength improvement by adding antioxidants is mainly attributed to the enhancement of the ceramic bonding rather than the protection of the carbon bonding. As a consequence, the use of antioxidants may not lead to a positive effect on strength improvement in the high temperature range where the presence of a large amount of glassy phase formed through reactions of antioxidants with the impurities from raw materials of brick constituents can certainly deteriorate the hot strength of bricks. Thus, similar to the roles on carbon protection, the improvement of strength by adding antioxidants can only work better in the low or medium temperature range where the carbon bond is the weakest phase in the bricks and determines the overall strength of bricks.

CHAPTER VII

Summary and Conclusions

The effects of graphite content, MgO grain-size distribution, amount of resin binder, and types of antioxidants on the decarbonizing behaviour of resin-bonded MgO-graphite refractories between 1000 and 1600°C in air and other atmospheres has been intensively studied in the present work.

7.1 The Process of Decarbonization

Decarbonization, as a function of both temperature and atmosphere in the reaction system, takes place mainly through carbon burnout by oxygen or/and MgO-C interaction. Carbon burnout by oxygen is a process of direct oxidation, while the process of MgO-C interaction occurs as indirect oxidation of carbon.

In the lower temperature range ($\leq 1400°C$), carbon burnout is the dominant decarbonizing reaction in an oxidizing atmosphere, and the overall rate of the decarbonizing process is largely determined by inward diffusion of oxygen from the atmosphere. At higher temperatures ($> 1400°C$) MgO decomposition becomes inevitable, and the presence of carbon materials enhances the decomposition due to the very low Po_2 in the reaction system. The chemical reactivity of MgO grains directly controls the

amount of oxygen contributing to the system in a given time for indirect oxidation. Outward diffusion of the gaseous products, Mg and CO, generated by MgO-C interaction is also very important to the overall rate of the process. The deposition of Mg vapour can not occur if carbon materials are present. However, the presence of a decarbonized layer does not necessarily make a MgO dense zone form unless a proper gradient of Po_2 is established. Since there is no possibility of self-protection by forming a MgO dense zone at low temperatures, decarbonization is often found more serious at low temperatures than that at high temperatures.

7.2 Control of Decarbonization

Reduction of brick porosity (material resistance) and Po_2 in the atmosphere (environmental condition) is most effective to the suppression of decarbonization in a temperature range where carbon burnout is more detrimental. Once Mg vapour is formed due to the MgO-C interaction, adjustment of Po_2 in the reaction system to allow the vapour to deposit within the decarbonized layer and form a MgO dense zone can significantly hinder further decarbonization through obstruction of diffusion channels.

Preventing outward diffusion of Mg(g) and CO(g) can effectively inhibit MgO-C interaction, thus reduction of material porosity is also important. Control of Po_2 in the reaction system can not only limit the MgO decomposition, but also enhances the formation of MgO dense zone. Besides, the reactivity of brick constituents, especially

MgO grains, also becomes crucial at high temperatures.

7.3 Effect of Brick Compositions on Oxidation Resistance

Increasing the graphite content in the bricks can reduce the extent of decarbonizing penetration by providing more flakes to be consumed, but at the same time, also produce a higher porosity after loss of the graphite phase. Thus, in consideration of the impact of material porosity, there is an optimum level of graphite content for oxidation resistance.

MgO grain-size distribution plays an important role on the brick porosity. Due to the factors of compaction, smaller size distribution can increase brick porosity significantly, especially after carbonization. This effect will be detrimental to the prevention of carbon oxidation. However, if the atmosphere is favourable, the smaller size distribution can also enhance the formation of MgO dense zone within the bricks (if the Po_2 is high enough), and thus hinder further decarbonization at high temperatures.

Increasing the amount of carbon binder does not result in a significant improvement of mechanical strength, especially at high temperatures, but increases the open porosity considerably after carbonization. Thus, in consideration of both mechanical strength and carbon oxidation resistance, only a minimum amount of binder is required in MgO-C bricks, and a selection of a binder with high carbon yield, low content of

volatile materials, and small volumetric contraction during carbonization is desirable.

7.4 Roles of Antioxidants on Carbon Protection

The instability of antioxidants in CO atmosphere indicates that the antioxidants can be transformed to their corresponding oxides within the brick body, depending on the temperature and time. These phase changes may be one of the reasons why in practice the amount of antioxidants becomes less and less before they are eventually exposed to an oxidizing atmosphere at the hot face. As the antioxidants gradually lose their chemical roles of carbon protection as a preferential oxygen getter, their physical roles, e.g. the induced volume expansion during transformation and enhancement of glassy phase formation, became prevailing. To improve the chemical roles of antioxidants on carbon protection, we should choose the antioxidants which can react quickly with oxygen, but be stable in the presence of CO(g). Selection of antioxidants with high volatility, large volume expansion after transformation, fast liquid formation and sintering with brick components, can improve their physical roles on carbon protection.

In the presence of antioxidants, the equilibrium P_{Mg} in the reaction system is increased. This effect can be either positive or negative to the protection of carbon, depending on the Po_2 in the reaction system. If the Po_2 meets the condition of the MgO dense zone formation, the antioxidants can enhance the role of the MgO dense zone in preventing further decarbonization; otherwise, more material loss is expected. At high

temperatures, the negative aspects of using antioxidants, i.e. enhancing MgO-C interaction and deteriorating hot strength, could prevail. Thus, unless carbon burnout in the low temperature range is the major concern or the Po_2 in the reaction system meets the condition of MgO dense zone formation, the addition of antioxidants should be cautious as a means to hinder decarbonization.

In the presence of Al or Si, nitrides may form as intermediate compounds in the region near the C-O_2 reaction interface, but not in the decarbonized layer or at the outer face when being exposed to air at high temperatures. Since AlN(s) and Si_3N_4(s) are more unstable than carbon at temperature below 1680°C, the nitrides will be oxidized preferentially. The transformation to nitrides increases the temperature of stability of antioxidants in CO gas and helps retard carbon oxidation in a higher temperature range. In addition, counter-diffusing of N_2 and reducing the porosity by volume expansion during oxidation of nitrides could contribute to inhibiting carbon oxidation. Based on this point, nitrides may be more effective than their corresponding carbides or metals for protection of carbon in the higher temperature range.

7.5 Changes of Brick Mechanical Strength

Before carbonization, the brick strength is mainly dependent on the graphite content. After carbonization, however, the cohesive strength of resin binder determines the overall strength of the composite body. After oxidation, the overall strength is still

controlled by the binder phase, but the extent of strength loss is related to the combined effects of material loss and sintering of MgO grains. Since the strength is largely determined by the type and amount of carbon binder after carbonization, the efforts of strengthening the bricks by modifying the size of either MgO grains or graphite flakes prove to be ineffective. The addition of antioxidants to improve the bonding shows a good result; thus, selection of a proper type of antioxidants and its amount is important.

The strength improvement by adding antioxidants is mainly attributed to the reinforcement of ceramic bonding rather than the protection of carbon bonding. Based on this point, the addition of Si or SiC may not lead to a positive result at high temperatures ($T \geq 1550^{\circ}C$) since the presence of a liquid phase can certainly deteriorate the hot strength of the bricks.

7.6 Characterization of Brick Properties

In practice, those portions of MgO-C bricks towards the permanent lining will go through thermal cycles in a reducing atmosphere, i.e. the process of carbonization, before they become hot-face furnace lining (after the previous hot face is worn out). Building awareness of the changes in the brick properties during this process will be beneficial to the proper usage of the bricks because these changes are essential to the brick performance in the later stage, reflect the brick performance more directly. Therefore, the evaluation of brick properties needs to be carried out in the state after carbonization.

Under a non-unidirectional oxidation condition, the measurement of weight change only gives a relative value and conceals the effect of sample geometry, including both size and shape. This condition is only suitable for a comparative study of different bricks in the same testing conditions. However, under an unidirectional oxidation condition, the sample geometry does not affect the value of weight change if expressed in per surface area dimensions. Also, the results from unidirectional tests better represent the effect of gas flow rate, flow direction, and the Po_2 in the flow, which are very important to evaluation of oxidation rate. On the other hand, the measurement of CO_2 concentration in the exhaust gas to estimate the rate of carbon burnout has been used in this study, which is also a successful experience and should be further improved.

For the bricks with antioxidants, the evaluation of oxidation resistance based only on the weight measurements is not meaningful because the oxidation of antioxidants contributes a weight gain to the overall weight change which makes assessing the amount of lost carbon difficult. The overall evaluation should be based on the change in phase composition, microstructure, physical properties (e.g. weight, dimension, bulk density, porosity, etc.), the depth of decarbonized layer, and the extent of strength loss.

7.7 Conclusions from Present Research Work

By adopting the proper experimental methods, the present work has investigated the behaviour and mechanisms of decarbonization in MgO-C bricks in a wide range of

temperature and atmosphere and has also evaluated the roles of antioxidants on carbon protection and strength improvement. In this work, the argument has been advanced that the process of decarbonization takes place in two different regimes as a function of both temperature and atmosphere in the reaction system. The important factors which control the overall rate of decarbonizing process have also been explained. Then, the roles of antioxidants which can be either positive or negative, changing with temperature and atmosphere in the reaction system, have been discussed. Therefore, a better understanding of the behaviour of decarbonization and the roles of antioxidants in MgO-graphite refractories has been achieved, and the initial three objectives for the present research project (see Chapter I) have been met with satisfaction.

In this chapter, the eight questions posed in Chapter I have been answered based on the present work. *Section 7.1* explained that there are two different regimes of decarbonization, i.e. direct and indirect oxidation of carbon as temperature and atmosphere change in the reaction system. This answer responds to *Questions 2* and *3* concerning the decarbonizing mechanisms and the effect of atmosphere. Besides, *Section 7.1* also revealed the relation of MgO dense zone formation with the Po_2 in the reaction system and the chemical reactivity of MgO grains, which is relevant to *Question 4*. *Section 7.2* answered *Question 2* concerning how to control decarbonization effectively as the decarbonizing regimes change. In *Section 7.3*, the effect of graphite content, MgO grain-size distribution, and amount of resin binder on the oxidation resistance of bricks

was clarified. This answer is for *Question 5*. The response to *Question 8* was given in both *Sections 7.4* and *7.5*, which provide a new insight on how antioxidants behave for carbon protection and strength improvement. *Section 7.6* explained how to characterize decarbonization more effectively, which is related to both *Questions 6* and *7*.

7.8 Recommendations on Further Research Work

The present research work has not been fully completed due to time limit on the study program. There are still some questions remaining, and even certain new questions have arisen from the experimental findings. Therefore, further research work on several subjects would be meaningful.

Although decarbonization is controlled by either inward diffusion of oxygen or outward diffusion of Mg(g) and CO(g), depending on which regime is in play, the chemical reactivity of materials also makes an important contribution to the overall process of decarbonization. So far, how the difference in chemical reactivity between secondary carbon and graphite contributes to the overall process rate has not been answered. Whether changing types of flakes or increasing flake size can significantly reduce the rate of carbon burnout is also unknown. Furthermore, confusion still exists as for how the nature of MgO grains, including the periclase size, impurity, and its precursor, affects decarbonization, especially MgO-C interaction.

Presently, only the phase evolution of bricks with antioxidants after heat treatments has been studied, which may not represent directly the brick phase composition because changes may take place during cooling. Thus, a direct investigation of phase evolution in MgO-C bricks with antioxidants at high temperatures as a function of the change of atmosphere would be meaningful for the kinetic study of oxidation of antioxidants. On the other hand, the antioxidants used in the present work do not perform very effectively in terms of carbon protection. The selection and testing of new antioxidants with higher reactivity with oxygen and higher volatility in CO atmosphere to improve the positive roles for carbon protection are necessary.

In order to simplify the calculation, assumption was made in the kinetic model presented in this work that diffusion is in a steady state; however, diffusion in an unsteady state is closer to the real system and should be considered when developing the kinetic equations. Modifying the present model to cover both direct and indirect oxidation is also meaningful. Since the rate constant for chemical reaction, k_c, is strongly dependent on the chemical reactivity of carbon materials, the k_c value needs to be correlated with brick properties, such as the percentage of graphite and carbon binder, the flake size, and the extent of graphite orientation.

References

[1]R. L. NACAMU, et al., "High Carbon-Magnesia Refractories in Basic Oxygen Steelmaking," Refractories J., 57 [4] 9-14 (1982).

[2]G. BUCHEBNER, "New Aspects in the Development of Carbon-Containing Magnesia Bricks for Basic Oxygen Steel Converters"; presented at the SIPRE Meeting, Terni, Italy, April, 1986.

[3]Y. L. LIN, et al., "Effects of Oxidation-Reduction Reactions in Magnesia-Graphite Compositions," Ceram. Eng. Sci. Proc., 7 [1-2] 27-39 (1986).

[4]I. PERETZ, et al., "Magnesia-Graphite Refractories for BOF Converters," Am. Ceram. Soc. Bull., 71 [9] 1383-90 (1992).

[5]R. E. MOORE, et al., "Research on Raw and Beneficated Minerals Systems for Steel Plant Refractories"; pp. 277-86 in Proceedings of the 75th Steelmaking Conference of the Iron and Steel Society of the AIME, Toronto, April 1992.

[6]G. C. PADGETT, "Refractory Materials - The Conflict with Nature," Refractories J., 59 [4] 6-14 (1984).

[7]T. ISHIBASHI, et al., "Behaviors of Flake Graphites and Magnesia Clinkers in Magnesia-Carbon Reaction," Taikabutsu Overseas, 3 [4] 3-13 (1983).

[8]B. H. BAKER, et al., "Dense Zone Formation in Magnesia-Graphite Refractories"; pp. 242-47 in Global Advances in Refractories, UNITECR'91 Proceedings. The German Refractories Association, Aachen, Germany, 1991.

[9]R. UCHIMURA, et al., "Development of High Performance Magnesia-Carbon Bricks for BOF," Interceram, Special Issue, 63-66 (1985).

[10]Y. NARUSE, et al., "Progress on Carbon-Bearing Refractories for the BOF," Ceram. Eng. Sci. Proc., 7 [1-2] 119-30 (1986).

[11]C. F. COOPER, "Graphite Containing Refractories," Refractories J., 55 [6] 11-21 (1980).

[12]M. SAKAGUCHI, et al., "Effect of Graphite Particle Size on Properties of MgO-C Bricks," Taikabutsu Overseas, 13 [1] 27-29 (1993).

[13]T. HORIO, et al., "Evaluation of Applicability of MgO-C Brick to Converters and Its Effect," Taikabutsu Overseas, 6 [1] 11-15 (1986).

[14]P. O. R. C. BRANT, et al., "Evolution of BOF Refractory Lining in Brazil"; pp. 1-12 in Global Advances in Refractories, UNITECR'91 Proceedings. The German Refractories Association, Aachen, Germany, 1991.

[15]A. BROWN, "The Properties of Ceramic Graphite Bodies," Refractories J., 58 [2] 7-10 (1983).

[16]H. KYODEN, et al., "Magnesia Carbon Tuyere Bricks for Combined Blowing in LD Converter," Taikabutsu Overseas, 3 [1] 10-16 (1983).

[17]S. YOSHINO, et al., "Wear of High-Graphite MgO-C Bricks," Taikabutsu Overseas, 3 [4] 21-23 (1983).

[18]N. C. LUBABA, et al., "Compaction Studies of MgO-Flake Graphite Mixtures Relevant to the Fabrication of Composite Refractory Materials," Br. Ceram. Trans. J.,

87 [5] 158-63 (1988).

[19]B. RAND, et al., "Carbon Binders from Polymeric Resins and Pitch: I. Pyrolysis Behaviour and Structure of the Carbons," Br. Ceram. Trans. J., 84 [5] 157-65 (1985).

[20]B. MCENANEY, et al., "Carbon Binders from Polymeric Resins and Pitch: II. Structure and Properties of the Carbons," Br. Ceram. Trans. J., 84 [6] 193-98 (1985).

[21]N. C. LUBABA, et al., "Effect of Carbon Binders on the Development of Porosity in MgO-Graphite Composite Refractories," Br. Ceram. Trans. J., 87 [5] 164-67 (1988).

[22]A. M. FITCHETT, et al., "Mechanical Properties of Carbon-Bearing Magnesia: I. Pitch-Bonded Magnesia," Br. Ceram. Trans. J., 83 [2] 54-58 (1984).

[23]A. M. FITCHETT, et al., "Mechanical Properties of Carbon-Bearing Magnesia: II. Pitch-Bonded Magnesia Graphite," Br. Ceram. Trans. J., 83 [2] 59-62 (1984).

[24]A. M. FITCHETT, et al., "Mechanical Properties of Carbon-Bearing Magnesia: III. Resin-Bonded Magnesia and Magnesia-Graphite," Br. Ceram. Trans. J., 83 [3] 73-76 (1984).

[25]G. ZOGLMEYR, "Technical and Environmental Aspects of the Use of Phenolic Resins in Modern-Day Refractories," Interceram, 42 [3] 145-49 (1993).

[26]P. L. SMITH, et al., "Equilibrium Relationships of Carbon-Metal Oxide Refractories," Br. Ceram. Trans. J., 84 [2] 62-69 (1985).

[27]R. BREZNY, et al., "Oxidation and Diffusion in Selected Pitch-Bonded

Magnesia Refractories," J. Am. Ceram. Soc., 67 [7] 480-83 (1984).

[28]T. RYMON-LIPINSKI, "Reactions of Metal Additives in Magnesia-Carbon Bricks in an Oxygen Converter," Stahl u. Eisen, 108 [22] 47-57 (1988).

[29]T. RYMON-LIPINSKI, "Oxidation Inhibiting Effect of Metal Additives in Refracotry Carbonaceous Materials," Stahl u. Eisen, 108 [25-26] 61-65 (1988).

[30]J. LEVEQUE, et al., "Converter Linings: A Compromise between Performance and Economy?"; pp. 109-43 in Proceedings of the 27th International Colloquium on Refractories, Refractories for Steelmaking Converters, Aachen, Germany, 1984.

[31]A. WATANABE, et al., "Behavior of Different Metals Added to MgO-C Bricks," Taikabutsu Overseas, 7 [2] 17-23 (1987).

[32]A. YAMAGUCHI, "Behaviors of SiC and Al Added to Carbon-Containing Refractories," Taikabutsu Overseas, 4 [3] 14-18 (1984).

[33]T. MATSUMURA, et al., "A Study on the Protection of Carbon Containing Bricks against Oxidation," Taikabutsu Overseas, 8 [4] 27-29 (1988).

[34]K. KURATA, et al., "Oxidizing Prevention of MgO-C Bricks for Converter," Taikabutsu Overseas, 11 [2] 17-22 (1991).

[35]Y. KIRYU, et al., "Application of MgO-C Brick to RH Lower Vessel," Taikabutsu Overseas, 7 [4] 50-53 (1987).

[36]H. TORITANI, et al., "Effect of Metallic Additives on the Oxidation-Reduction Reaction of Magnesia-Carbon Brick," Taikabutsu Overseas, 5 [1] 21-27 (1985).

[37]P. T. TROELL, et al., "Advances in the Development and Application of

Magnesia-Carbon Brick"; pp. 351-56 in Global Advances in Refractories, UNITECR'91 Proceedings. The German Refractories Association, Aachen, Germany, 1991.

[38]G. ZOGLMEYR, "Oxidation Behavior of Carbon Containing Basic Refractories," Radex-Rundschau, [2] 382-90 (1984).

[39]T. DARROUDI, et al., "Effects of Temperature and Several Gases on the Oxidation Characteristics of a Variety of Carbon-Magnesia Bricks and Their Raw Materials"; pp. 105-24 in Proceedings of the 1st International Conference on Refractories, Tokyo, Japan, 1983.

[40]R. J. LEONARD, et al., "Significance of Oxidation-Reduction Reactions Within BOF Refractories," J. Am. Ceram. Soc., 55 [1] 1-6 (1972).

[41]T. MATSUMURA, et al., "Properties of Magnesia Carbon Bricks Containing Aluminum or Aluminum Alloys," Taikabutsu Overseas, 8 [4] 24-26 (1988).

[42]P. O. R. C. BRANT, et al., "Refractories for BOF in Brazil"; pp. 82-107 in Proceedings of the 27th International Colloquium on Refractories, Refractories for Steelmaking Converters, Aachen, Germany, 1984.

[43]C. GUENARD, et al., "Characterization of the Properties of Magnesia-Carbon Bricks," Radex-Rundschau, [2] 391-400 (1984).

[44]B. H. BAKER, et al., "Role of Carbon in Steel Plant Refractories," Am. Ceram. Soc. Bull., 55 [7] 649-54 (1976).

[45]B. BREZNY, et al., "Microstructural and Chemical Changes of Pitch Impregnated Magnesite Brick under Reducing Conditions," Trans. J. Brit. Ceram. Soc.,

71 [6] 163-70 (1972).

[46]S. M. KIM, et al., "BOF Slag-Induced Formation and Destruction of Dense MgO Layers in Carbon-Containing Magnesites," Am. Ceram. Soc. Bull., 57 [7] 649-56 (1978).

[47]A. WATANABE, et al., "Mechanism of Dense Magnesia Layer Formation near the Surface of Magnesia-Carbon Brick," J. Am. Ceram. Soc., 69 [9] C-213-14 (1986).

[48]S. C. CARNIGLIA, "Limitations on Internal Oxidation-Reduction Reactions in BOF Refractories," Am. Ceram. Soc. Bull., 52 [2] 160-65 (1973).

[49]K. TABATA, et al., "A Study on Oxidation-Reduction Reaction in MgO-C Refractories," Taikabutsu Overseas, 8 [4] 3-10 (1988).

[50]K. L. KOMAREK, et al., "Reactions Between Refractory Oxides and Graphite," J. Electrochem., Soc., 110 [7] 783-91 (1963).

[51]X. LI, "Review on Decarbonization of Magnesia-Carbon Refractories"; Report for Predoctoral Examination, University of Montreal, 1991.

[52]C. F. COOPER, "Refractory Applications of Carbon: Flake Graphite, Its Function in Modern Refractories," Br. Ceram. Trans. J., 84 [2] 48-53 (1985).

[53]P. H. R. B. LEMON, "Refractory Applications of Carbon: Phenol Formaldehyde Polymers for the Bonding of Refractories," Br. Ceram. Trans. J., 84 [2] 53-56 (1985).

[54]I. MOCHIDA, "Roles of Carbons in Composite Refractories for Better Properties," Taikabutsu Overseas, 8 [4] 36-47 (1988).

[55]C. F. COOPER, "The Characterisation and Evaluation of Graphite Continuous Casting Refractories," Interceram, Special Issue, 1-6 (1987).

[56]R. H. HERRON, et al., "Slag Attack on Carbon-Bearing Basic Refractories," Am. Ceram. Soc. Bull., 46 [12] 1163-68 (1967).

[57]Y. MIYAGAWA, et al., "Improvement of MgO-C Lining for LD Converter," Taikabutsu Overseas, 6 [1] 16-21 (1986).

[58]G. D. PICKERING, et al., "Carbon-MgO Reactions in BOF Refractories," Am. Ceram. Soc. Bull., 50 [7] 611-14 (1971).

[59]M. LEFEBVRE, private communication, 1989.

[60]P. VELLUET, et al., "Oxidation Resistance of Magnesia-Carbon Bricks," Interceram, Special Issue, 95-98 (1985).

[61]D. J. GRIFFIN, et al., "Consideration for the Measurement and Improvement of Oxidation Resistance in Dolomite-Carbon and Magnesia-Carbon Refractories"; pp. 361-67 in Global Advances in Refractories, UNITECR'91 Proceedings. The German Refractories Association, Aachen, Germany, 1991.

[62]S. SAKAMOTO, et al., "Improvement of MgO-C Brick for Steel Making and Development of It's Evaluation Technique"; pp. 348-56 in UNITECR'89 Proceedings. Edited by L. J. Trostel, Jr., The American Ceramic Society Inc., 1989.

[63]Y. NARUSE, et al., "Results of Investigation of Mag-Carbon Bricks Used in Converter," Taikabutsu Overseas, 3 [2] 3-7 (1983).

[64]X. LI and M. RIGAUD, "Anisotropy of the Properties of Magnesia-Graphite

Refractories," J. Can. Ceram. Soc., 62 [3] 197-205 (1993).

[65]A. WOLFERT, et al., "Thermogravimetric Studies of Magnesia-Carbon Reactions"; pp. 367-71 in Global Advances in Refractories, UNITECR'91 Proceedings. The German Refractories Association, Aachen, Germany, 1991.

[66]O. S. OZGEN, et al., "Kinetics of Oxidation of the Graphite Phase in Alumina/Graphite Materials: I. Effect of temperature and initial pore structure at a fixed graphite content," Br. Ceram. Trans. J., 84 [2] 70-76 (1985).

[67]O. S. OZGEN, et al., "Kinetics of Oxidation of the Graphite Phase in Alumina/Graphite Materials: II. Materials with different graphite content, graphite flake size and with clay or carbon bonds," Br. Ceram. Trans. J., 84 [6] 213-18 (1985).

[68]H. ISHII, et al., "Reaction between Magnesia and Carbon at High Temperature," Taikabutsu Overseas, 11 [2] 9-16 (1991).

[69]R. E. MOORE, et al., "Reactions Between Magnesia-Graphite-Metal Components of B.O.F.-Type Refractories: Role of Impurities"; pp. 238-41 in Global Advances in Refractories, UNITECR'91 Proceedings. The German Refractories Association, Aachen, Germany, 1991.

[70]H. ISHII, et al., "Behavior of Impurities in Magnesia-Carbon Brick at High Temperatures," Taikabutsu Overseas, 10 [1] 3-8 (1990).

[71]R. F. LEINHOS, "Graphite for Refractories," Proc. Ceram. Eng. Sci., 4 [1-2] 194-99 (1983).

[72]N. C. LUBABA, et al., "Microstructure and Strength of MgO-Carbon

Composite Refractory Materials," Br. Ceram. Trans. J., 88 [2] 47-54 (1989).

[73]J. B. LEWIS, "Thermal Gas Reactions of Graphite"; pp. 129-99 in Modern Aspects of Graphite Technology. Edited by L. C. F. Blackman. Academic Press Inc. (London) Ltd., 1970.

[74]W. M. KENAN, "Hidden Properties of Graphite"; pp. 1463-70 in UNITECR'89 Proceedings, Vol. 2. Edited by L. J. Trostel, Jr. American Ceramic Society, Westerville, OH, 1989.

[75]J. SZEKELY, et al., "Reaction System Involving Single Particles"; Ch. 2 in Gas-Solid Reactions. Edited by J. Szekely, J. W. Evans, and H. Y. Sohn. Academic Press, Inc., 1976.

[76]R. L. NACAMU, et al., "Carbon Oxidation Rates as a Function of BOF Brick Texture," Am. Ceram. Soc. Bull., 54 [7] 647-49 (1975).

[77]T. M. REGAN, et al., "Mass Transfer," Ind. Eng. Chem., 62 [2] 41-53 (1970).

[78]A. YAMAGUCHI, "Thermochemical Analysis for Reaction Processes of Aluminium and Aluminium-compounds in Carbon-containing Refractories," Taikabutsu Overseas, 7 [2] 11-16 (1987).

[79]P. O. R. C. BRANT, et al., "Reactions of Silicon and Aluminium in MgO-Graphite Composites: I. Effects on porosity and microstructure"; pp. 247-50 in Global Advances in Refractories, UNITECR'91 Proceedings. The German Refractories Association, Aachen, Germany, 1991.

[80]A. YAMAGUCHI, "Affects of Oxygen and Nitrogen Partial Pressure on

Stability of Metal, Carbide, Nitride and Oxide in Carbon-Containing Refractories," Taikabutsu Overseas, 7 [1] 4-13 (1987).

[81]A. H. HEUER, et al., "Volatility Diagrams for Silica, Silicon Nitride, and Silicon Carbide and Their Application to High-Temperature Decomposition and Oxidation," J. Am. Ceram. Soc., 73 [10] 2789-803 (1990).

[82]A. YAMAGUCHI, et al., "Role and Behavior of Non-oxide Compounds Added to Carbon-Containing Refractories"; pp. 32-38 in Global Advances in Refractories, UNITECR'91 Proceedings. The German Refractories Association, Aachen, Germany, 1991.

[83]M. RIGAUD, X. LI, P. BOMBARD and B. GUEROULT, "Oxidation Resistance of Carbon-Bonded Basic Refractory Compositions"; pp. 307-15 in Proceedings of the 75th Steelmaking Conference of the Iron and Steel Society of the AIME, Toronto, April 1992.

[84]A. WATANABE, et al., "Some Properties of Magnesia-Carbon Bricks Containing Mg and Al," Taikabutsu Overseas, 5 [2] 7-12 (1985).

[85]A. YAMAGUCHI, et al., "The Effect of Al and Alloy Additives on the Properties of Carbon-Containing Refractories"; pp. 915-24 in Proceedings of the 2nd International Conference on Refractories, Tokyo, Japan, 1987.

[86]P. WILLIAMS, et al., "Charge Pad Refractory Developments in Basic Oxygen Steelmaking Converters"; pp. 25-31 in Global Advances in Refractories, UNITECR'91 Proceedings. The German Refractories Association, Aachen, Germany, 1991.

[87]E. TAMMERMANN, et al., "Influence of Experimental Conditions on Hot Mechanical Strength of Refractory Products Used in the Iron and Steel Industry"; pp. 192-97 in Global Advances in Refractories, UNITECR'91 Proceedings. The German Refractories Association, Aachen, Germany, 1991.

[88]D. A. BROSNAN, et al., "Oxidation Behavior of Carbon-Magnesite Refractories Containing Oxidation Inhibitors"; presented at the 93rd Annual Meeting of the American Ceramic Society in Cincinnati, April 1991.

[89]M. RIGAUD, et al., "Oxidation Kinetics of Graphite in Basic Refractory Compositions"; pp. 383-88 in Global Advances in Refractories, UNITECR'91 Proceedings. The German Refractories Association, Aachen, Germany, 1991.

[90]P. O. R. C. BRANT, "Microstructure and Porosity of Oxide-Graphite Refractory Composites"; Ph.D. Thesis. Univeristy of Sheffield, United Kingdom, 1988.

[91]A. D. PELTON, "Thermodynamics and Phase Diagrams of Materials"; Ch.1 in Materials Science and Technology, Vol.5. Edited by A. M. Alper. VCH Verlagsgesellschaft, Weinheim, Allemagne, 1991.

[92]V. L. STREETER, et al., "Fundamentals of Fluid Mechanics"; Part 1 in Fluid Mechanics, 7th Edition. Edited by V. L. Streeter and E. B. Wylie. McGraw-Hill, In., 1979.

APPENDIX I

Thermochemical Diagrams

Both predominance diagrams and volatility diagrams are two most useful tools for utilizing extensive thermodynamic data to understand and predict gas-solid reactions of various types - oxidation, reduction, evaporation, etc.

I.1 Predominance Diagrams

The predominance diagram is composed of areas or domains of stability of the various solid or liquid compounds. The conditions for co-existence of two and three solid or liquid phases are indicated respectively by the univariant lines and invariant (triple) points on the diagram. The condensed phase shown in the area is the one with the most negative Gibbs energy of formation. All the metastable species are not shown. If two compounds have the same Gibbs energy, they coexist on a univariant line providing that there are no other compounds that have a more negative value. Likewise, three compounds with the same (most negative) value define an invariant point.

Strictly speaking, the predominance diagram is not a true phase diagram because the area may not be the phase area, and the univariant line may not be the phase boundary if there are non-stoichiometric compounds or stable solution phases. On a true

phase diagram, the domains are associated with pure immiscible solid or liquid compounds and the lines are true phase boundaries. In the general case, the predominance diagram can be drawn with domains for completely miscible solid, liquid, or even gaseous compounds (always containing the base element). The diagram is calculated as if the compounds were immiscible. The boundary lines are then no longer phase boundaries, but are lines separating regions in which one species "predominates". Therefore, it is a simplified map of the relative stabilities or domains of predominance of compounds containing the base element. If there is no mutual solubility among the condensed phases, the univariant lines are actually phase boundaries. If this condition is not met, a diagram can still be constructed, but the phase boundary lines on the diagram will no longer be straight.

On the predominance diagrams the base element must be present in all the condensed phases. For the two-metal predominance area diagram, the chemical interactions should be considered. The number of gaseous components can be more than two if, for each additional component, the partial pressure of a gaseous species is held constant. However, it should be noted that the total pressure is not constrained on the predominance diagram. On the other hand, as the activity of a condensed phase is reduced, its corresponding area will be enlarged due to the increased stability.

The standard procedure for calculating a predominance diagram generally consists

of deriving expressions for the univariant lines of the diagram. The gradients of the univariant lines can be determined from the ratio between oxygen and the volatile species. If they are on the same side of the reaction equation, the gradient sign is negative, or otherwise it is positive. For further details about how to construct a predominance diagram, please refer to Reference No. 91.

I.2 Volatility Diagrams

Volatility diagrams are isothermal plots showing the partial pressures (p) of two gaseous species (typically, Po_2 and P_{MeOy} where Me stands for a metal and y can be zero or positive) in equilibrium with the various condensed phases possible in a system. On volatility diagrams, the univariant lines represent the maximum equilibrium vapour partial pressures of the volatile species.

Volatility diagrams are also not phase diagrams. The lines on volatility diagrams simply represent graphical solutions to the thermodynamics of various gas-solid reactions, and thus delineate "fields" where various condensed phases can be found.

The method of constructing a volatility diagram is very similar to that of constructing a predominance diagram. In Reference No. 81, Heuer et al. have already well explicated how to construct a volatility diagram combined with both isomolar and isobaric lines. Thus, there is no need to repeat here.

APPENDIX II

Oxidation Kinetics

II.1 Oxygen Concentration in Air Flow at Given Temperatures

Based on the principles of fluid mechanics,[92] the following governing equations can be derived:

1) continuity equation

$$\frac{d}{dx}(Cu) = 0 \tag{II-1}$$

2) momentum equation

$$\frac{d}{dx}(Cu^2) + \frac{dp}{dx} = 0 \tag{II-2}$$

together with the relations of parameters of gas flow with temperature:

$$u = M\sqrt{\gamma RT} \tag{II-3}$$

$$p = CRT \tag{II-4}$$

Integrating momentum equation (II-2) against the position of air flow gives:

$$C_1u_1^2 + p_1 = C_2u_2^2 + p_2 \tag{II-5}$$

or

$$p_1(1 + \frac{u_1^2}{RT_1}) = p_2(1 + \frac{u_2^2}{RT_2}) \qquad \text{(II-6)}$$

$$p_1(1 + \gamma M_1^2) = p_2(1 + \gamma M_2^2) \qquad \text{(II-7)}$$

if combined with the relations (II-3) and (II-4). Integrating continuity equation (II-1) against the position of air flow gives:

$$C_1 u_1 = C_2 u_2 \qquad \text{(II-8)}$$

or

$$\frac{p_1 M_1}{\sqrt{T_1}} = \frac{p_2 M_2}{\sqrt{T_2}} \qquad \text{(II-9)}$$

if combined with the relations (II-3) and (II-4). Dividing Equation (II-7) by (II-9) gives:

$$\frac{\sqrt{T_1}}{M_1}(1 + \gamma M_1^2) = \frac{\sqrt{T_2}}{M_2}(1 + \gamma M_2^2) \qquad \text{(II-10)}$$

By squaring the above equation on both sides, we can then obtain:

$$T_1(\frac{1}{M_1} + \gamma M_1)^2 = T_2(\frac{1}{M_2} + \gamma M_2)^2 \qquad \text{(II-11)}$$

Since T_1, p_1, u_1, M_1, C_1, and T_2 are known, both M_2 and p_2 can be easily solved from Equations (II-11) and (II-7). Thus, the oxygen concentration at testing temperature T_2 (at hot surface of oxidizing sample) can be calculated from:

$$C_2 = \frac{p_2}{RT_2} \qquad \text{(II-12)}$$

II.2 Rate of First-Order Chemical Reaction

Assume that a gas-solid reaction may be represented by the following:

$$A(g) + b\ B(s) \rightleftarrows c\ C(g)$$

and it is of first order with respect to only the gaseous reactant and product concentrations. Such a reaction can be described by the rate equation:

$$\mathbb{R} = k_1 C_A - k_{-1} C_C \qquad \text{(II-13)}$$

The rate constants k_1 and k_{-1} refer to the forward and reverse reactions, respectively. The difference in the forward and reverse reaction rate constants leads to an equilibrium constant K_E for the chemical reaction

$$K_E = \frac{k_1}{k_{-1}} \qquad \text{(II-14)}$$

Therefore,

$$\mathbb{R} = k_1 C_A - k_{-1} C_C \qquad \text{(II-15)}$$

$$= k_1 \left(C_A - C_C \frac{k_{-1}}{k_1}\right) \qquad \text{(II-16)}$$

$$= k_1 \left(C_A - \frac{C_C}{K_E}\right) \qquad \text{(II-17)}$$

k_1 can be considered to represent the overall rate constant k_c of the chemical reaction and thus we have

$$\mathbb{R} = k_c \left(C_A - \frac{C_C}{K_E}\right) \qquad \text{(II-18)}$$

II.3 Gas Phase Diffusivities

For binary nonpolar gas mixtures, the prediction of diffusion coefficients based on the Chapman-Enskog kinetic theory is usually preferred:[75]

$$D_{A-B} = \frac{1.8583\times10^{-27}\ T^{3/2}}{P\sigma_{AB}^2\ \Omega_{D,AB}} \sqrt{\frac{1}{M_A} + \frac{1}{M_B}} \qquad \text{(II-19)}$$

where

D_{A-B} = mutual diffusivity in binary gas mixture of A and B, m^2/s

T = absolute temperature, °K

M_A, M_B = molecular weights of gases A and B, g/mole

P = absolute pressure, atm

σ_{AB} = collision diameter, m

$\Omega_{D,AB}$ = collision integral, dimensionless

The values of σ_{AB} and $\Omega_{D,AB}$ in the above equation may be calculated from

$$\sigma_{AB} = \frac{\sigma_A + \sigma_B}{2} \qquad \text{(II-20)}$$

$$\frac{\epsilon_{AB}}{k} = \sqrt{\frac{\epsilon_A}{k} \times \frac{\epsilon_B}{k}} \qquad \text{(II-21)}$$

$$\Omega_{D,AB} = \frac{A}{(T^*)^B} + \frac{C}{\exp(DT^*)} + \frac{E}{\exp(FT^*)} + \frac{G}{\exp(HT^*)} \qquad \text{(II-22)}$$

where

ϵ_{AB} = maximum energy of attraction

k = Boltzmann's constant

$T^* = T \cdot (k/\epsilon_{AB})$

A = 1.06036	B = 0.15610	C = 0.19300	D = 0.47635
E = 1.03587	F = 1.52996	G = 1.76474	H = 3.89411

According to the book "Gas-Solid Reactions" of Szekely et al.,[75] the Lennard-Jones constants σ and ϵ for the gases O_2 (Mo_2 = 32.00) and CO (Mco = 28.01), which are the diffusion-gas-pair in our reaction system, are given in Table II-1.

Table II-1 Lennard-Jones constants σ and ϵ for the diffusion-gas-pair O_2 and CO (from Szekely et al.[75])

Gas	O_2	CO
σ x 10^{10} (m)	3.467	3.690
ϵ / k (°K)	106.7	91.7

APPENDIX III

Lists of Experimental Data and Their Statistical Analyses

For the sake of the thesis length, only part of the experimental raw data are listed in this appendix to show what is the range of data variation and how the data are treated.

Statistical analysis of the results of unidirectional oxidation tests

Brick samples for testing: 15 wt% graphite, regular MgO grain-size distribution, and 2.5 wt% resin binder; after carbonization at 1000°C for 10 h.

Test conditions: oxidation in an air flow of 500 ml/min for 5 h

Test No.	Oxidation temperature (°C)	Weight loss (g/cm^2)	Repeatability (%)
1	1000	0.23	96
2	1000	0.25	
3	1000	0.24	
1	1200	0.29	95
2	1200	0.28	
3	1200	0.31	
1	1400	0.37	94
2	1400	0.35	
3	1400	0.33	

Repeatability

The repeatability of the test results is calculated based on the following equation:

$$\textit{Repeatability}\ (\%) = 100 - \frac{\textit{Sample Standard Deviation}}{\textit{Arithmetic Mean}} \times 100\%$$

Level	Sample size	Mean (g/cm^2)	Standard deviation (g/cm^2)
1000°C	3	0.24	0.010
1200°C	3	0.29	0.015
1400°C	3	0.35	0.020

Analysis of Variance

The one-way analysis of variance is conducted to test the null hypothesis that the population means of the 3 temperature treatment groups are all equal.

Source of variation	Degrees of freedom	Sum of squares	Mean sum of squares	F	P
Between treatments	2	0.01816	0.009078	37.14	0.000
Within treatments (error)	6	0.00147	0.000244		
Total	8	0.01962			

Since $F = 37.14 > 10.92 = F_{0.01}(2,6)$, the null hypothesis, equality of the three means, can be rejected at the confidence level of 99%. In other words, these three temperature treatments do result in a difference in weight loss.

Analysis of Factor Level Effects

Estimation of the difference between two factor level means, i.e. contrast, is also made to compare the mean weight losses between two different temperature treatments, i.e. 1000 and 1200°C or 1200 and 1400°C. For the comparison of the mean weight losses at 1000 and 1200°C, the contrast is:

$$L_1 = \mu_{1000} - \mu_{1200}$$

and its desired 95 percent confidence interval is calculated as:

$$-0.08 \leq L_1 \leq -0.02$$

The result of analysis indicates that the mean weight loss at 1000°C falls below that at 1200°C by somewhere between 0.08 and 0.02 g/cm^2 per measurement. In the same way, by defining the contrast as:

$$L_2 = \mu_{1200} - \mu_{1400}$$

we can obtain the confidence interval:

$$-0.09 \leq L_2 \leq -0.03$$

Thus, we estimate with confidence coefficient 0.95 that the mean weight loss at 1400°C is greater than that at 1200°C by somewhere between 0.09 and 0.03 g/cm^2 per measurement.

Bulk densities of experimental bricks as-received

The bulk densities of experimental bricks as-received (8 bricks for each batch of total 9 mixes) were measured according to ASTM C 134-88.

Experimental bricks		Bulk density (g/cm^3)	
Identification	Description	Mean value	Standard deviation
G1-D1-B1	5 wt% graphite regular MgO grain-size distribution 2.5 wt% resin binder	3.01	8.33×10^{-3}
G2-D1-B1	10 wt% graphite regular MgO grain-size distribution 2.5 wt% resin binder	3.00	3.68×10^{-3}
G3-D1-B1	15 wt% graphite regular MgO grain-size distribution 2.5 wt% resin binder	2.98	3.20×10^{-3}
G4-D1-B1	20 wt% graphite regular MgO grain-size distribution 2.5 wt% resin binder	2.95	3.52×10^{-3}
G3-D2-B1	15 wt% graphite small MgO grain-size distribution 2.5 wt% resin binder	2.94	7.85×10^{-3}
G3-D1-B2	15 wt% graphite regular MgO grain-size distribution 3.5 wt% resin binder	2.95	4.17×10^{-3}
G3-D1-B1-A1	15 wt% graphite regular MgO grain-size distribution 2.5 wt% resin binder 4 wt% Al addition	2.95	5.77×10^{-3}
G3-D1-B1-A2	15 wt% graphite regular MgO grain-size distribution 2.5 wt% resin binder 4 wt% Si addition	2.95	2.40×10^{-3}
G3-D1-B1-A3	15 wt% graphite regular MgO grain-size distribution 2.5 wt% resin binder 4 wt% SiC addition	2.90	8.17×10^{-3}

Weight changes during carbonization

Brick samples for testing: G3-D1-B1 (as-received)

Test conditions: carbonization at 1000°C for 10 h

Sample number	Sample weight (g)		Weight loss (wt%)	Mean
	before carbonization	after carbonization		
1	180.29	177.28	1.67	1.70 wt%
2	179.19	176.14	1.70	Standard deviation
3	179.08	176.06	1.69	
4	180.85	177.72	1.73	0.022 wt%
5	180.73	177.64	1.71	

Measurement of the pycnometric volume change of a sample

Brick sample for testing: G3-D1-B1-A1 (after carbonization)

Test conditions: firing in CO at 1200°C for 5 h

Measurement Number	Pycnometric volume - cm^3 (before firing)	Mean 55.00	Pycnometric volume - cm^3 (after firing)	Mean 56.76	Change of pycnometric volume ($\Delta V/V_0$ %)
1	54.99		56.68		
2	54.92	Standard Deviation	56.72	Standard Deviation	3.20
3	55.00		56.83		
4	55.08	0.057	56.73	0.071	
5	55.02		56.84		

Changes of pycnometric volume during carbonization

Brick samples for testing: G3-D1-B2 (as-received)

Test conditions: carbonization at 1000°C for 10 h

Sample number	Pycnometric volume (cm^3)		Change of sample volume (vol %)	Mean value (vol %) -7.29
	before carbonization	after carbonization		
1	58.24	53.98	-7.31	
2	58.57	54.34	-7.22	Standard deviation 0.051
3	58.74	54.46	-7.29	
4	58.55	54.25	-7.34	

Measurement of relative cold crushing strength

Brick samples for testing: D1-B1 with different graphite contents (as-received)

Test conditions: carbonization at 1000°C for 10 h

Brick sample with graphite content (wt%)	Sample size		Maximum load before cracking (kgf)	Crushing strength (kgf/cm^2)
	Diameter (cm)	Height (cm)		
Before carbonization (as-received)				
5	4.38	4.01	2575	146.61
10	4.38	4.07	2250	126.22
15	4.38	4.10	1921	106.97
20	4.38	4.06	1450	81.54
After carbonization at 1000°C for 10 h				
5	4.38	4.03	443	25.10
10	4.40	4.13	457	25.18
15	4.40	4.12	465	25.65
20	4.41	4.08	465	25.88

Changes of pycnometric volume during unidirectional oxidation

Brick samples for testing: G3-D2-B1 (after carbonization)

Test conditions: oxidation in air at three different temperatures for 5 h

Oxidation temperature (°C)	Sample number	Sample volume (cm^3)		Sample diameter (cm)	Unidirectional volume loss (10^2 x cm^3/cm^2)	Mean value
		before oxidation	after oxidation			
1000	1	54.73	52.90	4.40	12.04	12.00
1000	2	54.83	53.02	4.39	11.96	
1200	1	54.25	52.05	4.40	14.47	14.43
1200	2	54.59	52.41	4.39	14.40	
1400	1	54.62	51.88	4.40	18.02	17.87
1400	2	54.18	51.50	4.39	17.71	

Weight changes during unidirectional oxidation

Brick samples for testing: G3-D1-B2 (after carbonization)

Test conditions: oxidation in air at three different temperatures for 5 h

Oxidation temperature (°C)	Sample number	Sample weight (g)		Sample diameter (cm)	Unidirectional weight loss (g/cm^2)	Mean value
		before oxidation	after oxidation			
1000	1	172.96	168.51	4.40	0.293	0.29
1000	2	174.55	170.35	4.39	0.277	
1200	1	173.73	168.61	4.41	0.335	0.34
1200	2	172.96	167.75	4.40	0.343	
1400	1	173.59	167.28	4.40	0.415	0.41
1400	2	171.21	164.98	4.40	0.410	

Measurement of the depth of a decarbonized layer

Brick sample for testing: G3-D1-B1 (as-received)

Test conditions: direct oxidation in air at 1200°C for 10 h

Measurement number	Measurement value (mm)	Measurement number	Measurement value (mm)	Depth of the decarbonized layer (mm)
1	10.65	16	9.75	
2	10.55	17	9.65	
3	10.40	18	9.70	Mean value
4	10.30	19	9.65	
5	10.00	20	9.75	10.14
6	9.95	21	9.80	
7	10.10	22	9.85	Standard deviation
8	10.40	23	9.70	0.3312
9	10.40	24	9.90	
10	10.50	25	10.05	Minimum
11	10.60	26	10.25	
12	10.50	27	10.35	9.65
13	10.20	28	10.40	Maximum
14	10.00	29	10.50	
15	9.80	30	10.55	10.65

ÉCOLE POLYTECHNIQUE DE MONTRÉAL
3 9334 00290464 5